

✓ NASA CR-167889
37255-8002-UT-00

INTEGRATED PROPULSION FOR NEAR-EARTH SPACE MISSIONS

VOLUME II: TECHNICAL

by C.L. Dailey, H.F. Meissinger, R.H. Lovberg, and S. Zafran



TRW Space and Technology Group
Redondo Beach, California 90278

prepared for
NATIONAL AERONAUTICS AND SPACE ADMINISTRATION

NASA Lewis Research Center
Contract NAS 3-22861

(NASA-CR-167889-Vol-2) INTEGRATED
PROPULSION FOR NEAR-EARTH SPACE MISSIONS.
VOLUME 2: TECHNICAL Final Report, 29 Sep.
1980 - 29 Sep. 1981 (TRW Defense and Space
Systems Group) 175 p HC 103/ME A01 CSCL 21C G3/20

N82-33425

Unclass
35305

ORIGINAL COPY
OF POOR QUALITY

1. Report No. CR 167889		2. Government Accession No		3. Recipient's Catalog No	
4. Title and Subtitle INTEGRATED PROPULSION FOR NEAR-EARTH SPACE MISSIONS, VOLUME II: TECHNICAL				5. Report Date October 1981	
				6. Performing Organization Code	
7. Author(s) C. L. Dailey, H. F. Meissinger, R. H. Lovberg, and S. Zafran				8. Performing Organization Report No. 37255-6002-UT-00	
9. Performing Organization Name and Address TRW Defense and Space Systems Group Redondo Beach, California 90278				10. Work Unit No	
				11. Contract or Grant No NAS 3-22661	
12. Sponsoring Agency Name and Address National Aeronautics and Space Administration Lewis Research Center Cleveland, Ohio 44135				13. Type of Report and Period Covered Final Report 29 Sep 1980 - 29 Sep 1981	
				14. Sponsoring Agency Code	
15. Supplementary Notes Project Manager, M. E. Valgora, Systems Analysis Office, NASA - Lewis Research Center					
16. Abstract The calculation approach is described for parametric analysis of candidate electric propulsion systems employed in LEO to GEO missions. Occultation relations, atmospheric density effects, and natural radiation effects are presented. A solar cell cover glass tradeoff is performed to determine optimum glass thickness. Solar array and spacecraft pointing strategies are described for low altitude flight and for optimum array illumination during ascent. Mass ratio tradeoffs versus transfer time provide direction for thruster technology improvements. Integrated electric propulsion analysis is performed for orbit boosting, inclination change, attitude control, stationkeeping, repositioning, and disposal functions as well as power sharing with payload on-orbit. Comparison with chemical auxiliary propulsion is made to quantify the advantages of integrated propulsion in terms of weight savings and concomittant launch cost savings.					
17. Key Words (Suggested by Author(s)) Electric propulsion Orbit analysis Large space structures			18. Distribution Statement Unclassified - unlimited		
19. Security Class. (of this report) Unclassified		20. Security Classif. (of this page) Unclassified		21. No of Pages 172	22. Price*

* For sale by the National Technical Information Service, Springfield, Virginia 22161

PRECEDING PAGE BLANK NOT FILMED

CONTENTS

	Page
1. INTRODUCTION.	1
2. ORBIT TRANSFER ANALYSIS	3
2.1 Calculation Approach	3
2.1.1 Climb Equations.	3
2.1.2 ΔV Maneuvers	8
2.1.3 Comparison of Performance Relations.	10
2.2 Spacecraft Parameters.	15
2.2.1 Thruster Efficiency.	15
2.2.2 Specific Mass.	16
2.2.3 Specific Power	18
2.2.4 Specific Area.	20
2.2.5 Propulsion Mass Ratio.	20
2.2.6 Propellant Mass Ratio.	20
2.2.7 Auxiliary Propulsion Mass Ratio.	20
2.3 Occultation Relations.	23
2.4 Space Environment Effects.	28
2.4.1 Atmospheric Density.	28
2.4.2 Radiation.	28
2.5 Solar Cell Cover Tradeoff.	28
2.6 Low Altitude Flight.	37
2.6.1 Power Factor in Feathered Flight	37
2.6.2 Orbit Transfer Starting Power.	48
2.6.3 Sustained Low Altitude Flight.	51
2.7 Plane Change	53
2.8 Orbit Transfer Times	57
2.8.1 Nominal Mission Performance.	57
2.8.2 Fast Orbit Transfer.	77
3. INTEGRATED PROPULSION ANALYSIS.	96
3.1 Scope of Study	96
3.1.1 System Concept and Assumptions	97
3.1.2 Spacecraft Description	98
3.2 Propulsion System Definition	101
3.2.1 Thruster Arrangement.	101
3.2.2 Thrust Modes	104
3.2.3 Thruster Function Allocation	107

CONTENTS (Continued)

	Page
3.3 System Requirements	108
3.3.1 Spacecraft Mass Characteristics	108
3.3.2 Disturbance Forces and Torques	112
3.3.3 Auxiliary Thruster Sizing	119
3.3.4 Principal On-Orbit ΔV Requirements	120
3.3.5 Use of Batteries	130
3.3.6 Thruster Cant Angle Requirements	131
3.3.7 Gravity Gradient Strategy	131
3.4 Integrated Propulsion Advantages	133
3.4.1 Comparison of Electric and Chemical APS.	133
3.4.2 Launch Cost Savings Achievable with Integrated Electric Auxiliary Propulsion.	134
3.4.3 Power Sharing in Orbit	140
4. DISCUSSION OF RESULTS	143
4.1 Orbit Transfer	143
4.1.1 Solar Cell Cover Thickness	143
4.1.2 Optimum Isp Range.	144
4.1.3 Importance of Efficiency and Specific Mass	145
4.1.4 Fast Orbit Transfer.	146
4.1.5 Low Altitude Flight.	147
4.2 Specific Mission Example	148
5. CONCLUSIONS	151
APPENDIX A East-West Stationkeeping ΔV Requirements Including the Effect of Spacecraft Mass Variation (Iterative Procedure).	153
REFERENCES.	158

ILLUSTRATIONS

		Page
1	Effect of ΔV and I_{sp} on Propulsion Payload Mass Ratio and Trip Time for Different Thruster to Payload Mass Ratios.	13
2	Thruster Efficiency Functions.	16
3	Estimated Specific Mass of Silicon Solar Cell Arrays vs Total Cell Thickness	19
4	Plane Containing Orbital Axis and Earth-Sun Line	24
5	View Toward Sun.	24
6	Earth Centered Coordinates	26
7	Atmospheric Density vs Altitude.	29
8	Fluence Rate vs Altitude for 0 and 30 deg Orbit Inclinations	30
9	Silicon Solar Cell Degradation Caused by Radiation	31
10	Effect of I_{sp} and Cover Thickness on Thrust time at $\frac{M_{EPS}}{M_{PL}} = 2$	33
11	Effect of I_{sp} and Cover Thickness on Thrust Time at $\frac{M_{EPS}}{M_{PL}} = 2$	34
12	Effect of I_{sp} and Cover Thickness on Thrust Time at $\frac{M_{EPS}}{M_{PL}} = 2$	35
13	Effect of I_{sp} and Cover Thickness on Thrust Time at $\frac{M_{EPS}}{M_{PL}} = 2$	36
14	Effect of Solar Cell Cover Thickness on Thrust Time for Different Combinations of Thruster α and η	38
15	Effect of Cover Thickness on Power Factor at GEO for Different Thruster Parameters (M_{EPS}/M_{PL}) = 2	39
16	Viewing Sphere Centered at Spacecraft.	40
17	Sun Angle Relative to Orbit Plane.	42
18	Feathered Array Power Factor vs Orbit Position Angle α for Different Values of β (no occultation)	44
19	Average Power Factor vs β for Feathered Array (no occultation)	45

ILLUSTRATIONS (Continued)

	Page
20 Average Power Factor vs Time After Summer Solstice for Feathered Array (28.5° Orbit Inclination, H = 250 km).	46
21 Percent Time Available vs Average Power Factor Per Day for Feathered Array (28.5° Orbit Inclination, H = 250 km).	47
22 Optimum Geometry to Initiate Ascent (B = -θ)	49
23 Maximum Average Power Factor at Start of Climb vs Days After Summer Solstice (no occultation)	50
24 Occultation Fraction vs Altitude (Summer Solstice ψ = 180°).	52
25 Comparison of Minimum Altitude for Feathered Solar and Nuclear Power.	54
26 ΔV for Different Plane Change Options (250 km initial orbit, GEO final orbit).	56
27 Effect of η and I _{sp} on Transfer Time for $\left(\frac{M_{EPS}}{M_{PL}}\right)_T = 1.0$	59
28 Effect of η and I _{sp} on Transfer Time for $\left(\frac{M_{EPS}}{M_{PL}}\right)_T = 2.0$	60
29 Effect of η and I _{sp} on Transfer Time for $\left(\frac{M_{EPS}}{M_{PL}}\right)_T = 3.0$	61
30 Effect of η and I _{sp} on Transfer Time for $\left(\frac{M_{EPS}}{M_{PL}}\right)_T = 4.0$	62
31 Effect of Payload Fraction on Minimum Transfer Time and Corresponding I _{sp}	63
32 Propulsion Mass Breakdown for 20% Payload Fraction	65
33 Propulsion Mass Breakdown for 25% Payload Fraction	66
34 Propulsion Mass Breakdown for 33% Payload Fraction	67
35 Propulsion Mass Breakdown for 50% Payload Fraction	68
36 Effect of η and I _{sp} on Transfer Time for $\left(\frac{M_{EPS}}{M_{PL}}\right)_T = 2.0$	69
37 Propulsion Mass Breakdown for 33% Payload Fraction	70

ILLUSTRATIONS (Continued)

	Page	
38	Percent of Total Propellant Used on-Orbit.	71
39	Comparison of Transfer Times for 5 and 10 Year Missions. . .	72
40	Effect of η on Transfer Time at Optimum I_{SP}	73
41	Effect of Specific Mass on Transfer Time for Case II $\eta = 45\%$ at 1750 sec.	75
42	Residual On-Orbit Power for Optimum I_{SP} Transfer and Case II Efficiency	76
43	Transfer Time Tradeoff - 10% Payload Fraction.	78
44	Transfer Time Tradeoff - 15% Payload Fraction.	79
45	Transfer Time Tradeoff - 20% Payload Fraction.	80
46	Transfer Time Tradeoff - 30% Payload Fraction.	81
47	Transfer Time Tradeoff - 40% Payload Fraction.	82
48	Transfer Time Tradeoff - 50% Payload Fraction.	83
49	Propulsion Mass Breakdown for 10% Payload Fraction	84
50	Propulsion Mass Breakdown for 15% Payload Fraction	85
51	Propulsion Mass Breakdown for 20% Payload Fraction	86
52	Propulsion Mass Breakdown for 30% Payload Fraction	87
53	Propulsion Mass Breakdown for 40% Payload Fraction	88
54	Propulsion Mass Breakdown for 50% Payload Fraction	89
55	Percent of Total Propellant Used On-Orbit.	90
56	Effect of Payload Fraction on Minimum Transfer Time and Corresponding I_{SP}	91
57	Resistojet Limitations for LEO and GEO Mission	93
58	Effect of Payload Fraction on Resistojet Transfer Time . . .	94
59	Reference Generic Spacecraft Configuration	99
60	Thruster Arrangement on Reference Configuration.	102

ILLUSTRATIONS (Continued)

		Page
61	Nominal Orbit Orientation of Vehicle.	106
62	Mass and Moments of Inertia of Reference Spacecraft/ Structure (Modular Antenna Structure) Extrapolated from Boeing Data (Ref. 2)	111
63	X Axis Forces (Ref. 2).	113
64	Y Axis Forces (Ref. 2).	114
65	Z Axis Forces (Ref. 2).	115
66	Pitch Torques (Ref. 2).	116
67	Yaw Torques (Ref. 2).	117
68	Roll Torques (Ref. 2)	118
69	Thrust Acceleration Required vs Duty Cycle in N-S Stationkeeping.	121
70	Stationkeeping ΔV Requirements vs A/M Ratio and Represent- ative A/M Ranges for Various Spacecraft Classes	123
71	Normalized Velocity Increment per Year for E-W Station- keeping as a Function of Duty Cycle with Eccentricity Ratio as a Parameter (Ref. 12).	126
72	Normalized Thruster Acceleration for E-W Stationkeeping as Function of Duty Cycle with Eccentricity Ratio as a Parameter (Ref. 12)	127
73	Performance Comparison of Chemical and Electric APS	136
74	Shuttle Launch Cost Contours in Terms of Cargo Weight and Length.	138
75	Examples of Launch Cost Savings Variation with Cargo Length.	139
76	Power Utilization Examples.	141
77	Iteratively Corrected Values of ΔV_s vs ΔV_{s0} (10-Year Mission).	156

TABLES

		Page
1	Low Thrust Chemical and Electric Propulsion Equation Summary.	11
2	Estimated Specific Mass for Advanced Argon Thruster Systems.	18
3	Electric Propulsion Specific Mass Estimates.	18
4	Range of α_E Parameter (kg/watt) and η for Cover Thickness Tradeoff	32
5	Mission Parameter Set.	57
6	Comparison of Optimum I_{sp} and I_{sp} for Minimum Transfer Time - Case II Efficiency.	64
7	Comparison of Orbit Transfer and On-Orbit Fluence Levels . . .	74
8	Thruster Function Allocations.	109
9	Auxiliary Thruster Functions and Numbers	109
10	Mass Properties Data for Three Spacecraft/Structure Classes (Ref. 2)	110
11	Scaling Relations for Modular Single Antenna (Ref. 2).	112
12	Characteristics of E-W Stationkeeping Maneuvers.	129
13	Spacecraft Attitude Maneuvers for Optimum Sun Alignment During Primary Thrust Phases	132
14	Auxiliary Propulsion V Requirements Other Than for E-W Stationkeeping (10-Year Mission) in m/sec.	134
15	ΔV and Mass Characteristics of Electric and Chemical APS Spacecraft (Reference Configuration: Modular Antenna System).	135
16	Effect of Thruster Efficiency on Transfer Time (33% Payload, $\alpha = 0.024$ kg/W).	146
17	Effect of α on Transfer Time (33% Payload, $\eta = 45\%$ at at 1750 sec I_{sp})	146
18	Effect of Payload on Transfer Time for Electric and Resistojet Thrusters	147

TABLES (Continued)

	Page
19 Specific Mission Requirements.	149
20 ΔV Requirements for APS, 60 m Modular Antenna Spacecraft . .	149
21 EPS Characteristics for 60 m Modular Antenna Spacecraft. . .	150
22 Solution of Equation A-5 for Iterative Correction of ΔV_S (Velocities in m/sec).	155

SYMBOLS

A	Total drag area = $A_{PL} + A_{EP}$ (meters) ²
A_{EP}	Electric propulsion drag area (meters) ²
A_{PL}	Payload drag area (meters) ²
A_{TH}	Propulsion system area (meters) ²
a	Acceleration, meters/(second) ²
a	Earth radius, kilometers
a_s	Stationkeeping acceleration, meters/(second) ²
B	Longitudinal separation of earth axis and orbit axis, degrees
b	Semiminor axis, meters
C_L	Length dependent cost, dollars
C_W	Weight dependent cost, dollars
C_D	Drag coefficient
D	Drag, newtons
d	Diameter, meters
E	Earth axis
E	Total energy = U + K, joules
F	Thrust, newtons
f	Occultation fraction
G	Universal gravitation constant, (meters) ³ /kilogram-(second) ²
g	Acceleration of gravity, meters/(second) ²
H	Altitude, meters

SYMBOLS (Continued)

I	Moment of inertia, kilogram-(meters) ²
I _{SP}	Specific impulse, seconds
i	Inclination, degrees
K	Kinetic energy, joules
k	Spacecraft characteristic (see Equation 61), (meters) ² /kilogram
L	Length, meters
ΔL _S	Longitude excursion between stationkeeping maneuvers, degrees
M	Mass, kilograms
M _{EP}	Electric propulsion dry mass, kilograms
M _{EPS}	Electric propulsion system dry mass, kilograms
(M _{EPS} /M _{PL}) _T	Total propulsion to payload mass ratio (see Equation 35)
M _{PL}	Payload mass, kilograms
M _{PP}	Propellant mass, kilograms
M _{PP0}	Initial propellant mass, kilograms
M _{TH}	Propulsion system mass, kilograms
MRE	Electric mass ratio = M _{EP} /(M _{PL} + ΔM _{PP})
MRP	Propellant mass ratio = M _{PP} /(M _{PL} + ΔM _{PP})
ΔM _{PP}	Auxiliary propulsion (propellant) mass, kilograms
m	Number of days to complete a stationkeeping maneuver
m	Spacecraft mass, kilograms
n	Stationkeeping fraction

SYMBOLS (Continued)

P	Angle between orbit axis and ecliptic pole, degrees
P	Power, watts
P_0	Beginning-of-life power, watts
P	Duty cycle
r	Orbit radius, kilometers
r	Power utilization ratio
r_F	Final orbit radius, kilometers
r_I	Initial orbit radius, kilometers
S	Solar constant, kilograms/meter-(second) ²
T	Orbit period, seconds
T	Thrust, newtons
T	Torque, newton-meters
t	Time, seconds
t_c	Stationkeeping cycle durations, days
t_θ	Time to complete repositioning, days
U	Potential energy, joules
ΔV	Velocity increment, meters/second
ΔV_s	Stationkeeping velocity increment, meters/second
v	Orbit velocity, meters/second
v_F	Final orbit velocity, meters/second
v_I	Initial orbit velocity, meters/second

SYMBOLS (Continued)

W	Weight, kilograms
x, y, z	Cartesian coordinates
Z	Ecliptic pole
α	Orbit position angle, degrees
α_C	Specific mass = M_{TH}/T , kilograms/newton
α_E	Specific mass = $M_{EP}/P_O = \alpha_S + \alpha_{TH}$, kilograms/watt
α_S	Solar array specific mass, kilograms/watt
α_{TH}	Specific mass of thruster subsystem, kilograms/watt
β	Angle between orbit plane and sun line, degrees (90 - β in Section 2.6.1)
β	Eccentricity ratio (see Equation 61)
β'	Angle between solar array and sun line, degrees
β_C	Specific thrust = T/A_{TH} , newtons/(meter) ²
β_E	Specific power = $P_O/A_{EP} = \text{watts}/(\text{meter})^2$
γ	Half-arc length for stationkeeping thrust, degrees
ϵ	Inclination of earth axis with ecliptic pole = 23.5 degrees
η	Thruster efficiency
θ	0.986 times the number of days after summer solstice, degrees
$\Delta\theta$	Repositioning transfer angle, degrees
λ_p	Power fraction = P/P_O
λ_{pp}	Propellant fraction (see Equations 17 and 25)
ρ	Atmospheric density, kilograms/(meter) ³

SYMBOLS (Continued)

δ	Angle between solar array and orbit plane, degrees
ϕ	Roll angle, degrees
ψ	Longitudinal separation of orbit axis and ecliptic pole, degrees
ω	Frequency, radians/second
ω	Orbit axis

1. INTRODUCTION

Previous studies established categories for primary and auxiliary electric propulsion in near-earth missions (References 1 and 2, respectively). In addition, Reference 3 characterized missions to be deployed from the Space Transportation System (STS) in low earth orbit. This study extended previous results to encompass integrated electric propulsion systems. The objectives of this effort were to establish the nature and characteristics of electric propulsion systems (1) that can provide the propulsion required for all phases of the LEO to GEO mission, starting with the spacecraft assembled in low earth orbit, and continuing through spacecraft disposal after conclusion of on-orbit operations, and (2) whose characteristics have minimum sensitivity to changes in mission requirements, thereby assuring as wide an applicability of the systems as possible.

During the study effort, a low thrust computer program was developed and implemented for parametric analysis of electric propulsion systems. The gravitational equation was solved for determination of thrusting time for orbit boosting as a function of payload mass ratio. The electric propulsion system mass included thrusters, power source, power conditioning, gimbals, propellant, propellant storage and distribution, structure and thermal control for propulsion equipment. The payload included all other mass deployed from the Shuttle Orbiter. In this manner, the power source for propulsion, which was sized for orbit transfer, was available for payload power sharing on-orbit.

The principal parameters of interest in the analysis included thruster efficiency, specific impulse, specific mass, specific power, specific area, power fraction, and propellant fraction in addition to mass ratios and maneuver times. For propulsive functions other than orbit boosting, the velocity increment (Δv) characterizing the maneuver was employed, and the rocket equation was implemented for analysis. The propulsion functions studied included orbit boosting, inclination change, attitude control, stationkeeping, repositioning, disposal, and power sharing on-orbit.

In order to compute transfer times for tradeoff comparisons, it was necessary to add the effects of atmospheric drag, occultation (shadowed

portions of each orbit), and radiation degradation to the climb equations. After these effects had been taken into account, it was determined that electric propulsion could be initiated at Shuttle's maximum cargo carrying altitude. It was further established that an optimum solar cell cover glass thickness could be used for orbit transfer. Strategies were developed for orienting solar arrays along the velocity vector to provide minimum drag area at low altitudes, and for rolling the spacecraft to achieve optimum array illumination during ascent. Plane change was initiated at higher altitudes to minimize radiation degradation.

The general mission parameter set investigated included payload fractions ranging from 20 to 50%, with 10 years operational lifetime at GEO. Transfer time calculations were performed for thruster efficiencies from 20 to 100% and specific impulse up to 5000 seconds. From the resulting tradeoff curves, and comparison with existing technology, recommendations for future technology efforts were made.

Integrated propulsion analysis was also performed to identify advantages of using electric propulsion for functions other than orbit transfer alone. These functions can be accomplished by using the electric propulsion system as an integrated part of the space vehicle rather than as a separate orbit transfer vehicle only. A generic spacecraft configuration, that is compatible with a single Shuttle launch, was chosen for analysis. Thruster arrangements, thrusting modes, and functional allocations were studied for all mission phases. Solar pressure effects on GEO stationkeeping requirements were found to be significant compared to gravitational requirements. Comparisons were made with chemical auxiliary propulsion systems to quantify the advantages of integrated propulsion in terms of weight savings and concomitant transportation cost savings.

During the integrated propulsion analysis, it was determined that gravity gradient torques could be used during ascent phases of the mission to assist in rolling the spacecraft to orient the solar array for optimum illumination. This was the general strategy employed during the study.

A summary of the technical effort is contained in Volume I of the final report. Details of the propulsion analysis are presented in this volume.

2. ORBIT TRANSFER ANALYSIS

2.1 CALCULATION APPROACH

"Primary propulsion" often refers to payload deployment only, with "secondary propulsion" covering everything else. There are two shortcomings of this viewpoint. One is that deployment is generally thought of as the sequence of events that starts with lift-off and ends with orbit insertion, with all propulsion events being done impulsively. This relegates low-thrust propulsion, i.e., continuous as opposed to impulsive, to orbit and attitude maintenance; and this may not be so. For large and/or flexible spacecraft, some of the deployment propulsion may necessarily be low thrust, whether chemical or electric. The other shortcoming is that it places orbit changes, both plane and altitude changes, in the same category as stationkeeping and attitude control. Thus a misleading distinction is drawn between a "secondary propulsion" maneuver and a "primary propulsion" one in terms of intent rather than the propulsion required for the maneuver.

A simple way around this confusion is to regard all orbital maneuvers as primary propulsion. Then propulsion used in deployment, disposal, return, retrieval and maneuvers that involve altitude and/or plane changes that may be needed for some missions, are all included in "primary propulsion"; while "secondary propulsion" encompasses attitude control, stationkeeping and docking requirements.

From this point of view, the orbit transfer portion of the present study is an example of low thrust primary propulsion that could be done either chemically or electrically. The other low thrust primary propulsion functions mentioned above could also be done with either chemical or electric propulsion.

2.1.1 Climb Equations

The calculation of transfer time is done by integrating the radial rate equation that describes the effect of essentially continuous tangential thrust applied to a quasi-circular orbit; i.e., it does not involve the "characteristic velocity" Δv . The relations are derived below in

parametric form for both electric and chemical low thrust to clarify the similarities and differences of the propulsion types.

From equilibrium of radial forces,

$$\frac{mv^2}{r} = \frac{GMm}{r^2} \quad (\text{gravitational equation})$$

so that

$$v^2 = \frac{GM}{r} \quad (1)$$

where v and r are orbit velocity and radius and m and M are spacecraft and Earth mass. G is the universal gravitation constant; g , used later, is the acceleration of gravity. Using the Earth radius, r in meters is the altitude H plus the Earth radius 6.37×10^6 ; in MKS units, $GM = 4.00 \times 10^{14}$.

The energy relations are:

Kinetic,

$$K = \frac{1}{2} m \left(\frac{GM}{r} \right) \quad (2)$$

potential,

$$U = \int_{\infty}^r \frac{GMm}{r^2} dr = - \frac{GMm}{r} \quad (3)$$

and total,

$$E = U + K = - \frac{GMm}{2r} \quad (4)$$

The net tangential force, thrust minus drag, increases the total energy according to the relation

$$(T - D) v = \frac{dE}{dt} \quad (5)$$

Thus, from Equations (1), (4) and (5)

$$T-D = \sqrt{\frac{GM}{r}} \frac{m}{2} \left(\frac{\dot{r}}{r} - \frac{\dot{m}}{m} \right)$$

or

$$\frac{\dot{r}}{r} = \frac{2}{m} \sqrt{\frac{r}{GM}} (T-D) + \frac{\dot{m}}{m} \quad (6)$$

Equation (6) applies to either chemical or electric propulsion. The subsequent developments are different for these cases but are done in a parallel way for ease of interpretation. The essential difference arises from the fact that dry propulsion mass for electric propulsion M_{EP} is more conveniently related to power than to thrust, while the reverse is true for chemical propulsion.

2.1.1.1 Low Thrust Electric

Thrust is given by,

$$T = \frac{2}{g} \left(\frac{\eta}{I_{SP}} \right) P \quad (7)$$

where P is power delivered to the thruster and η and I_{SP} are thruster efficiency and specific impulse.

Drag is

$$D = \frac{\rho C_D}{2} \left(\frac{A}{P} \right) v^2 P \quad (8)$$

where A is the total drag area including the payload A_{PL} and the electric propulsion system A_{EP} , v is flight velocity, ρ is atmospheric density and C_D is the drag coefficient related to the area A . Thus

$$\frac{A}{P} = \frac{A_{EP}}{P} + \frac{A_{PL}}{M_{PL}} \frac{M_{PL}}{M_{EP}} \frac{M_{EP}}{P} \quad (9)$$

With the definitions

$$\alpha_E = \frac{M_{EP}}{P_0} \quad (\text{power related specific mass}) \quad (10)$$

$$\beta_E = \frac{P_0}{A_{EP}} \quad (\text{specific power}) \quad (11)$$

$$\lambda_p = \frac{P}{P_0} \quad (\text{power fraction}) \quad (12)$$

ORIGINAL SOURCE
OF POOR QUALITY

Equation (9) becomes

$$\lambda_p \frac{A}{P} = \frac{1}{\beta_E} + \frac{\alpha_E}{\frac{M_{PL}}{A_{PL}} \frac{M_{EP}}{M_{PL}}} \quad (13)$$

where M_{EP} is electric propulsion dry mass and M_{PL} is payload mass.

Relating the mass flow rate to power gives,

$$\dot{m} = - \frac{2\eta P}{(gI_{SP})^2} \quad (14)$$

and the spacecraft mass m can be expressed in terms of payload mass in the form,

$$m = M_{PL} \left[1 + \frac{M_{EP}}{M_{PL}} + \lambda_{pp} \left(\frac{M_{PP}}{M_{PL}} \right)_0 \right] \quad (15)$$

where $(M_{PP})_0$ is the initial propellant mass and λ_{pp} is propellant fraction.

By combining Equations (10) and (12),

$$P = \frac{\lambda_p M_{EP}}{\alpha_E}$$

and using Equations (1), (7), (8), (13), (14) and (15) with Equation (6), the following climb equation is obtained:

$$\frac{\dot{r}}{r} = \frac{2\sqrt{\frac{r}{GM}} \left[\frac{2\eta}{gI_{SP}} - \frac{\rho C_D}{2\lambda_p} \frac{GM}{r} \left(\frac{1}{\beta_E} + \frac{\alpha_E}{\frac{M_{PL}}{A_{PL}} \frac{M_{EP}}{M_{PL}}} \right) \right] - \frac{2\eta}{(gI_{SP})^2}}{\frac{\alpha_E}{\lambda_p \frac{M_{EP}}{M_{PL}}} \left[1 + \frac{M_{EP}}{M_{PL}} + \lambda_{pp} \left(\frac{M_{PP}}{M_{PL}} \right)_0 \right]} \quad (16)$$

The propellant fraction comes from the relation

$$\lambda_{pp} = 1 + \frac{1}{(M_{PP})_0} \int_0^t \dot{m} dt$$

ORIGINAL PAGE IS
OF POOR QUALITY

By using Equations (10), (2) and (14) it is expressed in terms of the power fraction integral,

$$\lambda_{PP} = 1 - \frac{2\eta}{\alpha_E (gI_{SP})^2} \frac{\frac{M_{EP}}{M_{PL}}}{\left(\frac{M_{PP}}{M_{PL}}\right)_0} \int_0^t \lambda_p dt \quad (17)$$

2.1.1.2 Low Thrust Chemical

A parallel development is now done for the chemical case. Instead of relating \dot{m} and thrust to power, they are related directly to each other,

$$-\dot{m} = \frac{T}{gI_{SP}} \quad (18)$$

Drag is also related to thrust rather than power,

$$D = \frac{\rho C_D}{2} \left(\frac{A}{T}\right) v^2 T \quad (19)$$

and the specific area, in terms of thrust, is

$$\frac{A}{T} = \frac{A_{TH}}{T} + \frac{A_{PL}}{M_{PL}} \frac{M_{PL}}{M_{TH}} \frac{M_{TH}}{T} \quad (20)$$

where the subscript TH has replaced EP to specify the dry propulsion system area and mass. Also, for the chemical case,

$$\alpha_C = \frac{M_{TH}}{T} \quad (\text{thrust related specific mass}) \quad (21)$$

$$\beta_C = \frac{T}{A_{TH}} \quad (\text{specific thrust}) \quad (22)$$

so that Equation (20) becomes

$$\frac{A}{T} = \frac{1}{\beta_C} + \frac{\alpha_C}{\frac{A_{PL}}{M_{PL}} \frac{M_{PL}}{M_{TH}}} \quad (23)$$

ORIGINAL ...
OF POOR QUALITY?

Using Equations (1), (18), (19), (21), (22), and (23), Equation (6) becomes

$$\frac{\dot{r}}{r} = \frac{2\sqrt{\frac{T}{GM}} \left[1 - \frac{\alpha_C}{2} \frac{GM}{r} \left(\frac{1}{\beta_C} + \frac{\alpha_C}{\frac{M_{PL}}{A_{PL}} \frac{M_{TH}}{M_{PL}}} \right) \right] \frac{1}{gI_{SP}}}{\frac{\alpha_C}{\frac{M_{TH}}{M_{PL}}} \left[1 + \frac{M_{TH}}{M_{PL}} + \lambda_{PP} \left(\frac{M_{PP}}{M_{PL}} \right)_0 \right]} \quad (24)$$

For this case, the propellant fraction involves thrust related parameters. From Equations (18) and (21)

$$\dot{m} = - \frac{T}{gI_{SP}} = - \frac{M_{TH}}{gI_{SP} \frac{M_{TH}}{T}} = - \frac{M_{TH}}{\alpha_C gI_{SP}}$$

The propellant fraction is then

$$\lambda_{PP} = 1 - \frac{1}{\alpha_C (gI_{SP})} \frac{\frac{M_{TH}}{M_{PL}}}{\left(\frac{M_{PP}}{M_{PL}} \right)_0} \quad (t) \quad (25)$$

2.1.2 ΔV Maneuvers

For mission requirements expressed as a velocity change ΔV, the rocket equation is used to find the propulsion mass ratio and thrust time.

2.1.2. Low Thrust Electric

Using Equation (18) for thrust, the acceleration relation can be written,

$$- \dot{m} gI_{SP} = m \frac{dv}{dt}$$

After integration between limits corresponding to total propellant expulsion, this becomes,

$$\frac{m_0}{m} = e^{\frac{\Delta v}{gI_{SP}}} \quad (\text{rocket equation})$$

ORIGINAL COPY
OF POOR QUALITY

or, by using Equation (15),

$$\frac{M_{PL} + M_{EP} + M_{PP0}}{M_{PL} + M_{EP}} = e^{\frac{\Delta V}{gI_{SP}}} \quad (26)$$

The propulsion mass ratio is then,

$$\frac{M_{EP}}{M_{PL}} + \left(\frac{M_{PP}}{M_{PL}}\right)_0 = e^{\frac{\Delta V}{gI_{SP}}} \left(\frac{M_{EP}}{M_{PL}} + 1\right) - 1 \quad (27)$$

The thrust time is

$$t = -\frac{M_{PP0}}{\dot{m}} \quad (28)$$

with Equations (10) and (14) this becomes

$$t = \frac{(gI_{SP})^2 \alpha_E}{2\eta \lambda_p} \left(\frac{M_{PP}}{M_{EP}}\right)_0 \quad (29)$$

From Equation (26)

$$\left(\frac{M_{PP}}{M_{EP}}\right)_0 = \left(\frac{M_{PL}}{M_{EP}} + 1\right) \left(e^{\frac{\Delta V}{gI_{SP}}} - 1\right) \quad (30)$$

and the thrust time becomes

$$nt = \frac{\alpha_E}{2\lambda_p} (gI_{SP})^2 \left(\frac{M_{PL}}{M_{EP}} + 1\right) \left(e^{\frac{\Delta V}{gI_{SP}}} - 1\right) \quad (31)$$

2.1.2.2 Low Thrust - Chemical

Equation (27) remains the same for this case, except for the use of the subscript TH to designate the dry thruster mass. With this change, Equation (27) becomes

$$\frac{M_{TH}}{M_{PL}} + \left(\frac{M_{PP}}{M_{PL}}\right)_0 = e^{\frac{\Delta V}{gI_{SP}}} \left(\frac{M_{TH}}{M_{PL}} + 1\right) - 1 \quad (32)$$

Equation (28) also remains the same as for the electric thruster, but Equation (18) is used for the mass flow rate and Equation (21) is used for α_C . Thus in place of Equation (29), the thrust time becomes

$$t = \alpha_C gI_{SP} \left(\frac{M_{PP}}{M_{TH}} \right)_0 \quad (33)$$

Combining this with Equation (30) gives

$$t = \alpha_C gI_{SP} \left(\frac{M_{PL}}{M_{TH}} + 1 \right) \left(e^{\frac{\Delta V}{gI_{SP}}} - 1 \right) \quad (34)$$

2.1.3 Comparison of Performance Relations

The low thrust equations developed above are compared in Table 1 so that their similarities and differences can be more easily seen.

Except for the power fraction λ_p , and the different specific mass parameters α_E and α_C , the denominators of the orbit raising equations are the same. Also the drag terms in the numerator are essentially the same and become unimportant as ρ decreases rapidly early in the climb. The remaining two terms differ by the factor $2\eta/gI_{SP}$ in the electric equation. Thus, for equal electric propulsion mass ratios (dry thruster plus initial propellant mass divided by payload mass) the climb rates have the following relation:

$$\left(\frac{\dot{r}}{r} \right)_E = \frac{2\eta}{gI_{SP}} \frac{\alpha_C \lambda_p}{\alpha_E} \left(\frac{\dot{r}}{r} \right)_C \quad (35)$$

Also a comparison of time for the same ΔV maneuver, shows that

$$(t)_E = \frac{gI_{SP}}{2\eta} \frac{\alpha_E}{\alpha_C \lambda_p} (t)_C \quad (36)$$

which has the same meaning as Equation (35). For illustration, the comparison can be made more specific by using typical values for the parameters.

The value $\alpha_E = 0.024 \text{ kg/W}$ has been used for the electric thruster with an uncertainty range up or down of about a factor of 2. Similarly $\alpha_C = 0.34 \text{ kg/N}$ is a reasonable estimate for the chemical thruster, with

Table 1. Low Thrust Chemical and Electric Propulsion Equation Summary

ELECTRIC

$$\text{ORBIT RAISING: } \frac{r}{r} = \frac{2\sqrt{r} \left[\frac{2\eta}{gI_{SP}} - \frac{\rho C_D}{2\lambda p} \frac{GM}{r} \left(\frac{1}{\beta_E} + \frac{\alpha_E}{A_{PL}} \frac{M_{EP}}{M_{PL}} \right) \right] - \frac{2\eta}{(gI_{SP})^2}}{\frac{\alpha_E}{\lambda p} \frac{M_{EP}}{M_{PL}} \left[1 + \frac{M_{EP}}{M_{PL}} + \lambda_{PP} \left(\frac{M_{PP}}{M_{PL}} \right)_0 \right]}$$

where: $\lambda_{PP} = 1 - \frac{2\eta}{\alpha_E (gI_{SP})^2} \int_0^t \lambda_{PP} dt$

ΔV MANEUVERS: $\frac{M_{EP}}{M_{PL}} + \left(\frac{M_{PP}}{M_{PL}} \right)_0 = e^{\frac{\Delta V}{gI_{SP}}} \left(\frac{M_{EP}}{M_{PL}} + 1 \right) - 1$

$\eta t = \frac{\alpha_E}{2\lambda p} (gI_{SP})^2 \left(\frac{M_{PL}}{M_{EP}} + 1 \right) \left(e^{\frac{\Delta V}{gI_{SP}}} - 1 \right)$

PARAMETERS:

Specific Mass $\alpha_E = \frac{M_{EP}}{P_0}$

Specific Power/Thrust $\beta_E = \frac{P_0}{A_{EP}}$

Power Fraction $\lambda_p = \frac{P}{P_0}$

CHEMICAL

$$\frac{r}{r} = \frac{2\sqrt{r} \left[\frac{\rho C_D}{2} \frac{GM}{r} \left(\frac{1}{\beta_C} + \frac{\alpha_C}{A_{PL}} \frac{M_{TH}}{M_{PL}} \right) \right] - \frac{1}{gI_{SP}}}{\frac{\alpha_C}{M_{TH}} \frac{M_{PL}}{M_{PL}} \left[1 + \frac{M_{TH}}{M_{PL}} + \lambda_{PP} \left(\frac{M_{PP}}{M_{PL}} \right)_0 \right]}$$

where: $\lambda_{PP} = 1 - \frac{1}{\alpha_C (gI_{SP})} \int_0^t \lambda_{PP} dt$

ΔV MANEUVERS: $\frac{M_{TH}}{M_{PL}} + \left(\frac{M_{PP}}{M_{PL}} \right)_0 = e^{\frac{\Delta V}{gI_{SP}}} \left(\frac{M_{TH}}{M_{PL}} + 1 \right) - 1$

$t = \alpha_C gI_{SP} \left(\frac{M_{PL}}{M_{TH}} + 1 \right) \left(e^{\frac{\Delta V}{gI_{SP}}} - 1 \right)$

Specific Mass $\alpha_C = \frac{M_{TH}}{T}$

Specific Power/Thrust $\beta_C = \frac{T}{A_{TH}}$

ORIGINAL SOURCE OF POOR QUALITY

about the same uncertainty range. Using these values in Equation (36), with $g = 9.8$ and assuming $2\eta\lambda_p = 1.0$

$$(t)_E = 0.7 I_{SP} (t)_C \quad (37)$$

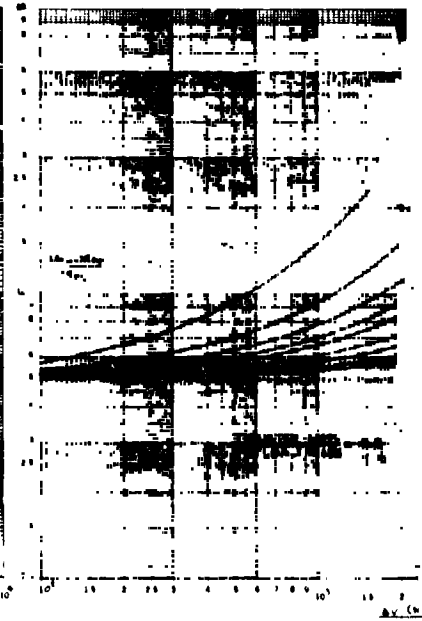
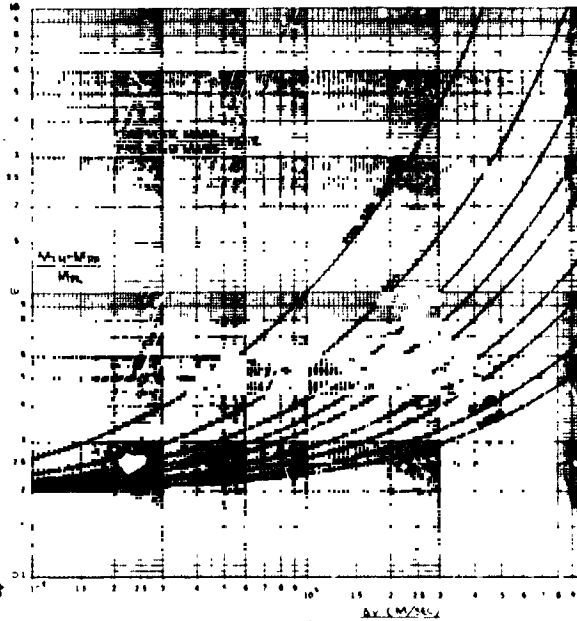
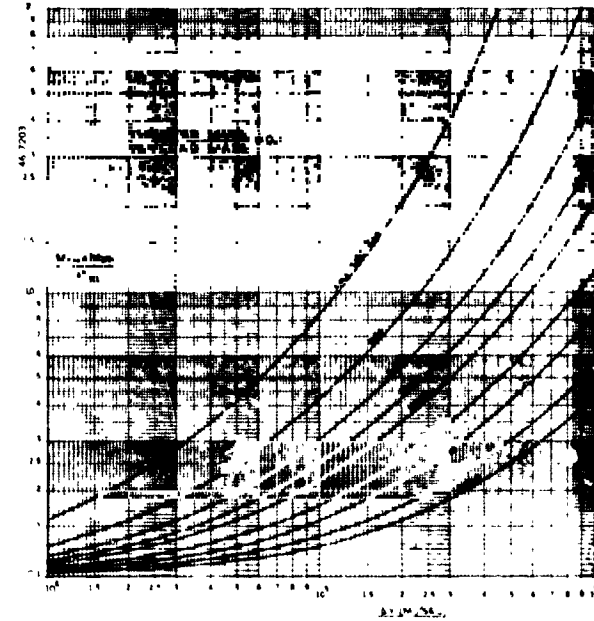
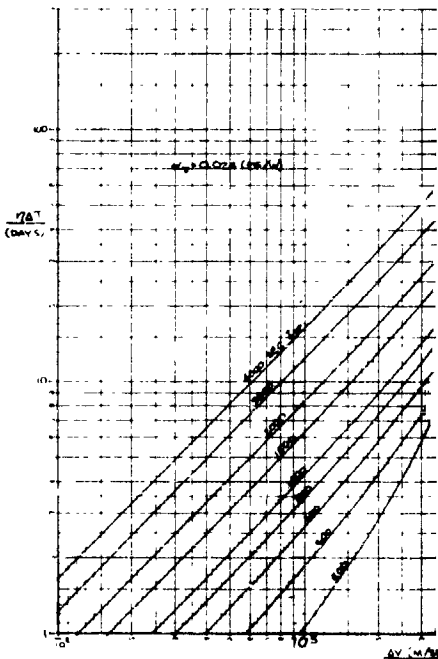
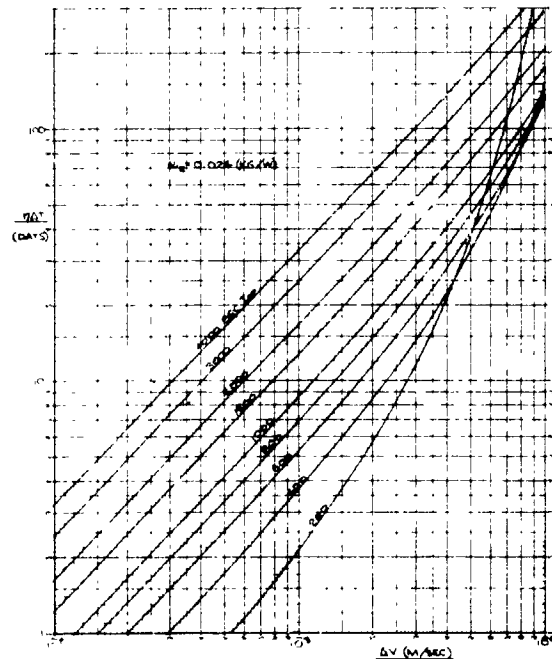
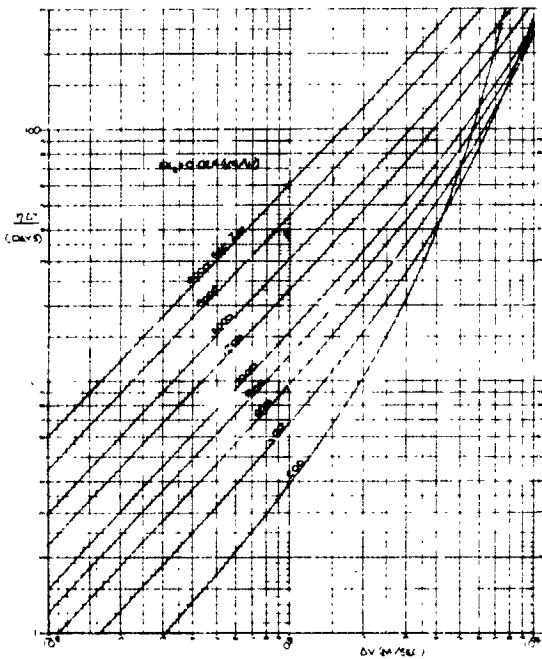
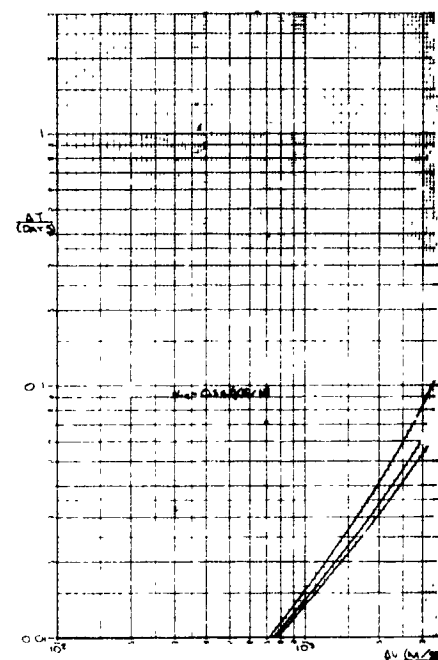
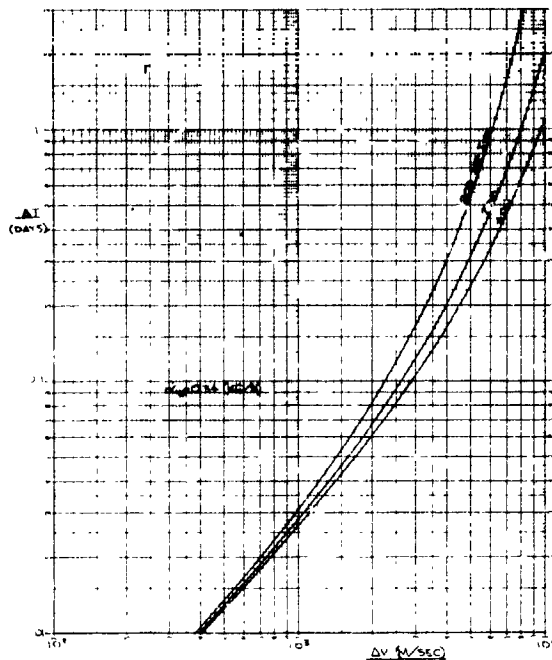
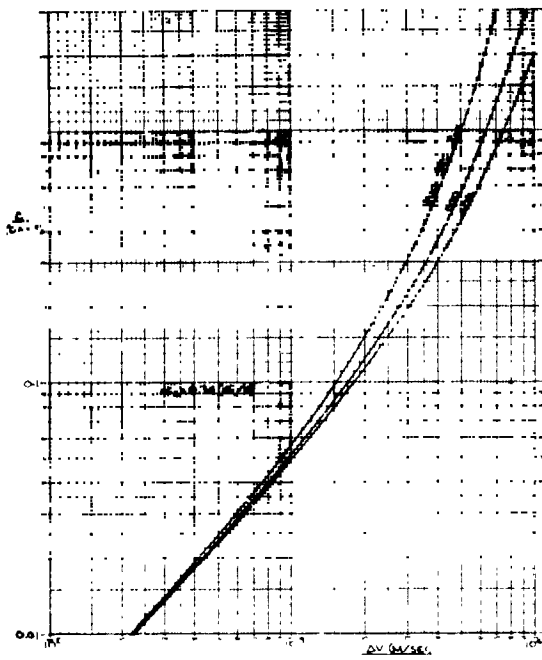
Equation (37) shows that, if a comparison were made on the basis of keeping the same propulsion-to-payload mass ratio, and the same I_{SP} , electric propulsion would take longer than chemical propulsion by the factor of $0.7 I_{SP}$. If the I_{SP} used for the comparison were 200 seconds, it would take 140 times as long for electric propulsion to do the same job; and for 4000 seconds I_{SP} it would take 2800 times as long as for chemical propulsion. This is the other side of the coin that must be kept in view when comparing the payload advantage of electric propulsion.

The payload advantage can be seen by comparing the mass ratio equation in Table 1. The conclusion is simply that the mass ratios are the same for both propulsion modes when the dry thruster to payload ratios, and the I_{SP} 's, are the same. The payload advantage of electric propulsion derives from its higher I_{SP} capability.

This effect is shown graphically in Figure 1. In the lower set of graphs the ratio of total propulsion mass to payload mass is plotted against ΔV for five different values of the thruster-to-payload mass ratio. All of the individual mass ratios can be found by using these plots.

The improvement in payload-to-propulsion mass ratio is apparent, but it should be noted that the effect is not linear with I_{SP} . It is a familiar result that propellant required for a given impulse is inversely proportional to I_{SP} . This intuitive idea is sometimes extended to indicate that payload mass for a given ΔV varies with I_{SP} in the same way. Figure 1 not only shows this is not true, but also that the I_{SP} advantage increases markedly with ΔV and by a different ratio depending on the thruster mass ratio. In general, the ΔV needed for a significant I_{SP} advantage to appear increases as the thruster mass ratio is increased.

For low thruster mass ratios, the payload ratio increases faster than the I_{SP} ratio (for large ΔV) while it is considerably less than the I_{SP} ratio for high thruster mass ratios. For example, at $\Delta V = 3000$ m/sec,



BOLDOUT FRAME

BOLDOUT FRAME

ORIGINAL PAGE IS
OF POOR QUALITY

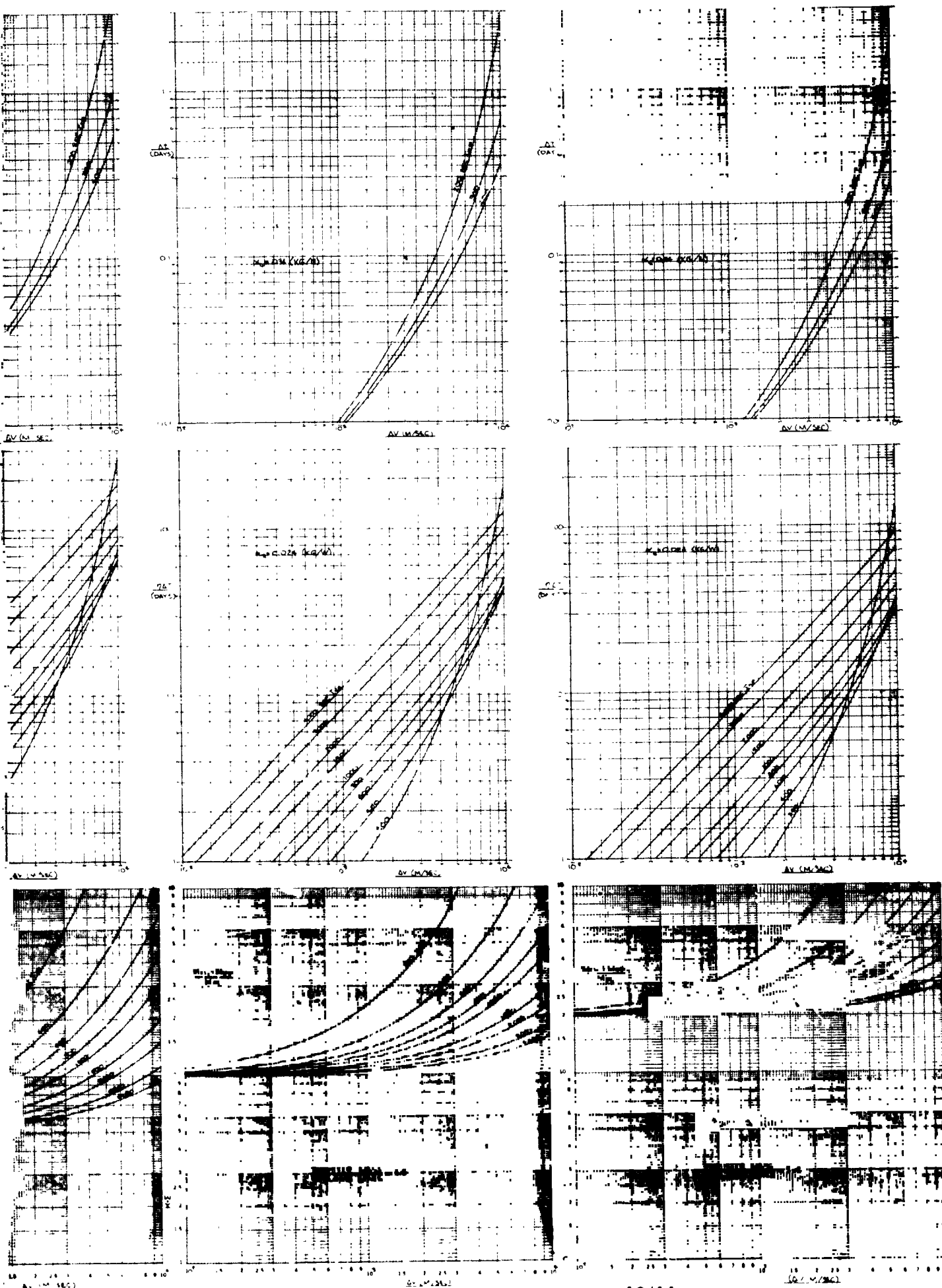


Figure 1. Effect of ΔV and I_{sp} on Propulsion to Payload Mass Ratio and Trip Time for Different Thruster Tc Payload Mass Ratios (Chemical and Electric Propulsion)

2

EXDOUT FRAME

the payload ratio is 14 for a 10-fold I_{SP} increase (from 200 to 2000 seconds) at a thruster mass ratio of 0.1, while it is only 6 for the same conditions at a thruster mass ratio of 1.0.

Because the thruster mass ratio is constant in each of these plots, the rise in propulsion mass ratio with increasing ΔV comes from increased propellant mass. The "base-line" in the plots corresponds to the thruster mass ratio. The rising base line increases the propulsion mass ratio relative to the payload mass, but it also reduces the trip time as shown in the center row of plots in Figure 1 for electric propulsion and in the upper row for chemical propulsion.

For electric propulsion, the trip time is shown as the product ηt , as indicated in Table 1. Consequently the actual time varies as $1/\eta$. This has a substantial effect. For example a 40% increase (e.g., $\eta = 40\%$ to 56%) results in a 30% reduction in trip time.

The difference between the linear and quadratic I_{SP} terms in Table 1 causes a qualitatively different effect of I_{SP} on trip time for the chemical and electric thrusters. For the former, time monotonically decreases with increasing I_{SP} while for the latter it generally increases. However at high ΔV there is an optimum I_{SP} (for minimum trip time). At $\Delta V = 10^4$ m/sec, this is about 800 seconds for all values of thruster mass ratio. At $\Delta V = 7 \times 10^3$ m/sec, the optimum I_{SP} has decreased to about 500 seconds.

The description above illustrates some of the important features of chemical and electric low thrust propulsion. More generally, it is a graphical representation of the Table 1 equations for chemical and electric propulsion maneuvers that can be prescribed in terms of ΔV requirement.

2.2 SPACECRAFT PARAMETERS

The spacecraft parameters for the low-thrust, electric, orbit transfer vehicle appear in Equation (16). They are discussed individually here.

2.2.1 Thruster Efficiency

As mentioned earlier, time varies inversely with thruster efficiency. This is shown explicitly in Table 1 for ΔV maneuvers and it is also true for orbit transfers in general. For this reason, considerable technology

development effort is devoted to thruster efficiency improvement. For the purpose of this study, the three efficiency functions shown in Figure 2 are defined. The Case I and Case II efficiency functions are lower and upper bounds respectively of present-day high performance electric thrusters. The Case III function is an estimated upper limit that may be approached with further development.

2.2.2 Specific Mass

The specific mass parameter is defined by Equation (10). It is the ratio of the total power-related mass to the beginning-of-life solar array power at normal sun incidence. The power-related masses comprise the total solar array mass (blanket, boom, supports, etc.) and the mass of the power conditioning and thruster hardware including the empty propellant tank and thermal control system. To put it more simply, it is the total electric propulsion system mass minus the propellant mass.

Table 2 lists estimated component masses for two types of advanced argon electric propulsion systems. One is the pulsed inductive plasma thruster and the other is the argon ion thruster.

The power processor is clearly the most important contributor. It is followed by the considerably smaller value of the thermal control system. The sum of these two components constitutes about 90% of the total electric propulsion system mass (excluding power source).

The solar power specific mass is affected by the cover thickness. A thin, advanced technology, silicon solar cell having a cell thickness of 2 mils and cover thicknesses equivalent to 1 mil of silica has been estimated to provide an array specific power of $\alpha_S = 0.005$ kg/watt (Reference 4). A linear variation of α_S with total thickness of cell plus covers was assumed for cover thicknesses of 1, 3 and 6 mils of silica on each side of the cell. These values are plotted in Figure 3. The SEPS solar cell, also shown in this figure, was used as a basis for extrapolating the solar cell array specific mass to a total thickness of 26 mils corresponding to the 2-mil cell with 12-mil covers on each side.

The above estimates of electric propulsion specific mass are summarized in Table 3 where the total electric propulsion specific mass is the sum of the thruster and solar array values: $\alpha_E = \alpha_{TH} + \alpha_S$.

ORIGINAL PAGE IS
OF POOR QUALITY

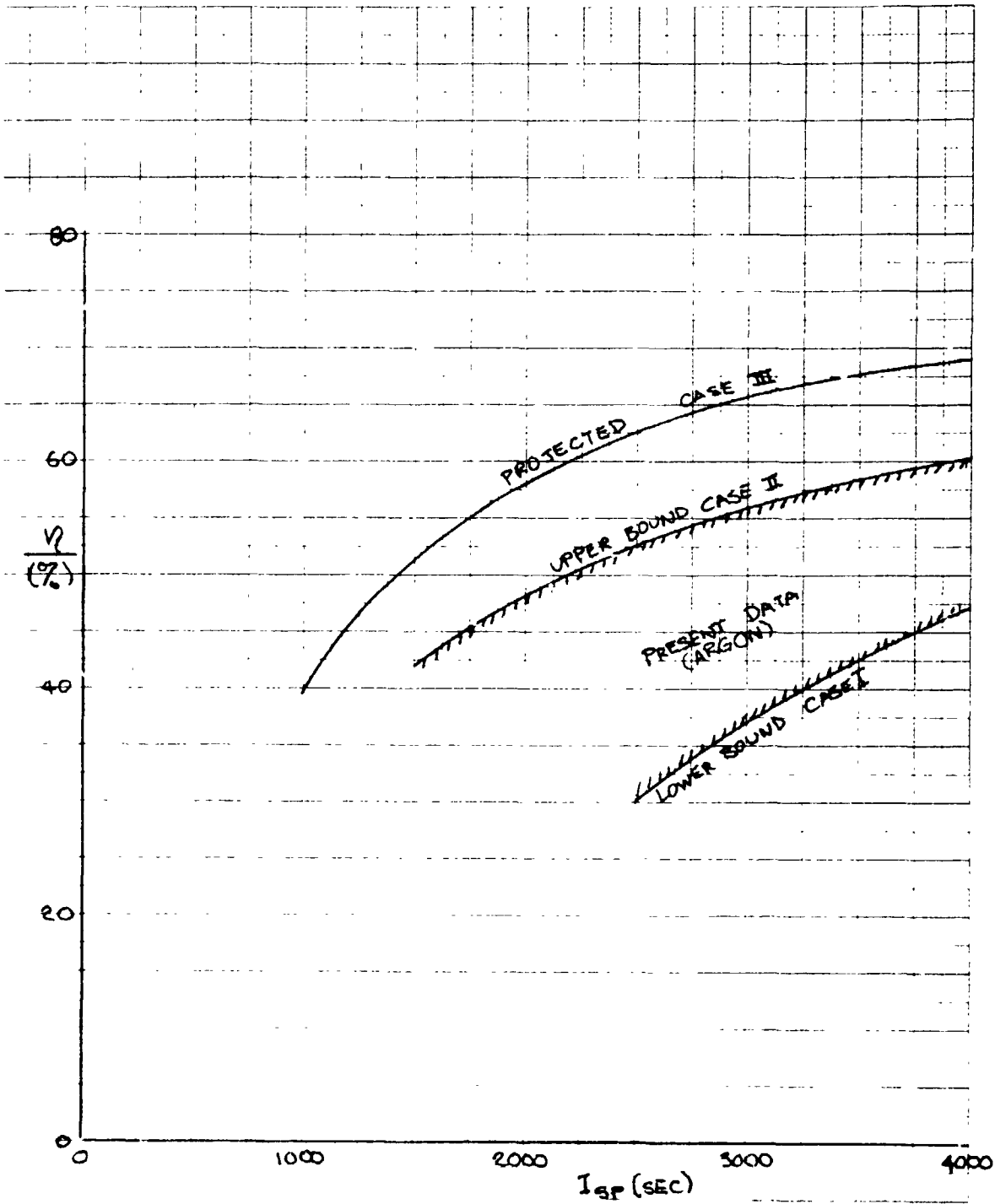


Figure 2. Thruster Efficiency Functions

Table 2. Estimated Specific Mass for Advanced Argon Thruster Systems

Component	Plasma (kg/kW)	Ion (kg/kW)
Power Processor	4.60	13.61
Thruster	0.36	0.18
Gimbals and Support	0.07	0.03
Thermal Control System	1.54	2.53
Propellant System (Dry)	<u>0.37</u>	<u>0.92</u>
Total	6.94	17.27

Table 3. Electric Propulsion Specific Mass Estimates

Thruster Type	α_{TH} (kg/W)	Cell Cover Thickness (mils)	α_S (kg/W)	α_E (kg/W)
Plasma	0.007	1	0.0050	0.012
		3	0.0059	0.013
		6	0.0085	0.016
		12	0.0250	0.032
Ion	0.017	1	0.0050	0.022
		3	0.0059	0.023
		6	0.0085	0.026
		12	0.0250	0.042

2.2.3 Specific Power

The specific power is defined by Equation (11). It is the ratio of the beginning-of-life power to the solar cell array frontal area. The projected value of $150 \text{ (w/m}^2\text{)}$ from Reference 4 was used for this parameter. The local power per unit mass at any instant during the climb is the quotient of the local power fraction λ_p with the specific mass α_E . The power fraction is the product of the individual power fractions for

ORIGINAL PAGE IS
OF POOR QUALITY

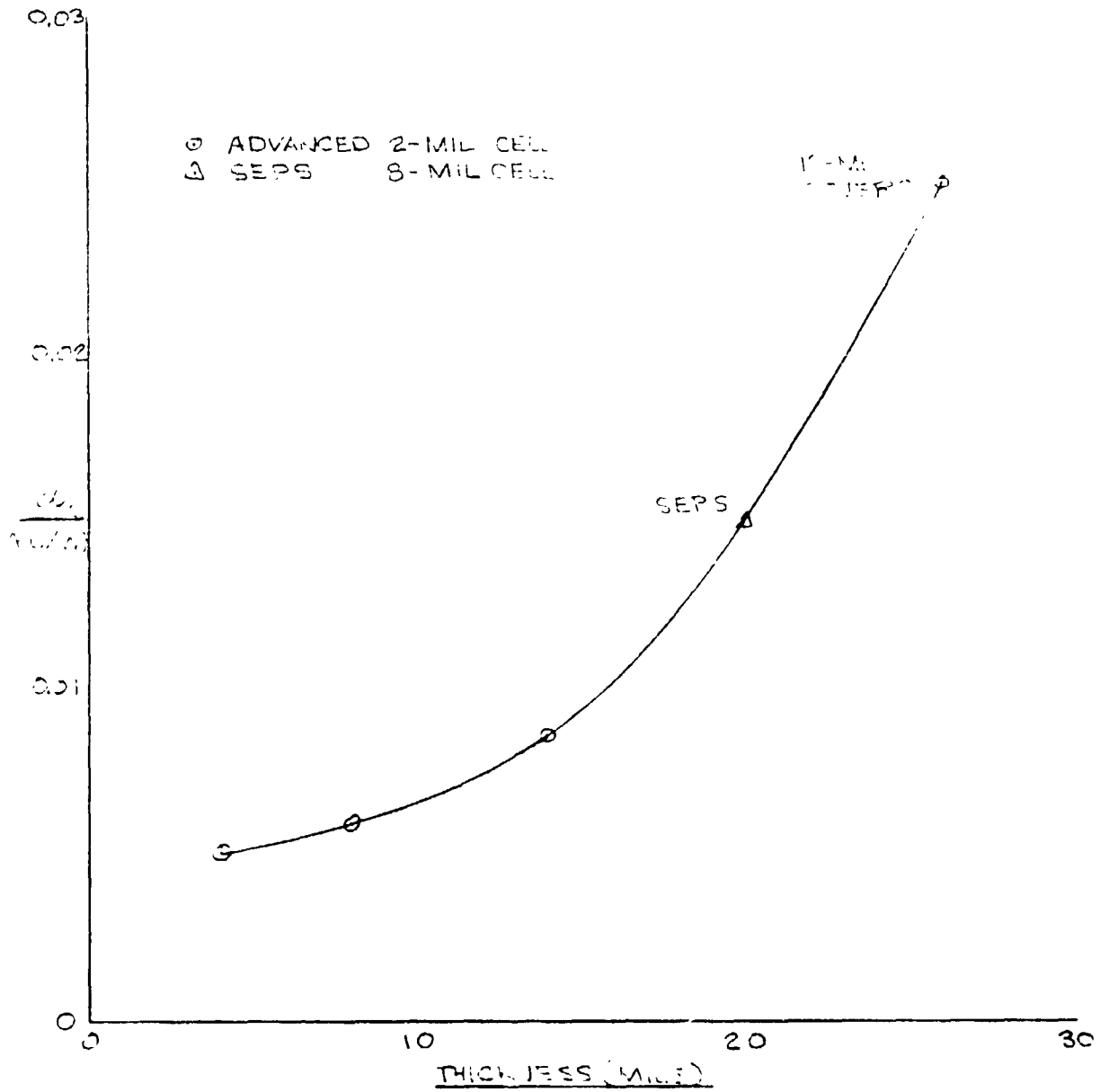


Figure 3. Estimated Specific Mass of Silicon Solar Cell Arrays vs Total Cell Thickness

occultation, reduced array illumination that can occur for some spacecraft orientations and solar cell degradation due to radiation.

2.2.4 Specific Area

The specific area M_{pL}/A_{pL} appears in the second term of the bracketed expression in the numerator of Equation (16). It is the ratio of the payload mass to the payload drag area. For the orbit transfer calculation a nominal value of 100 kg/m^2 was used. A lower value, 30 kg/m^2 , was used for low altitude flight calculations.

2.2.5 Propulsion Mass Ratio

The propulsion mass ratio M_{EP}/M_{pL} appears in Equations (15) and (16). It is the ratio of the electric propulsion system dry mass to the payload mass. This is the input parameter for Equation (16) that determines the rate of climb.

2.2.6 Propellant Mass Ratio

This ratio, (M_{pp}/M_{pL}) , also appears in Equations (15) and (16). It is the ratio of the propellant mass used for orbit transfer to the payload mass. This ratio determines the end-of-climb altitude. The propellant ratio at any instant during the climb is the product of the initial value of this ratio with the propellant fraction calculated by continuous integration of Equation (17). The climb is finished when this function reaches zero.

2.2.7 Auxiliary Propulsion Mass Ratio

The auxiliary propulsion mass is also expressed dimensionlessly in terms of payload mass, $\Delta M_{pp}/M_{pL}$. This ratio does not appear in the climb equations derived earlier. They describe orbit transfer for the special case of no auxiliary propulsion requirement. The procedure described here is used for the general case which does require auxiliary propulsion.

The following assumptions are made for this analysis:

- The auxiliary propulsion dry mass is ignorable compared to the main thruster system dry mass (of the order of 1%).
- Attitude control functions during orbit transfer (including inertia wheel unloading) are done by gimbaling the main thrusters, at effectively no cost in additional propellant mass.

- On-orbit attitude control propellant mass is ignorable compared to stationkeeping propellant mass.
- Attitude control during eclipse is done by an inertia wheel.

With these assumptions, the integrated electric propulsion system masses are those due to the main thrusters M_{EP} , the propellant used in orbit transfer M_{PP} , and the propellant used for on-orbit stationkeeping and disposal ΔM_{PP} .

The total electric propulsion mass ratio is therefore:

$$\left(\frac{M_{EPS}}{M_{PL}}\right)_T = \frac{M_{EP} + M_{PP} + \Delta M_{PP}}{M_{PL}} \quad (35)$$

where the subscript EPS refers to the electric propulsion system (dry thruster system including solar power and power conditioning) plus propellant; and the subscript T indicates the total system mass ratio when auxiliary propulsion is used. With the above assumptions, ΔM_{PP} is the auxiliary propulsion mass.

The orbit-raising calculation is done as described above except that, in this case, it is necessary to distinguish between the actual payload mass which is used as the reference mass in Equation (35) and the reference mass $M_{PL} + \Delta M_{PP}$ that is used in the computer program for the orbit transfer calculation. This is done with the following notation for "electric mass ratio"

$$MRE = \frac{M_{EP}}{M_{PL} + \Delta M_{PP}} \quad (36A)$$

and "propellant mass ratio"

$$MRP = \frac{M_{PP}}{M_{PL} + \Delta M_{PP}} \quad (36B)$$

The rocket equation is used to express ΔM_{PP} in terms of the characteristic velocity increment ΔV associated with the total on-station and disposal impulse requirements. Thus

$$\frac{M_{PL} + M_{EP} + \Delta M_{PP}}{M_{PL} + M_{EP}} = \text{Exp} \frac{\Delta V}{gI_{SP}} \quad (37)$$

ORIGINAL PAGE IS
OF POOR QUALITY

The state of the art auxiliary propulsion $I_{SP} = 3000$ seconds is used for all calculations.

By dividing the numerator and denominator by M_{PL} , this becomes, after rearrangement,

$$\frac{\Delta M_{PP}}{M_{PL}} = \left(1 + \frac{M_{EP}}{M_{PL}}\right) \left(\text{Exp} \frac{\Delta V}{g I_{SP}} - 1\right) \quad (38)$$

From Equation (36A)

$$\frac{M_{EP}}{M_{PL}} = \left(1 + \frac{\Delta M_{PP}}{M_{PL}}\right) MRE \quad (39)$$

so that Equation (38) becomes

$$\frac{\Delta M_{PP}}{M_{PL}} = \frac{(1 + MRE) \left(\text{Exp} \frac{\Delta V}{g I_{SP}} - 1\right)}{1 - MRE \left(\text{Exp} \frac{\Delta V}{g I_{SP}} - 1\right)} \quad (40)$$

Similarly to Equation (36A), Equation (36B) can be rearranged to give

$$\frac{M_{PP}}{M_{PL}} = \left(1 + \frac{\Delta M_{PP}}{M_{PL}}\right) MRP \quad (41)$$

With the use of Equations (39) and (41), Equation (35) becomes

$$\left(\frac{M_{EPS}}{M_{PL}}\right)_T = MRE + MRP + (MRE + MRP + 1) \left(\frac{\Delta M_{PP}}{M_{PL}}\right) \quad (42)$$

Finally, equation (40) is used with Equation (42) to give the following relation for the EPS mass ratio

$$\left(\frac{M_{EPS}}{M_{PL}}\right)_T = MRE + MRP + (MRE + MRP + 1) \left[\frac{(1 + MRE) \left(\text{Exp} \frac{\Delta V}{g I_{SP}} - 1\right)}{1 - MRE \left(\text{Exp} \frac{\Delta V}{g I_{SP}} - 1\right)} \right] \quad (43)$$

In general, the ΔV term in Equation (43) comprises all on-orbit functions such as stationkeeping, repositioning and disposal which are done by auxiliary propulsion at the I_{SP} shown in Equation (43).

ORIGINAL PAGE IS
OF POOR QUALITY

2.3 OCCULTATION RELATIONS

Figure 4 shows the circular satellite orbit of radius r around a spherical Earth of radius a . The occultation is the fraction of the time f that the satellite is in Earth's shadow.

Figure 4 depicts the Earth and the satellite orbit as seen on the plane containing the orbital axis (i.e., the angular momentum vector $\vec{\omega}$) and the Earth-Sun line. The orbit viewed toward the Sun is shown in Figure 5.

The semiminor axis of the perceived ellipse is

$$b = r \cos \beta \quad (44)$$

The equations of the ellipse and the Earth circle in this x-y plane are:

$$\begin{aligned} \frac{x^2}{r^2} + \frac{y^2}{b^2} &= 1, \\ \text{or } x^2 + \frac{y^2}{\cos^2 \beta} &= r^2 \end{aligned} \quad (45)$$

for the ellipse, and

$$x^2 + y^2 = a^2 \quad (46)$$

for the circle.

These intersect at a value of x obtained by simultaneous solution of Equations (45) and (46),

$$\begin{aligned} x^2 + \frac{(a^2 - x^2)}{\cos^2 \beta} &= r^2 \\ \text{or } x &= \pm \frac{\sqrt{a^2 - r^2 \cos^2 \beta}}{\sin \beta} \end{aligned} \quad (47)$$

Now,

$$x = r \sin \omega t = r \sin \frac{2\pi t}{T}$$

ORIGINAL PAGE IS
OF POOR QUALITY

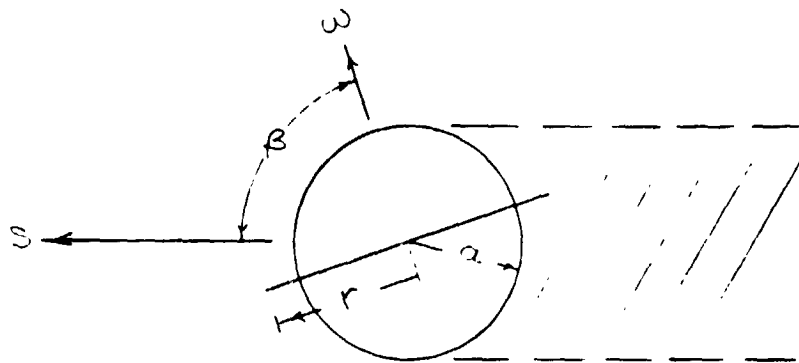


Figure 4. Plane Containing Orbital Axis and Earth-Sun Line

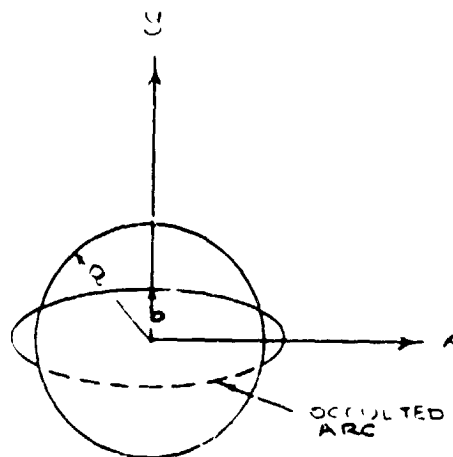


Figure 5. View Toward Sun

where t is orbit time and T is orbit period. The occultation time is twice the time for passage from $x = 0$ to $x = r \sin \omega t$. Hence, the occultation fraction f is:

$$f = \frac{2t}{T} = \frac{1}{\pi} \sin^{-1} \left[\frac{\sqrt{\left(\frac{a}{r}\right)^2 - \cos^2 \beta}}{\sin \beta} \right] \quad (48)$$

The problem then becomes that of finding β , given the orbital parameters and day of the year. It is convenient to adopt the Earth-centered coordinate system shown in Figure 6 where the x - y - z cartesian axes are referred to the fixed stars, x - y is the ecliptic plane, and z is the ecliptic pole. The Earth's axis E is fixed in the x - z plane and the Sun line is in the x - y (ecliptic) plane, with angle θ equal, in degrees, to 0.986 times the number of days after the summer solstice.

The satellite orbit axis ω is located by two coordinates: its inclination i with the Earth axis and ψ , the longitudinal separation of the orbit axis and the ecliptic pole. Angle B is the longitudinal separation of E and ω , referred to the ecliptic axis. $\epsilon = 23.5$ degrees, the inclination of E .

The angle β is determined by applying the law of cosines three times to the two spherical triangles drawn in Figure 6. Taking P as the angle between ω and Z , its arc on the sphere is:

$$\cos P = \cos i \cos \epsilon + \sin i \sin \epsilon \cos \psi \quad (49)$$

Also, since

$$\cos i = \cos \epsilon \cos P + \sin \epsilon \sin P \cos B,$$

P as determined in Equation (49) is used to solve for B :

$$\cos B = \frac{\cos i - \cos \epsilon \cos P}{\sin \epsilon \sin P} \quad (50)$$

Finally, from the larger triangle,

$$\cos \beta = \sin P \cos (\theta + B) \quad (51)$$

ORIGINAL PAGE IS
OF POOR QUALITY

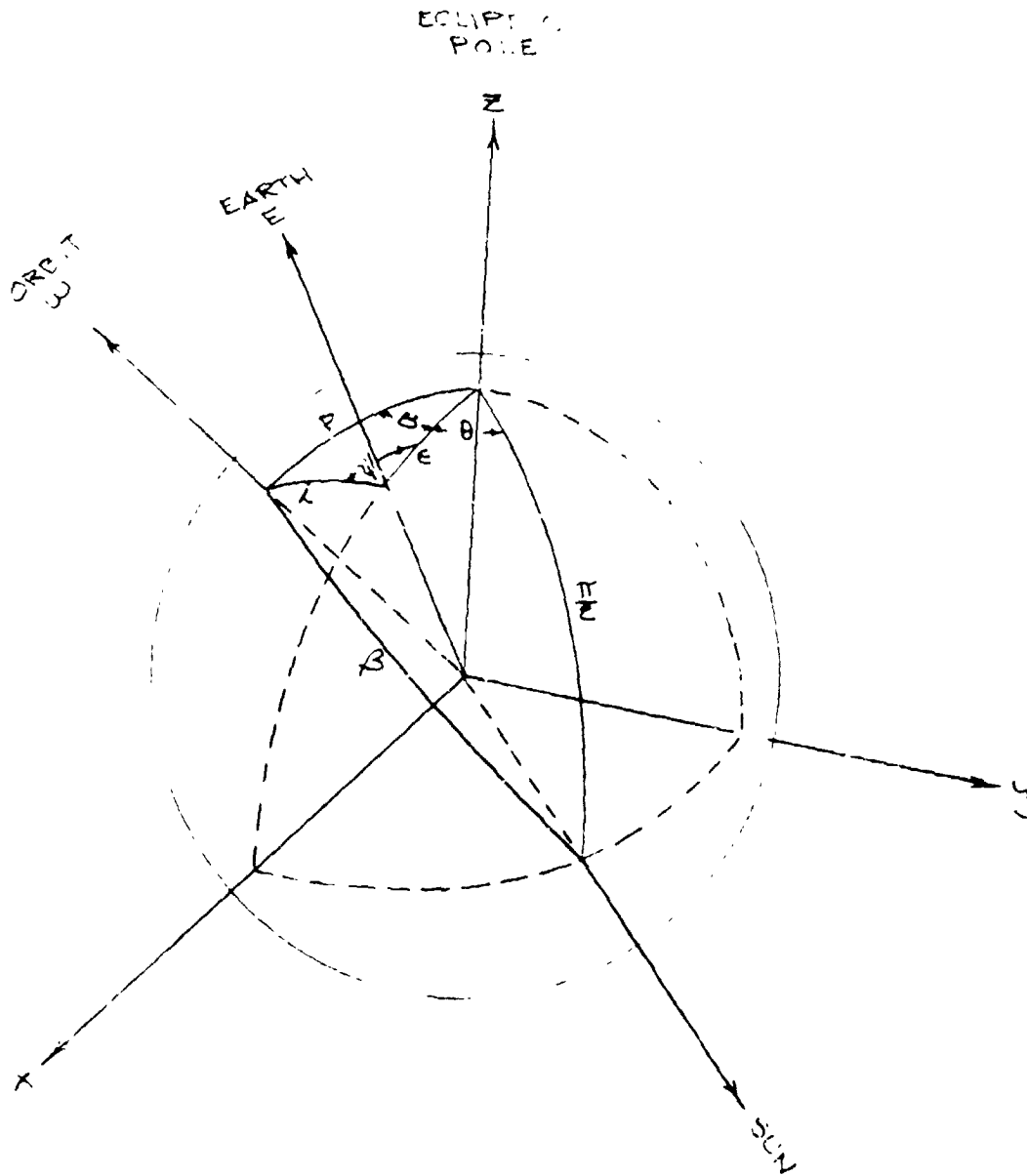


Figure 6. Earth Centered Coordinates (ϵ , i , P and B are Sides,
 ψ , B and θ are Longitude Angles)

Using $\theta(\text{deg}) = 0.986$ times the number of days after summer solstice, the orbit inclination i , the inclination of the Earth axis $\epsilon = 23.5$ degrees, and using $\dot{\psi} = -2.1 \times 10^{14} \cos i/r^{7/2}$ deg/day for the nodal regression rate (where r is orbit radius in kilometers), Equations (49), (50) and (51) are solved for β . The result is used in Equation (48) to calculate the occultation fraction f . The initial value of ψ depends on the time of day of the launch. This is accounted for by directly assigning an initial value to this angle.

The spherical triangle relations used above require that the angles be in the range from 0 to 180 degrees. This causes no difficulty in Equation (49), with the angles i and ϵ in the first quadrant. Also the angle ψ causes no problem. When the computer does not distinguish between $\cos \psi$ and $\cos (-\psi)$, the angle is automatically referred to the proper triangle location and geometry for all quadrants, so that P is correctly calculated.

The calculation of B in Equation (50) does require attention. When B increases through 180 degrees the computer may interpret the decreasing magnitude of the \cos as an angle less than 180 degrees. The correction procedure, then, is to let B be the value calculated from Equation (50) when $\sin B > 0$, and when $\sin B < 0$ the value calculated is replaced by $(360 \text{ deg} - B)$. The program then calculates occultation correctly as the climb progress from any starting conditions.

2.4 SPACE ENVIRONMENT EFFECTS

The two space environment effects of importance for orbit transfer from Shuttle altitude to geosynchronous orbit are atmospheric drag and the Van Allen radiation belt.

2.4.1 Atmospheric Density

Figure 7 shows the large variation in atmospheric density that occurs at high altitude, even when sunspot activity variations are averaged out (Reference 5). For the present study the nominal variation of density shown in Figure 7 is used.

It is seen in this figure that drag effects for transfer to GEO are significant only during the early stage of the flight when the altitude is below about 400 km. Drag is very important, however, in determining the minimum altitude for initiation of the transfer. This subject is discussed in Section 2.6.

2.4.2 Radiation

The radiation environment is shown in Figure 8 which shows fluence rate versus altitude for 0- and 30-degree inclination orbits. Data are from Reference 6. The fluence rate is the number of damage events per square centimeter per year expressed in terms of the number of 1-mev electrons required to produce the same damage. This is a function of cell type and cover protection. The data in Figure 8 are for silicon solar cells with 6-mil equivalent silica covers, and the fluence rates shown are for each side of the cell. For a free standing array, such as would be used for present missions, the numbers from Figure 8 are doubled to obtain the total damage rate. It is seen that the fluence rate for the equatorial orbit is more than twice that of the 30-degree orbit. This affects the choice of plane change strategy for transfer to GEO. This subject is discussed in Section 2.7.

The effect of the integrated fluence on silicon solar cell power is plotted in Figure 9 (Reference 6).

2.5 SOLAR CELL COVER TRADEOFF

Tradeoff calculations were made to find the optimum solar cell cover thickness for Shuttle orbit to GEO transfer missions. Although this was

ORIGINAL PAGE IS
OF POOR QUALITY

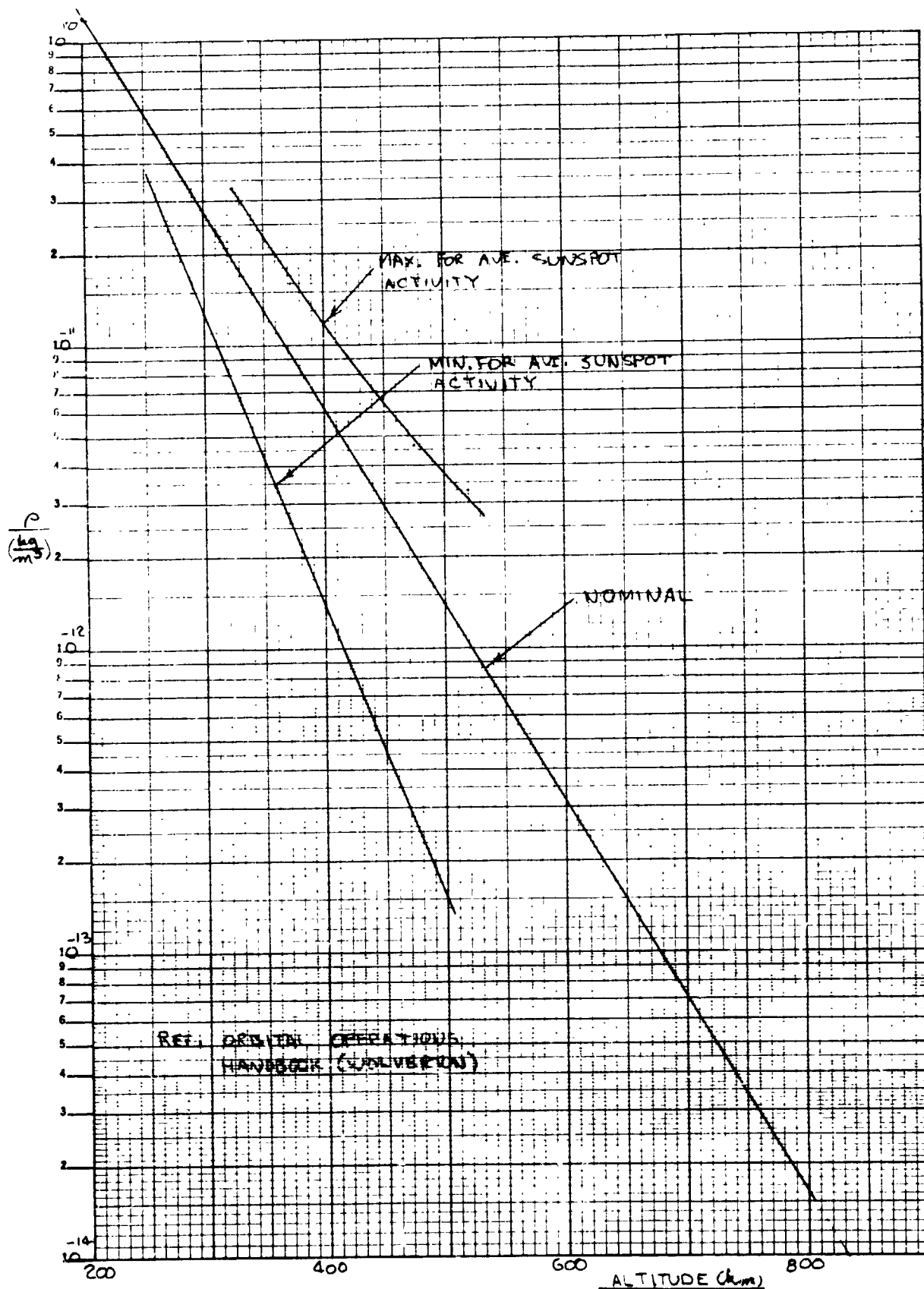


Figure 7. Atmospheric Density vs Altitude

ORIGINAL PAGE IS
OF POOR QUALITY

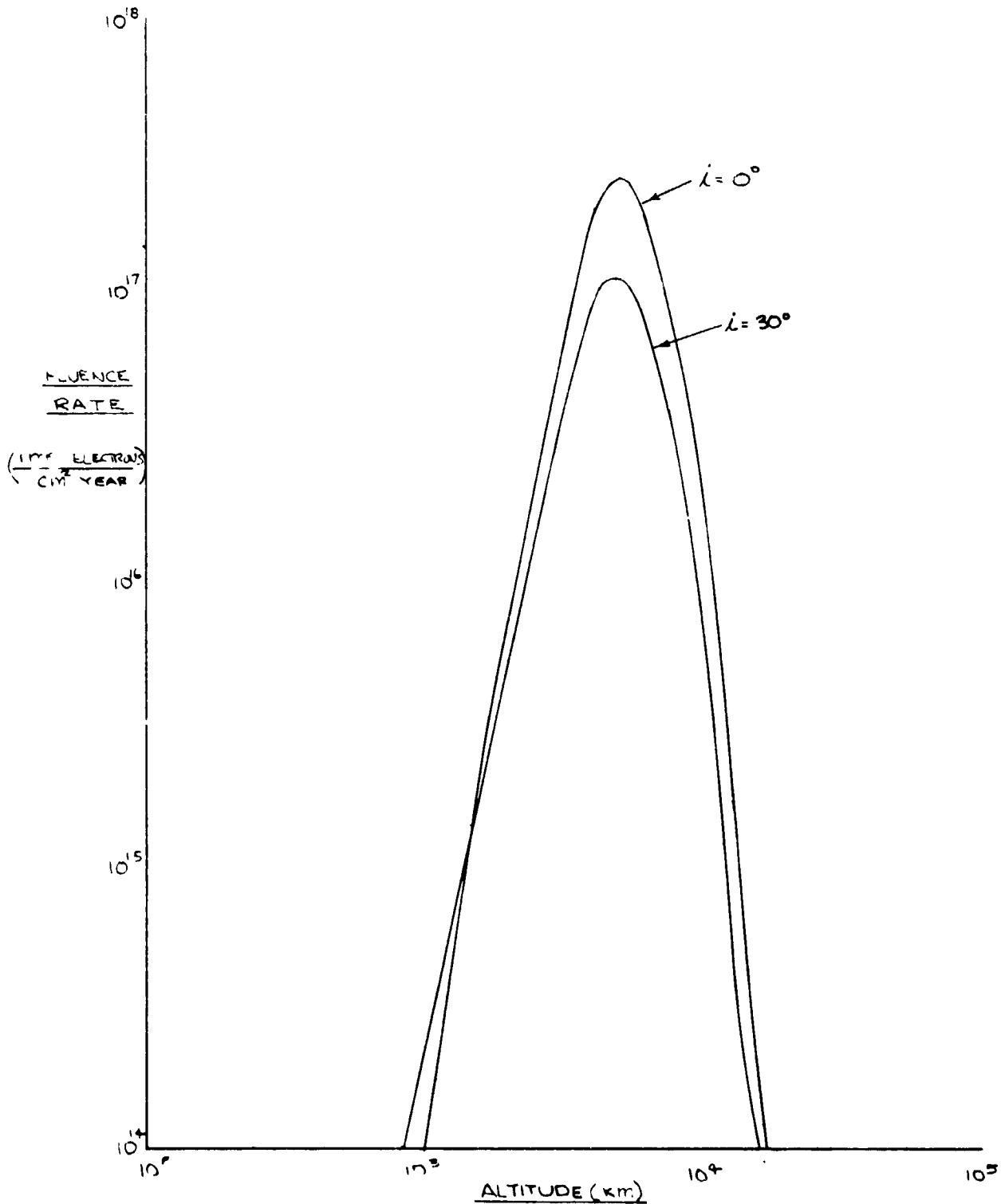


Figure 8. Fluence Rate vs Altitude for 0 and 30-deg Orbit Inclinations
(Each side for 6-mil covers - silicon solar cells)

ORIGINAL PAGE IS
OF POOR QUALITY

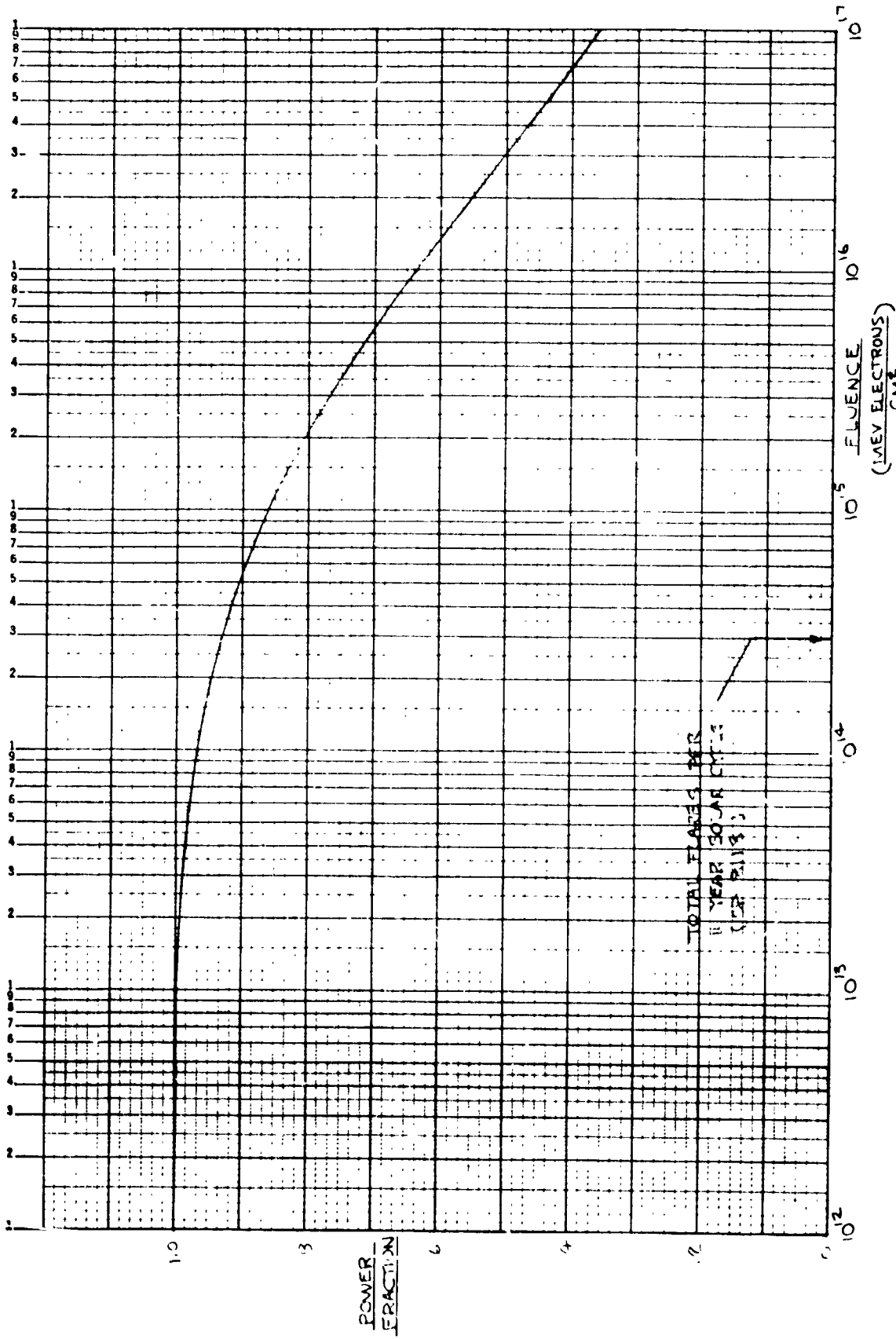


Figure 9. Silicon Solar Cell Degradation Caused by Radiation

done early in the study program before occultation was included in the climb program, the conclusions are believed to be applicable to the occulted case.

Table 4 lists the conditions used for the analysis. The solar power specific mass is the same function of cover thickness as that in Table 3 and the range of thruster specific mass brackets the thruster estimates. The lowest values of α_E were used with the highest thruster efficiency, the highest values with the lowest efficiency and the intermediate specific mass was examined with both the highest and lowest efficiency functions. In this manner, the full range of anticipated conditions was examined for intermediate and extreme cases. These extremes ranged from shortest to longest times at high radiation fluence.

Results for the four sets of conditions are plotted in Figures 10 through 13. Thrust time rather than transfer time is shown, reflecting the omission of occultation in this calculation. The I_{sp} is not a sensitive parameter; optimum values are roughly 1500 and 1700 seconds for the high efficiency case and 3700 and 3800 seconds for the low efficiency function. Cross-plots of time versus cover thickness at these I_{sp} values

Table 4. Range of α_E Parameter (kg/Watt) and η for Cover Thickness Tradeoff

α_{TH}	α_s	α_E	Covers (mils)	η Case
0.005	0.0050	0.0100	1	III
0.005	0.0059	0.0109	3	III
0.005	0.0085	0.0135	6	III
0.005	0.0250	0.0300	12	III
0.010	0.0059	0.0159	3	I III
0.010	0.0085	0.0185	6	I III
0.010	0.0250	0.0350	12	I III
0.020	0.0059	0.0259	3	I
0.020	0.0085	0.0285	6	I
0.020	0.0250	0.0450	12	I

ORIGINAL QUALITY
OF POOR QUALITY

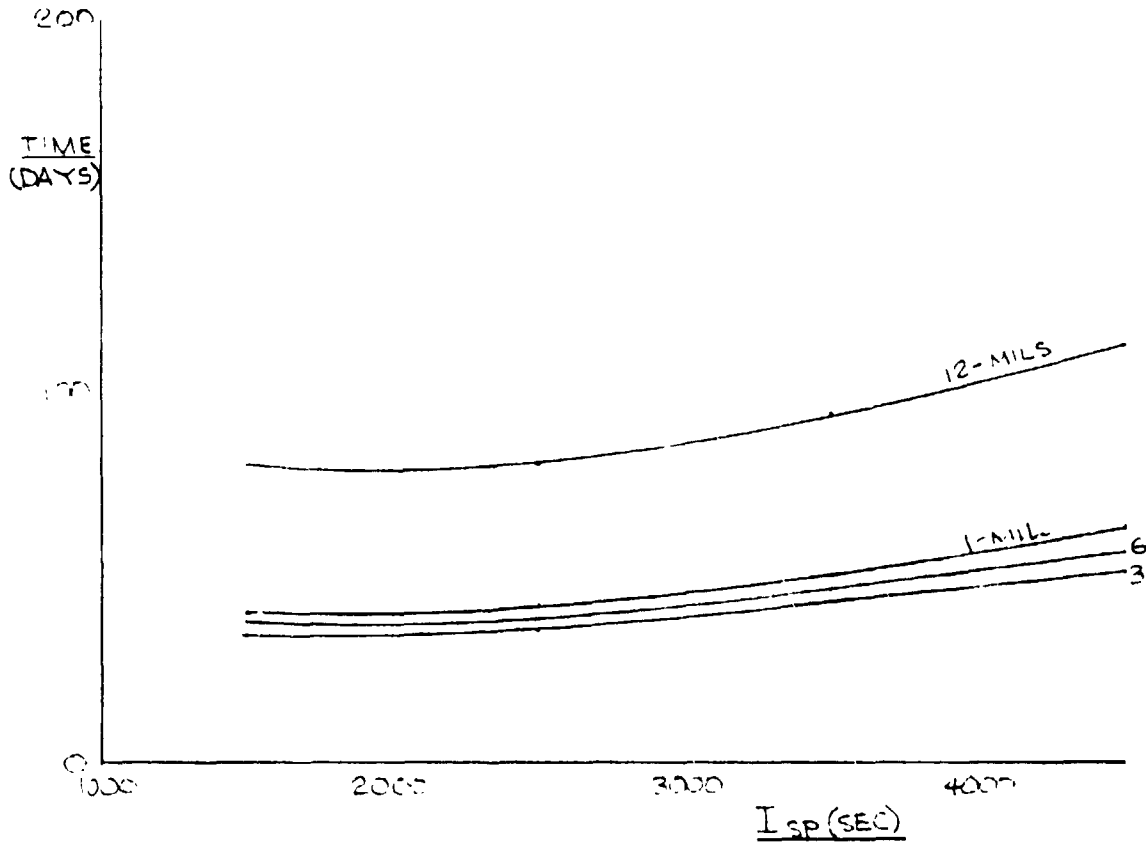


Figure 10. Effect of I_{sp} and Cover Thickness on Thrust Time at $\frac{M_{EPS}}{M_{PL}} = 2.0$
 ($\alpha_{TH} = 0.005$ kg/W, Case III n)

ORIGINAL PAGE IS
OF POOR QUALITY

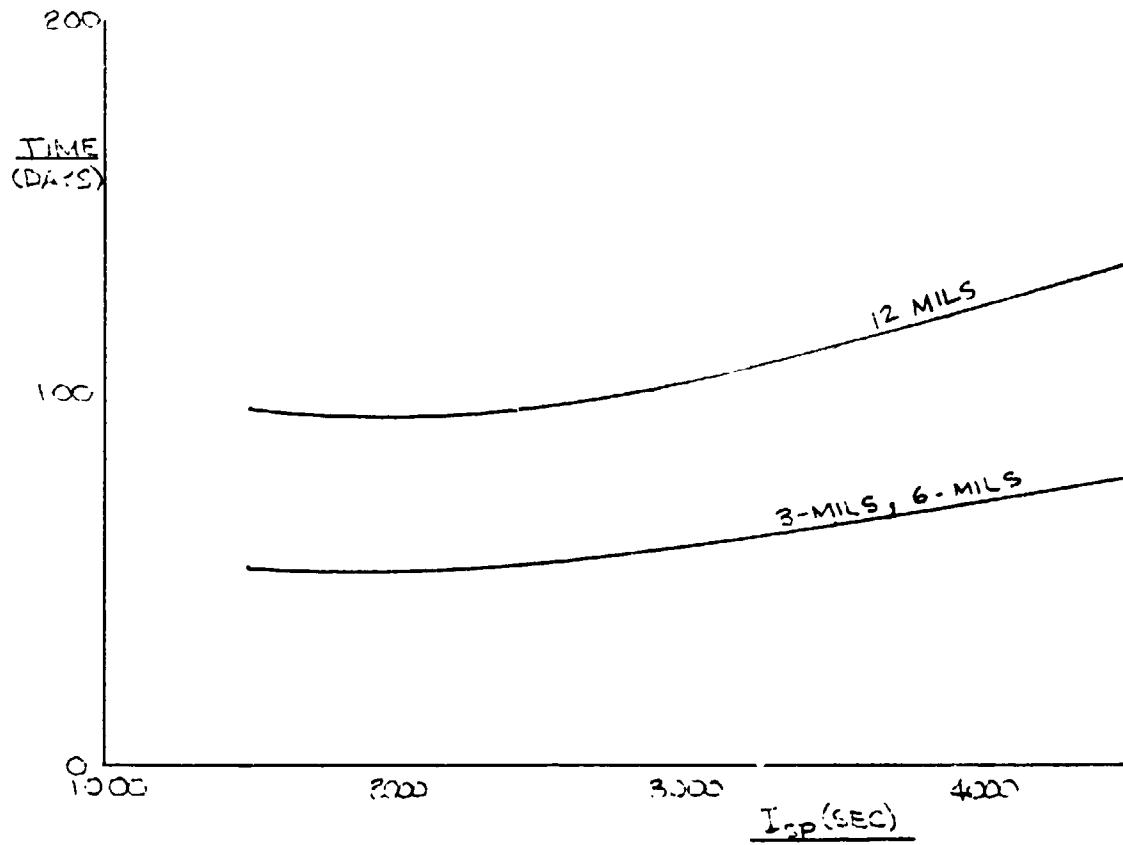


Figure 11. Effect of I_{sp} and Cover Thickness on Thrust Time at $\frac{M_{EPS}}{M_{PL}} = 2.0$
($\alpha_{TH} = 0.010$ Kg/W, Case III n)

ORIGINAL PAGE IS
OF POOR QUALITY

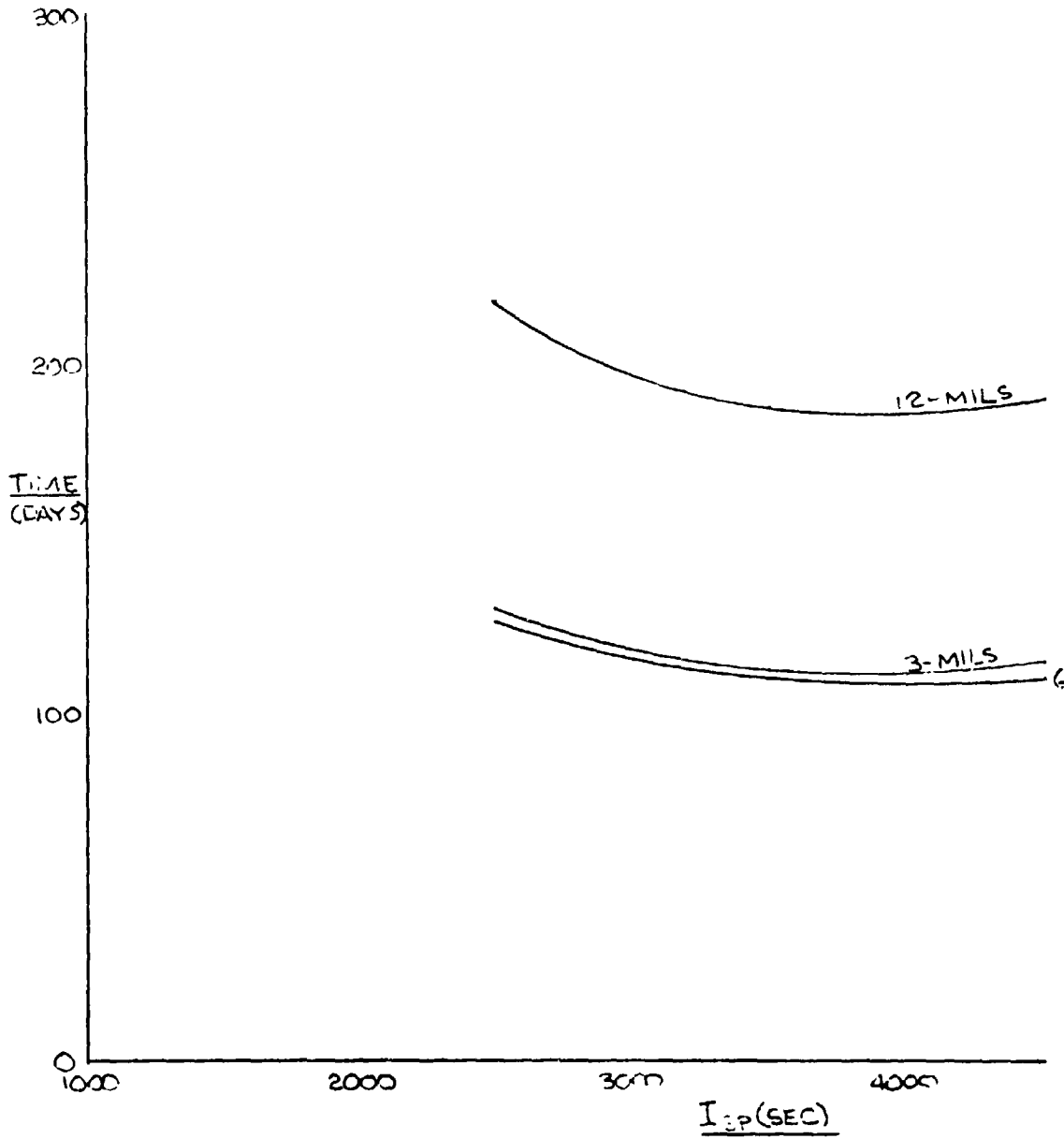


Figure 12. Effect of I_{SP} and Cover Thickness on Thrust Time at $\frac{M_{EPS}}{M_{PL}} = 2.0$
($\alpha_{TH} = 0.010$ Kg/W, Case I h)

ORIGINAL FACE IS
OF POOR QUALITY

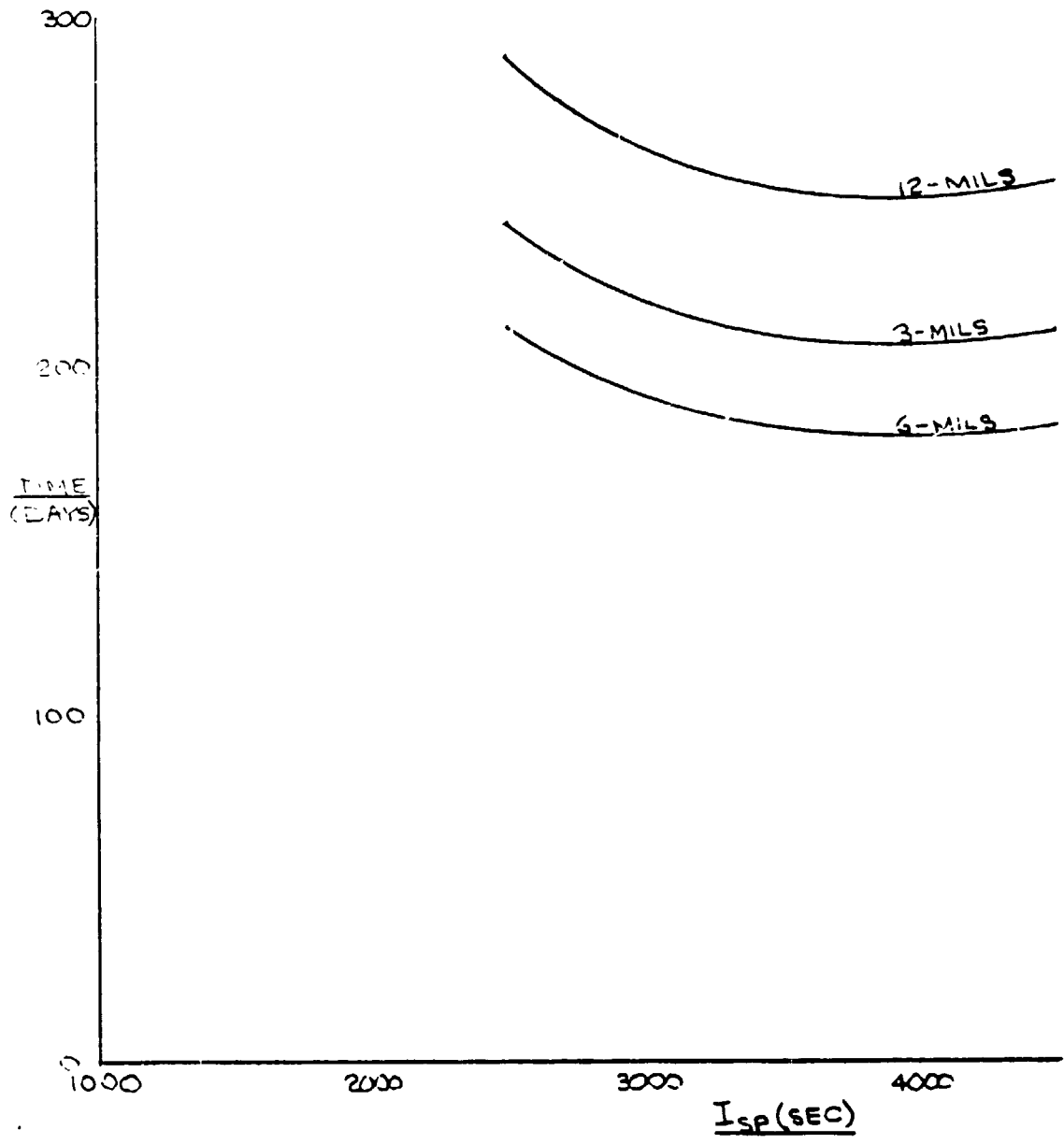


Figure 13. Effect of I_{sp} and Cover Thickness on Thrust Time at $\frac{M_{EPS}}{M_{PL}} = 2.0$
($\alpha_{TH} = 0.020$ Kg/W, Case I n)

are shown in Figure 14. Corresponding values of residual power factor are shown in Figure 15.

The 6-mil cover thickness gives thrust times very close to the minimum for all combinations of thruster efficiency and specific mass. In addition, this thickness results in a residual power factor high enough that further improvement would not be worth the additional time. However, the minima in Figure 14 are fairly broad so that increased thickness for the less efficient and heavier thrusters might offer enough improvement in residual power to be important for some payloads. In any event, cover thicknesses less than 6 mils do not appear to be needed for this orbit transfer mission.

2.6 LOW ALTITUDE FLIGHT

Conservative calculations of solar array drag effects based on total array area, i.e., with the array perpendicular to the flight direction, impose an unrealistic limitation on minimum useful altitude for solar power. The limit occurs well above the Shuttle parking orbit for maximum payload (about 250 km). This apparent limitation is readily removed by a feathered array strategy in which the array is oriented parallel to the flight direction and the spacecraft is rolled to the angle for maximum illumination. This reduces the available power but the drag area is reduced considerably more than the power with the result that the power per unit drag area β_{Σ} is increased by about a decade. Sustained flight is then possible at altitudes considerably lower than the Shuttle orbit, and electrically propelled spacecraft deployment directly from Shuttle becomes practical.

2.6.1 Power Factor in Feathered Flight

The geometric relations defining power factor and roll angle for maximum power in feathered flight are developed here.

Figure 16 shows the geometric relations as seen from the spacecraft, i.e., the viewing sphere is centered at the spacecraft. The velocity vector pierces the sphere at x which lies on the horizontal plane, the zenith is perpendicular to the horizontal plane at high noon and the orbit normal pierces the sphere at the right extremity. The angle α is zero at high noon and increases to 2π in one revolution; it reaches the terminator crossing at $\pi/2$ in 1/4 revolution. α is shown both as a great circle length on the sphere and as a longitudinal angle around the orbit normal.

ORIGINAL PAGE IS
OF POOR QUALITY

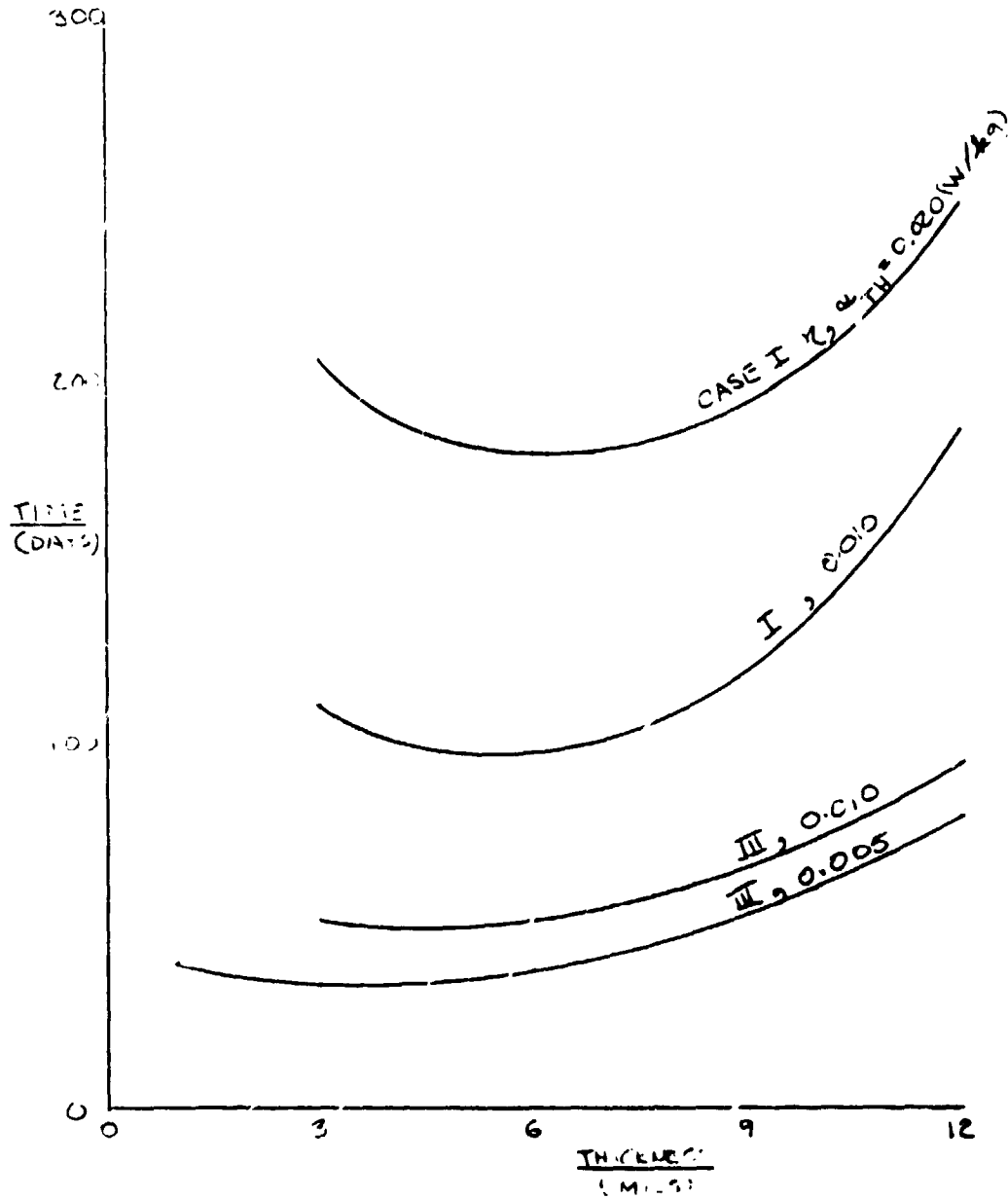


Figure 14. Effect of Solar Cell Cover Thickness on Thrust Time for Different Combinations of Thruster α and η

$$\left(\frac{M_{EPS}}{M_{PL}}\right) = 2.0$$

ORIGINAL DESIGN,
OF POOR QUALITY

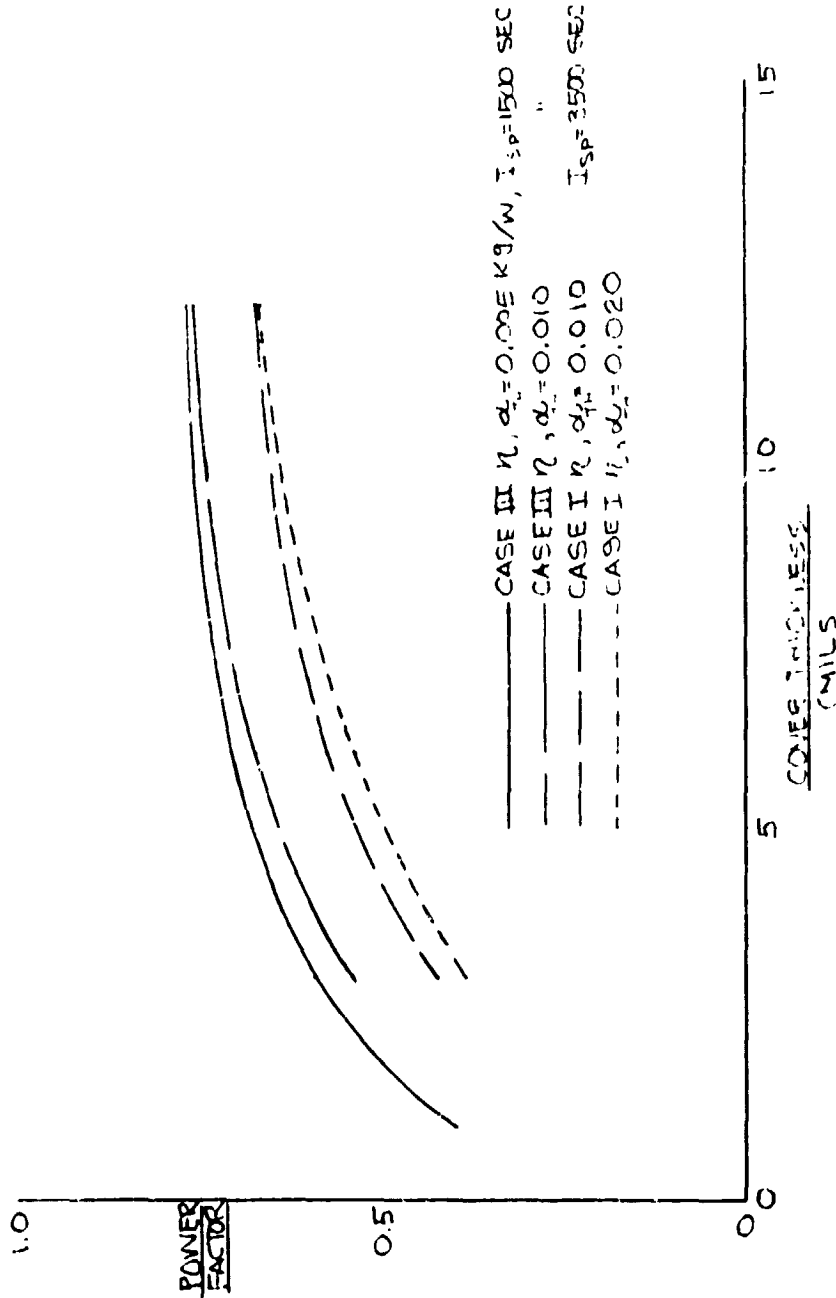


Figure 15. Effect of Cover Thickness on Power Factor at GEO for
Different Thruster Parameters ($M_{EPS}/M_{PL} = 2.0$)

The sun direction makes the angle $90 - \beta$ with the orbit plane. The sine of this angle is the power factor if the array is not rolled out of the orbit plane.

When the spacecraft is rolled for maximum illumination in feathered flight, the normal to the array makes the angle ϕ relative to the orbit plane. This angle is a minimum at high noon and $\alpha = 90$ degrees (at the terminator crossing). When the spacecraft is rolled through the angle ϕ , the Sun line makes the angle β' relative to the plane of the array.

The spherical right triangle XPS in Figure 16 has sides 90 degrees - α , 90 degrees - β , and hypotenuse β' . Using spherical triangle relations it can be shown that

$$\cos \beta' = \sin \alpha \sin \beta \quad (52)$$

and

$$\tan \phi = \frac{\cot \beta}{\cos \alpha} \quad (53)$$

The optimum roll angle is defined by Equation (53) and the power factor is $\sin \beta'$.

At high noon, when $\alpha = 0$, $\cos \beta' = 0$ so that $\sin \beta' = 1.0$; i.e., the array receives full illumination. At the terminator crossing, $\alpha = 90$ degrees and $\cos \beta' = \sin \beta$. At this location, $\sin (\cos^{-1} \sin \beta) = \sin (90 \text{ degrees} - \beta) = \cos \beta$ which is the correct value for the power factor when the array is parallel to the orbit plane.

Referring to Figure 6, the minimum value of β occurs at the summer solstice and when $\psi = 0$ degrees. At this point, $\beta = 90$ degrees - $(i + \epsilon) = 38$ degrees for an orbit inclination $i = 28.5$ degrees. β then varies within the range from 38 to 90 degrees as the time of the year varies and as the orbit regresses. This is shown in Figure 17 where the sun angle relative to the orbit plane ($90 - \beta$) is plotted versus the number of days after the summer solstice for an assumed altitude of 250 km.

ORIGINAL FILE
OF POOR QUALITY

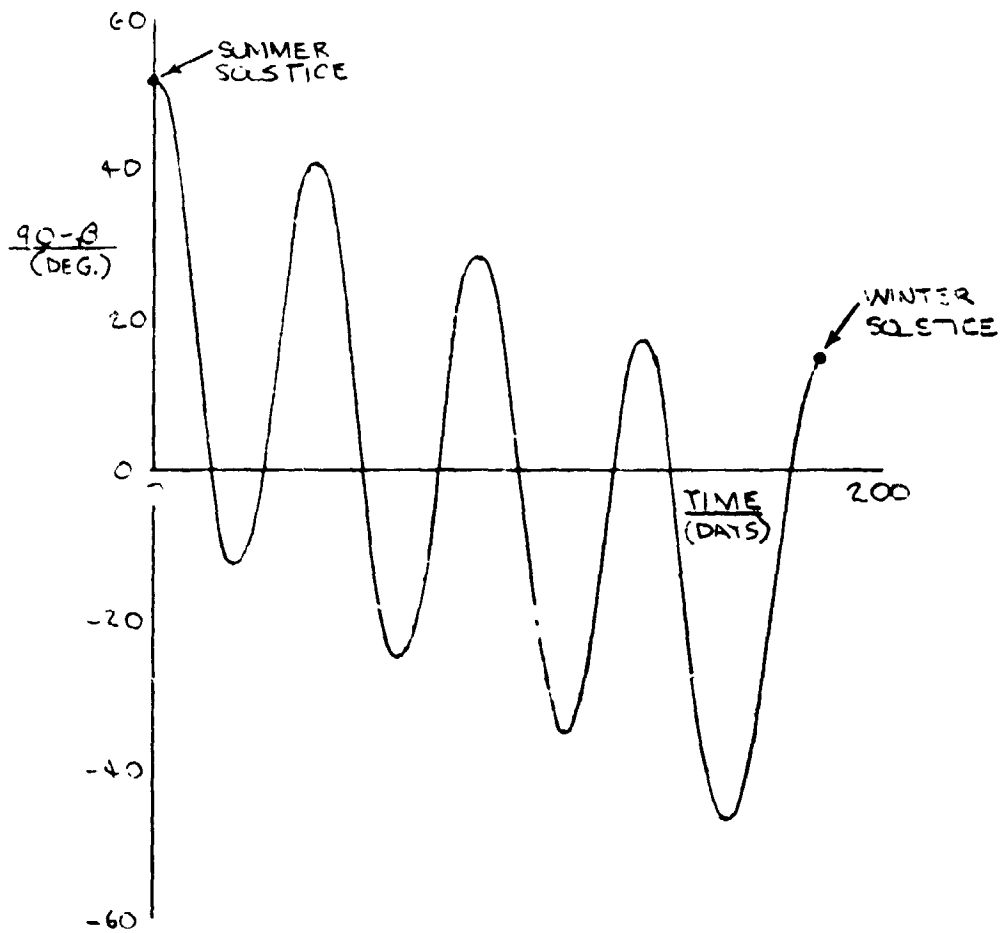


Figure 17. Sun Angle Relative to Orbit Plane (250 km Altitude, 28.5 deg Orbit)

Figure 18 shows the variation of the power factor (for the optimum roll angle ϕ) as a function of the spacecraft position in orbit, α , and for different values of the angle β between the orbit normal and the Sun direction, for the 250 km example. The value of this power factor, averaged over α , is plotted in Figure 19 as a function of β . The improvement in power factor at the optimum roll angle is impressive compared to $\cos \beta$ which is the power factor for the array parallel to the orbit plane. For example at $\beta = 90$ degrees, when the sun is in the orbit plane and $\cos \beta = 0$, the average power factor for the optimum roll angle is 0.64.

Since β varies with time as shown in Figure 17, the unocculted power available, averaged over the orbit period, is also a function of time. This variation can be calculated by finding β as a function of time from Figure 17 and looking up the corresponding average power factor in Figure 19. The result is shown as the upper curve in Figure 20. The occultation factor, calculated as explained in Section 2.3, is also shown in Figure 20 along with the occulted power which is the product of the feathered array power factor with the occultation power factor.

As mentioned earlier, the above illustrations apply for the assumed altitude of 250 km. When the equations for occultation and feathered flight are incorporated in a programmed calculation of the climb equation, the relations shown illustratively are calculated as continuous functions of time during the climb.

It is interesting to continue the 250 km example one step farther to estimate the average power available as a function of percentage of the time during the year that it is available. Both the occulted and non-occulted results are shown in Figure 21. For this example, which is the Shuttle parking orbit for maximum payload, 40% of the array power for full illumination is available at any time during the year. For 20% of the time, the average power over an orbit period is 50% of maximum power. This result is of particular importance for other than orbit transfer missions where the spacecraft may remain in a low altitude orbit for a substantial time.

ORIGINAL PAPER
OF POOR QUALITY

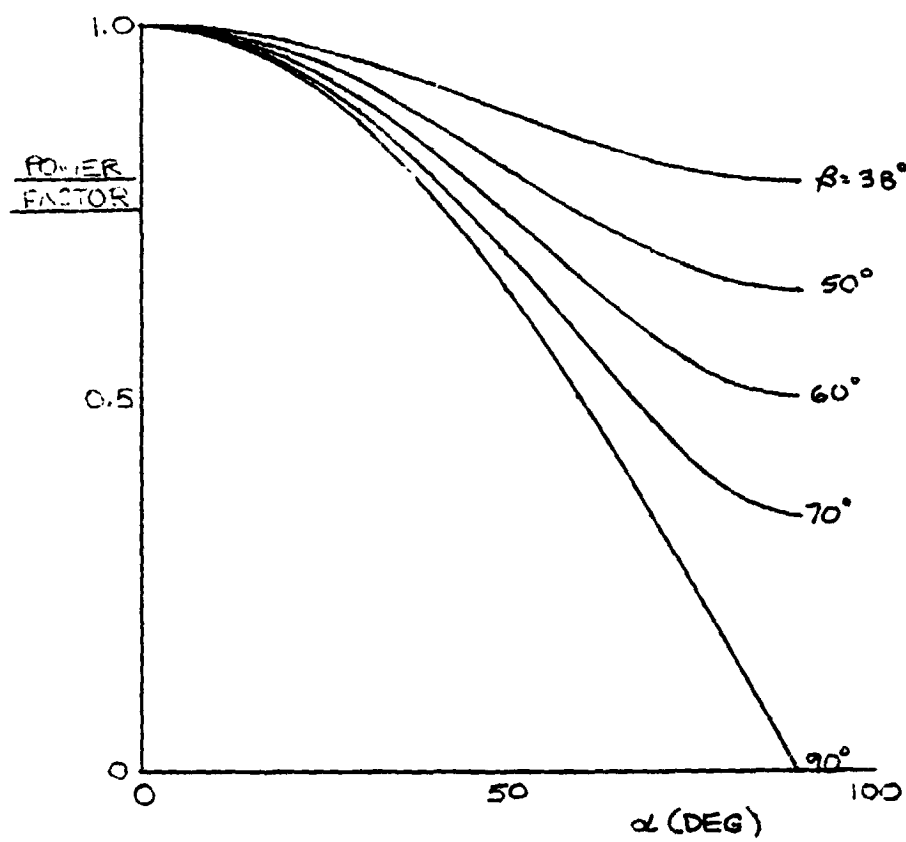


Figure 18. Feathered Array Power Factor vs Orbit Position Angle α for Different Values of β (no occultation)

ORIGINAL PAGE IS
OF POOR QUALITY

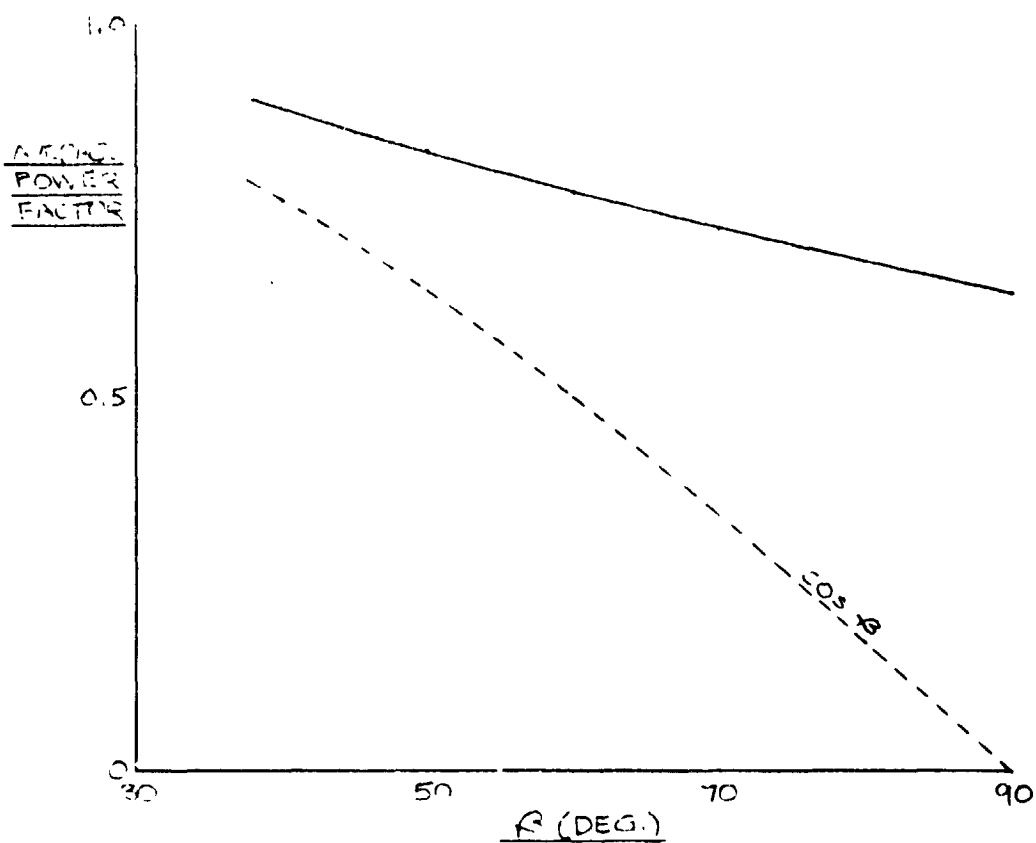


Figure 19. Average Power Factor vs β for Feathered Array
(No occlusion)

ORIGINAL PARTIAL
OF POOR QUALITY

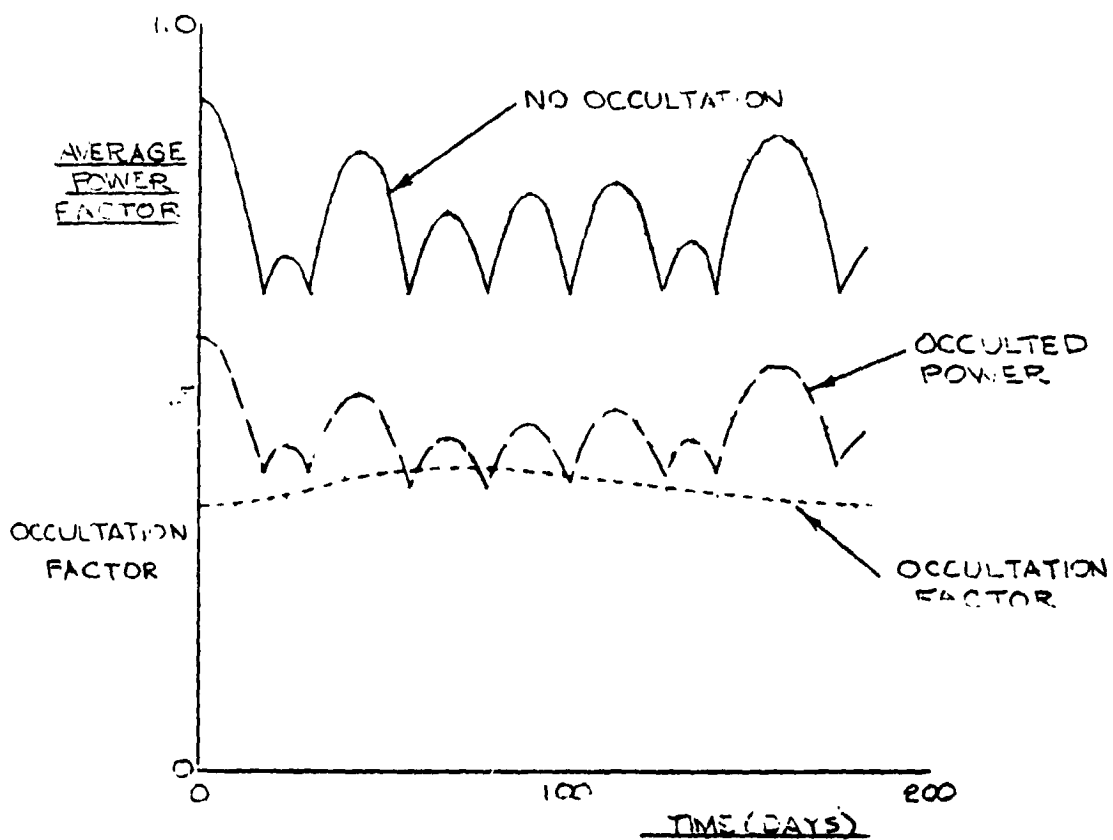


Figure 20. Average Power Factor vs Time After Summer Solstice
for Feathered Array (28.5° Orbit Inclination,
 $H = 250$ km)

ORBITAL PERIOD
OF POOR QUALITY

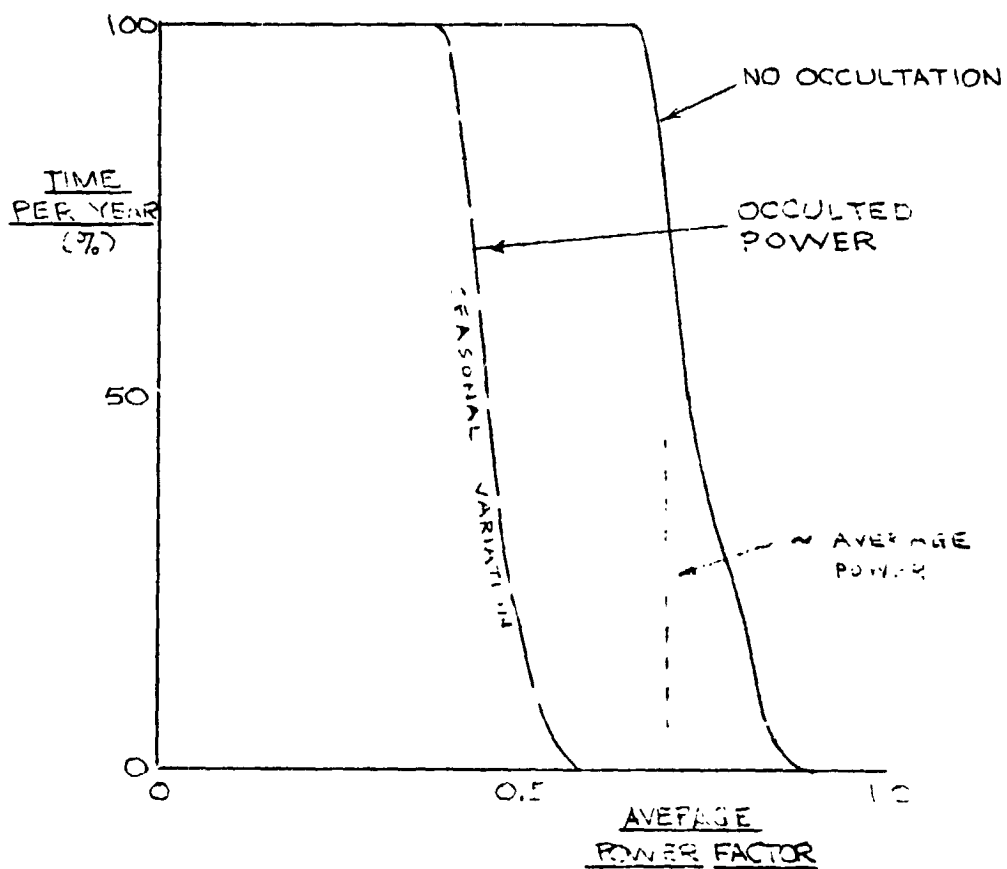


Figure 21. Percent Time Available vs Average Power Factor Per Day for Feathered Array (28.5° Orbit Inclination, H = 250 km)

2.6.2 Orbit Transfer Starting Power

For the orbit transfer mission, the spacecraft climbs quickly out of the drag region so that power loss associated with orbit regression is not an important consideration.

Referring to Figure 6, the optimum time of day to start the transfer is that for which $B = -\theta$ so that the orbit vector is coplanar with the ecliptic pole and the sun direction, as illustrated in Figure 22.

Equations (54) and (55) result from the law of cosines applied to the small triangle in Figure 22.

$$\cos f = \cos i \cos \epsilon + \sin i \sin \epsilon \cos \psi \quad (54)$$

$$\cos i = \cos \epsilon \cos P + \sin \epsilon \sin P \cos \theta \quad (55)$$

Since $P = 90 - \beta$,

$$\cos P = \sin \beta$$

$$\sin P = \cos \beta$$

Equations (54) and (55) can be rewritten as:

$$\sin \beta = \cos i \cos \epsilon + \sin i \sin \epsilon \cos \psi \quad (56)$$

$$\cos \theta = \frac{\cos i - \cos \epsilon \sin \beta}{\sin \epsilon \cos \beta} \quad (57)$$

Then with i and ϵ given, ψ is assigned to determine β from Equation (56) and this is used in Equation (57) to calculate θ . In this indirect way, β is found as a function of θ and Figure 19 is used to find the corresponding power factor averaged over the orbit. The occultation effect is accounted for in the ascent calculation.

Figure 23 shows the result of this calculation plotted as maximum average power factor at the start of the orbit transfer versus time in days after the summer solstice. The unocculted power available from the

ORIGINAL PAGE IS
OF POOR QUALITY

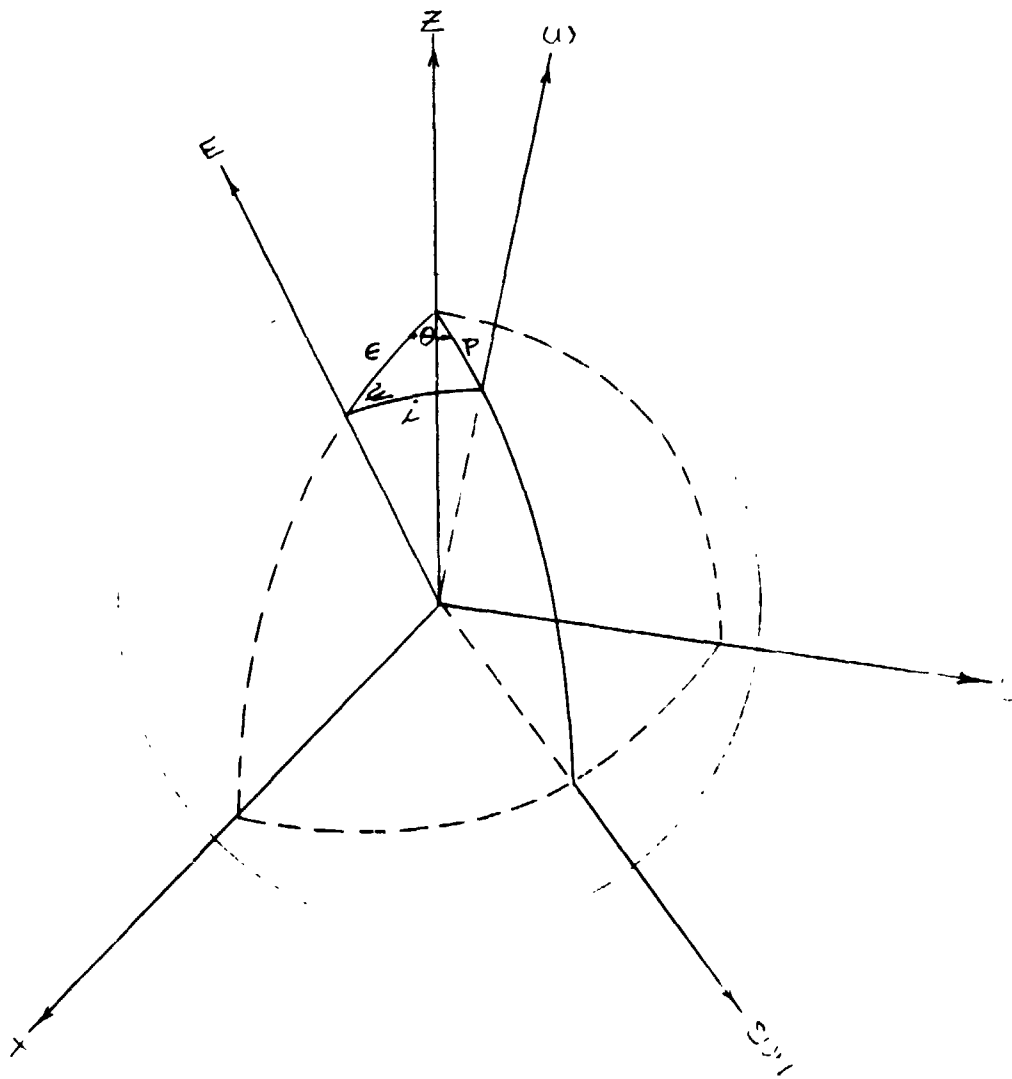


Figure 22. Optimum Geometry to Initiate Ascent ($B = -\theta$)

ORIGINAL FIGURE
OF POOR QUALITY

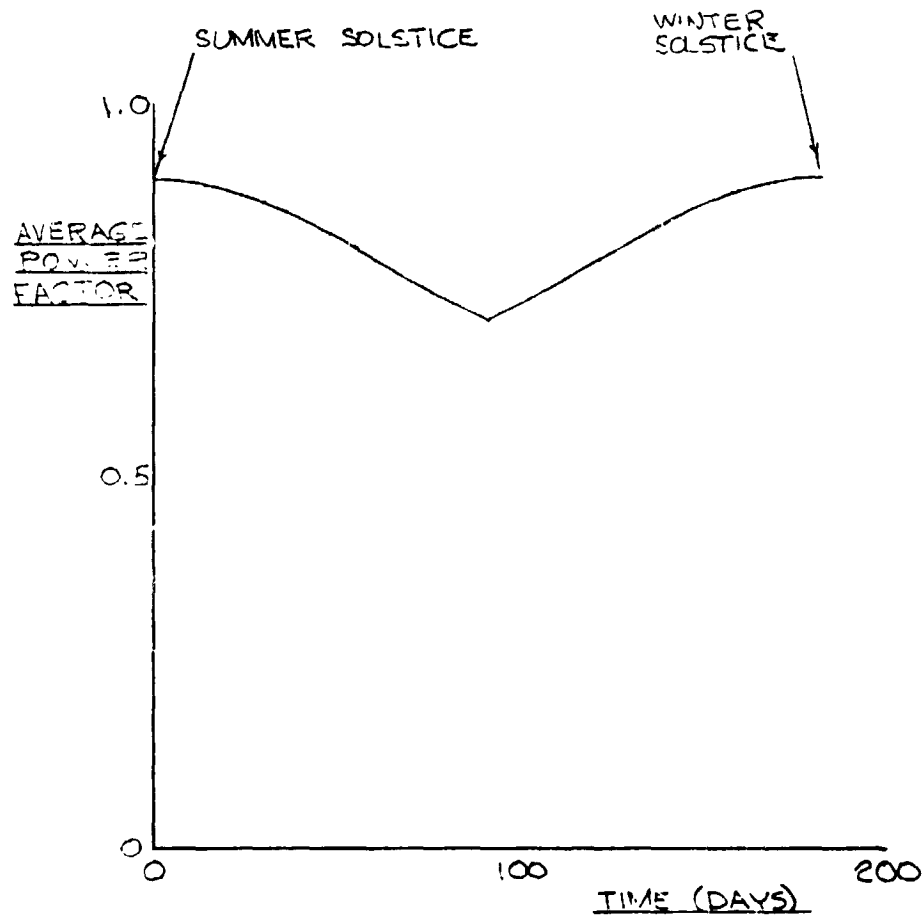


Figure 23. Maximum Average Power Factor at Start of Climb vs Days After Summer Solstice (no occultation)

feathered array varies from 70% to 90% of the full array power. For 2/3 of the year the available power is more than 80% of the full array power.

2.6.3 Sustained Low Altitude Flight

Both Figures 21 and 23 show that the feathered array, rolled for maximum illumination during an orbit, produces an average power of about 70% of the full array power. The starting power for the transfer mission is about 10% higher than the average value for sustained low altitude flight.

Figure 24 shows that the occultation fraction is not very sensitive to altitude in the neighborhood of 250 km where drag effects are large enough to require feathering the array, i.e., from 100 to 400 km. Therefore, a reasonable assumption is that an average power over the orbit period equal to 40% of the full array power is available over this altitude range and at any time of the year, for either low altitude sustained flight or for the low altitude end of an orbit transfer mission. The corresponding drag area in feathered flight is assumed to be 5% of the total array area.

The power per unit drag area is therefore increased by a factor of 8, from 150 to 1200 kg/W, in the feathered configuration as compared to the full blanket drag area and normal incidence power. This not only reduces the drag effect during the early stage of an orbit transfer to GEO, but it greatly reduces the minimum altitude for sustained flight.

This minimum is found by setting the numerator in Equation (16) equal to zero. After some rearrangement, the following expression is obtained for the required electric propulsion mass ratio:

$$\frac{M_{EP}}{M_{PL}} = \frac{\left(\frac{M_{PL}}{A_{PL}} \right)}{\left(\frac{n}{g I_{SP}} \frac{2}{\rho C_D} \frac{r}{GM} \right) \left(2 - \frac{\sqrt{GM}}{g I_{SP}} \right) - \frac{1}{\beta_E}} \quad (58)$$

OF POOR QUALITY

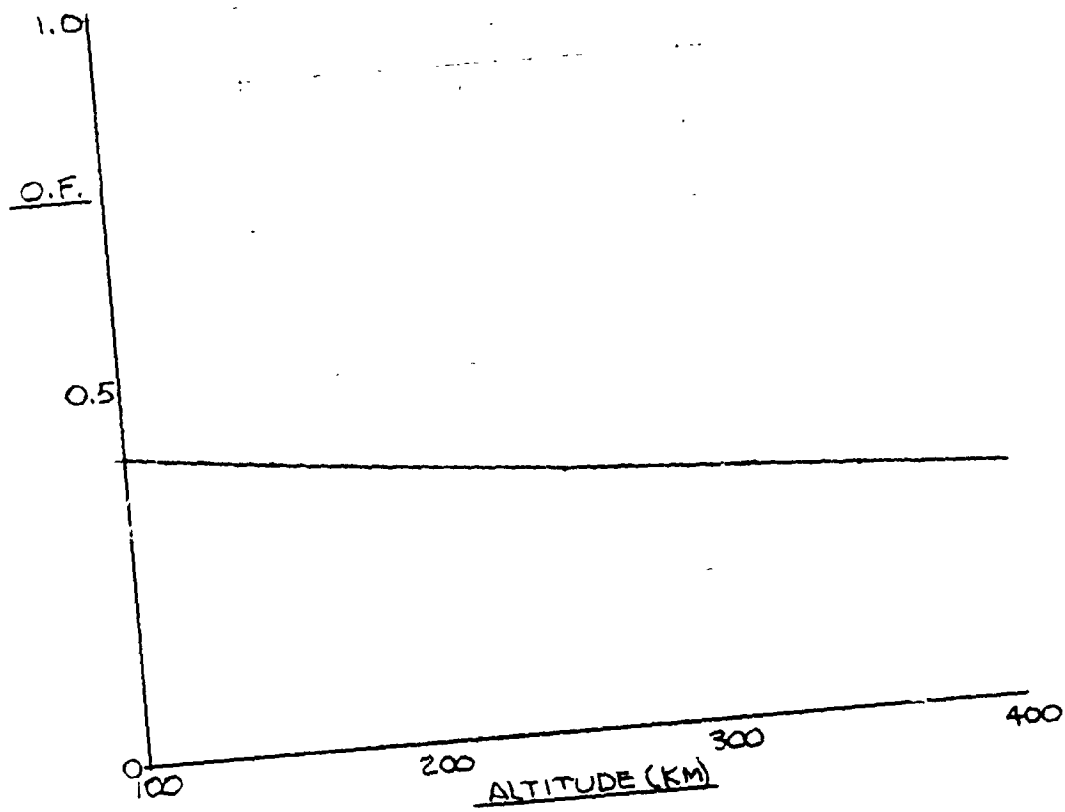


Figure 24. Occultation Fraction vs Altitude
(Summer Solstice, $\psi = 180^\circ$)

The drag contribution of the payload area appears in the numerator ratio which shows that the electric propulsion mass ratio increases linearly with the power supply specific mass and inversely with the payload specific mass. The drag effect of the power supply area appears in the denominator where it determines the condition for which the denominator becomes zero and the electric propulsion mass for equilibrium flight becomes infinite.

Equation (58) was used to plot the minimum altitude relations shown in Figure 25 for nuclear and solar power. The nuclear power source was estimated to have a specific mass $\alpha_E = 0.033$ while for solar power α_E ranged from 0.012 to 0.036 (kg/W).

The most important conclusion to be drawn from Figure 25 is that sustained flight with electric propulsion is practical down to 150 km, i.e., 100 km below the Shuttle parking orbit for maximum payload delivery. In this high drag region, the feathered solar array performs as well as the nuclear source. Thus, solar electric propulsion can be used directly to augment Space Transportation System capability without relying on intermediate chemical propulsion stages. Solar electric orbit transfer vehicles, servicing vehicles, or on-board propulsion systems may be deployed directly from the Shuttle Orbiter.

2.7 PLANE CHANGE

Edelbaum (Reference 7) has shown that the characteristic velocity ΔV required for low thrust orbit transfer with continuous plane change i , at constant I_{sp} , can be expressed by the equation,

$$\Delta V = \sqrt{v_I^2 - 2v_I v_F \cos \frac{\pi}{2} i + v_F^2} \quad (59)$$

where v_I and v_F are initial and final orbit velocities defined by Equation (1). By combining Equations (1) and (59), the characteristic velocity is expressed dimensionlessly in terms of the initial and final orbit radii and plane change angle,

$$\frac{\Delta V}{v_I} = \sqrt{1 - 2 \sqrt{\frac{r_I}{r_F}} \cos \frac{\pi}{2} i + \frac{r_I}{r_F}} \quad (60)$$

ORIGINAL
OF POOR QUALITY

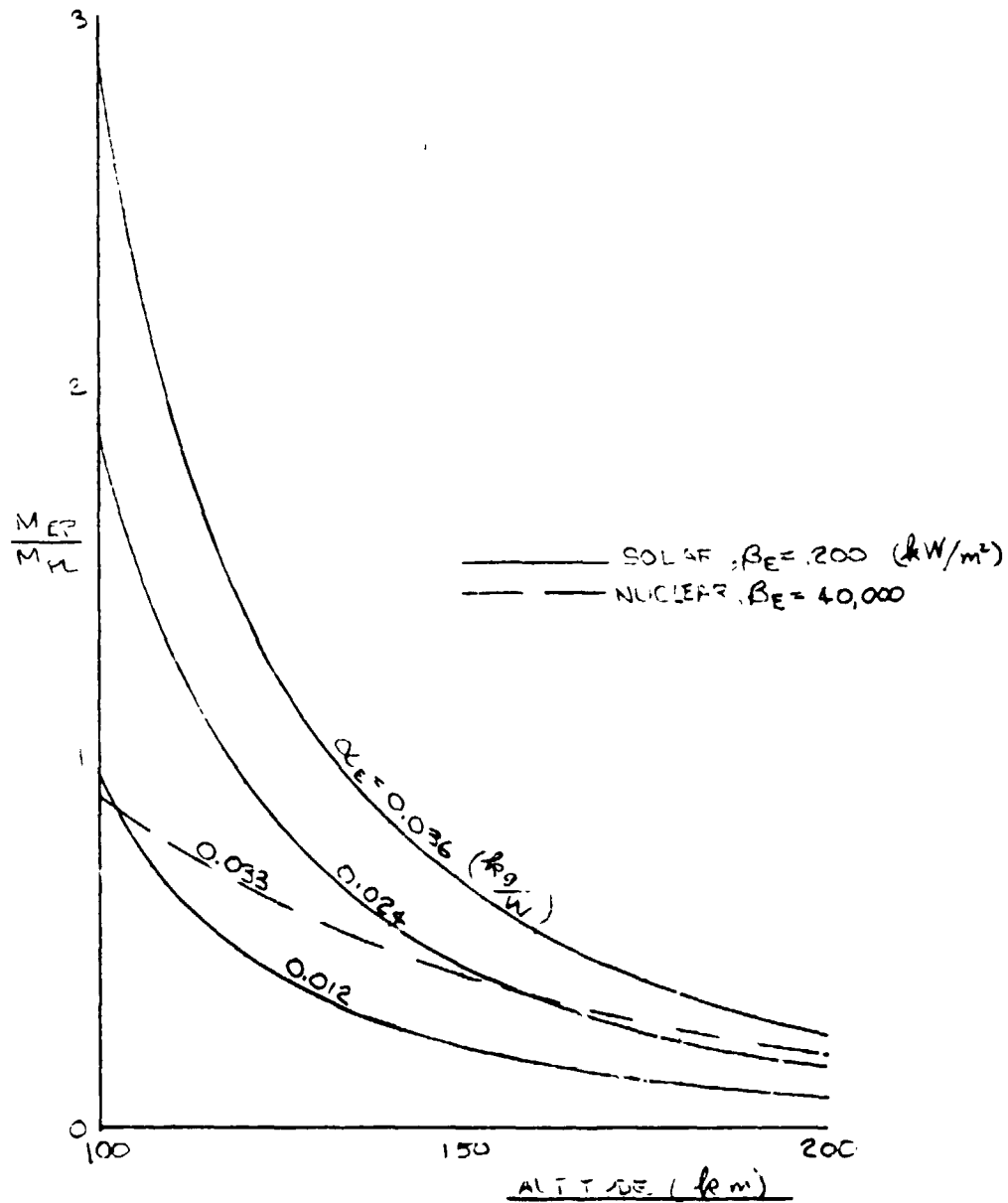


Figure 25. Comparison of Minimum Altitude for Feathered Solar and Nuclear Power
 $(\eta = 42\%, I_{SP} = 1500 \text{ sec}, M_{PL}/A_{PL} = 30 \frac{\text{kg}}{\text{m}^2})$

This equation can be used to compare four different ways to change the orbit plane angle during transfer from a low earth orbit of 250 km to GEO, as shown in Figure 26. The upper two curves compare the very inefficient approach of making the plane change at the initial altitude, with the more efficient one in which the plane change is made at GEO. The smallest ΔV requirement occurs when the plane rotation is done continuously during the transfer, according to an optimum thrust vector orientation schedule given in Reference 7. Although this minimizes ΔV , it has the disadvantage of producing a greater total radiation fluence for the case of a 28.5 degree launch followed by a plane rotation to 0 degrees. This effect is seen by comparing the fluence rate curves in Figure 8 for 0 and 30 degree inclination. The ratio of these rates increases from 1.0 at 1500 km to 2.3 at maximum fluence rate (5000 km) and to 2.9 at 10,000 km.

This suggests the alternate plane change approach in which the orbit inclination remains fixed up to 10,000 km after which it is rotated to the final value according to the optimum schedule. Figure 26 shows that the ΔV penalty relative to the optimum plane change is small. It is about 1/3 of that due to making the total plane change at GEO. In terms of ΔV , the transfer from 250 km to GEO, with i changing from 28.5 degrees at launch to 0 degrees at GEO, requires 5990 m/sec for the optimum schedule while an additional 349 m/sec (5.8%) more ΔV is needed when all of the change is made above 10,000 km.

R. DiEsposti, at NASA-LeRC, has calculated the power loss for both the optimum steering program and the alternate approach with plane change above 10,000 km. For a 3-mil shield thickness with infinite back-shielding, he found the residual power advantage of the alternate approach to be less than 2% greater than for optimum steering.* This suggests that optimum steering may be the preferred approach, although detailed trade calculations would be needed to verify this for a specific spacecraft design.

*Private communication.

ORIGINAL PAGE IS
OF POOR QUALITY.

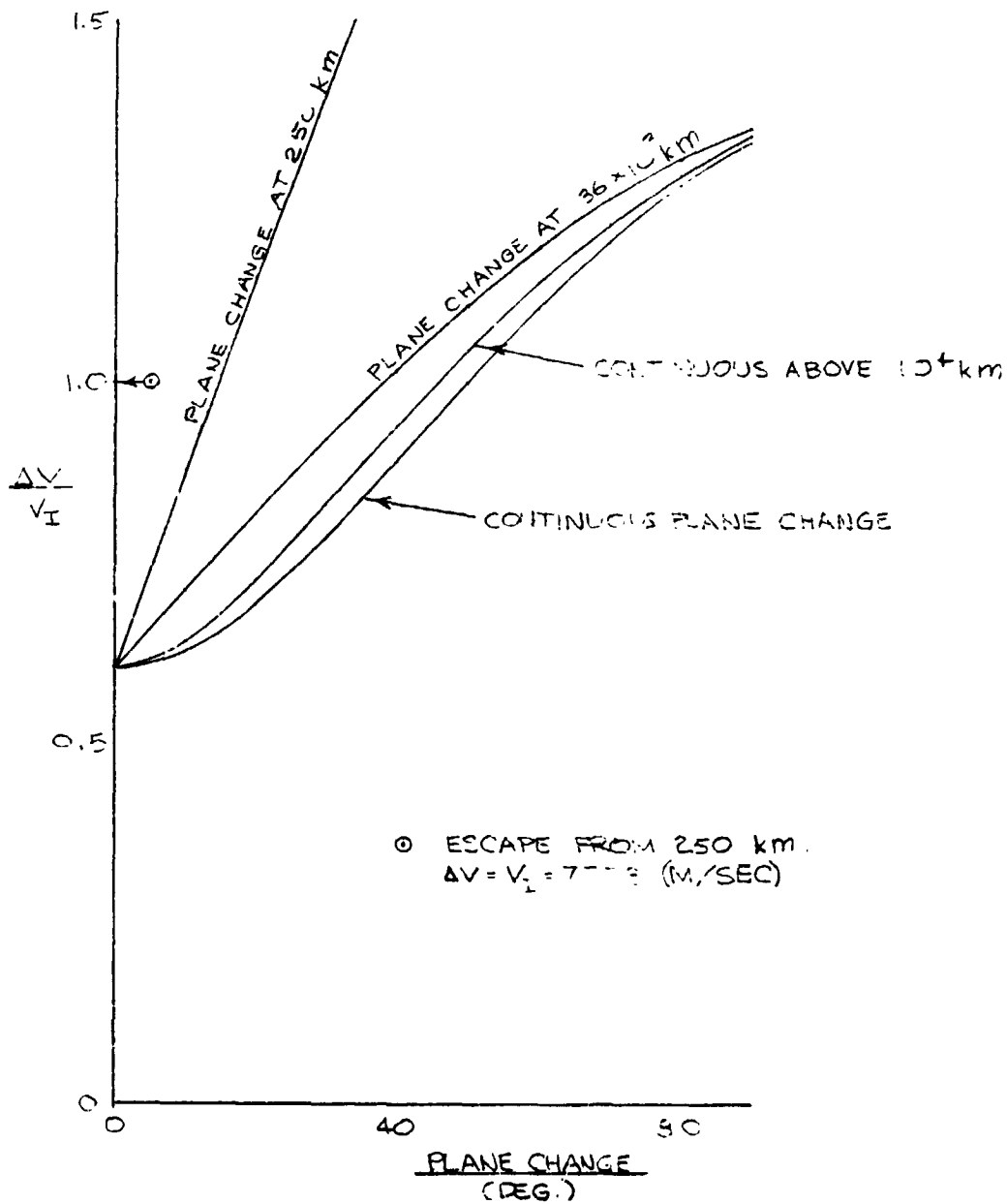


Figure 26. ΔV for Different Plane Change Options (250 km initial orbit, GEO final orbit)

2.8 ORBIT TRANSFER TIMES

Orbit transfer times presented here include all propulsion requirements for transfer from LEO to GEO followed by 5 and 10 year lifetimes and removal to a disposal altitude. Effects of occultation, drag and solar cell degradation are included. On orbit ΔV requirements are discussed in Section 3.

2.8.1 Nominal Mission Performance

The effect of thruster efficiency and I_{sp} on orbit transfer time is analyzed for different constant values of the electric propulsion system mass ratio. The calculation includes the effects of atmospheric drag, solar cell degradation and occultation for mission parameter sets shown in Table 5.

Table 5. Mission Parameter Sets

Mission Set No.	$\left(\frac{M_{EPS}}{M_{PL}}\right)_T$	Lifetime on Orbit (years)	ΔV on Orbit $\left(\frac{m}{sec}\right)$
1	1.0	10	1731
2	2.0	10	1731
3	3.0	10	1731
4	4.0	10	1731
5	2.0	5	949

Initial altitude, $H_o = 250$ km

Final operation altitude, $H_f = 35786$ km

Initial inclination, $i_o = 28.5^\circ$

Final operation inclination, $i_f = 0^\circ$ (equatorial orbit)

Disposal altitude, $H_d = 40786$ km

$\left(\frac{M_{EPS}}{M_{PL}}\right)_T$ represents the ratio of the total propulsion mass (primary thruster system dry, primary propellant and auxiliary propulsion required for stationkeeping and disposal) to the payload mass.

The spacecraft parameters are:

$$\alpha_E = 0.024 \text{ kg/W (thruster, solar array and processor)}$$

$$\beta_E = 150 \text{ W/m}^2 \text{ (solar array)}$$

$$\frac{M_{PL}}{A_{PL}} = 100 \text{ kg/m}^2 \text{ (payload)}$$

$$\eta = 20 \text{ to } 100\%$$

$$I_{SP} = \text{minimum to } 5000 \text{ seconds}$$

$\frac{M_{EP}}{M_{PL}}$ and $\frac{M_{PP}}{M_{PL}}$, electric propulsion dry mass ratios as required for the total electric propulsion system mass ratios in Table 5.

Figures 27 through 30 show the effect of thruster efficiency and specific impulse on orbit transfer time for total electric propulsion masses of 1, 2, 3 and 4 times the payload mass for 10-year missions. This mass accomplishes the total maneuver requirement of orbit transfer, inclination change, attitude control, stationkeeping and disposal. Each transfer time curve on these figures exhibits an optimum. To the left of the optimum, propellant mass requirements at low specific impulse are most influential. To the right of the optimum, power requirements at high specific impulse are more significant.

Figures 27 through 30 show that an optimum I_{SP} occurs that produces the shortest trip time for a given thruster efficiency; as seen in the figures, it is independent of η . Also plotted in these figures is the Case II efficiency relation, which shows the characteristic drooping toward lower I_{SP} 's. The net effect of this droop, as shown in Table 6, is that minimum trip time occurs at an I_{SP} higher than the "optimum" value.

A plot of I_{SP} and corresponding minimum transfer times is shown in Figure 31 as a function of payload fraction, i.e., the ratio of payload mass to total initial spacecraft mass. This fraction is related to the total electric propulsion mass ratio as shown below:

$$\text{Payload Fraction} = \frac{1}{\left(\frac{M_{EPS}}{M_{PL}}\right)_T + 1}$$

ORIGINAL FACE IS
OF POOR QUALITY

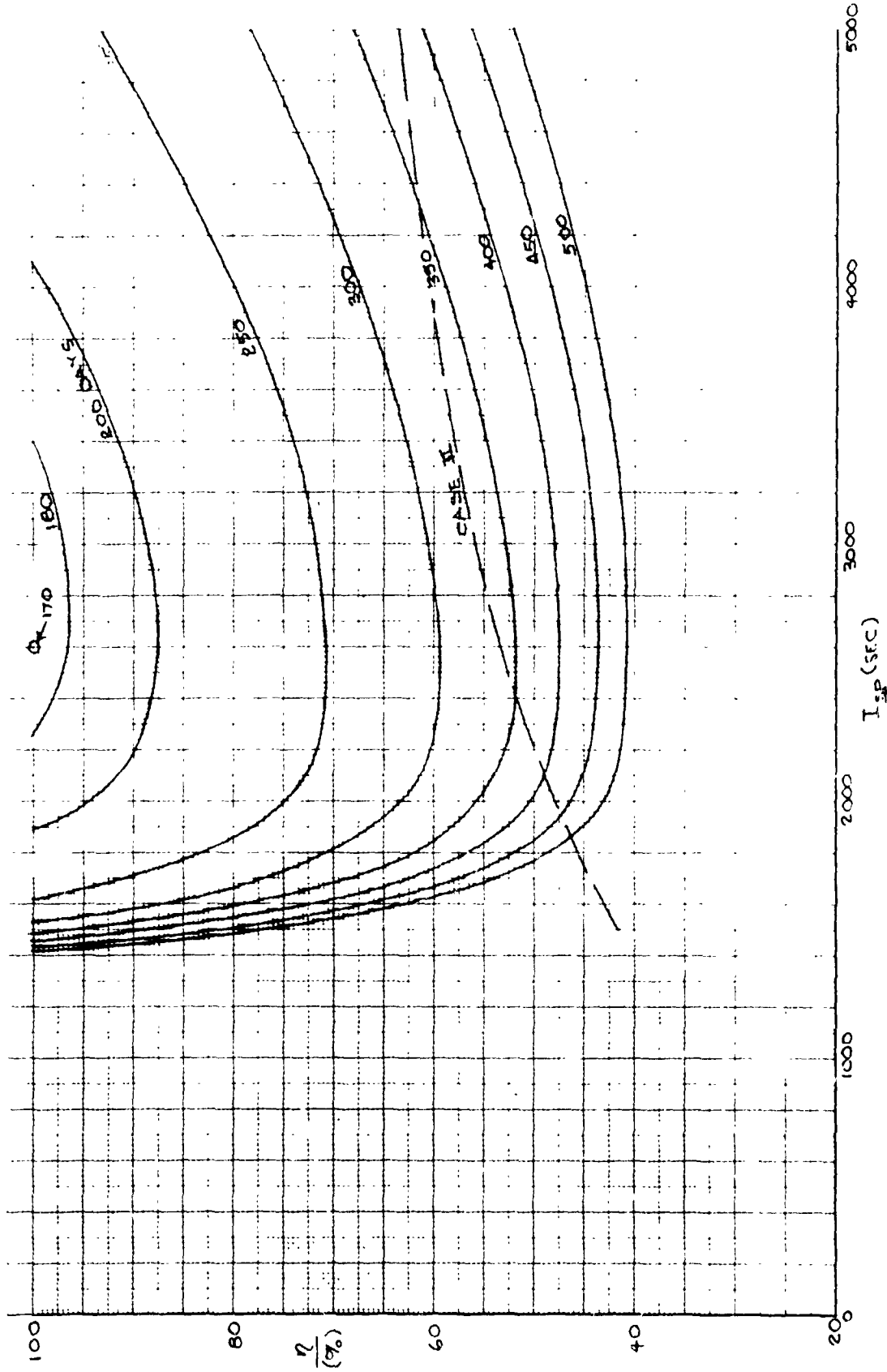


Figure 27. Effect of η & I_{sp} on Transfer Time for $\left(\frac{M_{EPS}}{M_{PL}}\right)_T = 1.0$

$$\left(\alpha = 0.024 \frac{\text{kg}}{\text{W}}, \beta = 150 \frac{\text{W}}{\text{m}^2}, \frac{M_{PL}}{A_{PL}} = 100 \frac{\text{kg}}{\text{m}^2}, 10 \text{ years}\right)$$

CHARACTERISTICS
OF ROOF SLABS

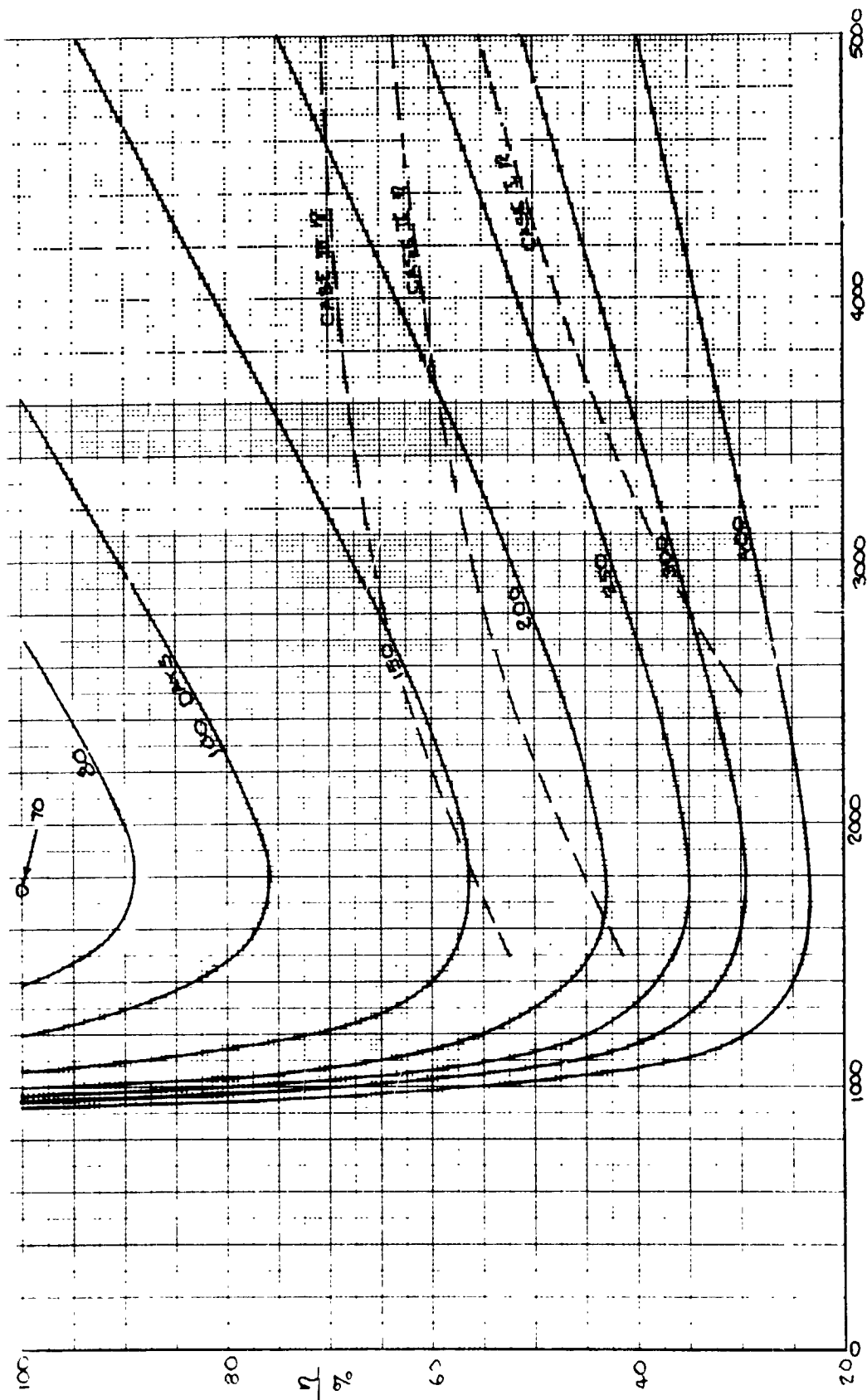


Figure 28. Effect of η & I_{sp} on Transfer Time for $\left(\frac{M_{EPS}}{M_{PL} T}\right) = 2.0$

$$\left(\alpha = 0.024 \frac{\text{kg}}{\text{W}}, \beta = 150 \frac{\text{W}}{\text{m}^2}, \frac{M_{PL}}{A_{PL}} = 100 \frac{\text{kg}}{\text{m}^2}, 10 \text{ years}\right)$$

ORIGINAL PAGE IS
OF POOR QUALITY

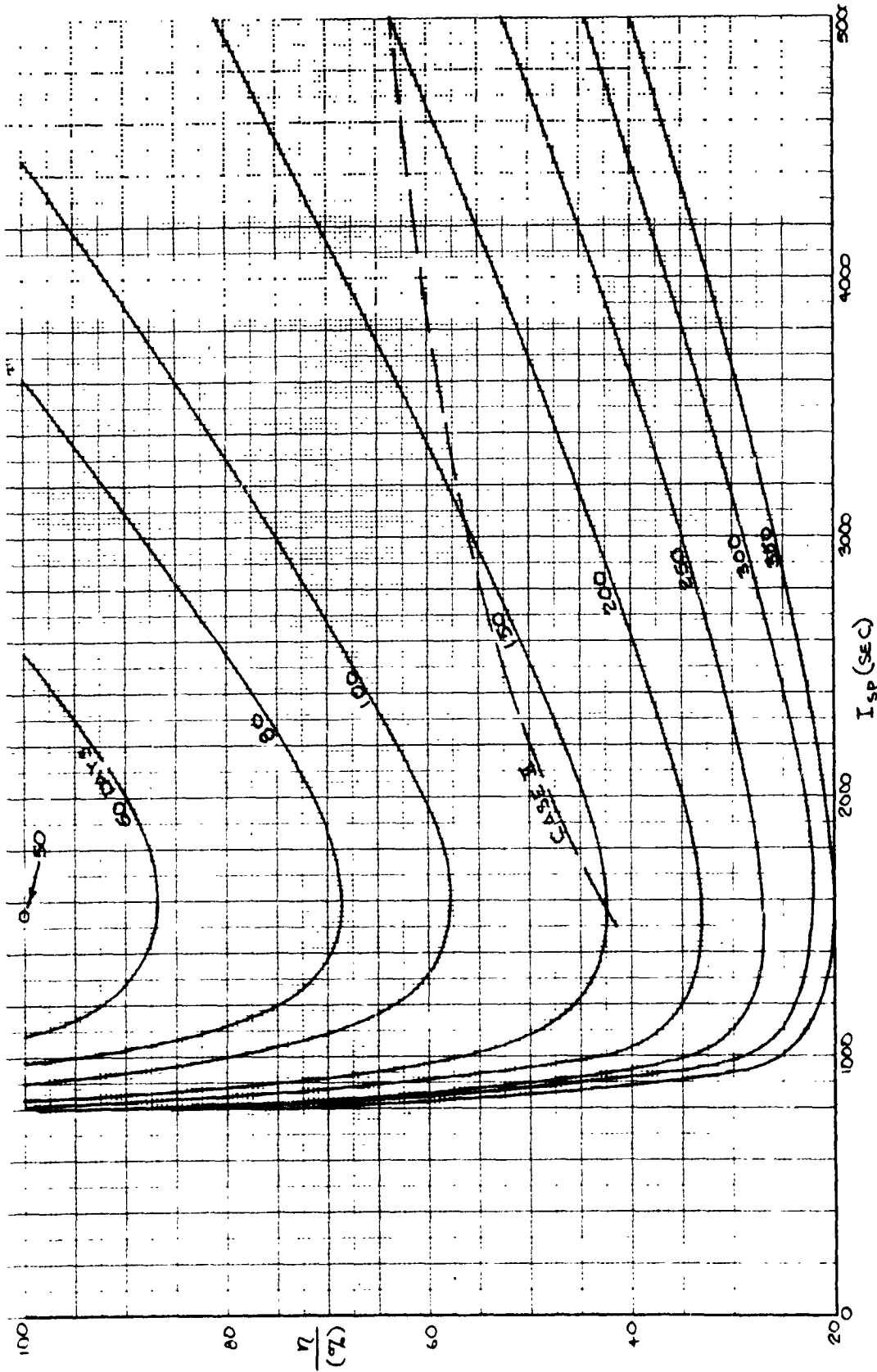


Figure 29. Effect of η & I_{sp} on Transfer Time for $\left(\frac{M_{EPS}}{M_{PL}}\right) T = 3.0$
 $\left(\alpha = 0.024 \frac{kg}{W}, \beta = 150 \frac{W}{m^2}, \frac{M_{PL}}{A_{PL}} = 100 \frac{kg}{m^2}, 10 \text{ years}\right)$

ORIGINAL PAGES
OF POOR QUALITY

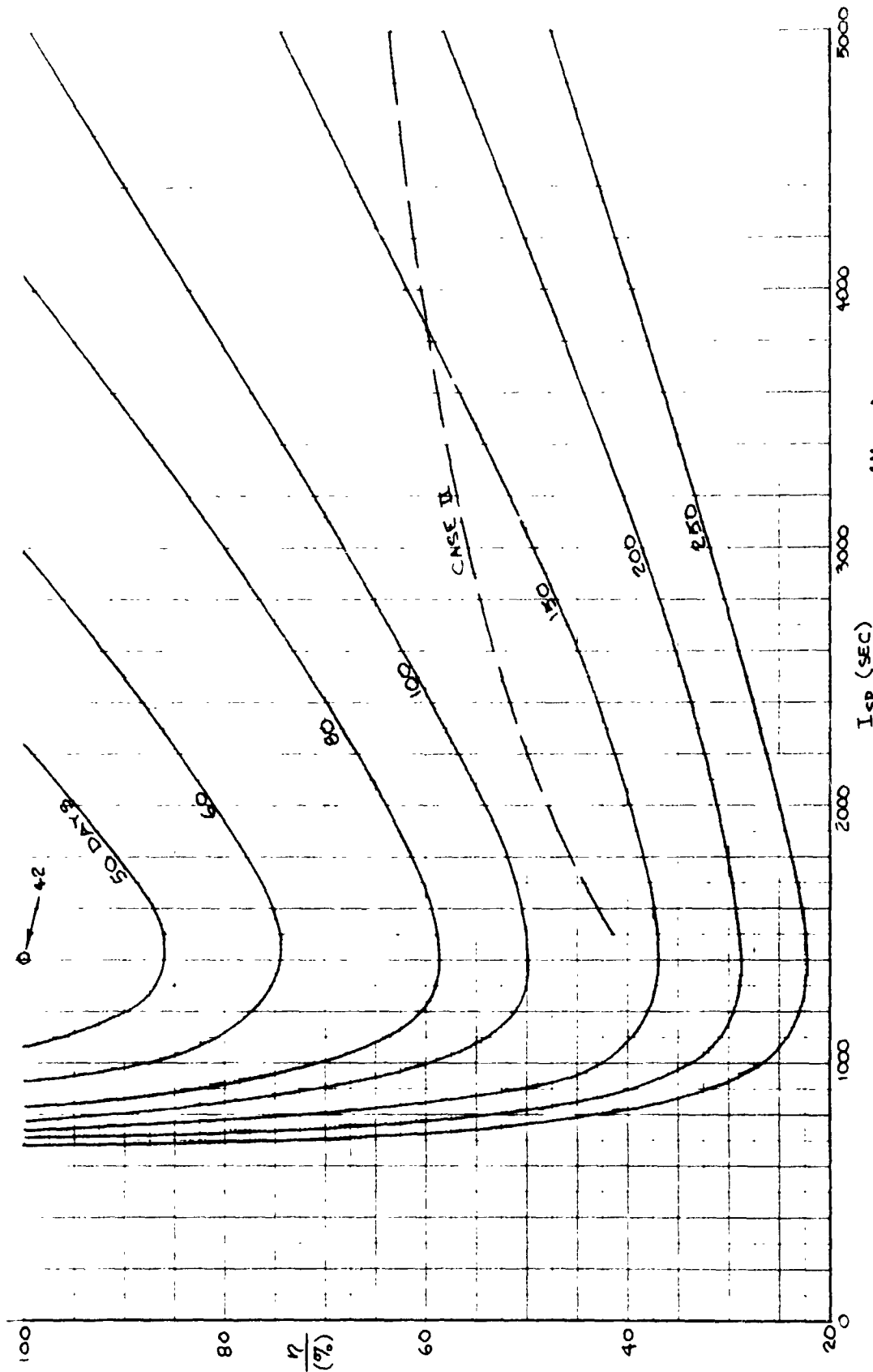


Figure 30. Effect of η & I_{sp} on Transfer Time for $\left(\frac{M_{EPS}}{M_{PL}}\right)^T = 4.0$
 $\left(\alpha = 0.024 \frac{kg}{W}, = 15() \frac{W}{m^2}, \frac{M_{PL}}{A_{PL}} = 100 \frac{kg}{m^2}, 10 \text{ years}\right)$

ORIGINAL PROBLEM
OF POOR QUALITY

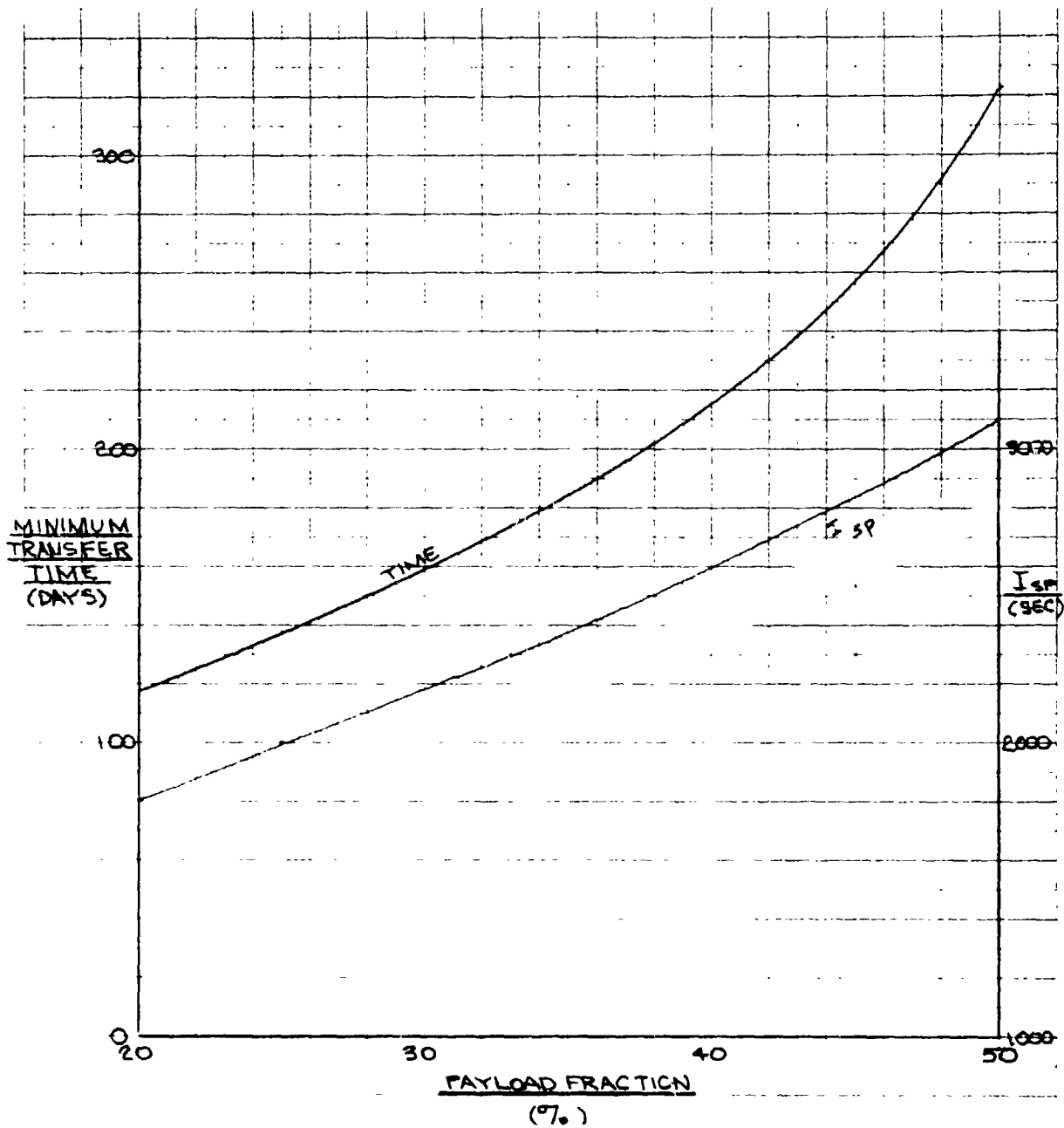


Figure 31. Effect of Payload Fraction on Minimum Transfer Time and Corresponding I_{sp} (Case II η , $\alpha = 0.024$ kg/W 10 Years)

Table 6. Comparison of Optimum I_{SP} and I_{SP} For Minimum Transfer Time - Case II Efficiency

$\left(\frac{M_{EPS}}{M_{PL}}\right)_T$	Optimum I_{SP} (sec)	I_{SP} For Minimum Transfer Time (sec)
1	2600	3100
2	1750	2300
3	1550	2000
4	1400	1800

It is shown in the figure as a percentage rather than a ratio.

From a system point of view, it is more economical to operate at an I_{SP} slightly lower than the minimum transfer time value in order to reduce the more expensive electric propulsion mass while increasing the less expensive propellant mass.

The relative magnitudes of these mass tradeoffs are seen in Figures 32 through 35 for the 10-year mission cases shown in Figures 27 through 30. The preferred I_{SP} conditions are shown as minimum transfer times in the figures.

The transfer time results for Mission Set 5 are plotted in Figure 36 and the mass ratio breakdown is shown in Figure 37. The greatly reduced on-orbit propellant for the shorter on-orbit life is apparent. It is also seen in Figure 38, which also shows the effect of payload fraction on the percent of total propellant that is used for on-orbit functions. The reduction of on-orbit propulsion from 12.6 to 7.3% of the total propellant mass results in a small reduction in transfer time. As shown in Figure 39, the transfer time for the 5-year mission is about 6% less than for the 10-year mission.

The two thruster parameters that have the greatest impact on transfer time are thruster efficiency and the electric propulsion specific mass parameter α . Figure 40 is a cross-plot of Figures 27 through 30 showing

ORIGINAL FIGURES
OF POOR QUALITY

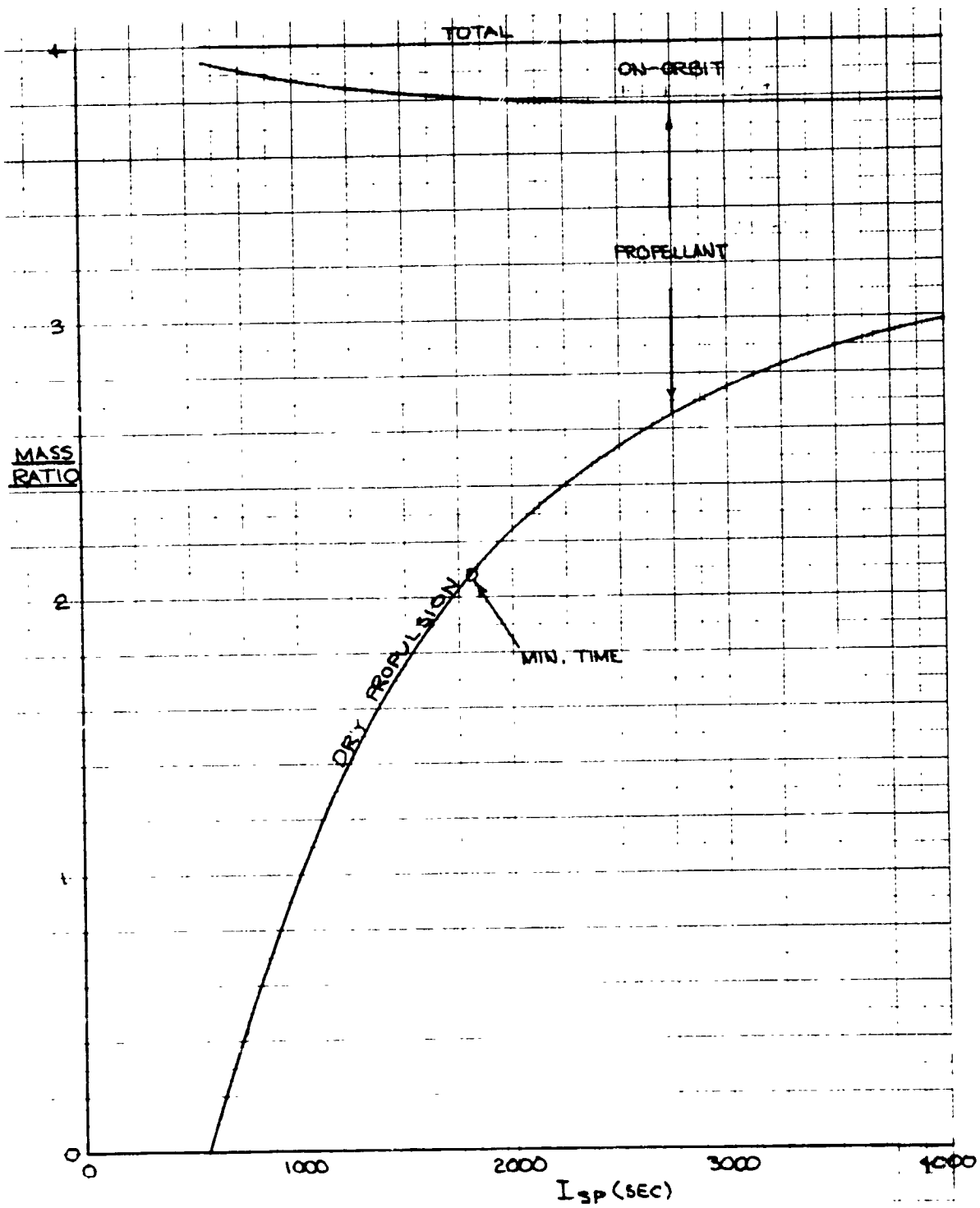


Figure 32. Propulsion Mass Breakdown for 20% Payload Fraction
(Case II η , $\alpha = 0.024$ kg/W, 10 Years)

CRITICAL DESIGN
OF POOR QUALITY

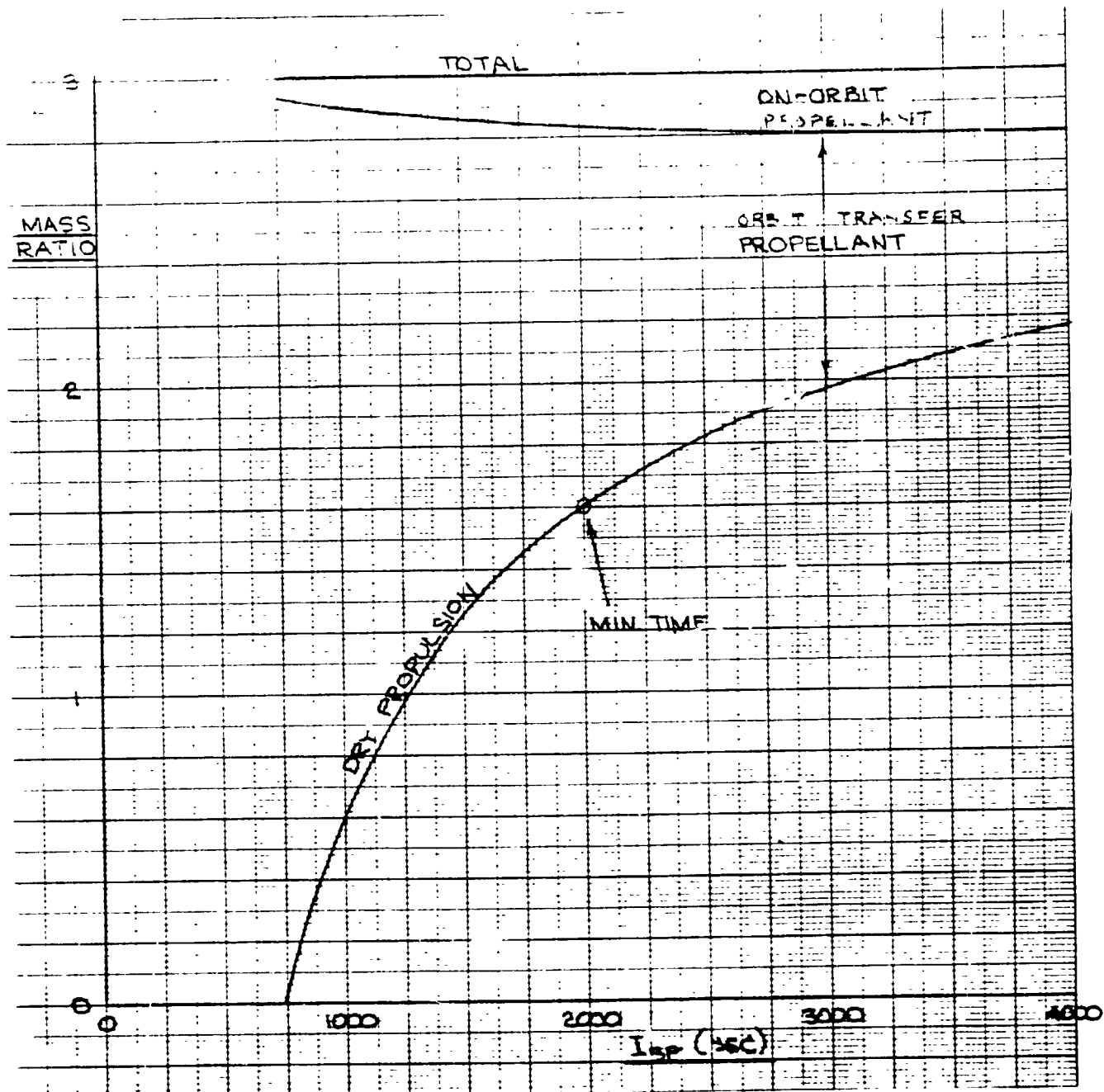


Figure 33. Propulsion Mass Breakdown for 25: Payload Fraction
(Case II η , $\alpha = 0.024$ kg/W, 10 Years)

ORIGINAL PAGE IS
OF POOR QUALITY

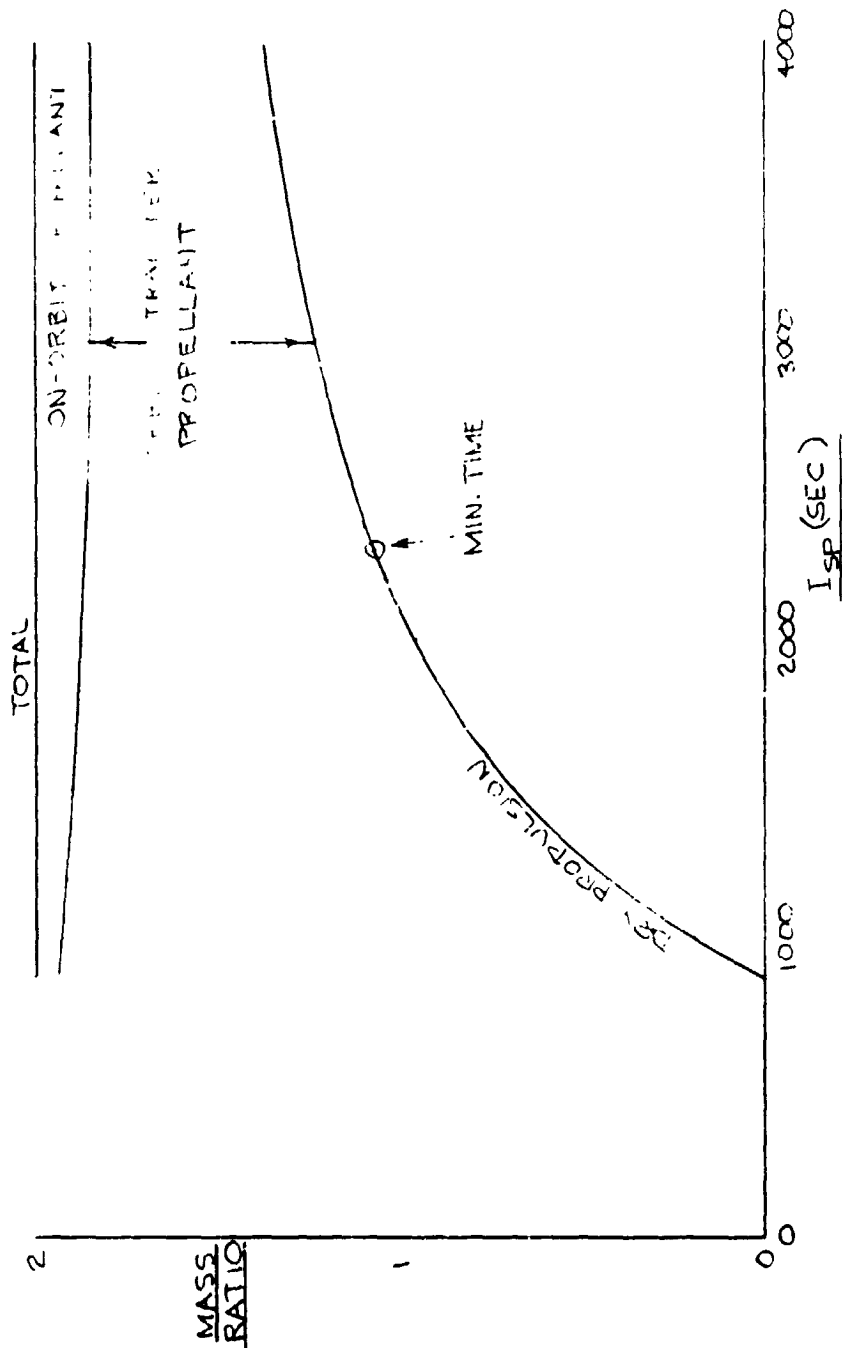


Figure 34. Propulsion Mass Breakdown for 33% Payload Fraction
(Case II n , $\alpha = 0.024$ kg/W, 10 Years)

OF POOR QUALITY

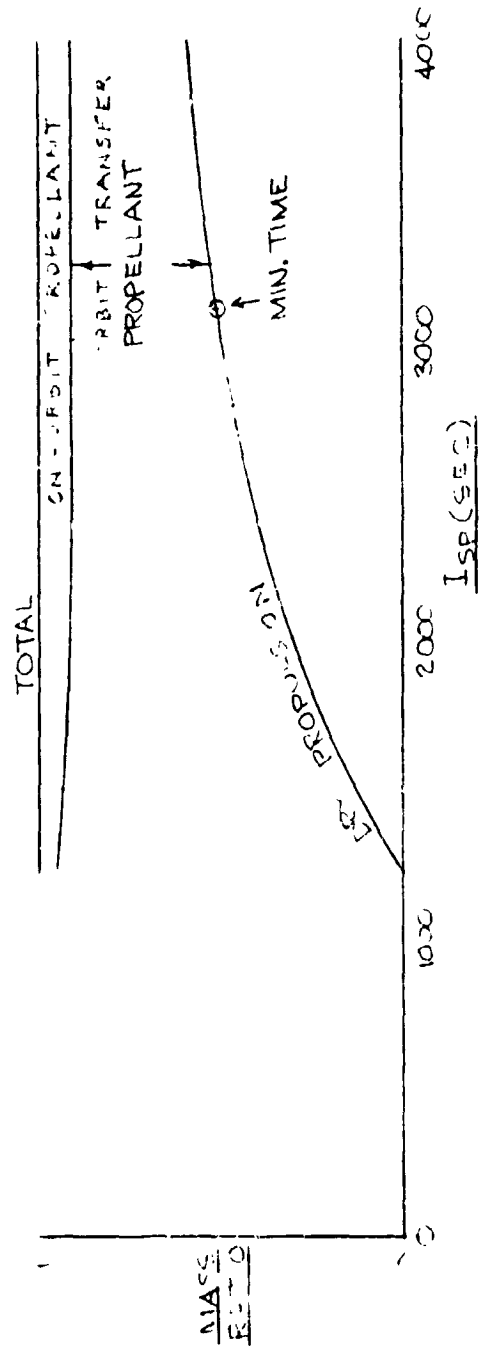


Figure 35. Propulsion Mass Breakdown for 50% Payload Fraction
(Case II η , $\alpha = 0.024$ kg/W, 10 Years)

ORIGINAL COPY
OF POOR QUALITY

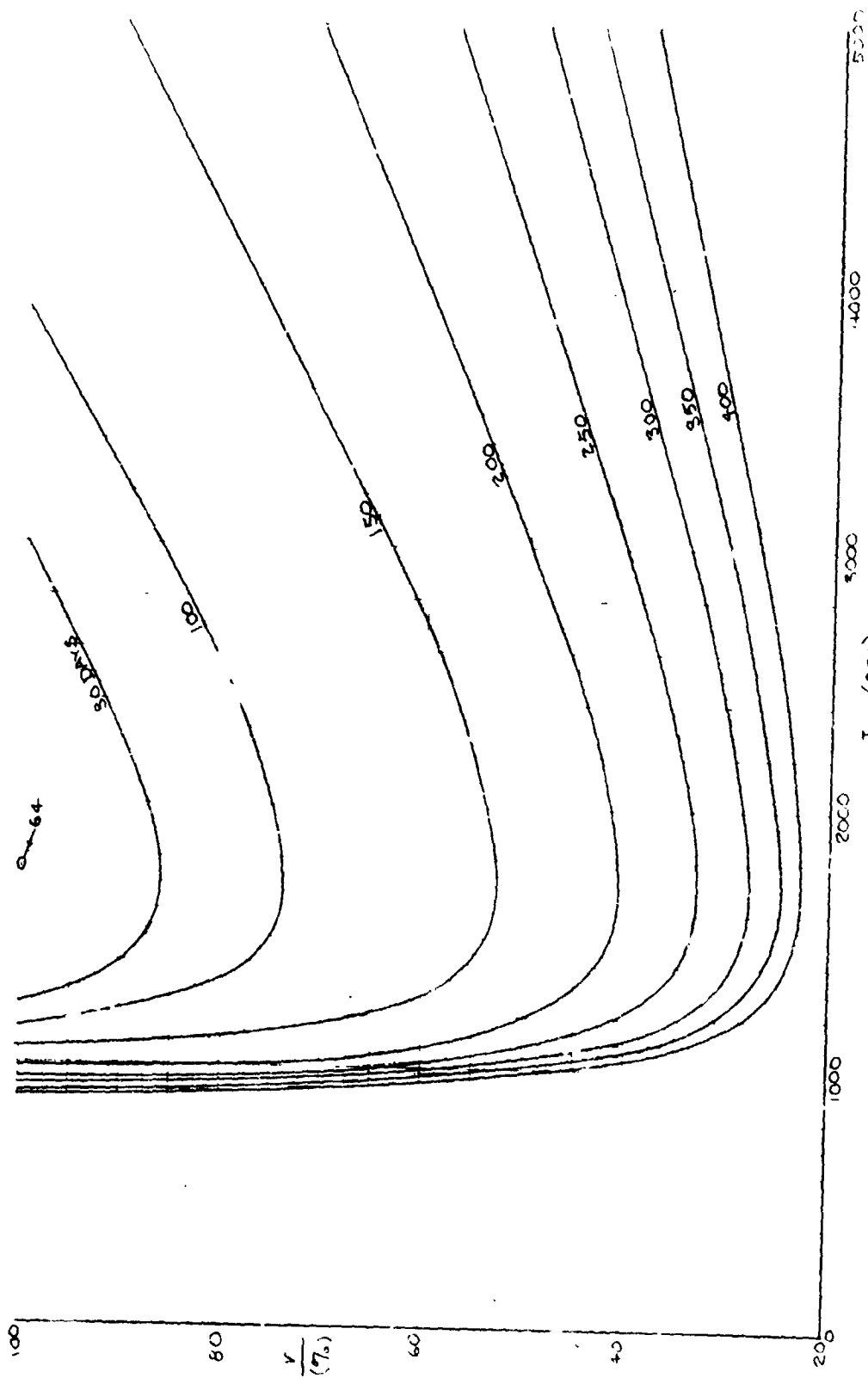


Figure 36. Effect of n and I_{sp} on Transfer Time for $\left(\frac{M_{EPS}}{M_{PL}}\right)_T = 2.0$

$$\left(\alpha = 0.024 \frac{\text{kg}}{\text{m}^2}, \beta = 150 \frac{\text{W}}{\text{m}^2}, \frac{M_{PL}}{A_{DL}} = 100 \frac{\text{kg}}{\text{m}^2}, 5 \text{ years}\right)$$

ORIGINAL PAGE IS
OF POOR QUALITY

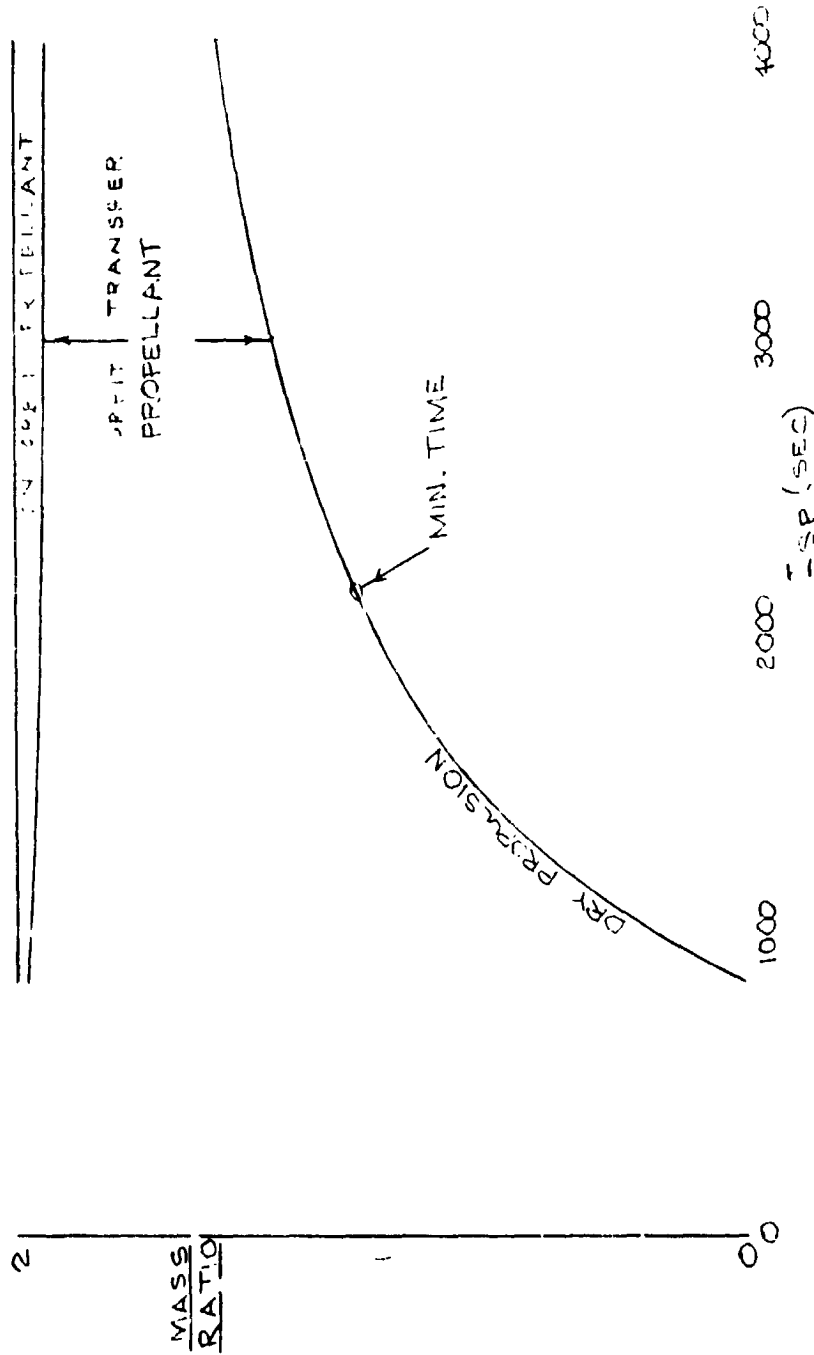


Figure 37. Propulsion Mass Breakdown for 33% Payload Fraction
(Case II η , $\alpha = 0.024$, 5 Years)

ORIGINAL ARTICLES
OF POOR QUALITY

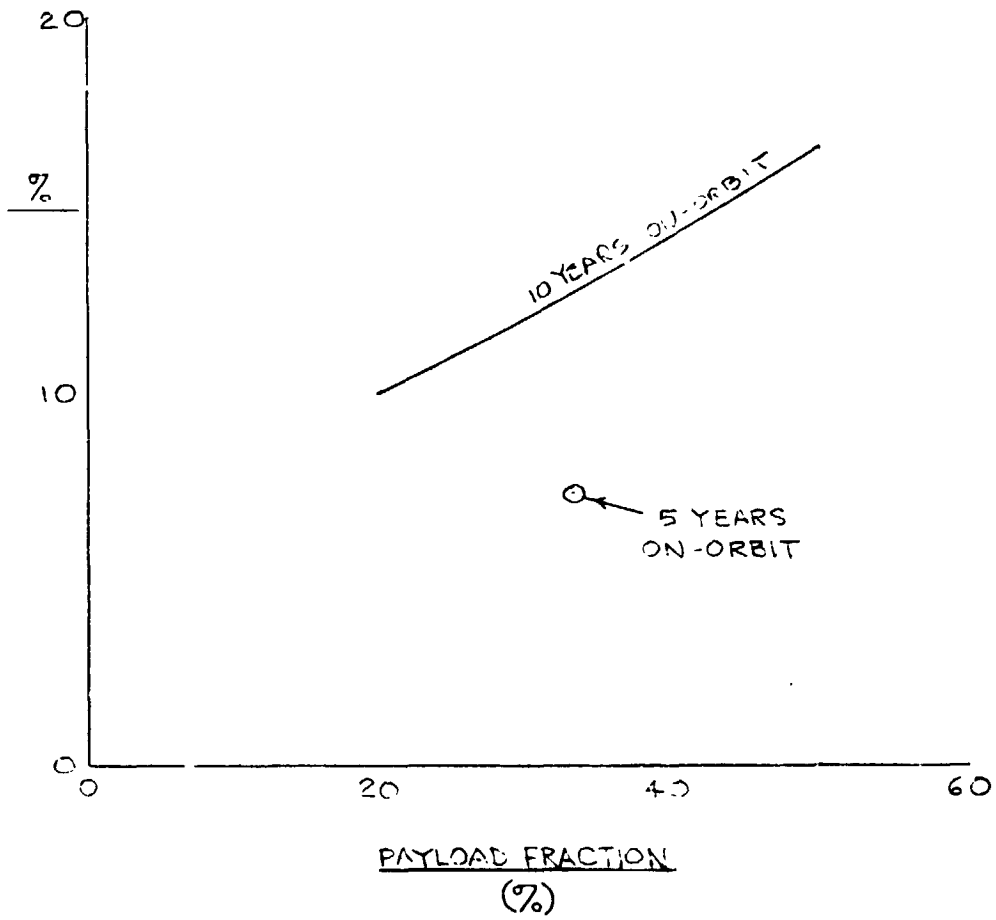


Figure 38. Percent of Total Propellant Used On-Orbit
(Case II $n, \alpha = 0.024, I_{sp}$ for Minimum Transfer Time)

ORIGINAL PAGE IS
OF POOR QUALITY

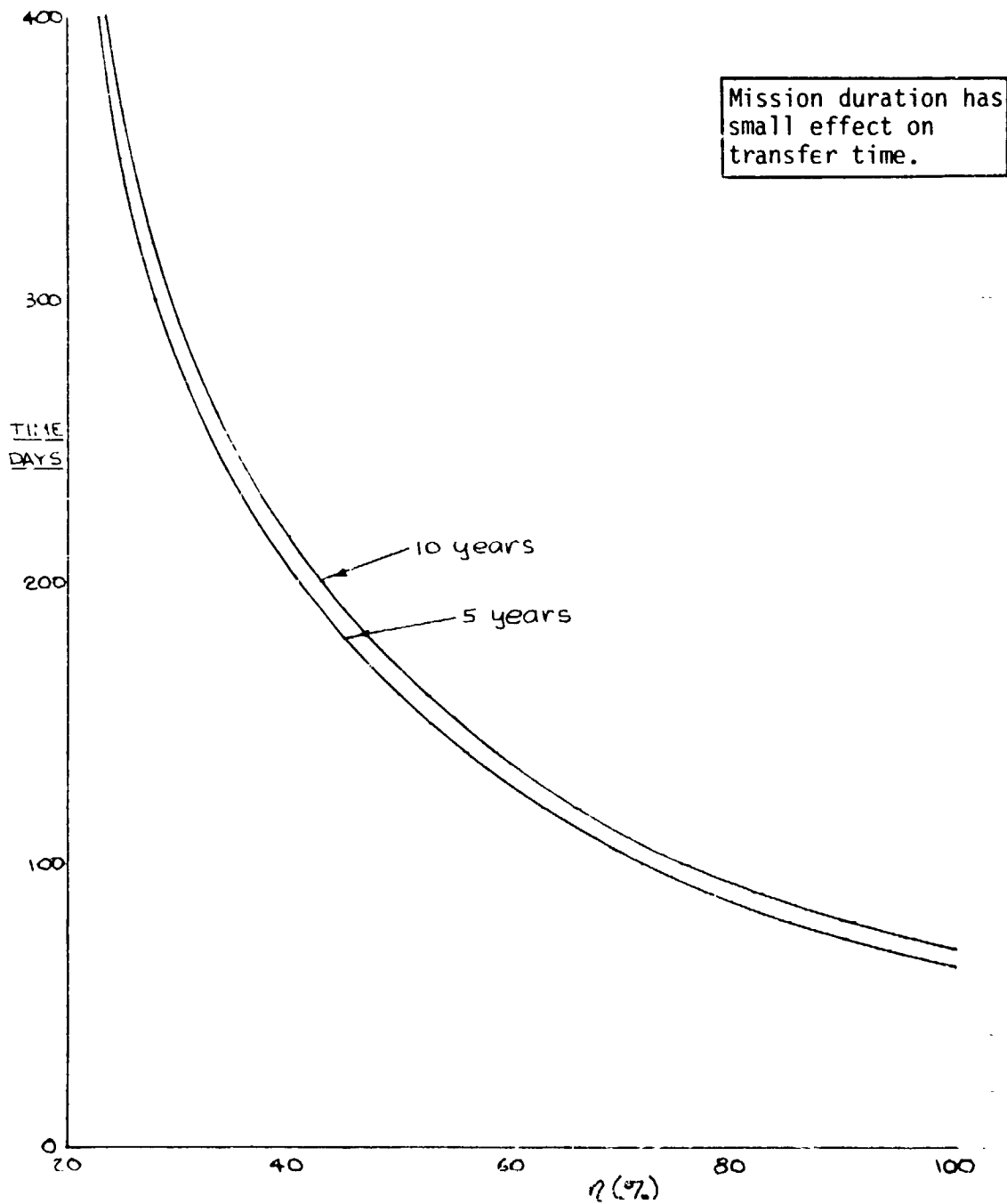


Figure 39. Comparison of Transfer Times for 5 and 10 Year Missions

$$\left(\alpha = 0.024 \frac{\text{kg}}{\text{W}}, \beta = 150 \frac{\text{W}}{\text{m}^2}, \frac{M_{\text{PL}}}{A_{\text{PL}}} = 100 \frac{\text{kg}}{\text{m}^2}, \text{Orbit Transfer } I_{\text{SP}} = 1750 \text{ sec}, \right.$$

$$\text{Auxiliary } I_{\text{SP}} = 3000 \text{ sec}, \left(\frac{M_{\text{FPS}}}{M_{\text{PL}}} \right)_T = 2.0)$$

ORIGINAL PAGE IS
OF POOR QUALITY

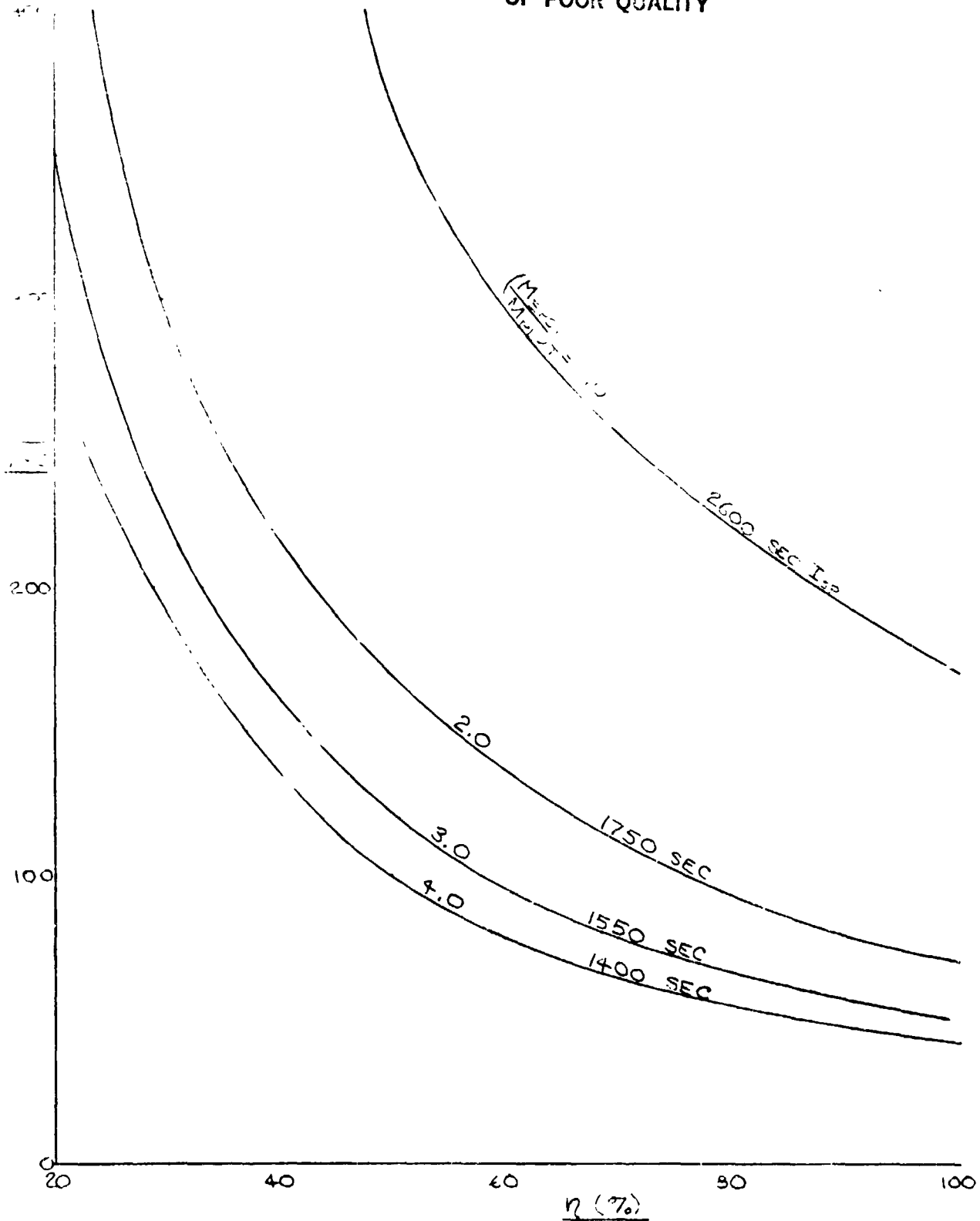


Figure 40. Effect of η on Transfer Time at Optimum I_{sp}

$$\left(\alpha = 0.024 \frac{\text{kg}}{\text{W}}, \beta = 150 \frac{\text{W}}{\text{m}^2}, \frac{M_{PL}}{A_{PL}} = 100 \frac{\text{kg}}{\text{m}^2}, 10 \text{ years} \right)$$

transfer time as a function of thruster efficiency at the optimum I_{SP} for the four different values of the total electric propulsion mass ratio. The corresponding optimum I_{SP} values are also shown. For the case of mass ratio equal to 2.0 at 50% efficiency, for example, the slope corresponds to a 3.7-day reduction in transfer time for a 1% improvement in thruster efficiency.

Figure 41 shows that transfer time varies essentially linearly with α . For a total electric propulsion mass ratio of 2.0 and a thruster efficiency of 45% at 1750 seconds I_{SP} , the slope at $\alpha = 0.024$ kg/W indicates a transfer time reduction of 20 days for a 10% reduction in α .

Figure 42 shows the power remaining after orbit transfer as a function of total EPS mass ratio, assuming the climb is conducted at optimum I_{SP} and Case II efficiency. In the mass ratio range of 2 to 4, the residual power ranges from 55 to 59% of the beginning of life value. At a mass ratio of 1.0, it is 50% of the initial value. The on-orbit power degradation is small. Table 7 compares the integrated fluence over a 10-year mission with that accumulated during orbit transfer and with the total fluence per 11 year solar cycle. The total on-orbit increment is about 2% of the orbit transfer value. Solar cell covers equivalent to 6 mils of fused silica were assumed for this calculation.

Table 7. Comparison of Orbit Transfer and On-Orbit Fluence Levels

$$\left(\frac{\text{meV electrons}}{\text{cm}^2} \right)$$

$\left(\frac{M_{EPS}}{M_{PL}} \right)_T$	Orbit Transfer	10-year Increment	Solar Flare	Total	Residual Power (%)
1.0	3×10^{16}	1.8×10^{14}	3×10^{14}	3.05×10^{16}	50
2.0	2.7×10^{16}	1.8×10^{14}	3×10^{14}	2.75×10^{16}	55
3.0	1.55×10^{16}	1.8×10^{14}	3×10^{14}	1.60×10^{16}	58
4.0	1.50×10^{16}	1.8×10^{14}	3×10^{14}	1.55×10^{16}	59

ORIGINAL PAGE IS
OF POOR QUALITY

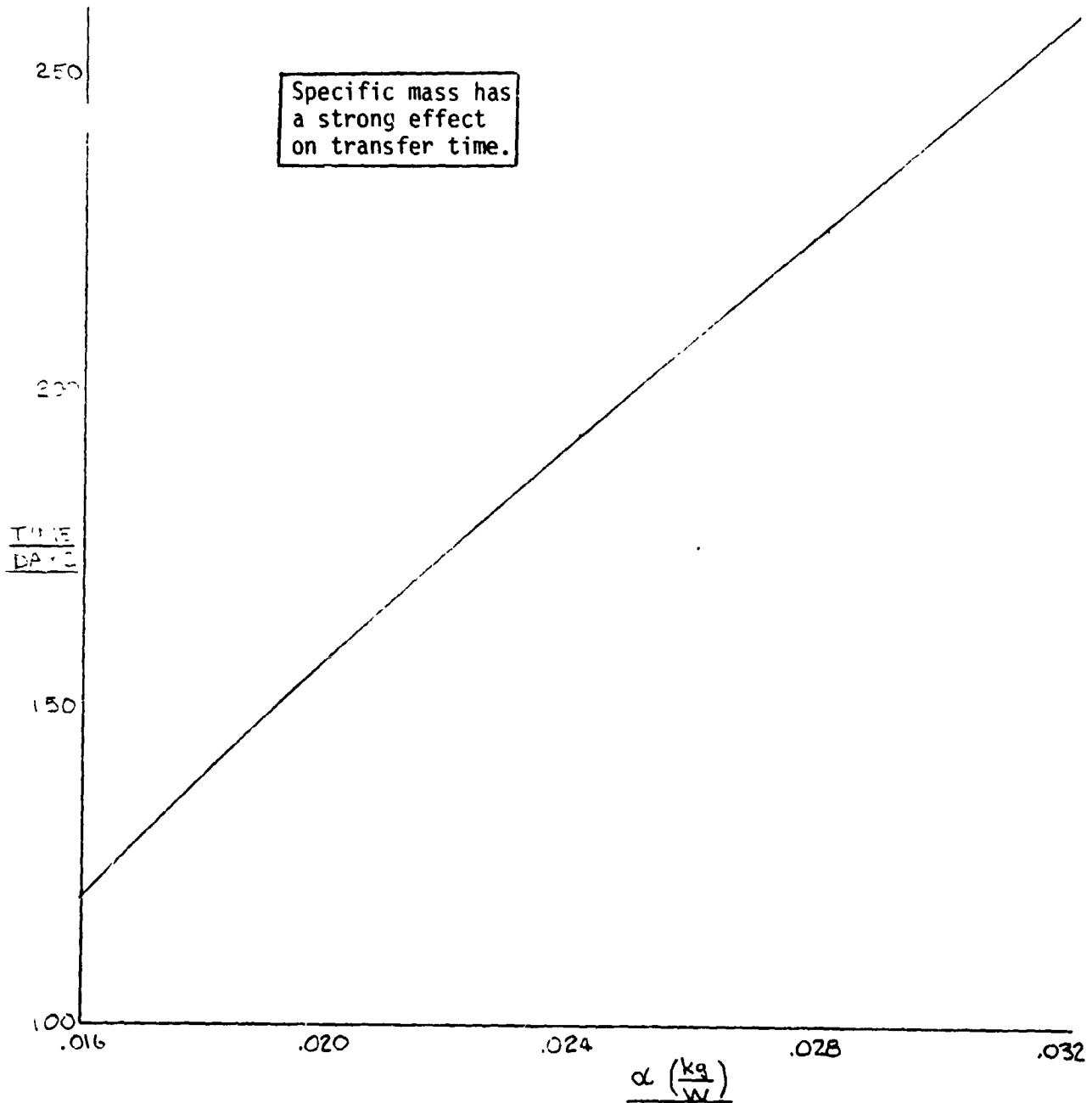


Figure 41. Effect of Specific Mass on Transfer Time for
Case II $\eta = 45\%$ at 1750 sec

$$\left[\beta = 150 \frac{W}{m^2}, \quad \frac{M_{PL}}{A_{PL}} = 100 \frac{kg}{m^2}, \quad \left(\frac{M_{EPS}}{M_{PL}} \right)_T = 2.0 \right]$$

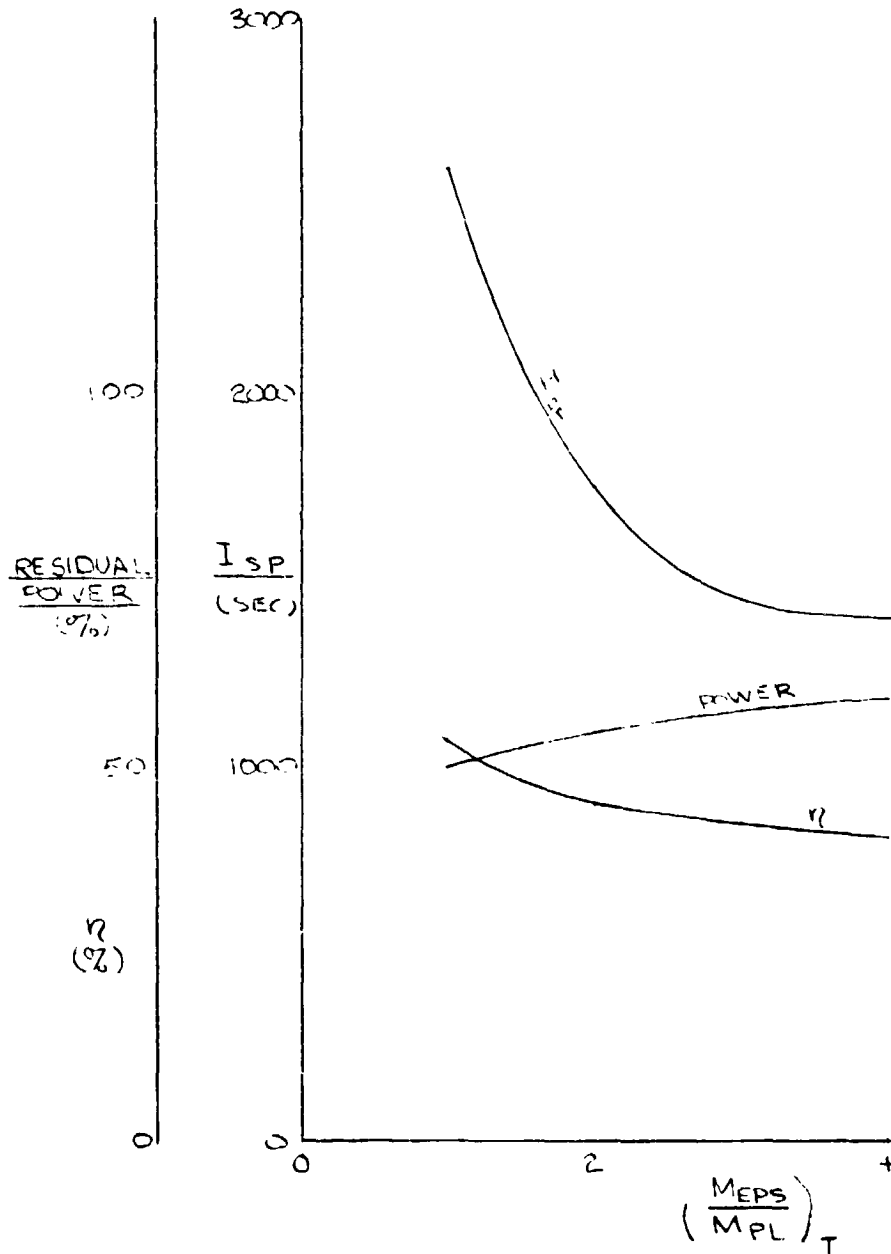


Figure 42. Residual On-Orbit Power for Optimum I_{SP} Transfer and Case II Efficiency
 $(\alpha = 0.024 \text{ kg/W}, \beta = 150 \text{ W/m}^2, M_{PL}/A_{PL} = 100 \text{ kg/m}^2, 10 \text{ years})$

2.8.2 Fast Orbit Transfer

The great attraction of electric propulsion is its ability to transfer large payload fractions and its greatest drawback is long transfer time. It is interesting to examine the payload penalty associated with fast orbit transfer for advanced technology thruster having the low values of α and the improved efficiency that might be anticipated.

The resistojet offers high efficiencies, in the range of 80 to 90% but is limited in I_{SP} to values less than 1000 seconds. The pulsed inductive thruster operates in the neighborhood of 50% efficiency in the range of 1500 to 2500 seconds. Both of these thruster types have lightweight power conditioning and appear to be possible candidates for fast transfer from Shuttle orbit to GEO.

To assess this possibility quantitatively, the parameter α was reduced from the value 0.024 kg/W, used previously, to 0.012 kg/W, the Case III efficiency function was used for the pulsed inductive thruster and two resistojet cases were examined: 90% at 900 seconds I_{SP} and 100% at 1000 seconds I_{SP} . The payload fraction was varied from 10% to 50%.

Figures 43 through 48 show the results of the transfer time calculations, assuming a 10-year duration on-orbit; the corresponding propellant breakdown plots are shown in Figures 49 through 54. These figures have the same characteristics seen in the previous section. Note, however, the steep slope of the transfer time curves at low specific impulse. Mission sensitivity to thruster operating characteristics in this region is extremely high. This will require strict adherence to performance specifications for any thruster operating in this range.

Figure 55 summarizes the 10-year on-orbit propellant fraction used for stationkeeping and disposal. The values range from 6% of the total propellant at 10% payload fraction, to 16% at 50% payload fraction. This increase is due to the decreased orbit transfer propellant requirement that results from the increase in I_{SP} for minimum transfer time as the payload fraction increases. This trend is seen in Figure 56 which shows the effect of payload fraction on the minimum transfer time and also on the corresponding I_{SP} for the assumed Case III efficiency.

At 10% payload fraction the I_{SP} for minimum transfer time is 1300 seconds and the time is only 31 days. This condition, however, is unrealistic

ORIGINAL PAGE IS
OF POOR QUALITY

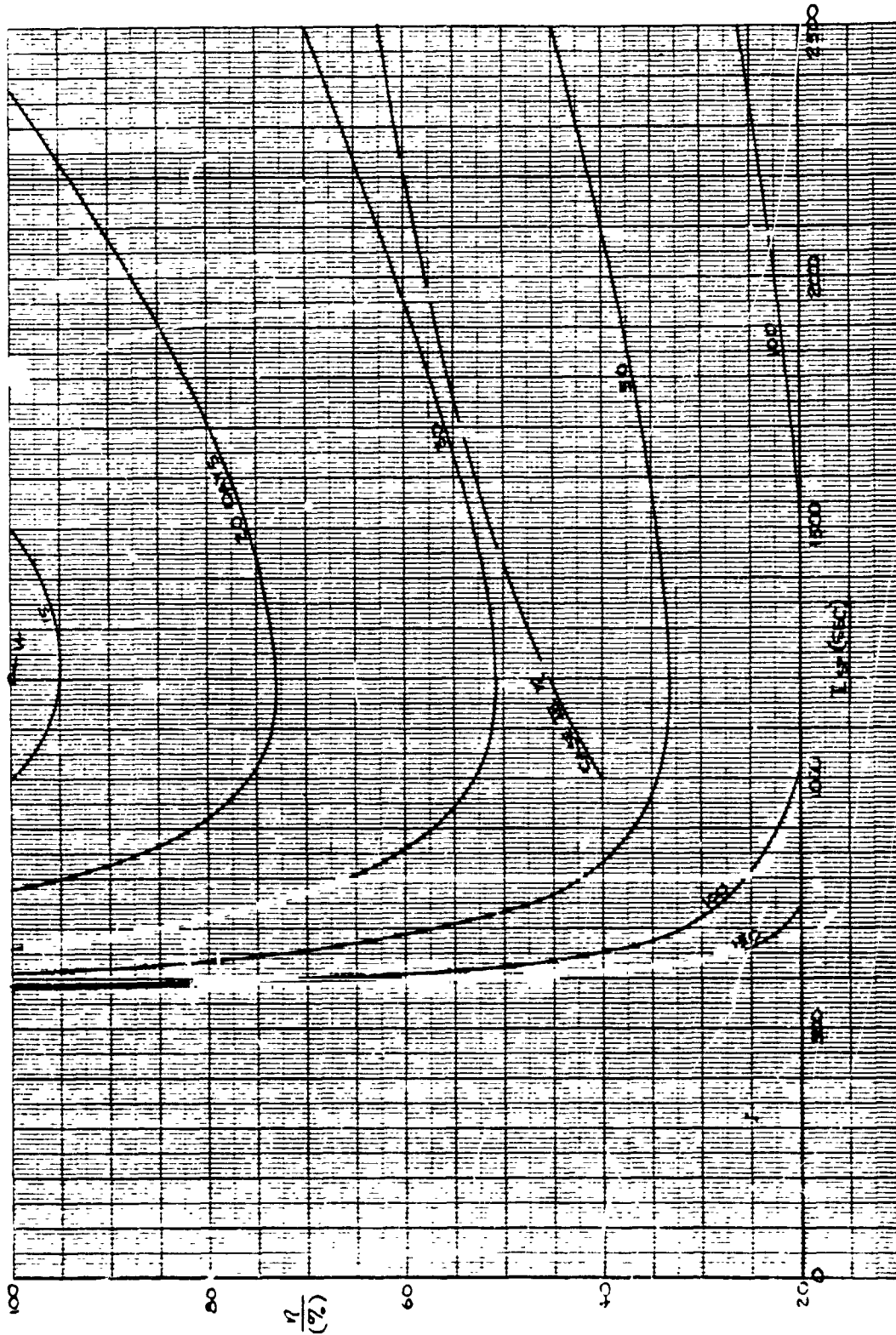


Figure 43. Transfer Time Tradeoff - 10% Payload Fraction
($\alpha = 0.012$ kg/W, 10 Years)

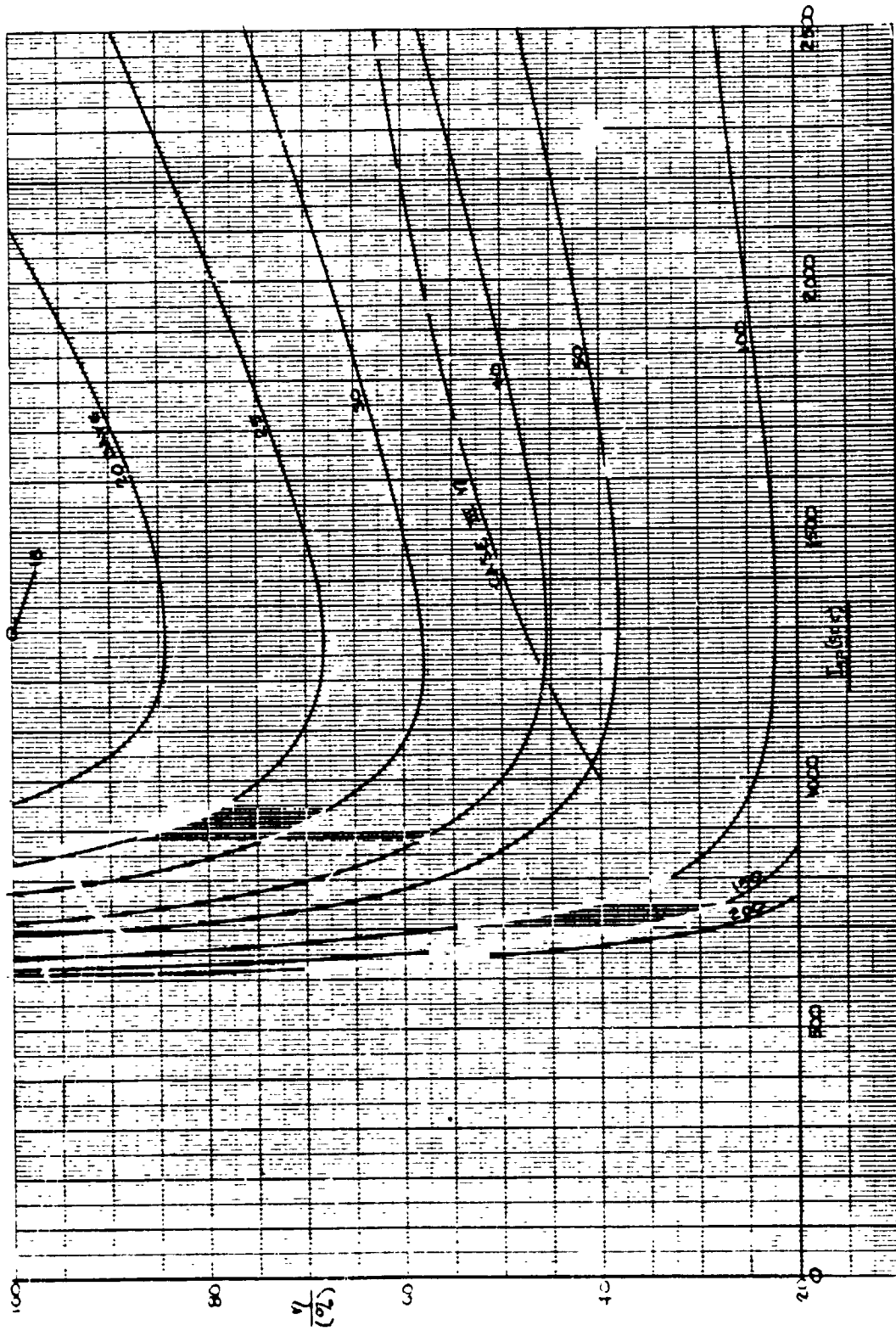


Figure 44. Transfer Time Trade-Off - 15% Payload Fraction
($\alpha = 0.012$ kg/W, 10 Years)

ORIGINAL PAGE IS
OF POOR QUALITY

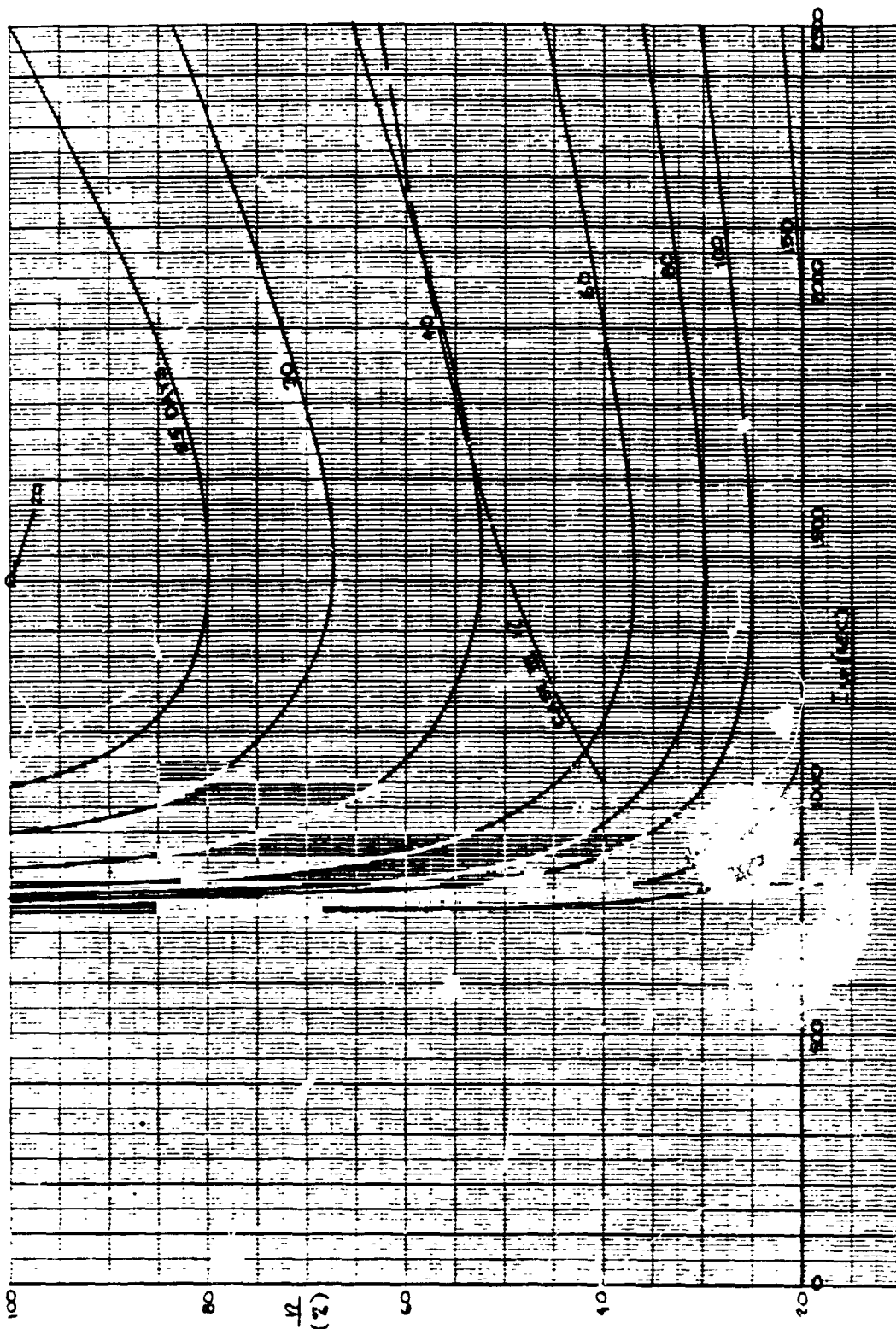


Figure 45. Transfer Time Trade-Off - 20% Payload Fraction
($\alpha = 0.012$ kg/W, 10 Years)

ORIGINAL PAGE IS
OF POOR QUALITY

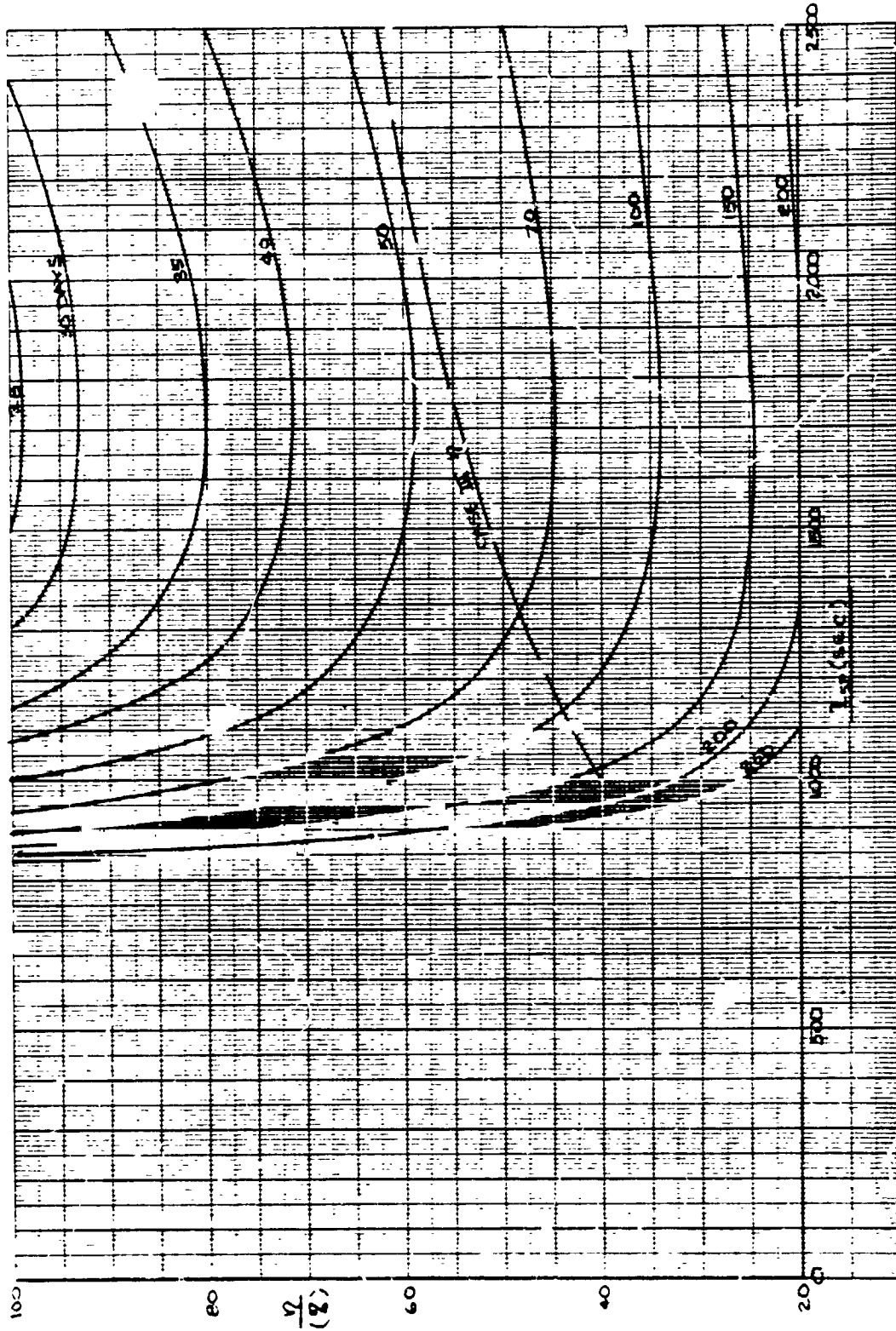


Figure 46. Transfer Time Trade-Off - 30% Payload Fraction
($\alpha = 0.012$ kg/W, 10 Years)

ORIGINAL PAGE IS
OF POOR QUALITY

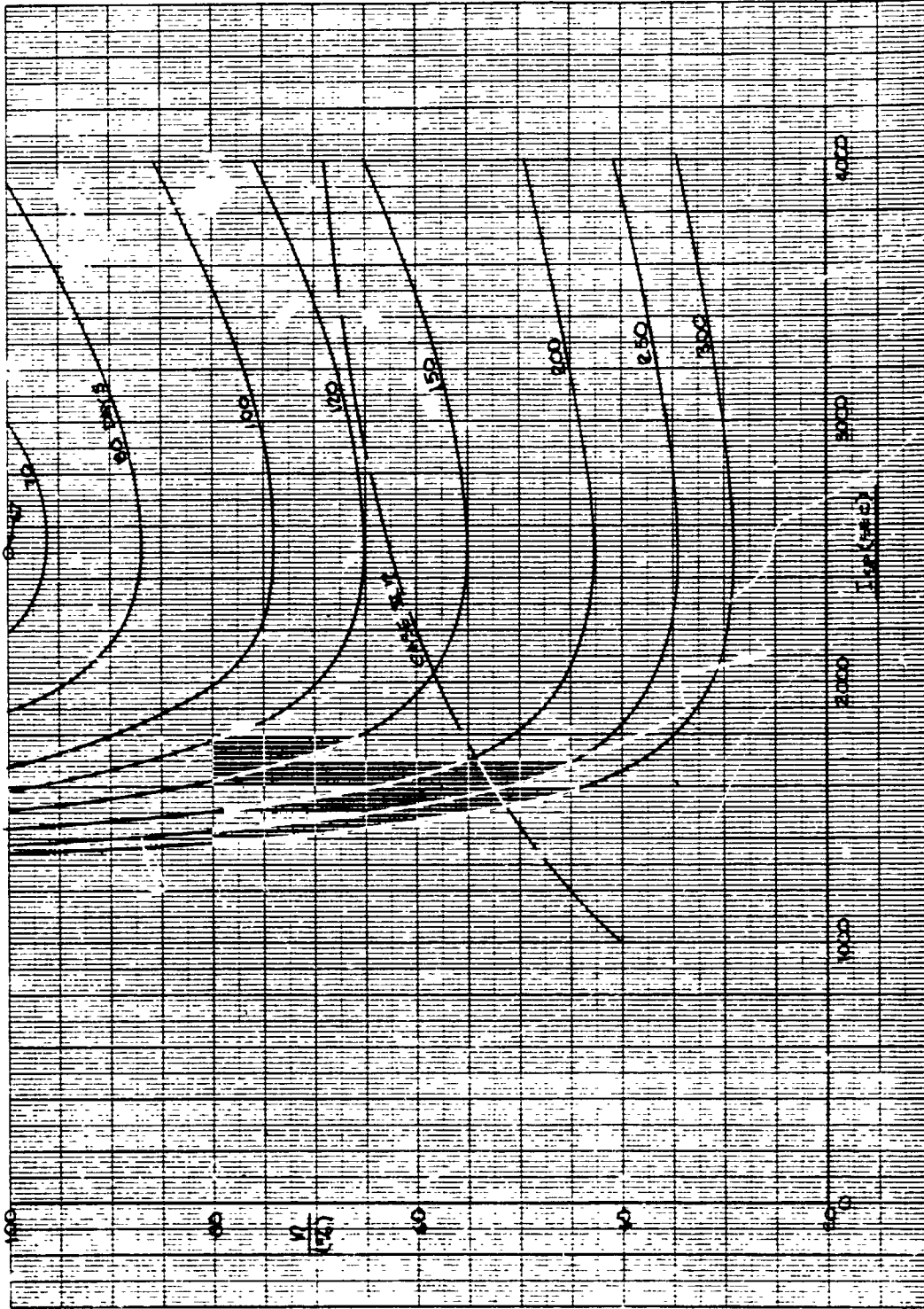


Figure 48. Transfer: Time Tradeoff - 50% Payload Fraction
($\alpha = 0.012 \text{ k} \cdot \text{W}, 10 \text{ years}$)

C-2

ORIGINAL PAGE IS
OF POOR QUALITY

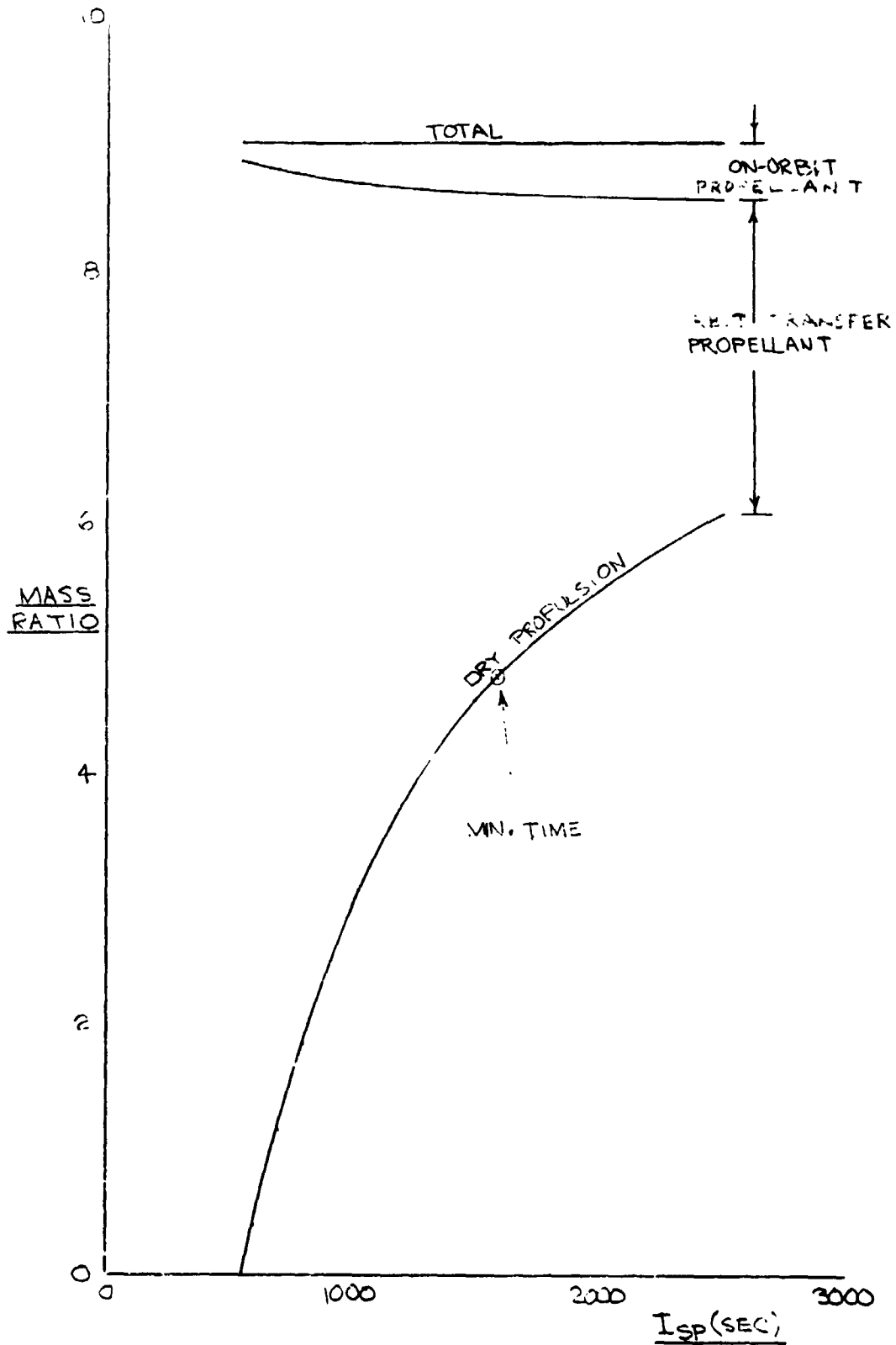


Figure 49. Propulsion Mass Breakdown for 10% Payload Fraction
(Case III $n, \alpha = 0.012$ kg/W, 10 Years)

ORIGINAL PAGE IS
OF POOR QUALITY

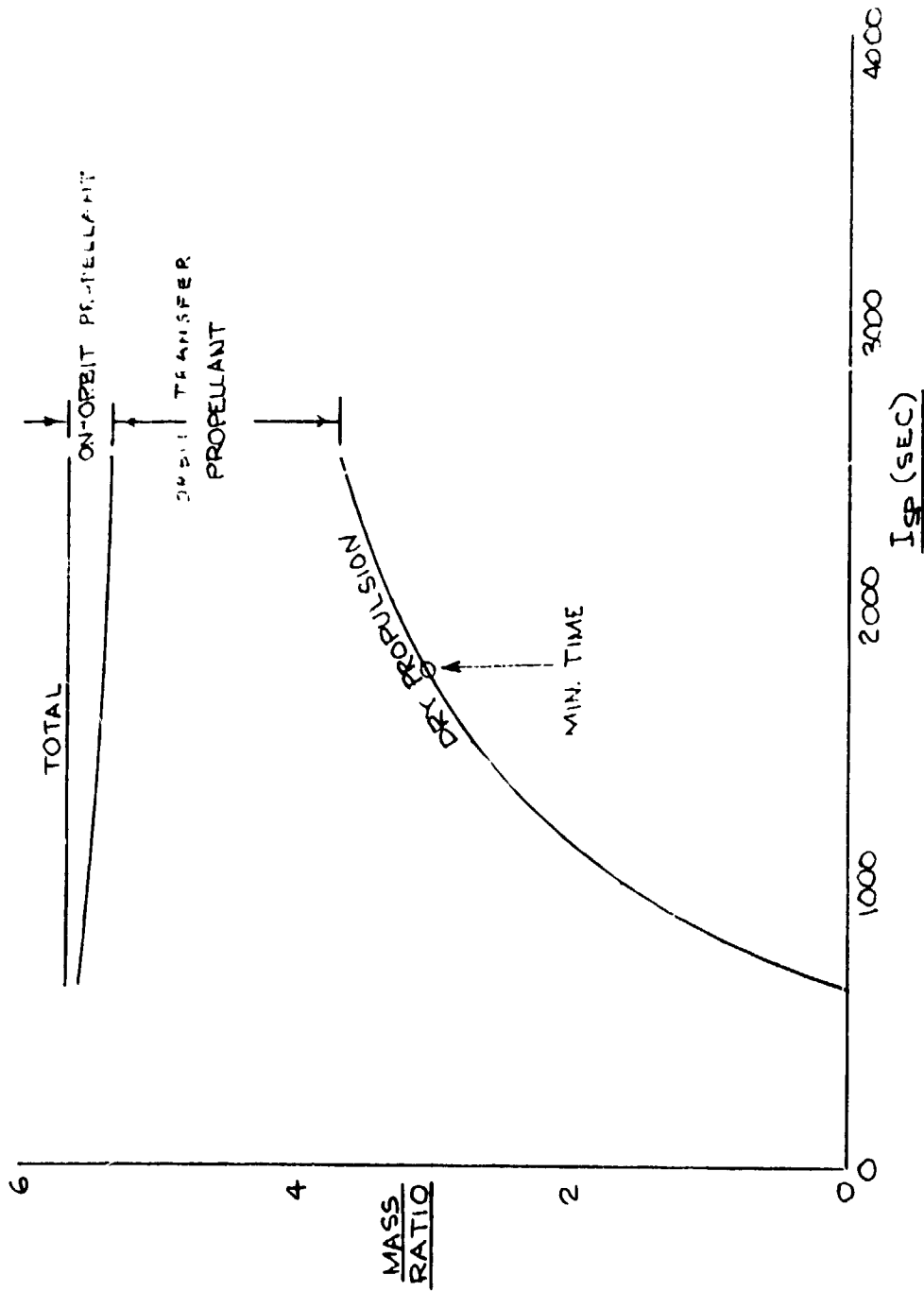


Figure 50. Propulsion Mass Breakdown for 15% Payload Fraction
(Case III η , $\alpha = 0.012$ kg/W, 10 Years)

ORIGINAL PAGE IS
OF POOR QUALITY

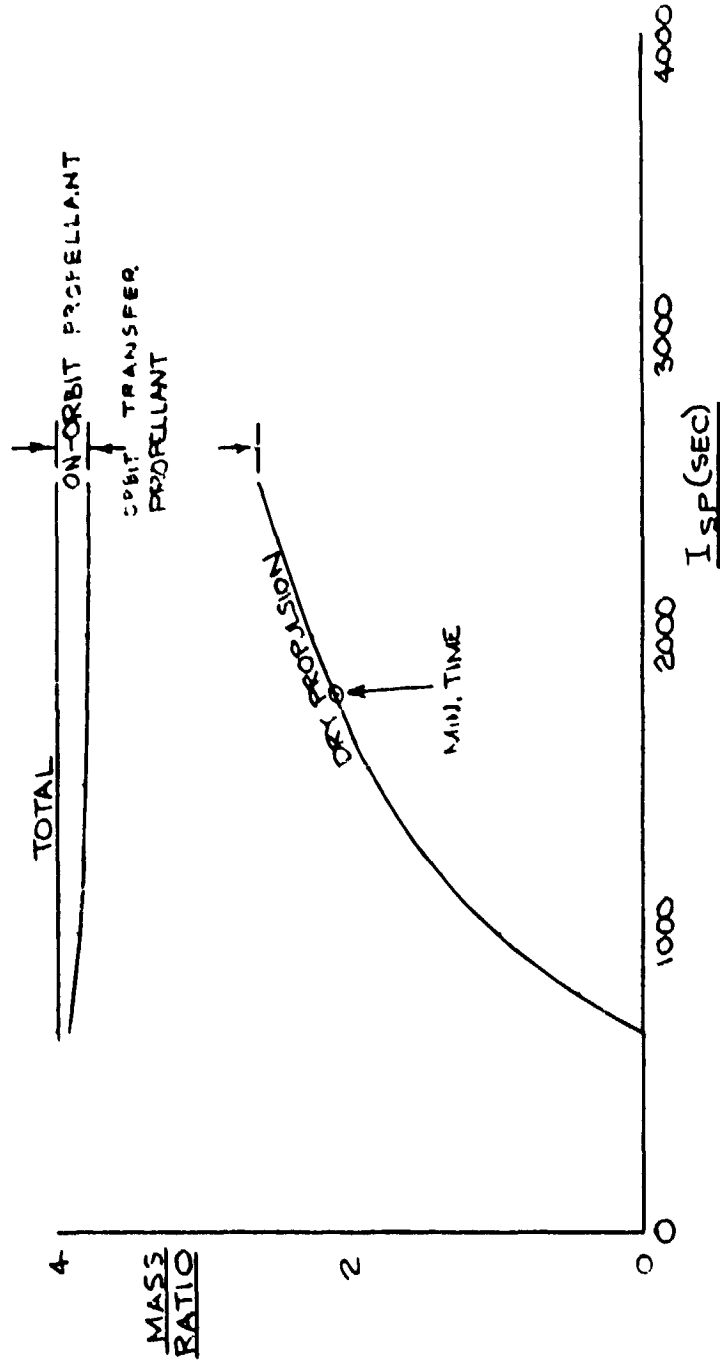


Figure 51. Propulsion Mass Breakdown for 20% Payload Fraction
(Case III η , $\alpha = 0.012$ kg/W, 10 Years)

ORIGINAL PAGE IS
OF POOR QUALITY

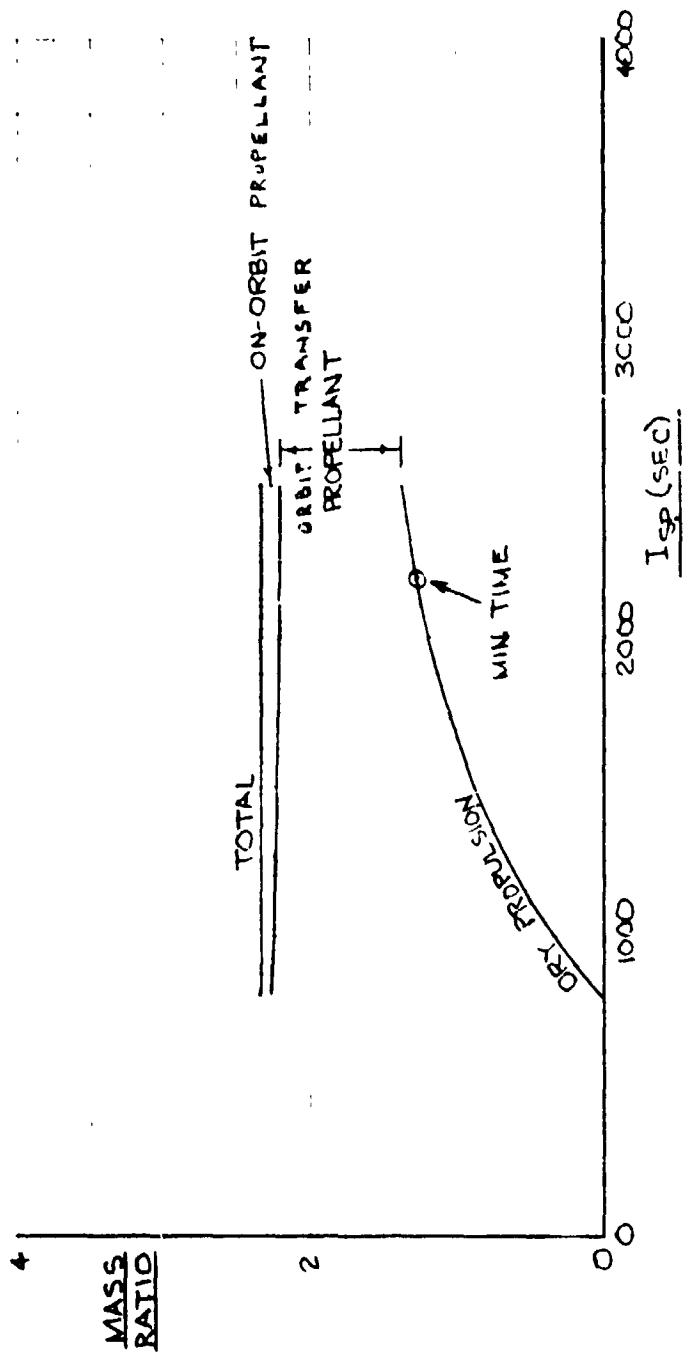


Figure 52. Propulsion Mass Breakdown for 30% Payload Fraction
(Case III η , $\alpha = 0.012$ kg/W, 10 Years)

ORIGINAL FACE IS
OF POOR QUALITY

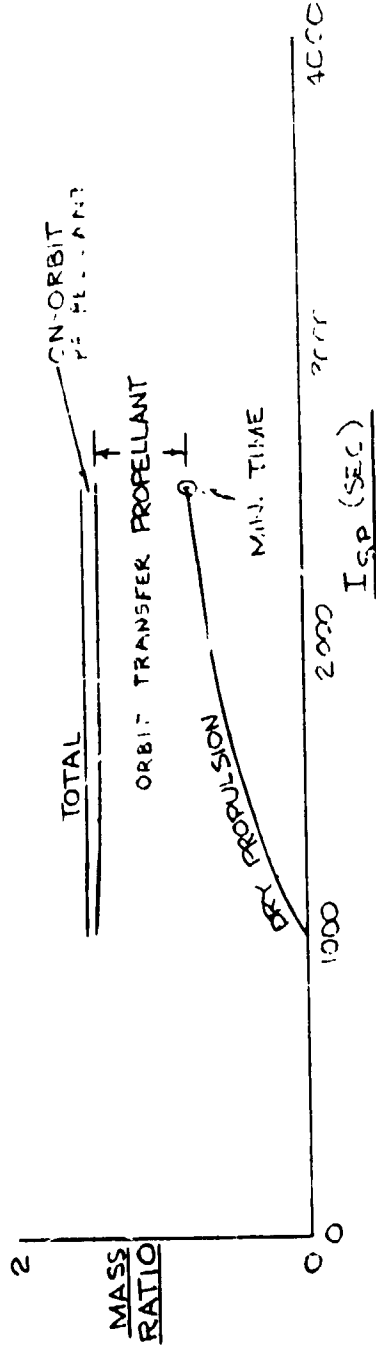


Figure 53. Propulsion Mass Breakdown for 40% Payload Fraction
(Case III η , $\alpha = 0.012$ kg/W, 10 Years)

ORIGINAL PAGE IS
OF POOR QUALITY

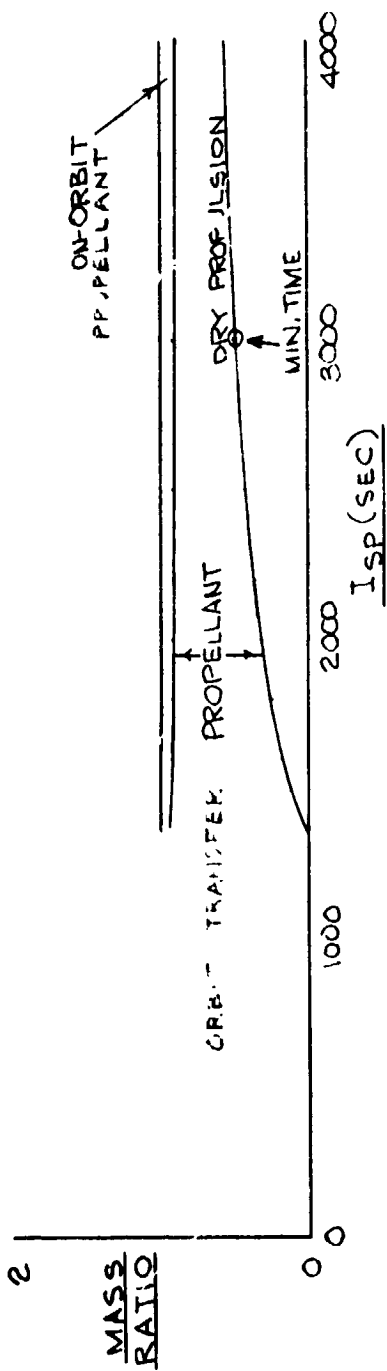


Figure 54. Propulsion Mass Breakdown for 50% Payload Fraction
(Case III n , $\alpha = 0.012$ kg/W, 10 Years)

ORIGINAL PAGE IS
OF POOR QUALITY

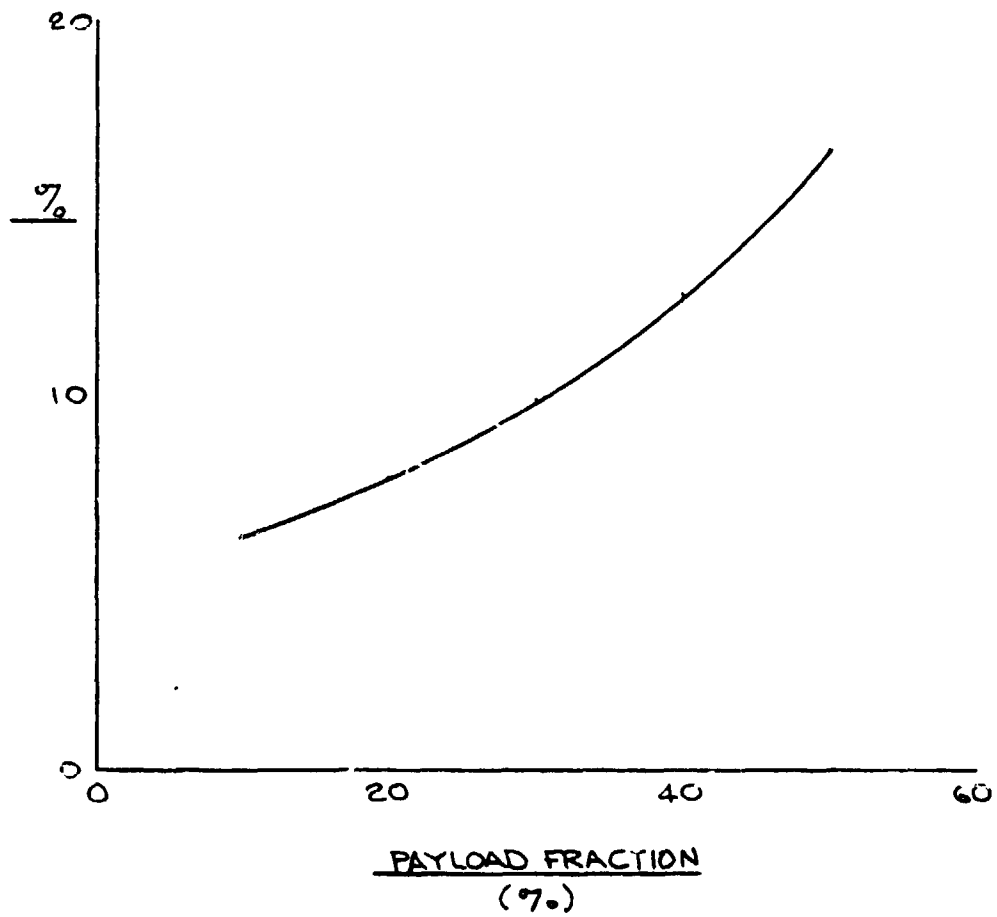


Figure 55. Percent of Total Propellant Used On-Orbit
(Case III $n, \alpha = 0.012$ kg/W, 10 Years)

ORIGINAL PAGE IS
OF POOR QUALITY

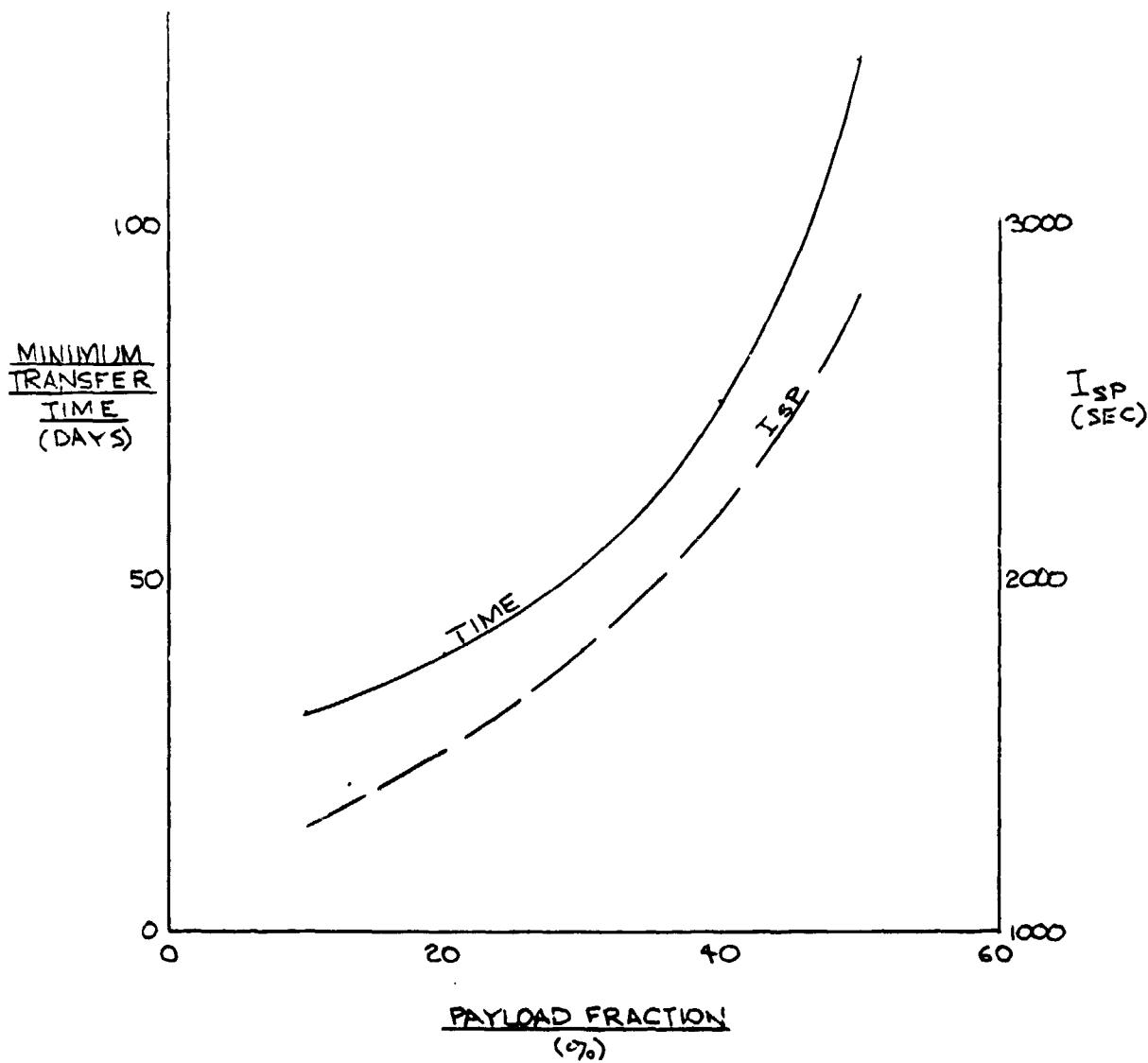


Figure 56. Effect of Payload Fraction on Minimum Transfer Time and Corresponding I_{sp}
(Case III η , $\alpha = 0.012$ kg/W, 10 Years)

because payload fractions as low as 10% can be managed by chemical propulsion with transfer times measured in hours rather than days. To be attractive, electric propulsion must transfer payload fractions that are significantly greater than the maximum capability of chemical propulsion.

A reasonable lower limit for payload fractions of interest for electric propulsion is 20%. Figure 56 shows a 40-day transfer time requirement for the plasma thruster at this payload fraction. Transfer time increases rapidly with payload fraction; at 30% it is 52 days, it is 75 days at 40% and at 50% payload fraction it has increased to 123 days. However, even these longer times are short compared to those previously indicated for conventional electric propulsion. The transfer time reduction of more than 50% is due both to the high thruster efficiencies of the Case III efficiency relation and the low value of specific mass α for the pulsed inductive plasma thruster.

The resistojet is capable of high efficiencies at I_{sp} values that are large compared to chemical rockets and low relative to electric thrusters that use either magnetic or electric fields for propellant acceleration. Conversion of thermal to kinetic energy is of the order of 90% until the I_{sp} limit fixed by material properties and heat loss is approached. For hydrogen propellant this might be about 900 seconds. Thus the resistojet range for the performance maps in Figures 43 through 48 is to the left of the optimum I_{sp} .

Figure 57 summarizes these zones of the performance maps for transfer times of 20, 30, 50 and 100 days. Again, 20% payload fraction is taken to be the minimum value of interest for electric propulsion. This limit and the maximum I_{sp} of 900 seconds are shown in Figure 57 for 90% thruster efficiency. For 20% propellant fraction the trip time is about 30 days. If the I_{sp} were reduced to 800 seconds, the time would be 50 days.

It is also seen in Figure 57 that trip time increases more rapidly with payload fraction for the resistojet than it does for the pulsed inductive thruster. For example, at 30% payload fraction it has increased to 100 days as compared to 52 days for the pulsed inductive thruster. Figure 58 shows this effect as a function of payload fraction for 90% efficiency at 900 seconds and also for the limiting case of 100% efficiency at 1000 seconds.

ORIGINAL PAGE IS
OF POOR QUALITY

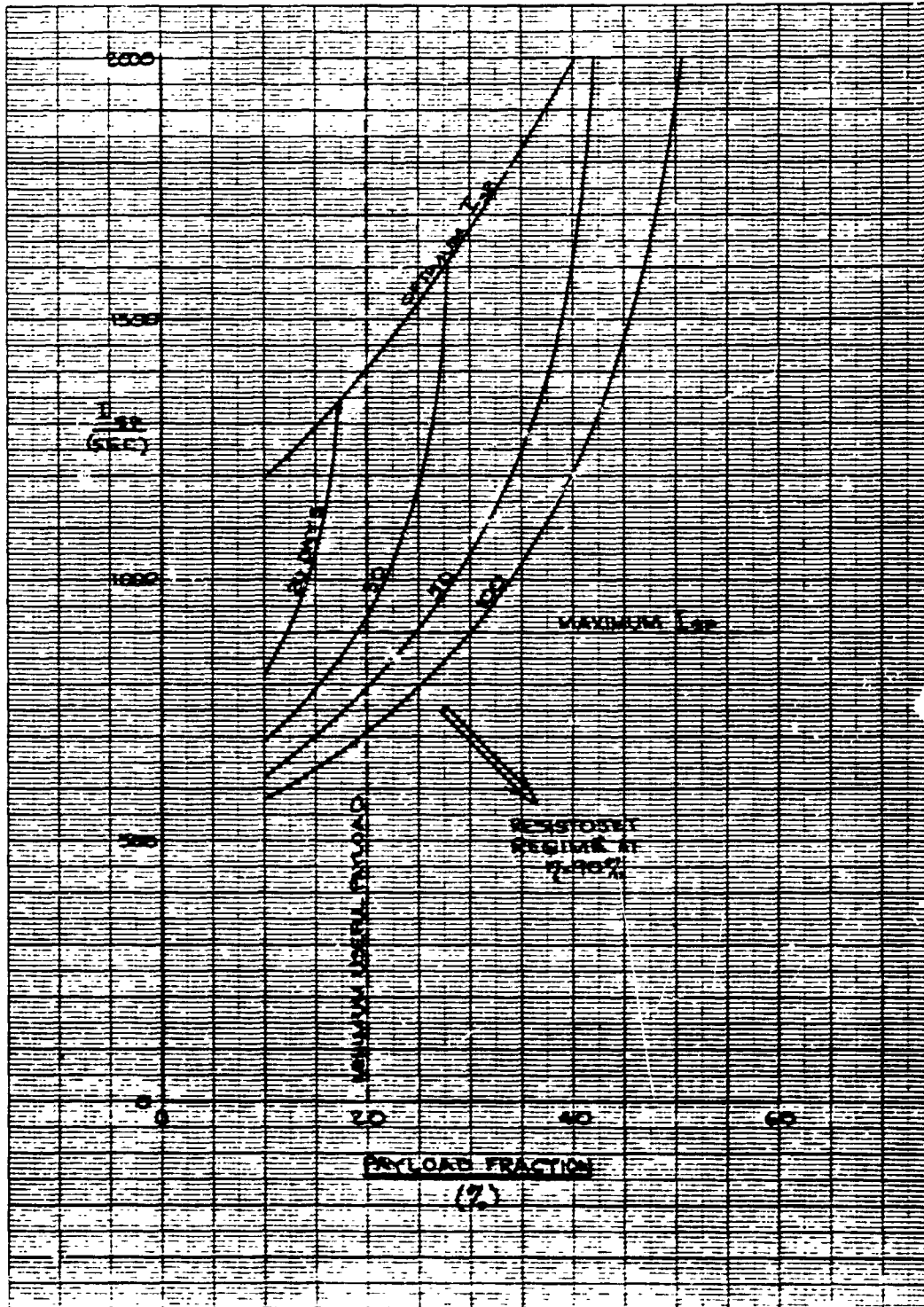


Figure 57. Resistojet Limitations for LEO to GEO Mission
($\alpha = 0.012 \text{ kg/W}$, 10 Years)

ORIGINAL PAGE IS
OF POOR QUALITY

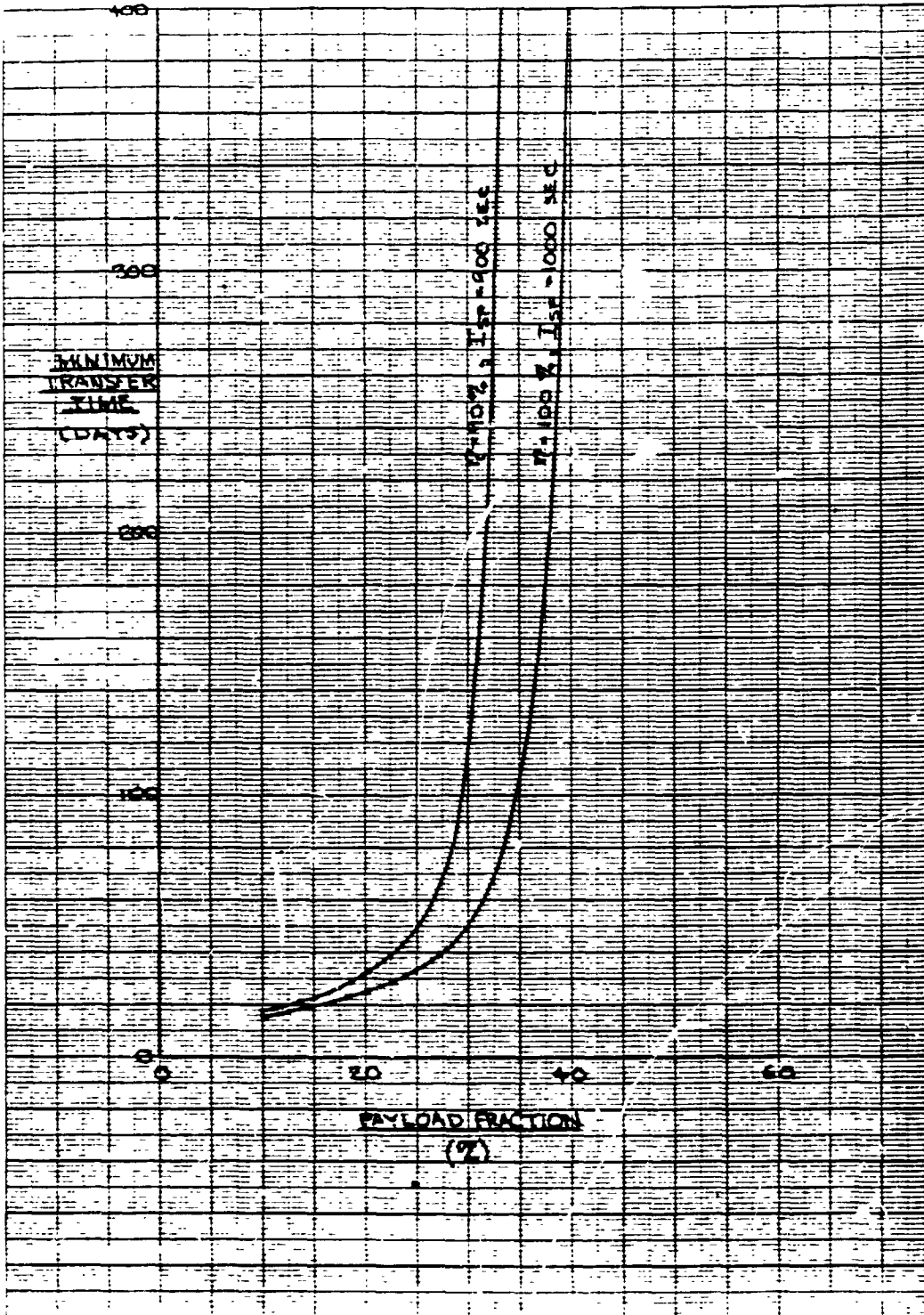


Figure 58. Effect of Payload Fraction on Resistojet Transfer Time
($\alpha = 0.012 \text{ kg/W}$, 10 Years)

Thus with foreseeable increases in thruster efficiency and reduction in specific mass (Case III efficiency relation and $\alpha = 0.012$ kg/W), Shuttle orbit to GEO transfer time can be reduced to 40 days for 20% payload fraction. At 50% payload fraction, the corresponding transfer time is only 123 days. Resistojet performance is only attractive for LEO to GEO transfer missions at low payload fractions. Its transfer times quickly become prohibitive with increasing payload fraction.

3. INTEGRATED PROPULSION ANALYSIS

The purpose of this investigation is to identify potential advantages of using electric propulsion not only for orbit raising to geosynchronous orbit but also for additional (auxiliary) functions that will be required during the ascent and orbital phases of the mission. These functions can be accomplished by using the EPS as an integrated part of the space vehicle rather than as a separate orbit transfer vehicle only.

3.1 SCOPE OF STUDY

For the integrated propulsion system, functions to be considered in addition to orbit transfer include:

- 1) Stationkeeping
- 2) Orbital repositioning
- 3) Spacecraft disposal at the end of the mission to an orbital altitude that precludes future interference with other satellites
- 4) Attitude control, including correction of perturbing torques due to gravity gradient and aerodynamic effects
- 5) Propulsion power sharing with the payload and with spacecraft housekeeping subsystems

Of these, the first three functions involve translation ΔV maneuvers, the fourth function, rotational maneuvers.

Results of the analysis are expressed in terms of weight and cost savings that result primarily from reduced propellant expenditure on orbit with the concomitant, even greater, reduction of propellant mass required for LEO to GEO transfer. It is these savings that translate into a reduction of total launch weight and, consequently, in Shuttle transportation cost savings.

Another important aspect of integrated propulsion is the question of thruster size and power requirements for adequately performing the auxiliary thrust functions, especially the correction of large disturbance torques. Also, the impact of sharing available power effectively between thrust operations and operation of other power consumers must be considered.

In addition to the integrated electric system, the use of a chemical auxiliary propulsion system is considered and the possible combination of electric and chemical thruster operations is also examined.

3.1.1 System Concept and Assumptions

The principal considerations in this investigation of integrated EPS functions are the following:

- 1) The orbit transfer from LEO to GEO is performed by means of a primary electric propulsion system.
- 2) Of primary interest are spacecraft of a size, i.e., total mass and dimensions, consistent with a single Shuttle launch rather than requiring multiple launches and assembly in orbit. The results, however, should be applicable for spacecraft requiring several launches.
- 3) The primary electric propulsion system is designed to exercise thrust vector control, by thruster gimbaling or thrust vector steering, as well as three-axis attitude control that can be done with moderate control torques. Auxiliary control will be provided to correct large disturbance torques during primary thrust operation and, in general, to perform attitude control during primary thrust off-periods.
- 4) Questions pertaining to attitude control of specific spacecraft configurations are generally not addressed. Also, questions of large structure deformation due to thrust forces and torques, and dynamic interactions, addressed in other recent studies, e.g., by Boeing Aerospace Company, are considered beyond the scope of this study task (Reference 2).
- 5) It is assumed that a major portion of the power available initially during LEO to GEO transfer will still be available for use by the EPS during the orbital mission phase, i.e., solar array degradation due to radiation damage during transfer will be about 4%.
- 6) Payload and spacecraft housekeeping functions may use a major part of the power available on orbit, thus imposing possible constraints on EPS thrust operations by power sharing.
- 7) North-south and east-west stationkeeping are to be performed without causing a change in the spacecraft nominal orientation, while orbital repositioning can be done by the main thrusters utilized during orbital transfer, if necessary by reorientating the spacecraft from its normal stationkeeping attitude. Final disposal can be done by either the main thrusters or the auxiliary stationkeeping thrusters.

- 8) Primary as well as auxiliary thrusters must be located and orientated so as to avoid or minimize thrust plume impingement on spacecraft appendages such as solar panels. However, details of thruster placement and articulation are not addressed during this task.
- 9) Attitude control torque requirements to control major disturbances are derived by extrapolation from existing data in the literature, e.g., Reference 2.
- 10) The state of the art Isp for auxiliary electric propulsion, 3000 seconds, is used for all calculations. Optimization to other values is not useful because of the low ratio of secondary to primary propulsion total impulse.

3.1.2 Spacecraft Description

This study makes use of results obtained from previous and concurrent studies of auxiliary electric propulsion systems on large space structures performed by Boeing Aerospace Company (Reference 2) under NASA Lewis Research Center Contract. Recent studies by TRW under NASA-LeRC and USAF Rocket Propulsion Laboratory contracts of auxiliary propulsion systems (References 8 and 9) also provide useful source data.

Data from the Boeing APS study used in this task include:

- Mass properties of various spacecraft structures
- Disturbance torque characteristics
- Attitude control and maneuver requirements
- Thruster sizing and placement
- Propulsion system design characteristics and propellant mass estimates

A wide range of spacecraft configuration categories, masses and dimensions are covered in the Boeing report, with emphasis on large structures that require multiple Shuttle launches and assembly in orbit. For the present analysis data applicable to a class of intermediate-sized vehicles with nearer-term mission application prospects were selected.

The data used pertain to a spacecraft category termed "modular antenna structure" (see Figure 59) with a mass ranging from 2000 to 27,000 kg. Spacecraft characteristics in the lower mass range are

ORIGINAL PAGE IS
OF POOR QUALITY

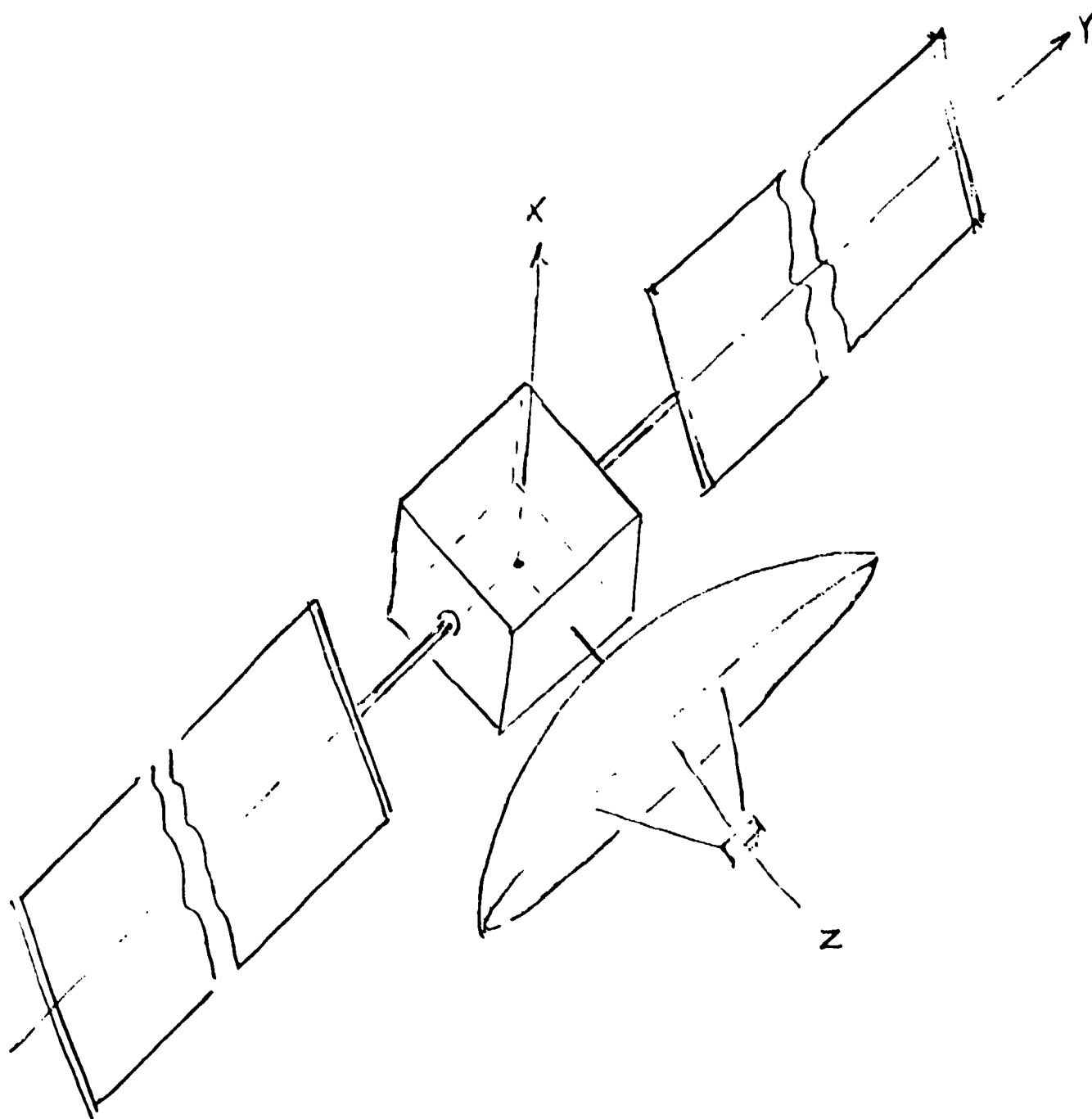


Figure 59. Reference Generic Spacecraft Configuration
(Based on Boeing Study, Reference 2)

compatible with a single Shuttle launch. The one-axis gimballed solar arrays provide primary propulsion power of several hundred kW. This implies array sizes of several thousand square meters with tip-to-tip dimensions of hundreds of meters. Data for this spacecraft class are presented in the Boeing report with antenna size as scaling parameter (d ranging from 15 to 200 m). Corresponding solar array dimensions range to 70 m panel length. Results obtained by Boeing are assumed to apply also to other intermediate-sized spacecraft of similar configuration where the payload is not necessarily a communication system or space radar.

The Boeing study concludes that the propellant mass required for auxiliary propulsion (E-W and N-S stationkeeping, solar pressure compensation and attitude control maneuvers) is determined primarily by the ΔV maneuver requirements, with attitude control expenditures being a small percentage of the total.* In the present study the ΔV maneuver requirements are increased by about 50% to include orbital repositioning and disposal maneuvers so that the relative proportion of attitude control propellant mass is thus further decreased. Consequently, attitude control propellant mass was neglected in the total propellant mass estimates.

Results of earlier TRW auxiliary propulsion integration studies (References 10 and 11) of existing satellite configurations designed for operation in geosynchronous (Intelsat V, MMS, DSCS III, DSP) and intermediate orbital altitudes (GPS) are applicable to this study in the following areas:

- Thruster location and operational sequence
- Thrust plume impingement avoidance
- Attitude control propellant mass data
- EMI and RFI interactions

These data are useful in auxiliary thruster placement and orientation trades, in bracketing propellant mass requirements and in defining areas of further study in controlling potential propulsion system/spacecraft interactions.

*Private communication from W. Smith, Boeing Study Manager.

3.2 PROPULSION SYSTEM DEFINITION

The integrated propulsion system comprises the main thrusters used for orbit transfer and an assembly of small thrusters to provide the much smaller forces needed for stationkeeping and the torques required for attitude control. Several configurations were examined before selection of the system described here.

3.2.1 Thruster Arrangement

Figure 60 shows the locations and orientations of the various electric thrusters used on the generic spacecraft design analyzed in this study.

A set of gimballed main thrusters is located at one end of the spacecraft center body, with the thrust axis normally pointing along the length axis (z-axis), such that propellant depletion does not produce a major thrust vector misalignment.

Four auxiliary electric thrusters are grouped around the main thrusters, pointing normal to the centerline along the x and y axes.

Two additional clusters of five thrusters each are located on outrigger booms extending in +x and -x directions with thrust orientations as indicated in the figure. The booms must be sufficiently long to prevent direct thrust plume impingement on nearby portions of the solar panels when these panels are oriented parallel or nearly parallel to the spacecraft x-y plane. The locations shown also provide favorable attitude control moments.

The x, y and z body axis designations shown in the sketch conform with the notation used in the Boeing study. The thrust designations F_x , T_y , F_y , T_z , etc., indicate in which direction the thrust forces (F), and around which axes the thruster torques (T), are acting. These designations, too, conform with the Boeing study.

The auxiliary thrusters shown can be operated in sets to produce either pure translation along any of the body axes or pure moments around the axes. For example, if pure translation maneuvers without

ORIGINAL
OF POOR QUALITY

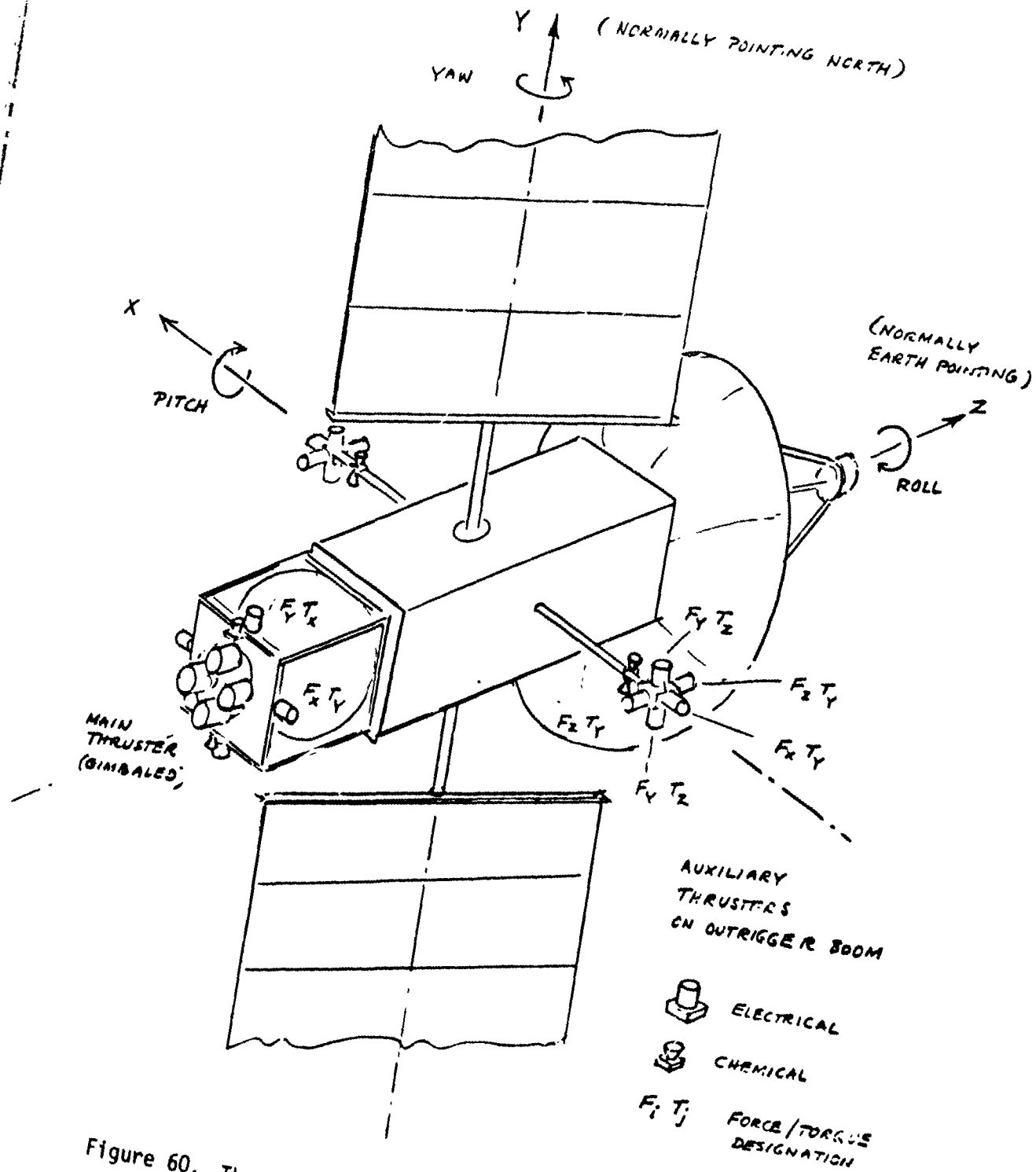


Figure 60. Thruster Arrangement on Reference Configuration

rotation are required the thrust magnitude or pulse length of thrusters used in combination must be controlled such that opposing torques cancel out. If pure rotation around a principal body axis is desired, care must be taken to cancel coupling effects by appropriate combination of several thrusters. Rotations around the x, y and z axes are referred to as pitch, yaw and roll, respectively. The thruster set is arranged to provide partial redundancy.

Gimballing of the main thrusters can correct thrust axis misalignment and can also be used to generate three-axis control moments. For pitch or yaw control the thrusters are gimballed jointly either around the x or the z axis. Roll control requires differential gimballing of at least two main thrusters. The auxiliary thrusters are assumed to be rigidly mounted at their respective locations.

Generally, during the primary thrust phases, most attitude control functions are performed by the main thrusters without requiring assistance from the electric APS thrusters. However, the control torques generated by the primary or auxiliary electric thrusters will not always be large enough to overcome maximum external disturbing torques such as may arise from gravity gradient or aerodynamic effects at low altitude. These conditions will occur for spacecraft with large appendages such as the solar arrays with tip-to-tip dimensions typical for the generic spacecraft configuration assumed here. Such spacecraft are characterized by large differences in maximum and minimum moments of inertia and large center-of-pressure/center-of-mass offsets. The moment of inertia differences are multiplying factors in the expressions for gravity gradient torques while the c.p./c.m. offset governs aerodynamic disturbing torques.

The Boeing study has shown that auxiliary chemical thrusters may have to be added to provide the necessary corrective torque capability which in the low and intermediate altitude region can be several orders of magnitude greater than that achievable by electric auxiliary thrusters of reasonable size. Data to substantiate this requirement for spacecraft mass and size characteristics considered here are shown in the next section.

Another factor to be considered is the periodic power cutoff due to eclipses that occur at low as well as high orbital altitudes. Although momentum storage devices can maintain normal attitude control functions during eclipse intervals, the use of chemical backup thrusters can effectively augment this capability. The alternative of using batteries with storage capacities of the order of 10 to 30 kW-hr to support auxiliary thrust operation does not appear to be practical or cost effective (see discussion in the next section).

Placement of the chemical thrusters at the locations shown in Figure 60 serves to control the largest external disturbance torques, namely those around the x and z axes. A minimum of six chemical thrusters is required.

3.2.2 Thrust Modes

In some instances during the ascent and the orbital mission phases, the desired maneuver modes require the thrust to be aligned with the orbital velocity vector; in others, an out-of-plane orientation at some angle or even normal to the velocity vector is required.

3.2.2.1 Ascent Phase Thrust Orientation

During the ascent phase the main thrusters operate continuously except during eclipses. The initial part of the transfer takes place without plane change to minimize exposure to Van Allen belt radiation. During this part of the ascent phase the thrust vector is oriented along the velocity vector.

During the final two-thirds of the ascent the thrust vector is oriented at an increasing out-of-plane angle to accomplish the required plane change into equatorial orbit by the time the vehicle reaches synchronous altitude, while the principal in-plane thrust component continues pointing along the velocity vector. Periodic reversals of the out-of-plane orientation are performed twice per orbital revolution, according to a steering program that places the midpoints of each successive out-of-plane deflection at the ascending and descending nodes of the orbit (see Reference 2, Section 4). In the preferred ascent profile

the rotational rates and accelerations around the local vertical that are required to achieve this steering program, however, are only about 25% of the maximum values quoted in Reference 2, since the out-of-plane maneuvers do not start before the orbital period has increased to about 6 hours. The required lateral steering torques can be provided by main thrust gimbal deflection assisted if necessary by the appropriate auxiliary thrusters.

In the low altitude region of ascent, periodic roll maneuvers are required to maintain optimum sun exposure of the feathered solar array panels (Section 2.6.1). This may present problems of excessive roll torque requirements since the roll moment of inertia I_{zz} is the largest one for the reference configuration being considered, and the maximum roll rates required to track the sun and achieve roll excursions of ± 75 degrees twice per orbit are as high as (\pm) 0.03 deg/sec. However, this occurs only under worst-case conditions, i.e., when the sun is within about 15 degrees of the orbit plane. The problem may be avoided by restricting the launch date and time-of-day so as to get a more favorable sun alignment, and/or by limiting the roll excursion at the expense of a small power loss.

A performance tradeoff between roll maneuver requirements for optimum sun exposure versus degraded power generation, and also versus required propellant expenditures for chemical thruster operation to support these maneuvers would be needed to define the best operation strategy.

3.2.2.2 On-Orbit Maneuvers

On-orbit operation normally requires the spacecraft z axis (length axis) to be Earth pointing, e.g., to perform typical Earth observation or communications relay tasks. This constraint prevents the use of the main thrusters for nonradially oriented ΔV maneuvers, such as E-W or N-S stationkeeping.

Figure 61 shows the spacecraft orientation during the orbital phase with the z axis pointing along the radius vector to earth, the x-axis is in the orbit plane. This orientation is consistent with best sun orientation of the solar panels which must perform one full revolution around

ORIGINAL PAGE IS
OF POOR QUALITY

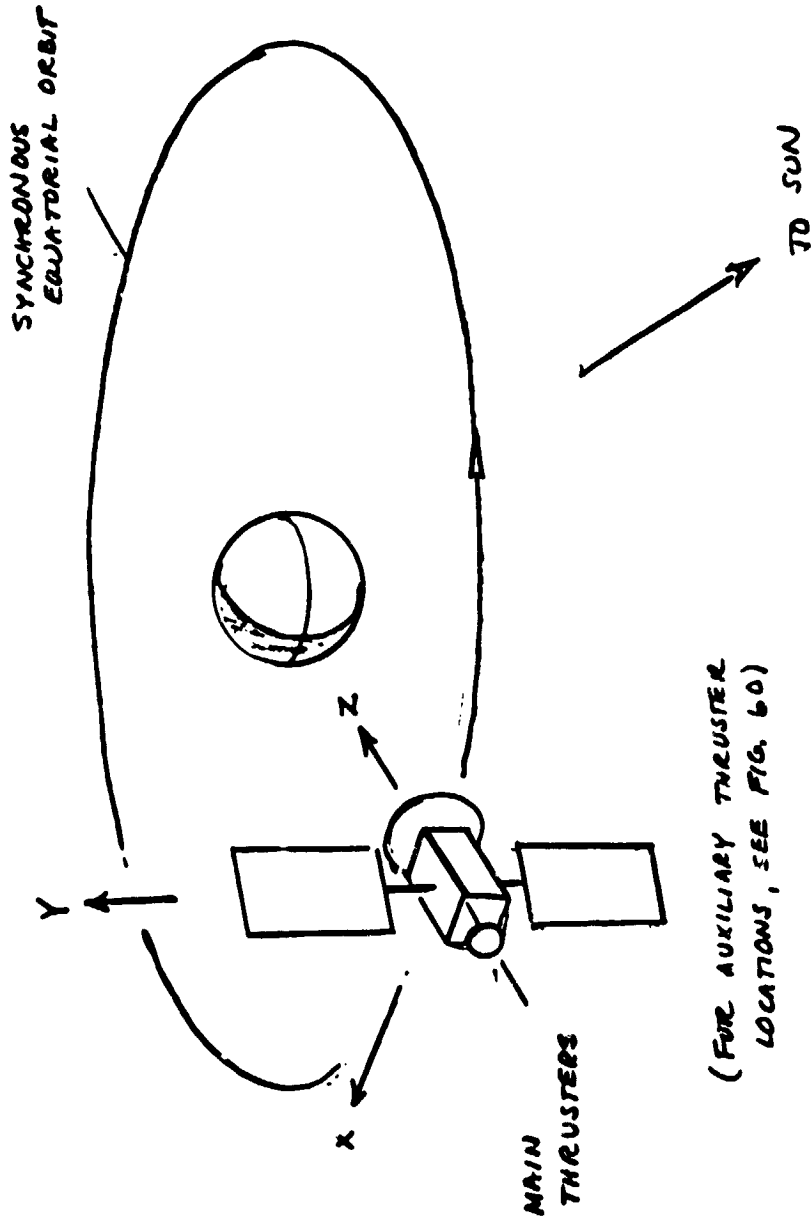


Figure 61. Nominal Orbit Orientation of Vehicle

their center line (the y-axis) per day. It is used by most three-axis controlled synchronous equatorial satellites today.

It is seen from Figure 60 that N-S stationkeeping, which requires a ΔV maneuver normal to the orbit plane, is performed by a combination of F_y thrusters, generally in sets of three, to nullify any pitch or roll torques that would be induced by individual thrusters. E-W stationkeeping requires thrust along the velocity vector or in the opposite direction and is performed by firing F_x thrusters.

The solar panels are in a worst case orientation for plume impingement from the boom-mounted F_y thrusters once every 12 hours, and similarly, but 6 hours later, for plume impingement from the F_y thrusters mounted near the main thruster assembly. These thrusters thus may require mounting at a fixed outward cant angle, depending on their position relative to the solar panel edges.

For satellites with large Earth pointing antennas, centered on the z-axis, a similar outward cant angle may be required for the forward firing F_z thrusters.

The required cant angle varies inversely with boom length. A trade between extra boom structure mass and extra propellant mass expenditure due to the cant angle is involved in determining the best arrangement for plume impingement avoidance.

Orbital repositioning maneuvers to a different longitude may be required several times during the spacecraft life. For these maneuvers the major ΔV impulses, one in prograde and one in retrograde direction, are required at the beginning and the end of the transfer in a sequence that depends on whether eastward or westward repositioning is intended. Since normal payload operations, e.g., communications relay functions, can be suspended during the repositioning phase which may last for several weeks, the vehicle can be reoriented again to permit utilization of the main thrusters.

3.2.3 Thruster Function Allocation

From the foregoing discussion it is apparent that the use of auxiliary electric thrusters is a practical approach to performing

translational and rotational maneuvers during the orbital mission phase and to providing attitude control support during the ascent phase. However, chemical backup thrusters may be needed: (1) to meet peak control torque requirements that exceed the capability of auxiliary electric thrusters of reasonable size, and (2) to substitute for electrical thrusters under eclipse conditions (unless momentum storage devices can fill this need).

Table 8 lists the thruster types required and their utilization modes versus mission operation phases, to summarize the results of this discussion. Table 9 summarizes the thruster locations and orientations assumed, their functions in translational and rotational maneuvers and the minimum number of thrusters employed.

3.3 SYSTEM REQUIREMENTS

This section presents performance data, design characteristics and other parameters needed in assessing the applicability of integrated auxiliary electric propulsion as compared with an alternative chemical APS. These data are required to substantiate assessments previously quoted from the Boeing APS study (see Section 3.1) and also, to support propellant mass evaluations and related analyses in Section 3.4. Applicable data derived from the reference study are presented as appropriate.

3.3.1 Spacecraft Mass Characteristics

Table 10 lists the net spacecraft mass and moments of inertia of the selected reference spacecraft class ("modular antenna system") and two other spacecraft classes of larger and smaller size investigated in the Boeing study. These spacecraft categories are defined by Boeing as "large erectable antenna structures" and "concentrated mass with appendages," respectively. In each case the mass and moment-of-inertia values are listed for the parametric range investigated. The mass characteristics of the selected reference system fall into an intermediate range between those of the other two.

Figure 62 shows spacecraft masses and the largest and smallest moments of inertia, I_{zz} and I_{yy} , versus antenna diameter, d , in the range

ORIGINAL PAGE IS
OF POOR QUALITY

Table 8. Thruster Function Allocations

THRUST PHASES	THRUST FUNCTIONS				
	MAIN THRUST ΔV	3-AXIS CONTROL BY TVC	ΔV	AUXILIARY THR ACS	ACS
THRUSTER TYPE	ELECTRIC	ELECTRIC	ELECTRIC	CHEMICAL BACKUP	
<u>ASCENT PHASE</u>					
MAIN THRUST ON	✓	✓	-	(✓)	✓
MAIN THRUST OFF	-	-	-	✓	✓
<u>ORBITAL PHASE</u>					
MAIN THRUST ON	r ✓	✓	-	(✓)	✓
	not r ✓	✓	-	(✓)	✓
MAIN THRUST OFF	-	-	✓	✓	✓

Table 9. Auxiliary Thruster Functions and Numbers

THRUSTER DESIGNATION	ELEC. AUXILIARY THRUSTERS			CHEMICAL BACKUP THRUSTERS		
	THRUSTER FUNCTIONS ΔV	LOCATION	MIN. NO.	FUNCTION ACS	LOCATION	MIN. NO.
$F_x T_y$	E-W	YAW	BOOM	-		-
			MAIN ASS'Y			
$F_y T_x$	N-S	PITCH	MAIN ASS'Y	PITCH	MAIN ASS'Y	2
$F_y T_z$	N-S	ROLL	BOOM	ROLL	BOOM	4
$F_z T_y$	FORE-AFT	YAW	BOOM	-		-
TOTAL			12	TOTAL 6		

Table 10. Mass Properties Data for Three Spacecraft/Structure Classes
(Reference 2)

Parameter/Mass Characteristics	Large Erectable Structure	Modular Antenna System	Concentrated Mass with Appendages
Scaling Parameter	Length	Antenna Diameter	Antenna Diameter
Parameter range (m)	82 to 1300	15 to 200	15 to 60
Mass range (kg)	1.23×10^4 to 1.95×10^5	2.03×10^3 to 2.7×10^4	3×10^3 to 1.2×10^4
Moments of Inertia Range ($\text{kg}\cdot\text{m}^2$)			
I_{xx}	3.47×10^7 to 1.37×10^{11}	1.35×10^5 to 1.08×10^8	7.11 to 3.66×10^5
I_{yy}	1.38×10^7 to 5.49×10^{10}	1.17×10^4 to 8.79×10^7	7.93×10^4 to 3.12×10^5
I_{zz}	3.45×10^7 to 1.37×10^{11}	1.35×10^5 to 1.66×10^8	3.01×10^4 to 1.03×10^6

ORIGINAL PAGE IS
OF POOR QUALITY

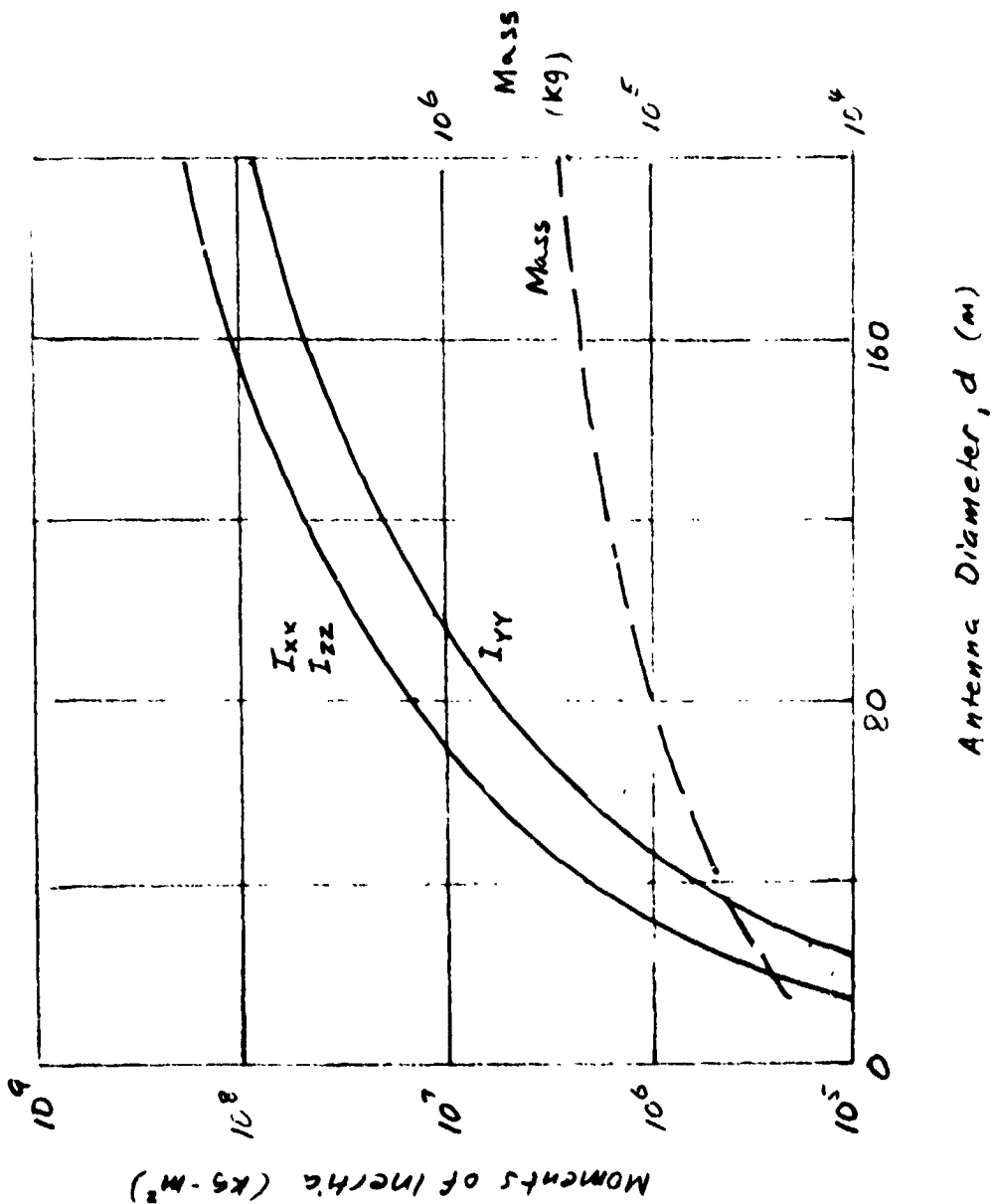


Figure 62. Mass and Moments of Inertia of Reference Spacecraft/Structure (Modular Antenna Structure) Extrapolated from Boeing Data (Reference 2)

of 15 to 200 m. The scaling relations used to express other spacecraft characteristics in terms of antenna size are listed in Table 11. The antennas were taken to be solid, as opposed to mesh, construction for the following analysis.

3.3.2 Disturbance Forces and Torques

Figures 63 through 65 show disturbance forces in the x, y and z directions acting on the reference spacecraft for the range of antenna sizes considered. Figures 66 through 68 show the corresponding disturbance torques. The curves represent maximum disturbances in LEO and GEO, and nominal disturbances in the normal on-orbit orientation in GEO. For a given vehicle size these forces differ by a factor of 1-1/2 to 4 and the torques by 1-1/2 to 2-1/2 orders of magnitude between LEO and GEO, reflecting the very much larger disturbances, dominantly due to gravity gradient and aerodynamic effects, acting on the vehicle at low orbital altitude. The disturbance forces and torques vary by about 2 orders of magnitude over the vehicle size range investigated, except for y-axis torques which vary by 4 orders of magnitude.*

Table 11. Scaling Relations for Modular Single Antenna
(Reference 2)

Scale Factor = Antenna Diameter = d (meters)
Range = 15-200 (meters)
Antenna Power = 1.5 x d (kW)
Antenna Mass = 0.36 x d ² (kg)
Array Area = Antenna Power x 8.96 (meters ²)
Array Length = 8.85 x Width (meters)
Array Mass = Antenna Power x 13.41 (kg)
Mass Total = 135 x d (kg)
Mass Avionics = Mass Total + Antenna Mass - Array Mass
Dimensions Avionics Cube = (Mass Avionics/19) ^{1/3} = L (meters)

*The very large torques around the y-axis apparently are due to the high ratio of antenna to solar panel dimensions in this configuration. Normally the torques around the x and z-axes would be expected to dominate.

ORIGINAL PAGE IS
OF POOR QUALITY

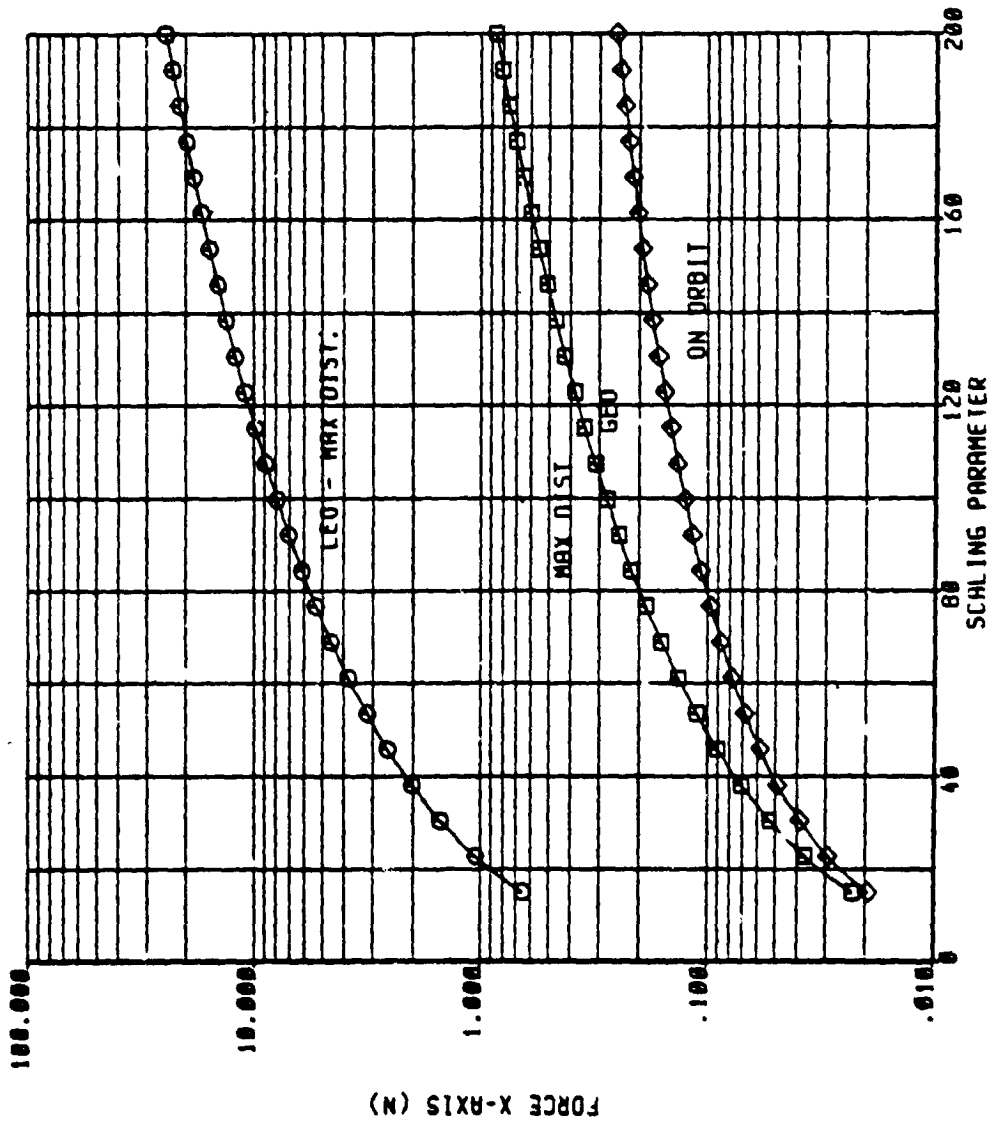


Figure 63. X Axis Forces (From Reference 2)

ORIGINAL PAGE IS
OF POOR QUALITY

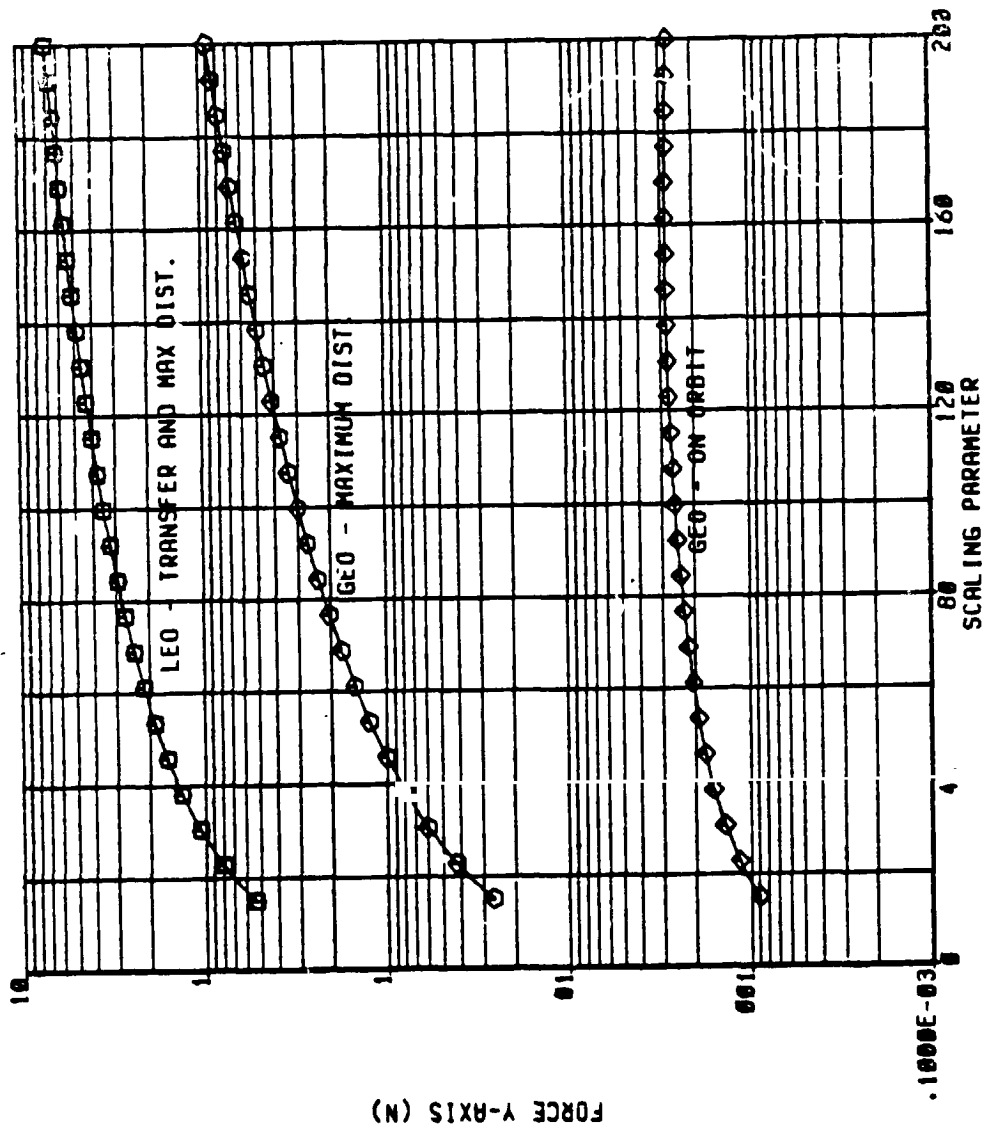


Figure 64. Y Axis Forces (From Reference 2)

ORIGINAL PLOT
OF POOR QUALITY

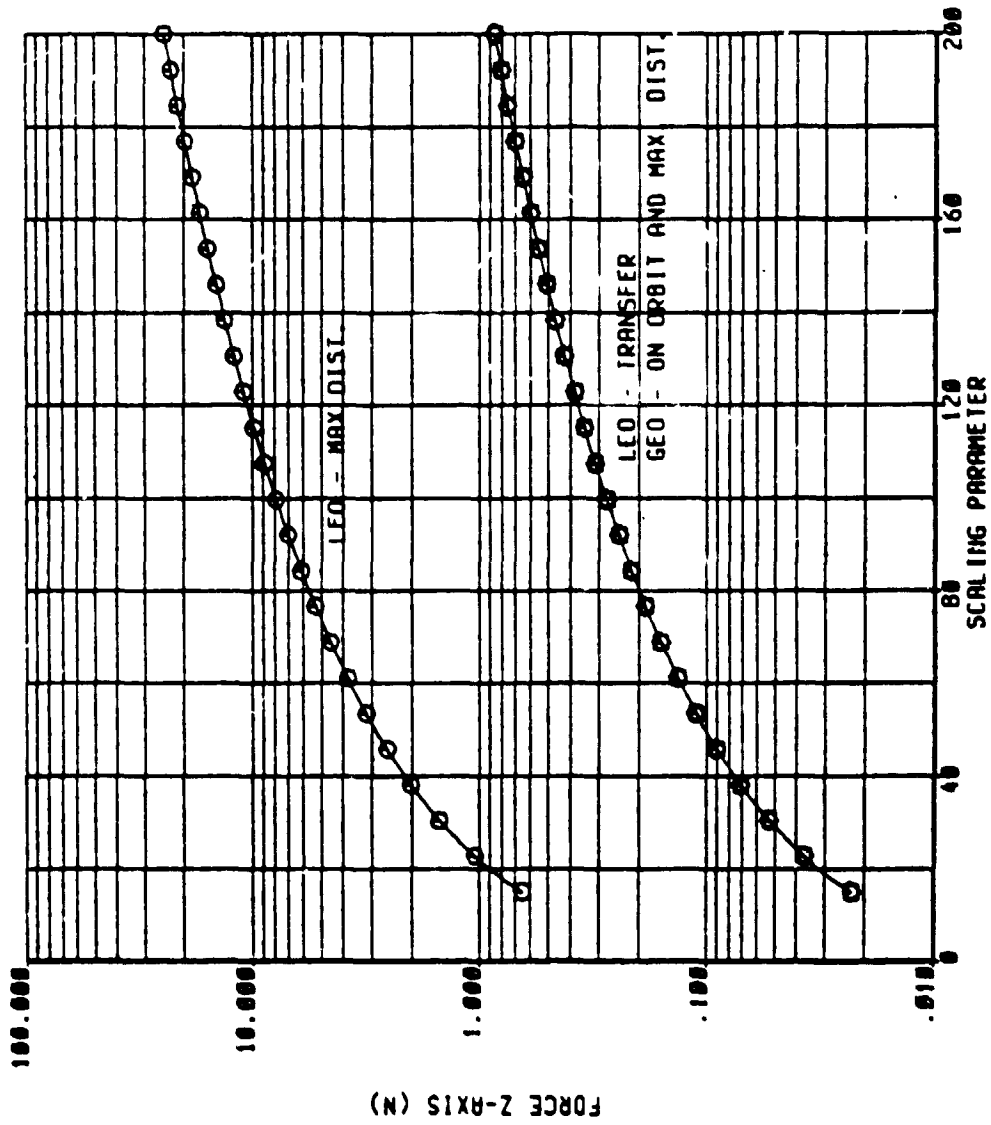


Figure 65. Z Axis Forces (From Reference 2)

ORIGINAL PAGES
OF POOR QUALITY

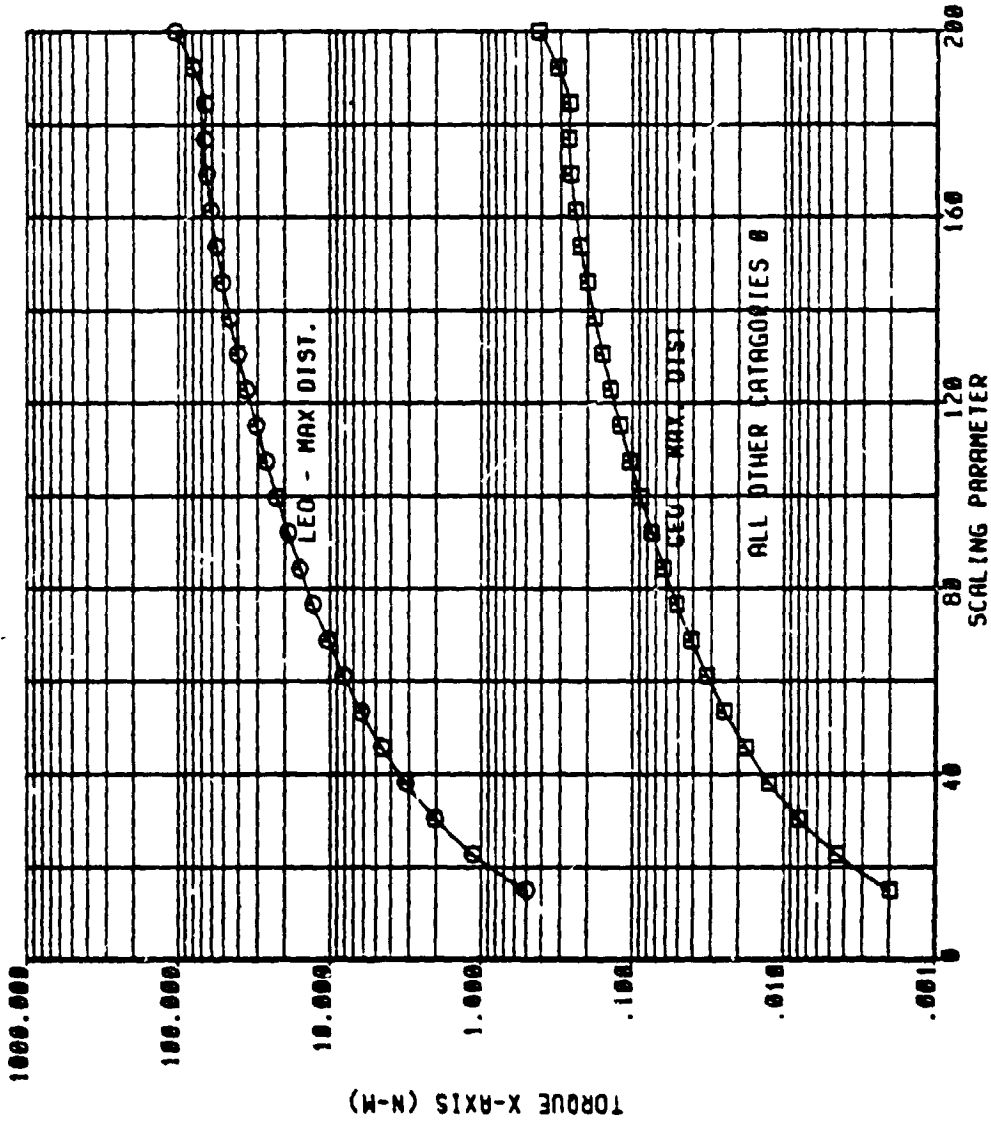


Figure 66. Pitch Torques (From Reference 2)

ORIGINAL PAGE IS
OF POOR QUALITY

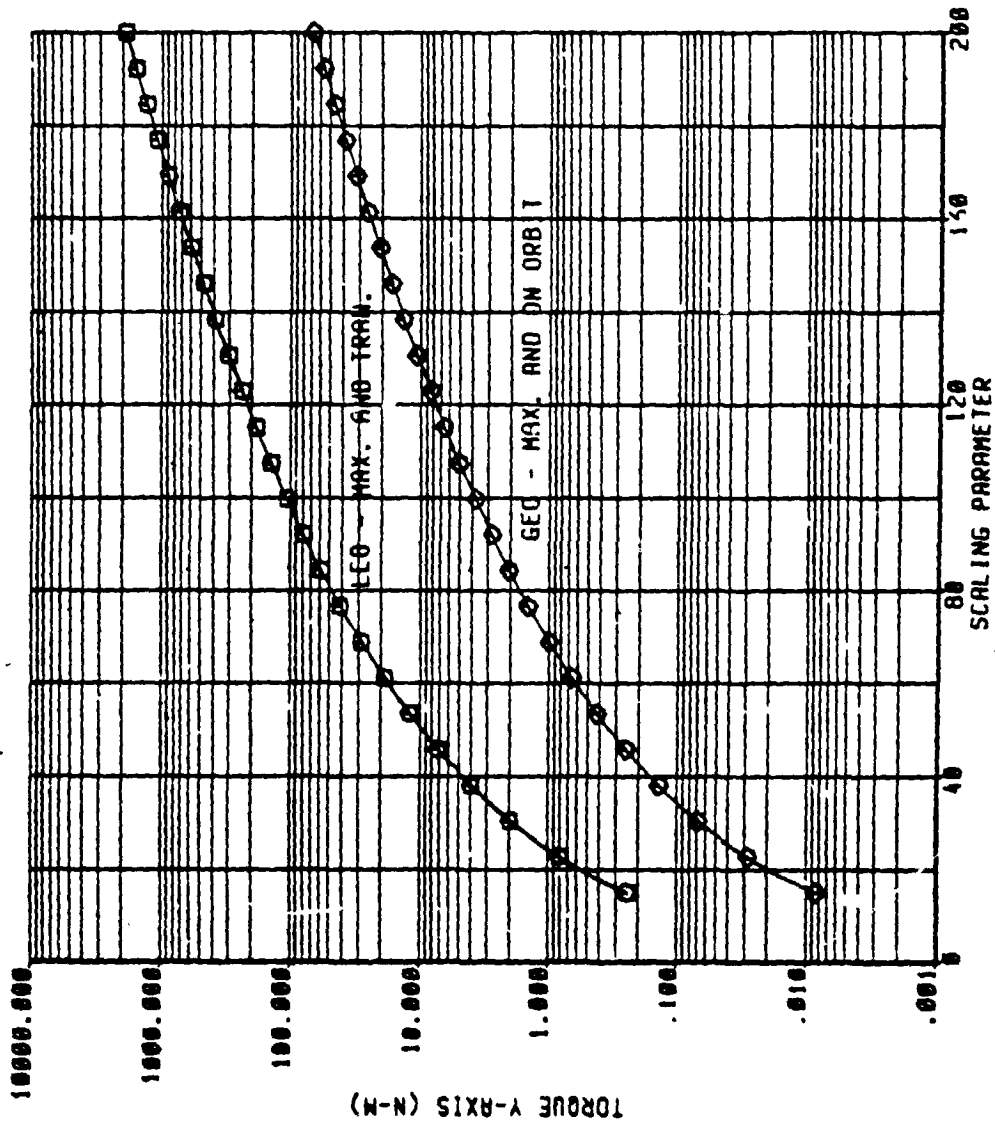


Figure 67. Yaw Torques (From Reference 2)

ORIGINAL PAGE IS
OF POOR QUALITY

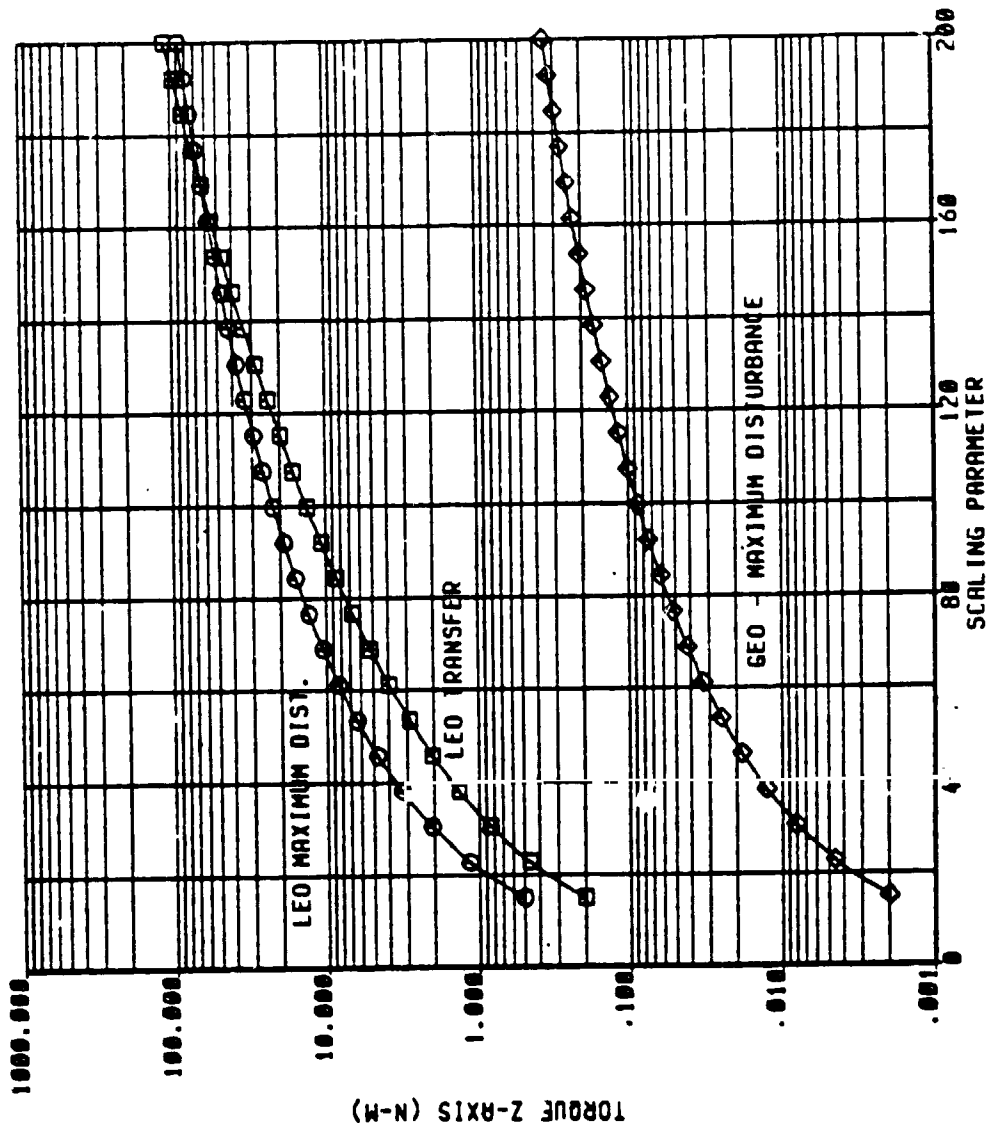


Figure 68. Roll Torques (From Reference 2)

Intermediate vehicle sizes with antenna diameters of 80 to 100 m correspond to the maximum vehicle mass range that can be accommodated by a single Shuttle launch, i.e., the range from 12,000 to 18,000 kg (see Section 3.4). For these sizes the maximum disturbance torques around the x and z axes, in low orbit, are about 20 N-m; those around the y-axis, about 100 N-m.

Based on these data it is apparent that an electric auxiliary thruster of any reasonable size, i.e., 0.05 to 0.10 N, cannot provide the maximum control torques required in LEO even if the atypically large yaw torques shown are disregarded. With a long (10 m) moment arm provided by the outrigger booms, the $F_y T_z$ thrusters (see Figure 60), used in pairs, would not produce control torques greater than typically 1 to 2 N-m. Gimbaling of the main thrusters would not yield more than about 2 to 5 N-m for representative thruster sizes and locations.

Even for much smaller vehicle sizes, electric auxiliary thrusters of practical size would not meet control torque requirements in low orbit. This control task may therefore require the addition of chemical backup thrusters, as previously discussed in Section 3.2.3.

3.3.3 Auxiliary Thruster Sizing.

Auxiliary thruster sizing for the selected reference configuration was keyed to north-south stationkeeping requirements and the control of geosynchronous maximum disturbance torques, as discussed in the Boeing report. Based on the results obtained in that study, the required thruster size ranges from 0.001 N per thruster for a vehicle in the 15-m antenna class to 0.01 N per thruster for a 60-m antenna vehicle, assuming a set of six thrusters acting together. In the configuration shown in Section 3.2 (Figure 60), with three thrusters firing in +y or -y direction for N-S stationkeeping, the required thruster size would be 0.002 to 0.02 N, and still somewhat larger for vehicles in the 80 m antenna class.

Results of an independent calculation of N-S stationkeeping thrust requirements are presented below.

Let $1/n$ be the fraction of time each day that is assigned for continuous N-S stationkeeping thrust operation. (Or equivalently, assume a full

day of thrust operation is needed every n'th day.) The thrust acceleration a required to maintain such a schedule depends on n and γ :

$$\frac{a}{g} = 2.3 \times 10^{-7} \frac{n}{\sin \gamma}$$

where γ is the arc length on each side of the nodal point over which thrusting continues. $\gamma = 90$ degrees, implies continuous thrusting in north and south directions, respectively. The term $\sin \gamma$ expresses the loss of thrusting efficiency associated with thrust arc extension away from the nodes.

Figure 69 shows a/g versus n with γ as a parameter. The limiting case is $n = 1, \gamma = 90$ degrees, which represents continuous thrusting every day. For a 15,000 kg spacecraft the total thrust force required under this condition would be 0.04 N. For $n = 2$ (thrusting every other day) the thrust would have to be increased to 0.08 N.

Assuming a 3000-second specific impulse and Case-I thruster characteristics, the stationkeeping power requirement for continuous thrust operation ($n = 1$) for a 15,000 kg spacecraft mass would be approximately 1.5 KW. This compares with 80 to 100 kW required to operate main thrusters of about 6 N thrust force, assuming Case-II thrusters at $I_{SP} = 1500$ seconds.

3.3.4 Principal On-Orbit ΔV Requirements

The principal ΔV requirements include stationkeeping, repositioning maneuvers and the final satellite disposal maneuver to a higher orbital altitude. A 10-year life in orbit is assumed.

3.3.4.1 North-South Stationkeeping

Data derived from the Boeing study indicate 10-year stationkeeping requirements ranging from 552 m/sec for the smallest vehicle of the referenced category (15 m antenna) and 570 m/sec for an intermediate size vehicle (60 m antenna), to 613 m/sec for the largest size (200 m antenna). The increase is due to radiation pressure compensation requirements. N-S stationkeeping alone would require 457 to 518 m/sec depending on the calendar years of the mission.

The intermediate requirement above is assumed for propellant mass estimates calculated in Section 3.4. Taking a loss in thrust efficiency

ORIGINAL PORTION
OF POOR QUALITY

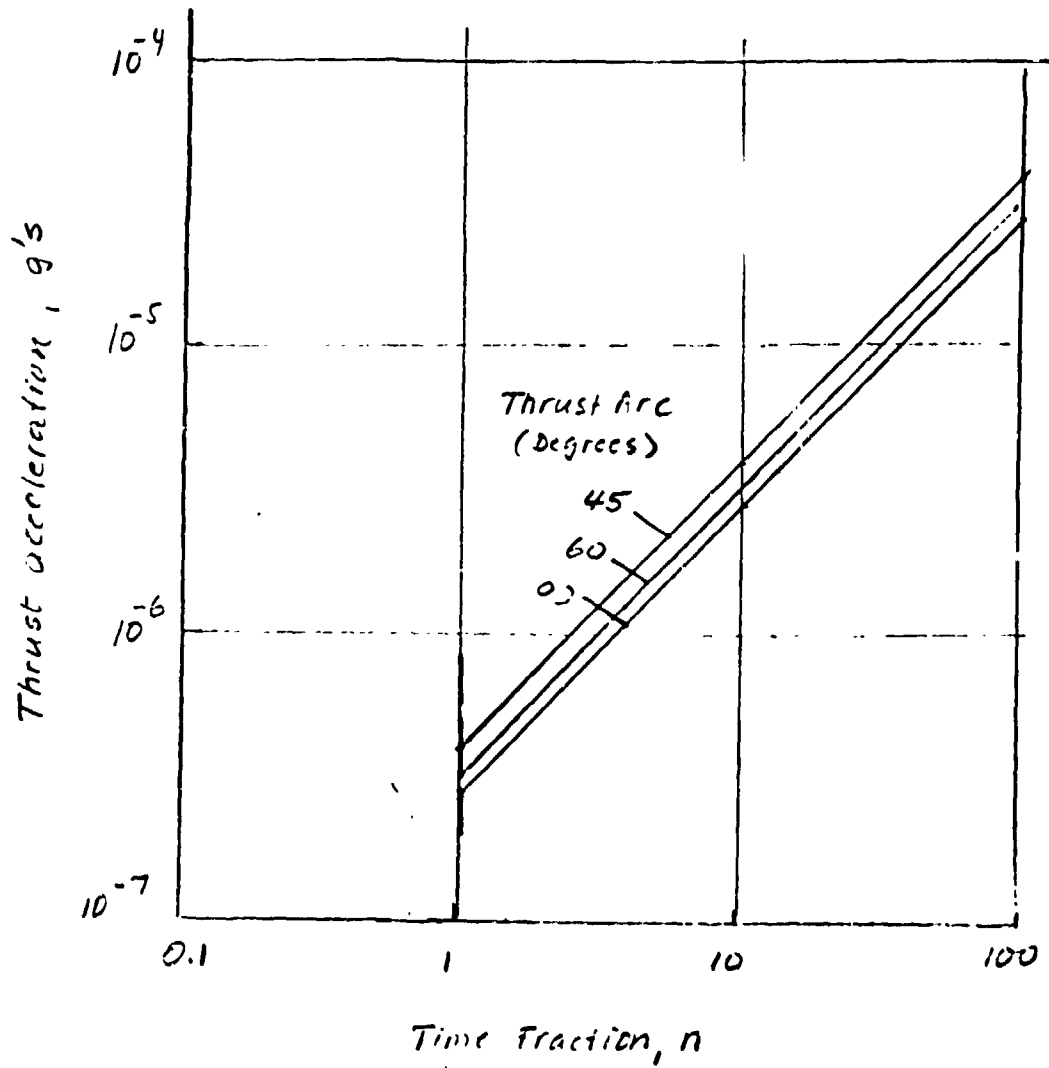


Figure 69. Thrust Acceleration Required vs Duty Cycle in N-S Stationkeeping

for distributed thrusting about +45 degrees centered at the nodal crossings resulted in a N-S ΔV requirement of 639 m/sec. This requirement corresponds to those calendar years requiring the most stationkeeping.

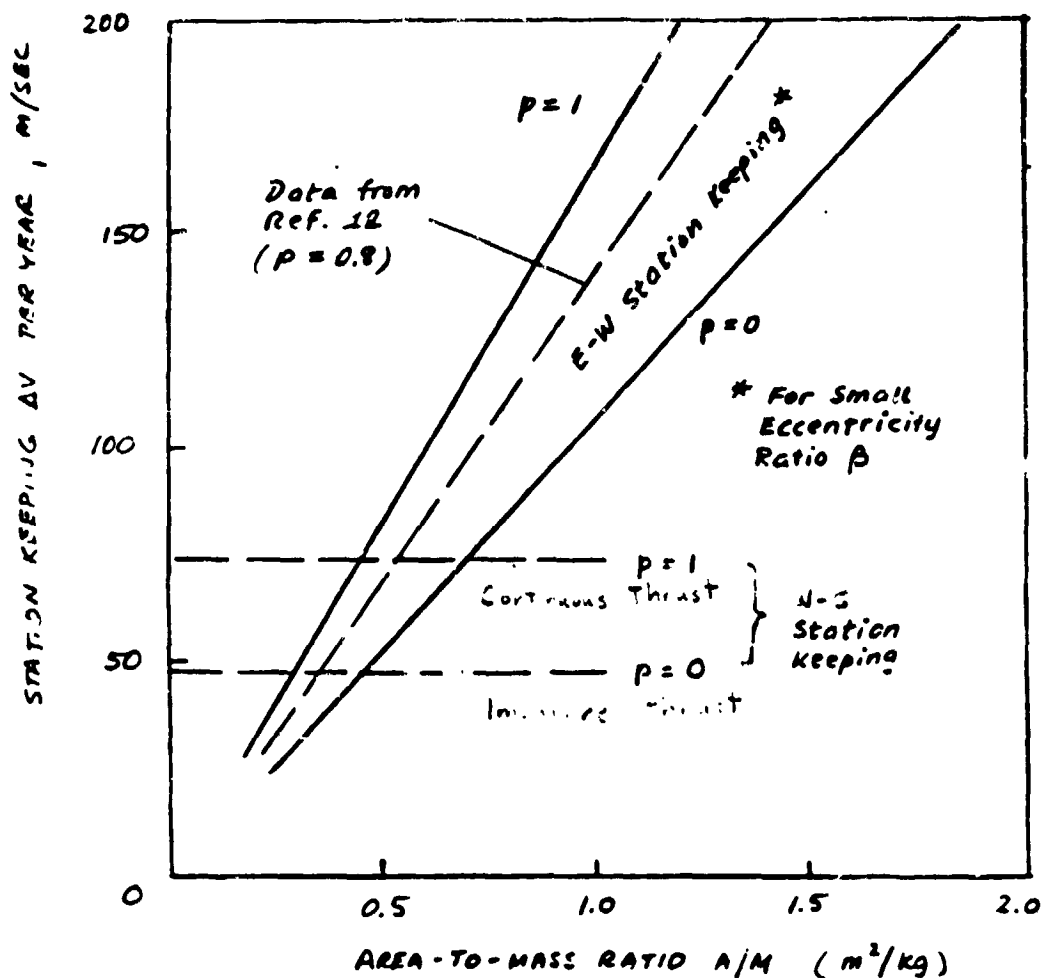
3.3.4.2 East-West Stationkeeping

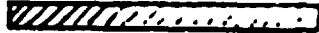
For large spacecraft structures with high area-to-mass ratios, A/M, such as those considered in this study, the annual E-W stationkeeping ΔV expenditures required to compensate for the effects of earth's triaxiality are negligible by comparison.

Based on data from the Boeing study (Reference 2) and from a NASA report by R. R. Lovell and T. A. O'Malley (Reference 12), the E-W stationkeeping ΔV required to compensate for solar pressure is shown in Figure 70 as function of the A/M ratio, with the duty cycle p as parameter. N-S stationkeeping requirements are also shown for comparison. The value $p = 0$ corresponds to impulsive thrusting, $p = 1.0$ to continuous thrusting over the entire orbit during days when stationkeeping maneuvers are being performed. In low thrust operation, both E-W and N-S stationkeeping ΔV requirements increase with the length of the duty cycle. The penalty factor is $\pi/2 = 1.571$ for $p = 1.0$ relative to impulsive thrust maneuvers (where $p = 0$). Figure 70 shows that the ΔV required for E-W stationkeeping exceeds the N-S stationkeeping ΔV if the A/M ratio is greater than $0.45 \text{ m}^2/\text{kg}$, assuming the same duty cycle is used in either case.

Typical ranges of A/M values for seven classes of large spacecraft investigated in the Boeing study are indicated below in the abscissa in Figure 70. The "box structure" class of spacecraft is represented by the largest range of A/M values, reaching $A/M = 1.67 \text{ m}^2/\text{kg}$ for a characteristic length L of 1000 m. Such a spacecraft would require a yearly ΔV of 180 m/sec for E-W stationkeeping if impulsive thrust maneuvers are assumed, i.e., 3.8 times more than for N-S stationkeeping. For the "modular antenna" class of spacecraft assumed as typical in the present study, the E-W stationkeeping requirements range from 20 to 100 m/sec per year as A/M varies between 0.17 and $0.90 \text{ m}^2/\text{kg}$, i.e., for antenna diameters ranging from 20 to 140 m. In this case the E-W stationkeeping requirements exceed those for N-S stationkeeping if $d > 60 \text{ m}$.

ORIGINAL PROJECT
OF POOR QUALITY



-  Cross
-  Series of Antennas
-  Antenna Form
-  Plate
-  Mastpole Antenna
-  Modular Antenna Config.
- $d=20\text{ m}$ 40 m
-  Box Struct.
- $L=80\text{ m}$ 1000 m

Representative A/M Ranges of S/C Investigated by Boeing
(Reference 2)

Figure 70. Stationkeeping ΔV Requirements vs A/M Ratio and Representative A/M Ranges for Various S/C Classes

The above data were shown only in summary form. A more detailed discussion, based on equations and parameters that govern stationkeeping maneuver requirements, are presented in the following discussion.

Analysis of ΔV Requirements for E-W Stationkeeping

In Reference 12 the ΔV requirements for various methods of E-W stationkeeping to compensate for solar pressure effects are derived. It is shown that circumferential thrust in E or W direction requires only one-half the ΔV expenditure that would be used by the alternative of radial thrusting. It is also shown that this thrust mode requires 18% more ΔV expenditure than one of direct solar pressure compensation where continuous thrust parallel to the sun line would be applied. Considering the nominal earth-pointing spacecraft orientation, however, it is apparent that intermittent thrusting in a fixed E or W direction is much simpler than applying thrust components along the three spacecraft axes in periodically varying combinations so as to produce a continuously sun-pointing thrust vector. The circumferential thrust mode (termed method 2 in Reference 12) therefore will be adopted as the nominal mode in the remainder of this analysis.

According to the derivation in Reference 12 the annual ΔV requirement is given by

$$\Delta V_s = \left(\frac{3\pi S k}{2 \dot{\lambda}} \right) \left(\frac{p\pi}{2 \sin \frac{p\pi}{2}} \right) \left(\frac{\beta}{\sin^{-1} \beta} \right) \quad (61)$$

where

$k = (1 + \sigma) \frac{A}{M}$ (with σ average reflectivity of satellite, ≈ 0.3)

$S =$ solar constant, $4.5 \times 10^{-6} \text{ kg m}^{-1} \text{ sec}^{-2}$

$\dot{\lambda} =$ mean angular velocity of earth motion around sun, 1.99×10^{-7} rad/sec

$p =$ duty cycle

$\beta =$ eccentricity ratio e^*/e_p (with $e^* =$ max. allowable eccentricity and $e_p =$ peak eccentricity that would occur if the initial orbit were circular ($e_0 = 0$) and no stationkeeping were applied.)

The parameter β which defines the desired stationkeeping accuracy can also be expressed by the relation

$$\beta = 0.4 \frac{\Delta L_S}{k} \quad (62)$$

where ΔL_S is the allowable longitude excursion (in degrees) between stationkeeping maneuvers. (β is a dimensionless quantity.) For very small values of ΔL_S , and hence β , the term $(\beta/\sin^{-1}\beta)$ in Equation (61) approximately equals 1.0, and therefore stationkeeping accuracy will have little if any influence on ΔV_S in this case.

The thruster acceleration required in performing E-W stationkeeping is given by

$$a_s = \left(\frac{Sk}{m}\right) \left(\frac{3\dot{\theta}_E}{8\dot{\lambda}}\right) \left(\frac{\beta}{\sin \frac{p\pi}{2}}\right) \quad (63)$$

where

m = number of days to complete a stationkeeping correction

$\dot{\theta}_E$ = angular velocity of earth's axial rotation,

= 7.29×10^{-5} rad/sec

Using results obtained in Reference 12, Figure 71 shows the normalized velocity increment $\Delta V_S/k$ in (m/sec)/(m²/kg) as function of the duty cycle p with β as parameter, based on Equation (61), and Figure 72 shows the normalized thruster acceleration (m/k) a_s in g's/(m²/kg), based on Equation (63).

The curves in Figure 71 show the influence of the principal parameters p and β on ΔV_S . However, for representative k values ranging between 0.2 and 2.0 m²/kg and for longitude excursions ΔL_S assumed to be less than 0.1 degree, β is restricted to the range of 0.02 to 0.2, and the ΔV requirements are those given by the top curve in Figure 71. For these small β values and given values of k , the only way to achieve a reduction in ΔV requirements below the maximum is by reducing the duty cycle p to less than 1.0, taking advantage of the fact that ΔV_S is most sensitive to a p reduction in the upper range of its values.

The multiplicative effect of the A/M ratio, and hence k , on ΔV_S requirements was previously exhibited in Figure 70 for $p = 0$ and 1.0 assuming low β values.

ORIGINAL PAGE IS
OF POOR QUALITY

Table 12 shows results of a parametric evaluation of yearly ΔV_s requirements for spacecraft with antenna diameters ranging from 20 to 140 m. The velocities shown are those for duty cycles $p = 1.0, 0.3$ and 0 (impulsive thrust) in circumferential thrusting (method 2) and also the corresponding values for direct compensation by thrusting in sun direction (method 1). The selected maneuver mode ($p = 0.3$) requires 34% less ΔV expenditure than operation at $p = 1$ and 22% less than operation in the direct solar pressure compensation mode. The A/M values used in this calculation are based on data given in Reference 2 for the modular antenna class of spacecraft that is considered in this analysis. Accordingly, the dependence of A/M on the antenna diameter is given by

$$\frac{A}{M} = \frac{1}{135} \left(\frac{\pi d}{4} + 13.44 \right) \text{ in } m^2/kg \quad (64)$$

where

$$M = 135 \times d \text{ (kg), (d in meters).}$$

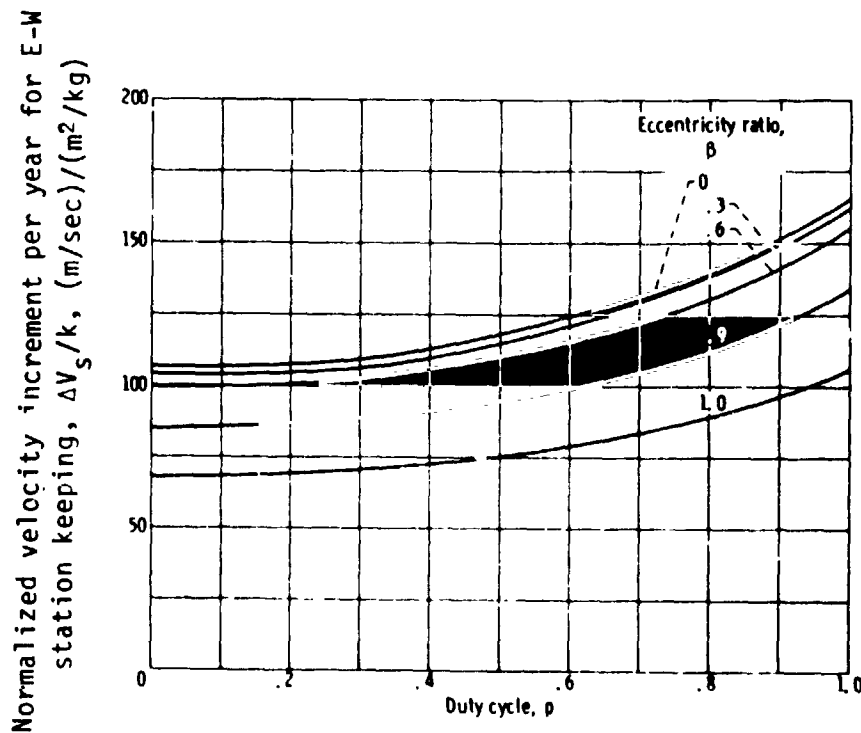


Figure 71. Normalized Velocity Increment per Year for E-W Station-keeping as Function of Duty Cycle with Eccentricity Ratio as a Parameter (from Reference 12)

ORIGINAL PAGE IS
OF POOR QUALITY

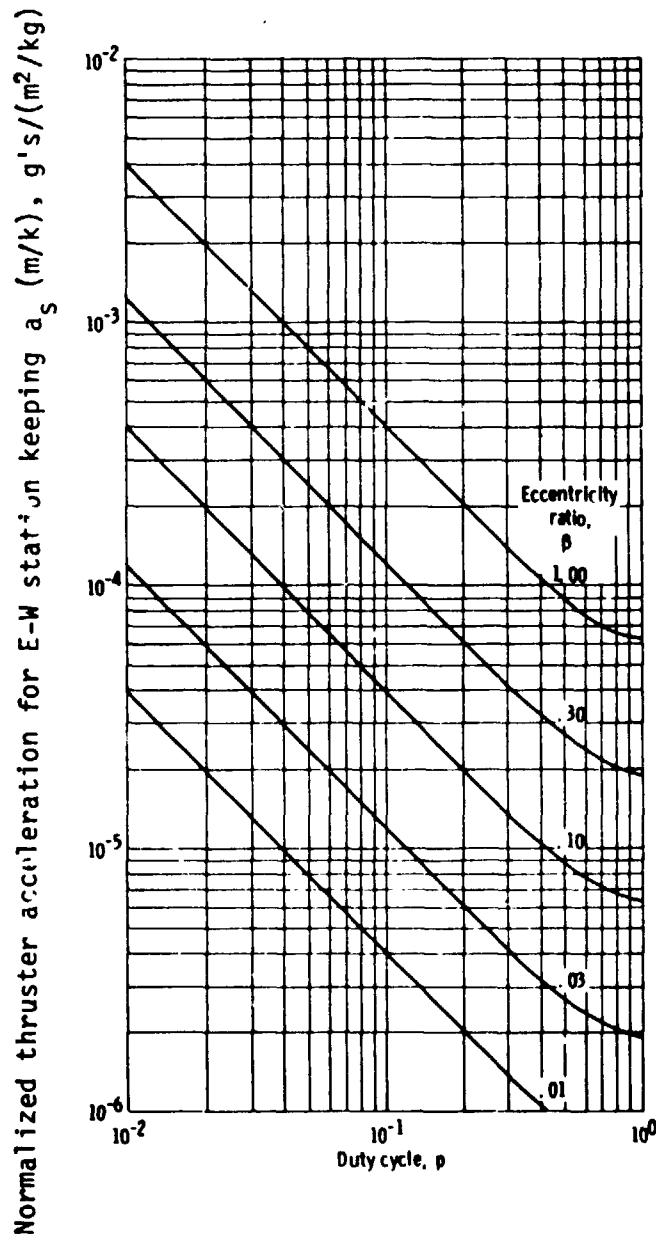


Figure 72. Normalized Thruster Acceleration for E-W Station-keeping as Function of Duty Cycle with Eccentricity Ratio as a Parameter (from Reference 12)

In addition Table 12 lists nominal spacecraft mass and power and assumed stationkeeping thrust, thruster power and acceleration characteristics as functions of antenna diameter, and derives values of a_s (m/k) for $p = 0.3$ based on Equation (63) for two stationkeeping accuracy requirements $\Delta L_s = 0.05$ and 0.10 degrees. Finally the number of days (m) is calculated during which stationkeeping maneuvers at a 30% duty cycle are to be performed. Also listed is the stationkeeping cycle duration t_c (in days) for the specified ΔL_s values. t_c is given by the relationship, derived in Reference 12,

$$t_c = \frac{\sin \beta}{\pi} \times 365 \approx \frac{\beta}{\pi} \times 365 \text{ days for } \beta \ll 1 \quad (65)$$

The results show that stationkeeping cycles for $\Delta L_s = 0.1$ degree range from 5.3 to 16.5 days, each cycle requiring 5 days of stationkeeping maneuvers lasting for 7.2 hours per day (30% duty cycle). For $\Delta L_s = 0.05$ deg, the stationkeeping cycles would have to occur twice as often requiring 7.2 hours of thrusting per day for 2.5 days, but leaving the total annual ΔV expenditure unchanged.

Mass Variation Effect on Solar Pressure Perturbation

It should be noted that the ΔV_s values derived in Table 12 are based on fixed values of spacecraft mass. Actually, since solar pressure effects depend on A/M and mass varies with propellant expenditure, a more precise derivation of ΔV_s expenditures requires that the variation of A/M be taken into account. The iterative technique used for this purpose is discussed in Appendix A.

3.3.4.3 Repositioning

A total of five repositioning maneuvers of 180 degrees each is assumed as an upper limit in a 10-year mission. For low thrust the maneuver requirement is expressed by

$$\Delta V = 5.70 \frac{\Delta \theta}{t_\theta} \text{ (in m/sec)} \quad (66)$$

where

$\Delta \theta$ = transfer angle (in degrees)

t_θ = time to complete the transfer (in days)

Table 12. Characteristics of E-W Stationkeeping Maneuvers

d (m)	A/M ⁽¹⁾ (m ² /kg)	k = 1.3 A/M (m ² /kg)	ΔV _s for E-W Stationkeeping (m/sec) per Year		M _N ⁽¹⁾ (kg)	P _N ⁽¹⁾ (kW)	T ⁽²⁾ (N)	P _T ⁽²⁾ (kW)	a _s /k ⁽³⁾ ($\frac{g's}{m^2/kg}$)
			Method 1 p = 1.0	Method 2 p = 0.3					
20	0.216	0.281	39.8	31.1	2700	30	0.03	1.2	3.95 x 10 ⁻⁶
40	0.332	0.432	61.3	47.8	5400	60	0.06	2.4	2.57
60	0.449	0.583	82.6	64.5	8100	90	0.09	3.6	1.91
80	0.565	0.735	104.2	81.3	10800	120	0.12	4.8	1.52
100	0.681	0.886	125.6	98.0	13500	150	0.15	6.0	1.25
d (m)	a _s x m/k ⁽⁴⁾ ($\frac{g's}{m^2/kg}$) ΔL _s = 0.1° 0.05°	m (days) ⁽⁵⁾	β ⁽⁶⁾	t _c (days) ⁽⁷⁾	Derivation of above results:				
		0.1 0.05°	0.1° 0.05°	0.1° 0.05°	(1) Based on nominal S/C model, Ref. 2				
					(2) Assumed values				
					(3) Calculated from preceding data				
					(4) From Equation (63)				
					(5) From preceding columns				
					(6) From Equation (62)				
					(7) t _c = $\frac{365 \beta}{\pi}$				
Assumed Duty Cycle p = 0.3									
20	2.0x10 ⁻⁵	0.95x10 ⁻⁵	5.06	2.53	0.142	0.071	16.5	8.25	
40	1.30	0.650	↓	↓	0.093	0.046	10.76	5.38	
60	0.963	0.482	↓	↓	0.069	0.034	7.98	3.99	
80	0.767	0.384	↓	↓	0.054	0.027	6.32	3.16	
100	0.634	0.317	↓	↓	0.045	0.023	5.26	2.63	

Allowing 20 days for each transfer, the total ΔV requirement for five repositioning maneuvers becomes 256.5 m/sec. In impulsive maneuvers this ΔV requirement would be reduced by 2.

3.3.4.4 Orbit Raising Maneuver for Satellite Disposal

The maneuver requirements are given by

$$\Delta V_1 = v_{co} \left(\sqrt{\frac{2r_2 r_0}{r_1(r_1+r_2)}} - \sqrt{\frac{r_0}{r_1}} \right) \quad \text{initial impulse} \quad (67)$$

$$\Delta V_2 = v_{co} \left(\sqrt{\frac{2r_1 r_0}{r_2(r_1+r_2)}} - \sqrt{\frac{r_0}{r_2}} \right) \quad \text{final impulse} \quad (68)$$

where

$$v_{co} = \sqrt{\frac{GM}{r_0}} = \text{circular velocity at } r_0, 7908 \text{ m/sec}$$

$$r_0 = \text{Earth radius} - 6378 \text{ km}$$

$$r_1 = 6.614 r_0 = \text{radius at synchronous altitude}$$

$$r_2 = \text{radius at altitude of disposed orbit}$$

The velocity requirement ($\Delta V_1 + \Delta V_2$) for disposal to 40,785 km altitude is 166.5 m/sec.

3.3.5 Use of Batteries

The question of whether auxiliary propulsion functions might be supported at times (e.g., during eclipse) by the use of batteries was investigated.

Assuming a storage requirement of 10 kW-hr and a voltage of 120 V, about one hundred 80-amp-hr cells would be required, at a discharge voltage of 1.25 V/cell. Depth-of-charge of 80% is acceptable for this application since only 60 charge/discharge cycles per year are required. Total losses of 20% was assumed, 10% each during charge and discharge operation. The battery set would have an estimated mass of 450 kg including battery charger.

The use of batteries for this purpose does not seem weight efficient since chemical backup thrusters will be available in any case, as discussed previously, and can substitute for electric auxiliary thrusters when power is unavailable. Secondly, momentum storage devices, being carried to handle routine ACS operations, would obviate the use of electric ACS thrusters during the 72-minute eclipse periods occurring at the spring and fall equinox seasons.

The use of batteries as a buffer against peak power demands by the eclipse APS, for example to avoid a conflict with payload power requirements, does not appear necessary. Power sharing in the orbital mission phase often involves under-utilization of the available power, rather than a need for managed power allocation under peak loads as is discussed in Section 3.4. In missions with unusually large payload power requirements this question may require further study.

3.3.6 Thruster Cant Angle Requirement

Auxiliary thruster location and orientation generally require detailed design trades depending on overall spacecraft configuration and mission profiles. Significant constraints will be imposed on thruster placement and orientation to avoid thruster plume impingement on the arrays, especially for spacecraft with large solar arrays, as discussed in Section 3.2.

Referring to Figure 60, the boom-mounted F_y thrusters may require an offset or cant angle large enough to avoid plume impingement on the nearest solar panel areas under worst-case panel orientation which will occur twice each day. To define the best arrangement a trade is required between the propellant penalty due to the cosine-loss resulting from canting the thrusters versus the mass of added boom structure that would be required to reduce the cant angle.

3.3.7 Gravity Gradient Strategy

During the ascent phase of the mission, gravity gradient torques can be employed to assist in orienting the spacecraft for optimum array illumination. The spacecraft attitude maneuvers required are summarized in Table 13. In the atmospheric drag region, the solar arrays are feathered for minimum drag. The spacecraft is either maintained fixed at ϕ (roll

Table 13. Spacecraft Attitude Maneuvers for Optimum Sun Alignment During Primary Thrust Phases

1. Lowest Altitude (ARRAY FEATHERED FOR MINIMUM DRAG)	Roll Only	Excursions $\pm 38^\circ$ for Sun Angle = 52° $\pm 75^\circ$ for Sun Angle = 15° Fixed 90° for Sun Angle $\leq 15^\circ$
2. Low-to-Intermediate Altitudes (ARRAY ARTICULATED)	Roll Only	SAME AS ABOVE
3. Intermediate-to-High Altitudes (ARRAY ARTICULATED; PLANE CHANGE SIMUL- TANEOUSLY WITH ORBIT RAISING)	Roll Yaw	Modified Periodic Excursion in Same Range Excursions to $\pm 45^\circ$ GENERALLY NOT IN PHASE WITH ROLL EXCURSIONS, DEPEND- ING ON NODAL POSITION RELATIVE TO SUN LINE

angle) = 90 deg or rolled from ± 38 to ± 75 degrees on sun angle (see Section 2.6.1 for a discussion of seasonal sun angle variation relative to the orbit plane). Gravity gradient is useful in providing restoring torques towards $\phi = 0$. The maximum gravity gradient torques are near $\phi = \pm 45$ deg, which are consistent with maneuver requirements. The best utilization of gravity gradient occurs when the period of roll motion is close to that of the orbital period. At low to intermediate altitudes, above the drag region, the solar arrays are rotated about their axis, and the roll motion is the same as described above. At intermediate to high altitudes, when combined orbit boosting and plane change are implemented, the roll motion is similar to that described above, but is modified to accommodate additional yaw motion for optimum solar array illumination.

The gravity gradient assist is most useful at low altitudes, where torque requirements are greatest, for reducing the size of inertial momentum storage devices in the attitude control system. Since the roll motion is driven primarily by gravity gradient, rather than by spacecraft attitude control moment gyroscopes or reaction control, solar array deformations are also reduced. If possible, spacecraft mass distribution should be chosen to permit gravity gradient operation slightly below the natural oscillation frequency. Thus, inertial design of the spacecraft would be constrained, but large roll angles could be maintained with small driving torques.

3.4 INTEGRATED PROPULSION ADVANTAGES

The advantages of integrated electric propulsion are assessed by weight and concomitant transportation cost comparisons with chemical propulsion. On-orbit power sharing with electric propulsion is another advantage examined for the reference generic spacecraft.

3.4.1 Comparison of Electric and Chemical APS

The ΔV requirements for APS were presented in Section 3.3.4. They are summarized here in Table 14, which lists requirements other than those for E-W stationkeeping. The iterative procedure described in Appendix A was used for determining ΔV_s , the E-W stationkeeping requirements.

Comparison was made between a chemical APS operating at 300 seconds I_{sp} , and an electric APS at 3000 seconds I_{sp} . As discussed in Section 3.1.1, repositioning and disposal in the electric case were performed by the main thrusters (in the integrated EPS) at 1500 seconds I_{sp} . Table 15 lists ΔV requirements and resulting mass characteristics for the electric and chemical APS cases for spacecraft with 20, 60, and 100 m antenna diameters as well as the differences in total mass launched. The mass characteristics are shown graphically in Figure 73 for comparison.

Note, that for the 60 m antenna spacecraft, the use of electric APS saves over 7000 kg of total launched weight.* At the Shuttle cargo limit of 29,500 kg, electric APS affords about a 50% increase in reference spacecraft mass.

In Table 15 the total mass values M_{TL} and $M_{TL} + FSE$ are derived from the initial mass in orbit M_{TI} by adding the propellant mass consumed during low thrust ascent from LEO to GEO ($\Delta V = 6015$ m/sec) and the mass of mission-peculiar flight support equipment (FSE), such as payload cradles, which is assumed to be 5% of the gross mass M_{TL} . The primary electric propulsion system mass including tankage is included in the reference mass M_N . The auxiliary propulsion system dry mass is included in M_0 .

*The terms weight and mass are used interchangeably in this discussion.

ORIGINAL PAGE IS
OF POOR QUALITY

Table 14. Auxiliary Propulsion ΔV Requirements
Other Than for E-W Stationkeeping
(10-Year Mission), in m/sec

ELECTRIC APS	
1. N-S Stationkeeping (Assuming $\pm 45^\circ$ thrusting arc)	
- Low Value	564
- High Value	639*
2. Repositioning (5 Events)	256.5
3. Disposal to 40,785 km Altitude	166.5
CHEMICAL APS	
1. N-S Stationkeeping	
- Low Value	508
- High Value	575*
2. Repositioning (5 Events)	128.3
3. Disposal to 40,785 km Altitude	166.5

*This value used in subsequent analysis

3.4.2 Launch Cost Savings Achievable with Integrated Electric Auxiliary Propulsion

NASA's Shuttle Launch cost reimbursement policy (Reference 13) defines weight dependent and length dependent user charges, respectively, as

$$C_W = 1.333 \times \frac{\text{spacecraft total weight}}{\text{total weight capacity}} \times (\text{dedicated launch cost})$$

$$C_L = 1.333 \times \frac{\text{spacecraft total length}}{\text{total length capacity}} \times (\text{dedicated launch cost})$$

Table 15. ΔV and Mass Characteristics* of Electric and Chemical APS Spacecraft
(Reference Configuration: Modular Antenna System)

d (m)	M_N	M_O	ΔV_S	ΔV_{NS} (m/sec)	ΔV_{SK}	ΔV_r	M_{PP2} ($I_{sp} = 3000$ s, 1500 s)	M_{PP3}	M_{TI}	M_{TL}	$M_{TL} + M_{FSE}$	ΔM
	<u>Electric APS</u>											
20	2,700	2,865	316	639	955	423	95	86	3,046	4,584	4,813	-
60	8,100	8,400	623		1262		368	256	9,024	13,578	14,257	-
100	13,500	14,040	925		1564		767	432	15,239	22,928	24,075	-
	<u>Chemical APS</u>											
20	2,700	2,800	245	575	295	1,115	M_{PPA} ($I_{sp} = 300$ sec)					
60	8,100	8,600	475			1,345	1,291	4,989	4,091	6,155	6,463	1,650
100	13,500	14,500	690			1,560	4,989	10,150	13,589	20,444	21,466	7,209
									24,650	37,086	38,940	14,865

* Mass in kg

d - Antenna diameter

M_N - Reference S/C mass (incl. primary EPS dry mass)

M_O - $M_N +$ APS dry mass

M_{PP2} - Stationkeeping propellant mass

M_{PP3} - Other APS propellant mass

M_{PPA} - Total APS propellant

M_{TI} - Total initial mass in orbit

M_{TL} - Total S/C mass launched

M_{FSE} - Flight supp. syst. mass (= 0.05 M_{TL})

ΔM - Mass reduction through integrated electric APS

ΔV_S - E-W stationkeeping requirement due to solar pressure

ΔV_{NS} - M-S stationkeeping requirement

ΔV_{SK} - Total stationkeeping requirement

ΔV_r - Other APS velocity requirements (repositioning and disposal)

ORIGINAL PAGE IS
OF POOR QUALITY

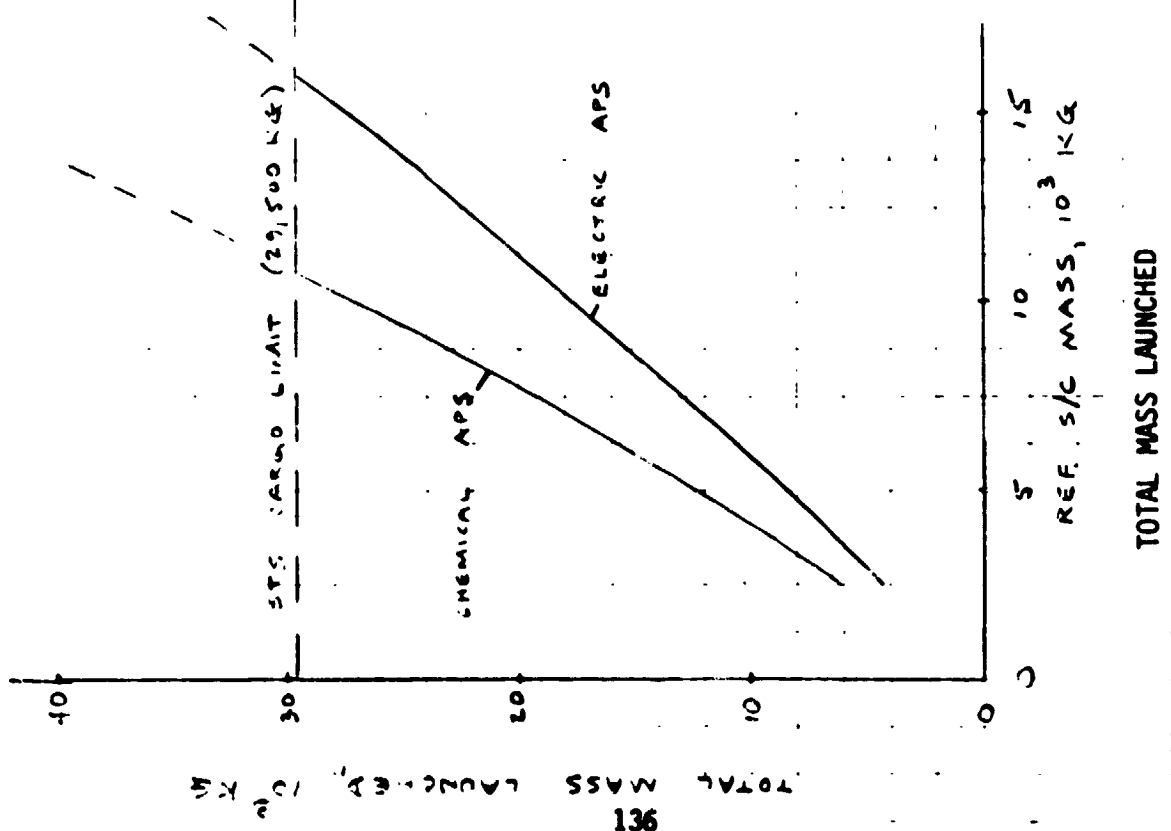
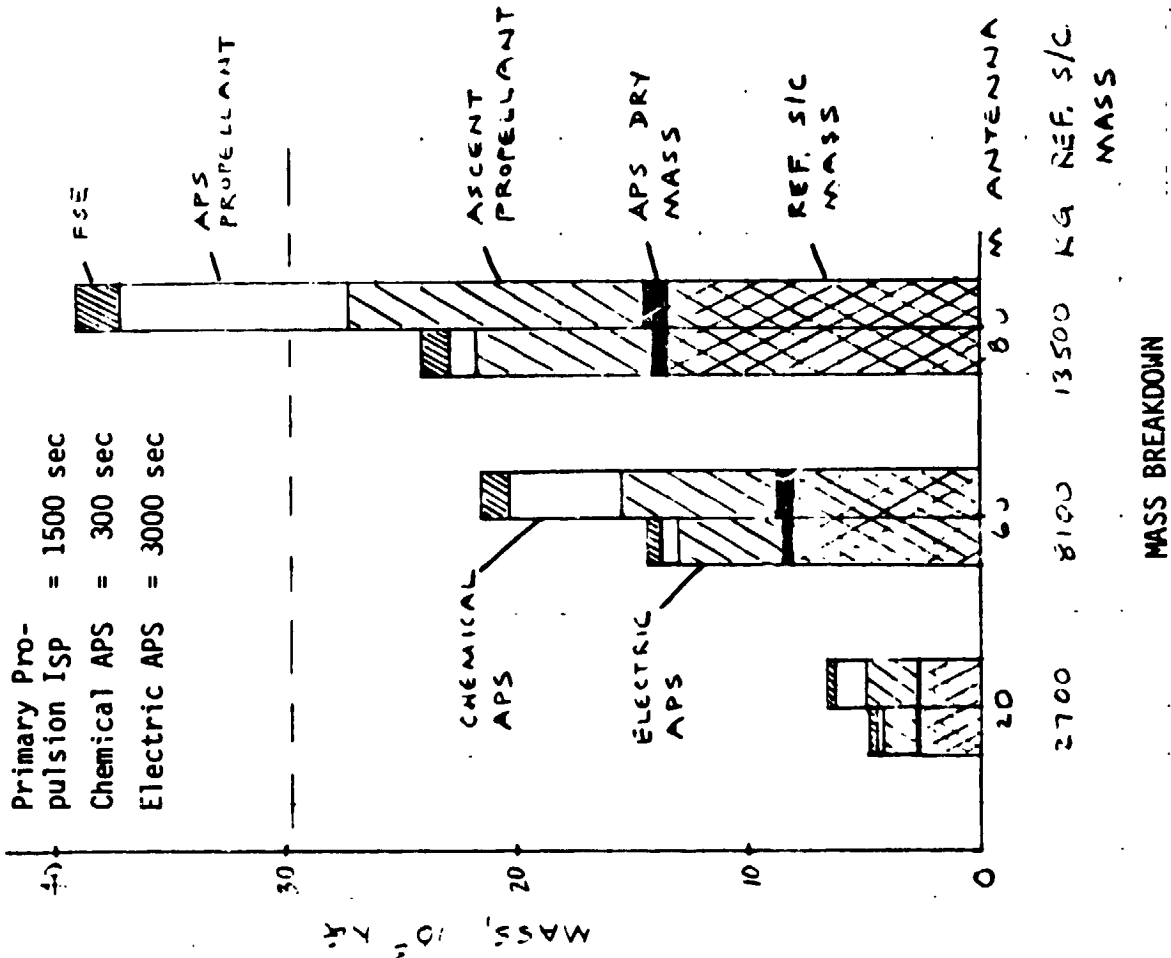


Figure 73. Performance Comparison of Chemical and Electric APS

where dedicated launch cost is given as \$ 30.2 million (1981 dollars). The user will be charged the larger of the two cost figures. The full dedicated launch cost will be charged if either spacecraft weight or length exceed 75% of full capacity, i.e., 22,110 kg or 13.72 m, respectively.

Figure 74 illustrates this reimbursement policy in terms of cost contours plotted in a mass versus length diagram. The graph shows the fixed cost plateau reached when mass or length exceed the 75% of capacity level. The dashed diagonal designates the breakeven points of weight and length dependent charges. Using the dedicated Shuttle launch cost, the weight and length dependent charges are

$$C_W = \$1.384 \text{ million per } 1000 \text{ kg}$$

$$C_L = \$2.30 \text{ million per meter}$$

The slope of the breakeven line is defined by

$$\frac{W}{L_{BE}} = \frac{2.30}{1.384} = 1.611 \times 10^3 \text{ kg/m}$$

If launch charges were always weight-dependent and varying linearly, the launch cost savings due to weight reduction would be defined simply by the relation

$$\Delta \text{cost} = \$1.384 \Delta M \text{ (millions per } 1000 \text{ kg)}$$

For example, the 7,209 kg weight savings for the nominal 8,100 kg spacecraft mass (see Table 15) would translate into a launch cost saving of approximately \$10 million.

Actually, under certain conditions these savings will not always be fully realized under the NASA launch cost reimbursement policy, for example, if spacecraft dimensions make the launch cost length-dependent. Figure 75 shows bars of weight savings ΔM for several values of assumed spacecraft length. In one case, the entire ΔM is in the weight-critical region, in the second case it straddles the cost breakeven line and in the third case it is entirely in the length critical region of the cost

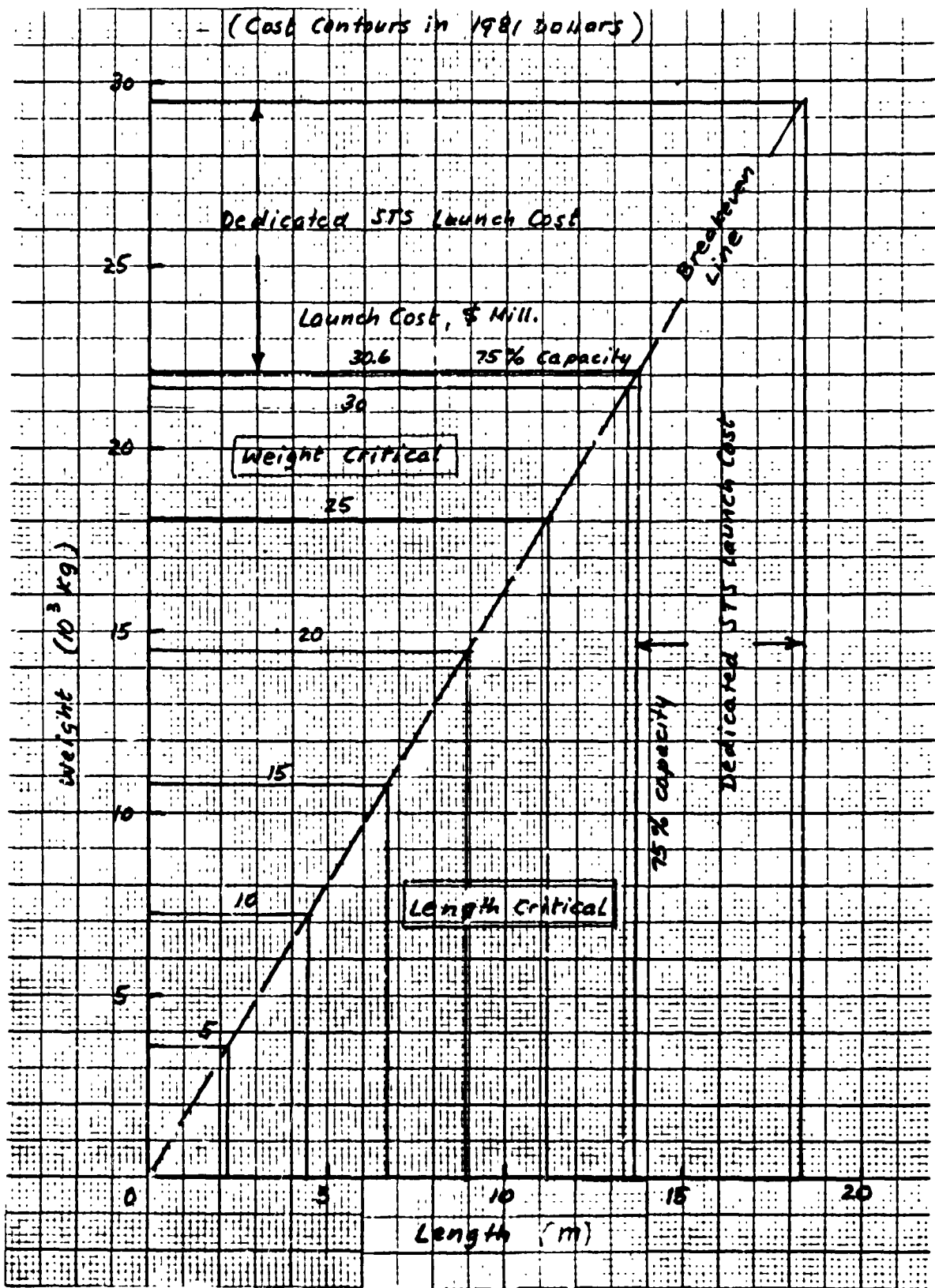


Figure 74. Shuttle Launch Cost Contours in Terms of Cargo Weight and Length

ORIGINAL
OF POOR QUALITY

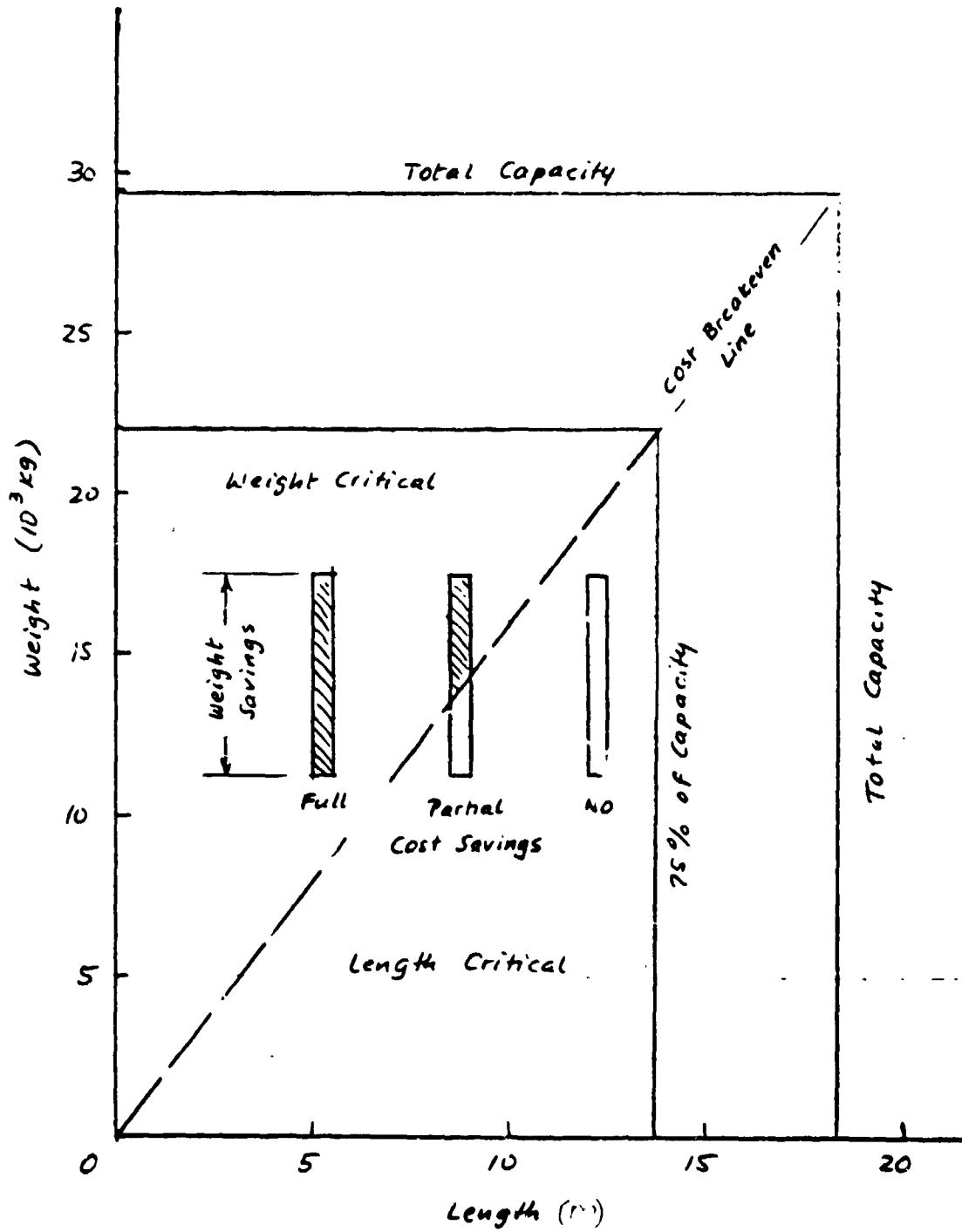


Figure 75. Examples of Launch Cost Savings Variation with Cargo Length

contour diagram. Accordingly, the cost savings reflect either all or part of the weight savings; or, in the third case, no cost savings are realized at all in spite of large weight savings.

Another effect of NASA's nonproportional cost allocation is the partial loss of potential savings if the gross weight exceeds the 75% limit.

Significant launch cost savings with integrated electric propulsion are anticipated for weight dependent payload configurations. Length dependent configurations will also benefit because of the reduced volume required for propellant storage when compared with chemical propulsion.

3.4.3 Power Sharing in Orbit

Shared use of available solar array power by the integrated electric APS and the spacecraft housekeeping systems and payload(s) during the orbital mission phase tends to increase overall system cost-effectiveness, a further incentive for adopting the integrated APS concept.

To characterize the degree of power utilization during the mission, the ratio of power used on-orbit to power used in ascent is introduced. This ratio, r , serves as a measure of power utilization effectiveness. Figure 76 shows contours of constant r in a graph of on-orbit versus ascent power requirements on a logarithmic scale.

Consider as an example a mission which requires 200 kW initially for orbit-transfer by primary electric propulsion. After a power loss of about 40% during the transfer phase due to solar array radiation damage, the remaining power level would be 120 kW. On orbit power required by the payload and housekeeping subsystems is assumed to be 30 kW, i e., calling for only 25% utilization of available power (Case 1).

By using auxiliary electric propulsion with a nominal power allocation of 30 kW for on-orbit maneuvers the utilization effectiveness is raised to 50% (Case 2A). At times of primary propulsion use for major on orbit maneuvers, however, all available power is allocated to the EPS, thus raising the utilization effectiveness to 100% (Case 2B).

Considering the launch weight reduction achievable through use of the integrated electrical APS as discussed in Section 3.4.1, the solar array size could actually be reduced by 30 to 35% without reducing the initial

ORIGINAL PAGE IS
OF POOR QUALITY

PAYLOAD POWER 30 KW
EPS POWER (PRIMARY) 200 KW
REDUCED EPS POWER
BECAUSE OF WEIGHT SAVINGS 130 KW

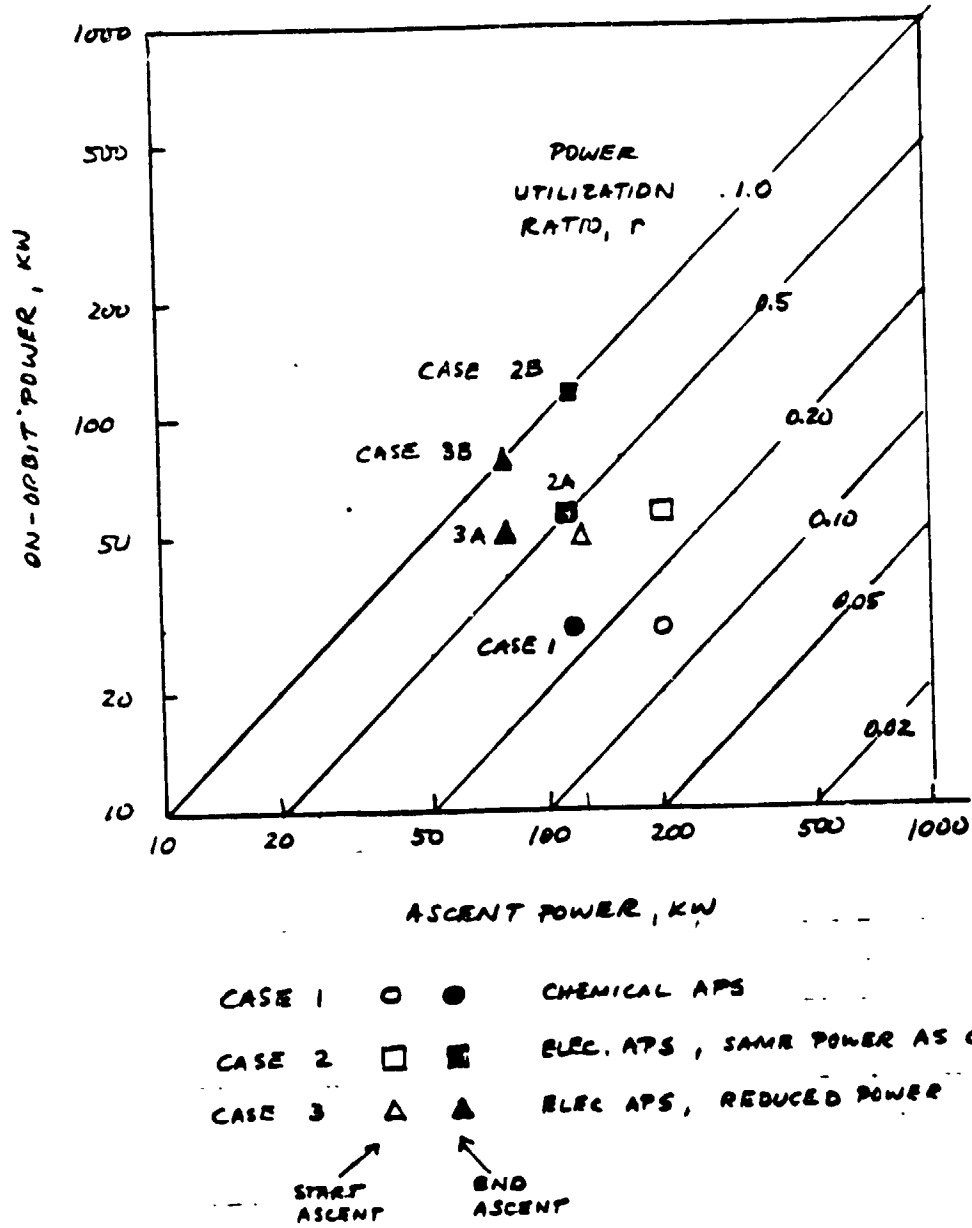


Figure 76. Power Utilization Examples

thrust acceleration. The solar array power would be 130 kW initially, the degraded power level about 80 kW. Assuming the same payload and auxiliary propulsion power requirements on orbit as before, the utilization factor becomes $\frac{60}{80} \times 100 = 75\%$ (Case 3A) with an occasional increase to 100 percent during major maneuvers (Case 3B).

In summary, the integrated APS concept will increase power utilization by a factor of 3 (or 4) in Case 3, while also permitting a one-third reduction in launch weight, solar array and primary electric propulsion size.

In Case 2 where the spacecraft uses the same solar array and primary electric propulsion system as in Case 1 with a one-third reduction in launch weight, the time required for orbital ascent would be substantially less than in Cases 1 or 3. The power utilization factor would be raised by 2 (or 4) compared with Case 1.

4. DISCUSSION OF RESULTS

This study has been primarily concerned with the LEO to GEO mission. Several results from the study, such as solar cell cover thickness optimization, optimum I_{SP} range, importance of thruster efficiency, and low altitude flight apply to orbit transfer portions of the analysis. They are discussed separately below. Next, a specific mission has been selected to illustrate how study results can be applied to particular configurations of interest. Results from both orbit transfer and integrated propulsion analysis are used to define the integrated EPS.

4.1 ORBIT TRANSFER

4.1.1 Solar Cell Cover Thickness

It was found that, for the LEO to GEO transfer mission, there appears to be no compelling reason to reduce the thickness of solar cell covers much below 6 mils. The calculations were made for an assumed payload fraction of 33%. For the lowest assumed thruster efficiency function the cover thickness for minimum transfer time ranged from 5.5 mils to 6.5 mils as the specific mass α varied from 0.01 to 0.02 (W/kg). For the highest assumed thruster efficiency function the corresponding cover thicknesses ranged from 3-1/2 to 4-1/2 mils for specific masses varying from 0.005 to 0.01 (W/kg). For the shortest transfer time case (highest efficiency and lowest α), the transfer time for 6-mil covers was only 12% larger than the minimum time for the 3-1/2 mil covers. However, the corresponding residual power on orbit was 15% greater for the 6-mil covers.

Tradeoff calculations for a given mission would be needed to define an optimum thickness for a specific application. However the weak dependence of orbit transfer time on cover thickness, i.e., the flatness of the minimum, shows that cover thickness is not a sensitive parameter so that 6 mils is a near-optimum thickness for a wide range of parameters. Improved solar array performance might be expected from thinner covers for missions below the Van Allen belt; but for the LEO to GEO application, 6-mil covers appear to be adequate.

4.1.2 Optimum I_{SP} Range

The optimum I_{SP} for transfer from LEO to GEO is the value that gives the shortest transfer time for a given efficiency. It depends on payload fraction but is essentially independent of both the specific mass parameter α and the efficiency. Its value ranges from 2600 seconds at 50% payload down to 1400 seconds at 20% payload.

The functions relating η to I_{SP} for a fixed transfer time are fairly flat near the optimum I_{SP} . Because η generally increases with I_{SP} for electric thrusters, the I_{SP} for minimum transfer time for a given type thruster occurs at a higher value than the optimum I_{SP} , the difference being larger for the less efficient thrusters than for the more efficient ones. For example at 33% payload, the least efficient thruster had an I_{SP} of 4000 seconds for minimum transfer time as compared to 2100 seconds for the most efficient thruster.

In the neighborhood of the minimum transfer time (when the slope of the efficiency function is equal to that of a constant transfer time line), variation of I_{SP} has very little effect on transfer time. But it does have a strong effect on the trade between dry propulsion mass and propellant mass. Reducing the I_{SP} only slightly results in a large reduction in the more expensive dry propulsion mass that is compensated by a nearly equal gain in the less expensive propellant mass. For example, using the intermediate efficiency relation at 33% payload, the minimum transfer time is 174 days for an I_{SP} of 2300 seconds. The corresponding values of dry propulsion mass and propellant mass are 1.06 and 0.80 times the payload mass. If the I_{SP} were reduced to the optimum value of 1750 seconds, for this case, these values would become 0.84 for dry propulsion and 1.14 for propellant. The transfer time, however, would be increased from 174 days to 190 days, or about 9%.

A reasonable compromise is to select an I_{SP} midway between the optimum value and the minimum transfer time value, about 2000 seconds for the present example. The transfer time is then about 180 days, the dry propulsion mass is 0.96 and the propellant mass is 0.92 times the payload mass. Using this approach, the I_{SP} ranges from 2850 seconds at 50% payload to 1700 seconds at 20% payload for the intermediate efficiency relation.

Higher values of I_{SP} are encountered for planetary missions that require much greater total impulse than that needed for LEO to GEO transfer. Lower values are optimum for lower impulse missions such as small changes in orbit altitude ranging from the Shuttle parking orbit to the beginning of the radiation belt for spacecraft using integrated propulsion. For these missions high energy chemical rockets and resistojets become attractive. However, for the total impulse range of LEO to GEO missions, the useful I_{SP} range is roughly from 1500 to 2500 seconds. This may also be true for multimission spacecraft, such as an electric tug, making several low altitude orbit changes. This aspect of Shuttle capability extension needs further study.

4.1.3 Importance of Efficiency and Specific Mass

The two most important thruster system parameters affecting transfer time from LEO to GEO are the thruster efficiency (the ratio of ideal beam kinetic power to input electric power) and the thruster specific mass (mass per unit input electric power of the dry propulsion system). The importance of efficiency is illustrated by the 33% payload example having a specific mass of 0.024 kg/W. For the lowest efficiency function assumed for the study the minimum transfer time is 272 days at 4000 seconds I_{SP} and 48% efficiency. For the intermediate efficiency function the time is reduced to 174 days at 2300 seconds I_{SP} and 51% efficiency. For the most efficient thruster the time is only 147 days at 2100 seconds I_{SP} and 59% efficiency. These values are shown in Table 16.

The Case I and Case II efficiencies are based on present data; the Case III function is an estimated performance that may be attainable in the near future. It is not so much the efficiency differences that are important as it is the combination of increased efficiency with reduced I_{SP} . For instance, the Case II example is only 3% higher efficiency than Case I, yet the transfer time is reduced by 98 days as a consequence of the I_{SP} reduction from 4000 to 2300 seconds.

A slightly different example, Case II efficiency at optimum I_{SP} and 33% payload, is used to show the importance of the specific mass parameter α on transfer time. Table 17 compares results for α ranging from 0.016 to 0.032 (kg/W) for this case.

Table 16. Effect of Thruster Efficiency on Transfer Time
(33% Payload, $\alpha = 0.024$ kg/W)

Efficiency Function	η (%)	Isp (sec.)	Transfer Time (days)
Case I	48	4000	272
Case II	51	2300	174
Case III	59	2100	147

Table 17. Effect of α on Transfer Time
(33% Payload, $\eta = 45\%$ at 1750 seconds I_{SP})

α (kg/W)	Transfer Time (Days)
0.016	120
0.024	193
0.032	259

The specific mass parameter is clearly of great importance. The transfer time is reduced 66 days by reducing α from 0.032 to 0.024 (kg/W).

For the LEO to GEO transfer mission, thruster technology effort should be focused on increasing efficiency at moderate I_{SP} (1500 to 2500 seconds) and reducing the specific mass as much as possible. Any thruster capable of achieving both of these objectives simultaneously would be very attractive for this mission.

4.1.4 Fast Orbit Transfer

In addition to reduction of LEO to GEO transfer time through efficiency improvement and specific mass reduction, it is always possible to achieve further reductions by giving up payload. At some point this defeats the primary advantage of electric propulsion which is its ability to transport larger payloads than can be handled by chemical propulsion. Table 18 summarizes the trade between payload and transfer time for the low specific mass of 0.012 kg/W and the highest efficiency function assumed for an electric thruster. Transfer times for the resistojet, operating at

Table 18. Effect of Payload on Transfer Time for Electric and Resistojet Thrusters

Payload Fraction (%)	Transfer Time (Days)	
	Electric	Resistojet
10	31	18
20	39	32
30	52	118
40	75	-
50	123	-

90% efficiency and 900 seconds I_{SP} are also shown for comparison of this thruster type.

This table further illustrates the importance of high efficiency at moderate I_{SP} , combined with low specific mass. It also shows that the resistojet may not be suitable for the integrated LEO to GEO mission. It shows an advantage only for small payload fractions, for the assumed I_{SP} of 900 seconds. It would quickly lose this advantage if the I_{SP} were reduced even slightly below this value. For example, at 800 seconds I_{SP} and 90% efficiency, the time would be increased from 32 days to 60 days for 20% payload.

4.1.5 Low Altitude Flight

It was found during the course of this study that solar electric propulsion could be extended to altitudes well below the optimum Shuttle parking orbit. For an assumed specific mass of 0.024 (kg/W), $\eta = 42\%$ at 1500 seconds I_{SP} and an area density of 30 kg/m² a spacecraft with 60% payload could maintain altitude at 150 km. This is done by feathering the solar array for minimum drag (oriented edge-on to the flight direction) and rolling it for maximum illumination to produce an average occulted power of about 40% of the full array power. The greatly increased ratio of solar array power to drag area opens up the possibility of continuous flight in the aerodynamic drag range of altitudes that extend from 500 km down to 150 km. Previously the lower end of this range was considered to be unacceptable for solar electric propulsion (Reference 14).

A comparison of the feathered flight mode with a nuclear power source shows comparable performance down to 150 km.

4.2 SPECIFIC MISSION EXAMPLE

The specific mission chosen to illustrate application of integrated electric propulsion systems is summarized in Table 19. It is a modular antenna spacecraft with a 60 m diameter antenna. Its reference configuration is illustrated in Figure 60 (page 102). The mission is to operate the spacecraft for 10 years in geosynchronous equatorial orbit after having transferred it from Skuttle's parking orbit at 250 km altitude and 28.5 degrees inclination. Stationkeeping requirements on-orbit are ± 0.1 degree. Upon conclusion of on-orbit operations, the spacecraft is transferred to higher altitude for disposal.

The APS ΔV requirements for this mission are summarized in Table 20. N-S stationkeeping requirements are derived from Section 3.3.4.1. E-W stationkeeping requirements are taken from Table 12 in Section 3.3.4.2 (page 129) for Method 2, $\sigma = 0.3$. The E-W requirements are several percent high because the effect of spacecraft mass variation, discussed in Appendix A, was not taken into account. Disposal requirements are given in Section 3.3.4.4 (page 130). A contingency of 20% has been added to account for momentum wheel unloading during attitude control operations, and for propellant residuals. Since the total ΔV on-orbit is very close to the value used in Section 2.8.1 (see Table 5, page 57), the results shown in that analysis may be used directly.

The beginning-of-life power can be estimated from the anticipated residual on-orbit power shown in Figure 42 (page 76). A residual power in excess of 50% is anticipated for the specific case chosen. The residual power requirement of 90 kW (Table 19) thus results in a value of 180 kW BOL. Using a specific mass, $\alpha_E = 0.024$ kg/W, the EPS dry mass is $(0.024)(180)(1000) = 4320$ kg. The payload mass is then the spacecraft dry mass from Table 19 less the EPS dry mass. Hence, the payload mass = $13,500 - 4320 = 9180$ kg.

For a thruster exhibiting Case II efficiency characteristics, the tradeoff curves in Figures 27 through 30 (pages 59-62) apply to this example. At 33% payload fraction, for instance, Figure 28 is applicable.

Table 19. Specific Mission Requirements

Configuration	Modular Antenna (see Figure 60)
Antenna Diameter	60 m
Spacecraft Dry Mass	13,500 kg
Initial Altitude	250 km
Final Operation Altitude	35786 km
Initial Inclination	28.5°
Final Operation Inclination	0° (equatorial orbit)
Disposal Altitude	40786 km
Lifetime On-Orbit	10 years
On-Orbit Stationkeeping Accuracy	±0.1°
On-Orbit Power	90 kw

Table 20. ΔV Requirements for APS, 60 m Modular Antenna Spacecraft

Maneuver	ΔV (m/sec)
North-South Stationkeeping	639
East-West Stationkeeping	545
Disposal	<u>167</u>
Sub-total	1451
20% Contingency	<u>290</u>
Total	1741

Minimum transfer time occurs at 2300 I_{sp} (see Table 6, page 64), but it is better to operate at slightly lower I_{sp} for the reasons given in Section 2.8.1. Selecting 2000 sec as the operating point yields a thruster efficiency of 47.5% and 187 days transfer time at an electric propulsion system mass = (2.0) (9180) = 18,360 kg. The total spacecraft mass launched in the Shuttle cargo bay (excluding flight support equipment) is then 18,360 + 9180 = 27,540 kg. The BOL thrust level for the primary thrusters is computed from Equation (7) to be 8.7 N.

The APS thrusters operate at 3000 sec I_{SP} and approximately 0.1 N thrust as discussed in Section 3.3.3. At Case I efficiency, the APS thrusters consume 4.0 kW per Equation (7). Checking on-orbit power capability, Figure 42 (page 76) shows 53% residual power at 2000 sec I_{SP} close to 33% payload ratio. This corresponds to 95.4 kW at beginning of orbital operations, which is sufficient to support the payload plus the APS thrusters.

The EPS characteristics for the 60 m modular antenna spacecraft are summarized in Table 21.

Table 21. EPS Characteristics for 60 m Modular Antenna Spacecraft

BOL Power	180 kW
Mass Properties	
Dry Weight	4320 kg
Propellant Weight	14040 kg
Total Weight	18360 kg
Orbit Boosting Thrusters	
BOL Thrust	8.7 N
Specific Impulse	2000 sec
Efficiency	47.5%
APS Stationkeeping Thrusters	
Thrust	0.1 N
Specific Impulse	3000 sec
Efficiency	37%
Power	4.0 kW
LEO to GEO transfer time	187 days
Orbital lifetime	10 years

5. CONCLUSIONS

- (1) For a wide range of spacecraft and mission parameters, 6-mile covers are near optimum for LEO to GEO transfer.
- (2) The most favorable I_{sp} range for primary propulsion for this mission is roughly from 1500 to 2500 seconds.
- (3) High efficiency in this I_{sp} range, and low specific mass are very important for short transfer times.
- (4) Fairly short transfer times are feasible with near term technology. With demonstrated thruster efficiency, the transfer time is about 175 days for 33% payload.
- (5) Very short transfer times may be possible with further technology advances. For the assumed Case II thruster efficiency and $\alpha = 0.012$ kg/W, the transfer time for 30% payload is 52 days.
- (6) The resistojet is only attractive at low payload fractions for this mission.
- (7) With the feathered solar array, rolled for optimum illumination, continuous flight is possible at altitudes above 150 km.
- (8) Substantial residual power is available for on-orbit power sharing with payload. At 33% payload, 57% of BOL power is available.
- (9) Large propellant mass savings, through integrated electric APS, results in 50% increase of maximum Shuttle launched reference spacecraft mass. These savings are realized principally through reduction in auxiliary propellant mass and the resulting, even larger, reduction in primary propellant mass requirements.
- (10) The launch weight reduction from integrated electric APS can lead to Shuttle launch cost savings as large as \$10 million for a spacecraft of 8100 kg net mass studied herein. However, the results are strongly influenced by the spacecraft stowed length under NASA's Shuttle launch cost reimbursement policy.
- (11) Electric APS and primary EPS thrust vectoring meet attitude control requirements. Chemical auxiliary thrusters only provide a backup function.
- (12) Gravity gradient torques can be used to sustain spacecraft roll maneuvers for optimum solar panel illumination during primary thrust phases of the mission. Operation near resonance should greatly reduce control moment gyroscope requirements.

- (13) With the initial gross weight reduction achieved through integrated electric APS, the solar array and primary EPS used for LEO to GEO transfer can be significantly reduced in size while still producing a similar acceleration as before. Alternatively, if not reduced in size, the system would achieve a faster transfer due to increased acceleration.
- (14) East-west stationkeeping ΔV due to solar pressure on large spacecraft structures can be three to four times greater than north-south stationkeeping ΔV . There is practically no effect of east-west stationkeeping accuracy on ΔV requirements.

APPENDIX A

EAST-WEST STATIONKEEPING ΔV REQUIREMENTS INCLUDING THE EFFECT OF SPACECRAFT MASS VARIATION (ITERATIVE PROCEDURE)

Spacecraft mass variation due to stationkeeping propellant expenditures are relatively minor, i.e., only a few percent, in the case of electric auxiliary propulsion. However for an accurate performance comparison with chemical auxiliary propulsion maneuvers where such propellant expenditures will be very much larger, the effect of mass variation of solar pressure perturbation must be taken into account.

Using the ΔV_s requirements derived in Section 3.3.4.2 (Table 12) as a first step in an iterative process, a good approximation of actual ΔV_s requirements and the corresponding propellant expenditures is obtained by the algorithm derived below.

We use the average spacecraft mass defined by

$$M_{ave} = M_o + \frac{1}{2} M_{pp} = M_o \left[1 + \frac{1}{2} \left(e^{\Delta V / I_{sp} g} - 1 \right) \right] \quad (A-1)$$

$$= \frac{1}{2} M_o \left(1 + e^{\Delta V / I_{sp} g} \right)$$

in approximating an average value of k

$$k_{ave} = 1.3 \frac{A}{M_{ave}}$$

in Equation (61) which derives ΔV_s as a function of k or A/M.

The term ΔV used in Equation (A-1) is the total ΔV expended on orbit, for stationkeeping and other maneuvers. ΔV_s is only a part of this total ΔV expenditure and must be separated from the other part designated by ΔV_r . In the equation relating ΔV_s to A/M_{ave} ,

$$\Delta V_s = Q \cdot k_{ave} \approx 1.3 Q \frac{A}{M_{ave}} \quad (A-2)$$

**ORIGINAL PAGE IS
OF POOR QUALITY**

the terms ΔV_s and ΔV_r used in defining M_{ave} must be segregated as follows

$$\Delta V_s = 1.3 \cdot Q \frac{2A}{M_0} \frac{1}{(1 + e^{(\Delta V_r + \Delta V_s)/I_{SP}g})} \quad (A-3)$$

The coefficient Q used as a simplifying notation in Equation (A-2) and (A-3) is the product of all factors except $k = A/M$ that appear on the right side of Equation (61).

To further simplify Equation (A-3) we substitute the terms

$$e^{\Delta V_r/I_{SP}g} = S_r$$

$$e^{\Delta V_s/I_{SP}g} = S_s$$

$$1.3 Q \frac{A}{M_0} = \Delta V_{s0}$$

where the quantity ΔV_{s0} is the ΔV_s value that was previously obtained by assuming a constant mass M_0 (Table 12). With these substitutions Equation (A-3) is reduced to

$$\Delta V_s (1 + S_r S_s) = 2 \Delta V_{s0} \quad (A-4)$$

or

$$\Delta V_s (1 + S_r e^{\Delta V_s/I_{SP}g}) = 2 \Delta V_{s0} \quad (A-5)$$

From this equation the corrected values of ΔV_s can be readily derived given S_r and ΔV_{s0} .

Note that the principal approximations made in this procedure are the assumptions that the average mass M_{ave} is the mean between the masses at the beginning and end of the orbital mission phase and that k_{ave} is proportional to $1/M_{ave}$. The approximations are better for electric propulsion where the propellant expenditure is relatively minor than for the chemical APS case. However, for purposes of this analysis the approximations inherent in the above approach are considered adequate.

Note also that a differentiation of I_{SP} values between those maneuvers performed by the main and the auxiliary electric thrusters is approximate

and should be made in calculating the corrected ΔV_s values using an equation similar to (A-5). In these calculations we assumed specific impulse values of 1500 seconds for the main and 3000 seconds for the auxiliary electric thrusters vs 300 seconds for chemical thrusters in auxiliary propulsion system performance comparisons. Table 14 lists ΔV requirements other than those for E-W stationkeeping, i.e., the partial ΔV requirements adding up to ΔV_r in Equation (A-3) to be used as input terms in solving for ΔV_s .

Table 22 gives the results of relating corrected and initial ΔV_s values for electric and chemical propulsion maneuvers, based on the above I_{SP} data. (In solving the transcendental velocity equation (A-5) for the unknown variable, ΔV_s is assumed as input and ΔV_{SO} obtained as output quantity.) The results are plotted in Figure 77 which shows that in the range of interest the corrected ΔV_s values for electric propulsion are

Table 22. Solution of Equation A-5 for Iterative Correction of ΔV_s
(Velocities in m/sec)

ΔV_s	S_s	ΔV_{NS}	S_{NS}	ΔV_r	S_r	ΔV_{SO}
<u>ELECTRIC APS</u> ($I_{SP} = 3000$ s)		(3000 s)		(1500 s)		
300	1.0102	639	1.022	423	1.0292	309
600	1.0206	639	1.022	423	1.0292	621
900	1.0311	639	1.022	423	1.0292	937
1300	1.0452	639	1.022	423	1.0292	1363
<u>CHEMICAL APS</u> ($I_{SP} = 300$ sec)						
300	1.1074	870	1.344			367
600	1.2264	870	1.344			794
900	1.3581	870	1.344			1271
1300	1.5561	870	1.344			2009

ORIGINAL PAGE IS
OF POOR QUALITY

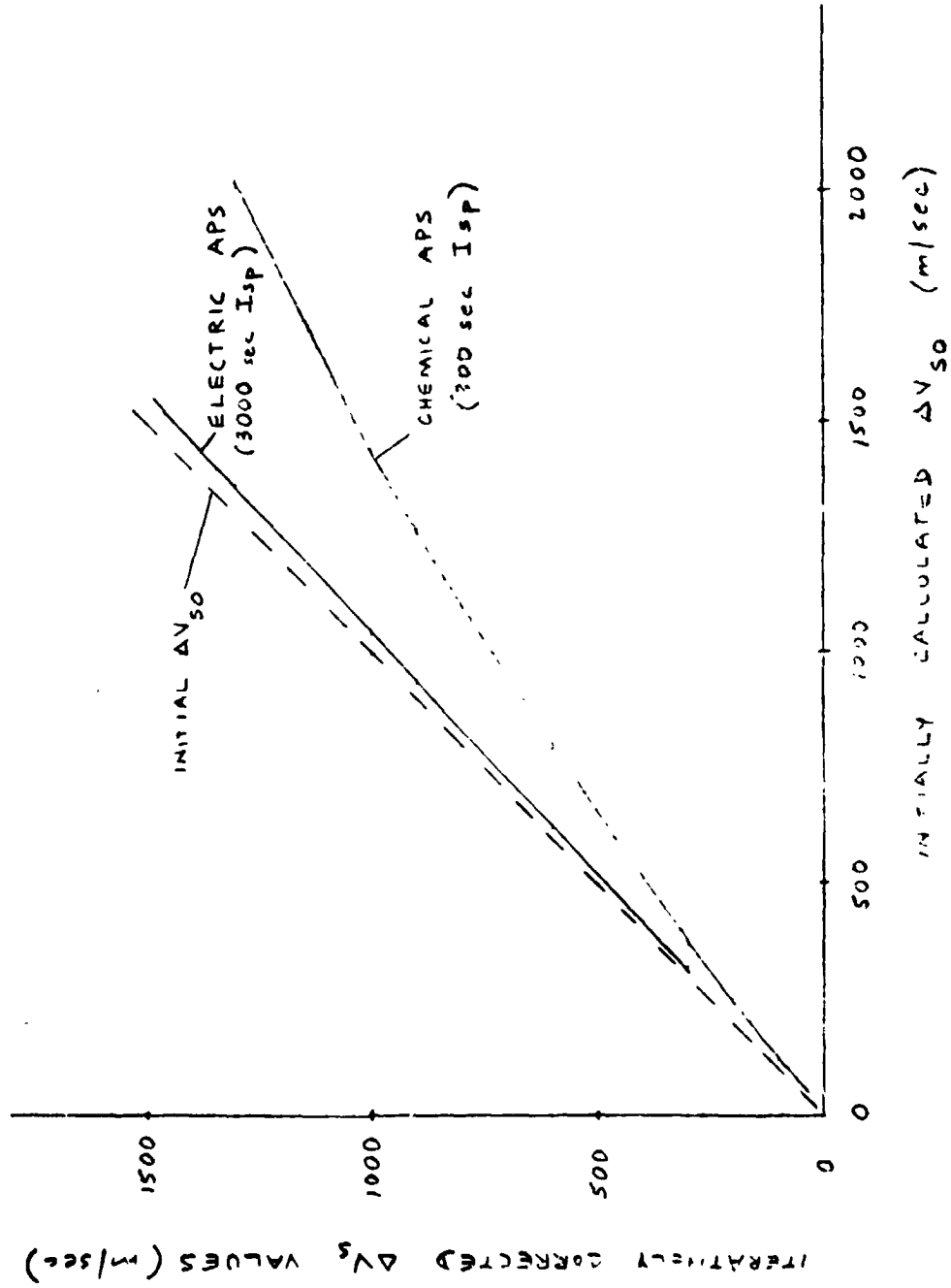


Figure 77. Iteratively Corrected Values ΔV_s Versus ΔV_{so} (10 Year Mission)

3 to 5 percent less than the initial values ΔV_{SO} , while for chemical propulsion the differences can be as large as 35%. As previously explained, these reductions are due to the use of average A/M ratios in the ΔV_S calculation rather than the initially assumed higher A/M_0 ratios that did not take propellant mass variations into account. Clearly, this effect is much larger in the chemical propulsion case.

REFERENCES

1. C.H. Terwilliger and W.W. Smith, "Electric Propulsion for Near-Earth Space Missions," NASA CR-159736, NASA-LeRC Contract NAS 3-21346, January 1980.
2. W.W. Smith and J.P. Clark, "Study of Electrical and Chemical Propulsion for Auxiliary Propulsion of Large Space Systems," NASA CR-165502, NASA-LeRC Contract NAS 3-21952, March 1981.
3. W.E. Pipes, III, "Advanced Spacecraft Deployment System Study," AFRPL-TR-80-43, AFRPL Contract F04611-79-C-0032, September 1980.
4. J.A. Scott-Monck, "Prospects for Enhancing SEPS Array Performance," NASA Contract NAS7-100.
5. R.W. Wolverton, ed., Flight Performance Handbook for Orbital Operations, John Wiley & Sons, N.Y. 1963.
6. H.Y. Tada and J.R. Carter, "Solar Cell Radiation Handbook," NASA-JPL Publication 77-56, November 1, 1977.
7. T.N. Edelbaum, "Propulsion Requirements for Controllable Satellites," ARS Journal, August 1961.
8. "8-cm Mercury Ion Thruster Subsystem Users Manual," prepared by TRW for NASA-LeRC, July 1977.
9. "Pulsed Plasma Propulsion System/Spacecraft Design Guide," AFRPL-TR-80-38, June 1980.
10. S. Zafran, ed., "Ion Engine Auxiliary Propulsion Applications and Integration Study," NASA-CR-135312, July 1977.
11. M. Huberman, et. al., "Mission Integration Study for Solid Teflon Pulsed Plasma Millipound Propulsion System," AFRPL-TR-80-37, June 1980.
12. R.R. Lovell and T.A. O'Malley, "Station Keeping of High Power Communication Satellites," NASA TM X-2136, November 1970.
13. "Space Transportation System Reimbursement Guide," NASA, JSC-11802, May 1980.
14. S. Zafran, M.H. Gran, and V.V. Fosnight, "Ion Engine Propulsion Module (IPM)," Final Report, NASA-GSFC Contract NAS 5-26008, January 1981.